Greenhouse climate: from physical processes to a dynamic model

Promotor: dr. ir. J. Schenk, hoogleraar in de
technische natuurkunde

G. P. A. Bot

Greenhouse climate: from physical processes to a dynamic model

Proefschrift

ter verkrijging van de graad van
doctor in de landbouwwetenschappen,
op gezag van de rector magnificus,
dr. C. C. Oosterlee,
hoogleraar in de veeteeltwetenschap,
in het openbaar te verdedigen
op woensdag 14 december 1983
des namiddags te vier uur in de aula
van de Landbouwhogeschool te Wageningen.

Schrijven is gewoon blijven zitten tot het er staat

(vrij naar Kees van Kooten)

Voor Vera,
Ivo, Marjolein, Heroen en Gerwin

Voorwoord

Bij het gereedkomen van dit proefschrift wil ik gaarne mijn erkentelijkheid uitspreken voor de medewerking die ik daarbij van zeer velen heb gehad.
Prof. dr. ir. J. Schenk heeft mij als mijn promotor enorm gestimuleerd. Het is bij het schrijven van een proefschrift uitermate belangrijk dat de eerste pennevruchten kunnen rijpen in een intensieve samenwerking tussen promovendus en promotor. Jaap, je aanwijzingen, gebaseerd op je diepe fysisch inzicht en je streven naar nauwkeurige formuleringen hebben ervoor gezorgd dat het rijpingsproces voorspoedig verliep. Graag wil ik je voor deze fijne samenwerking bedanken.
In de beginfase van het onderzoek is nauw samengewerkt met prof. ir. J. van Dixhoorn. Jan, de toepassing van de systeemleer op de kasklimaatsbeheersing, zoals door jou geïntroduceerd, klinkt in dit proefschrift door. Voor je samenwerking en je aanstekelijk enthousiasme kan ik je nu bedanken.
Het hier beschreven onderzoek werd gedragen door de informele werkgroep "optimalisering kasklimaat ten behoeve van de teelt van kasgewassen". Hierin wordt door dr. ir. H. Challa (Cabo), dir. ir. J. v.d. Vooren (destijds Proefstation Naaldwijk, nu Proefstation Aalsmeer), dr. ir. A.J. Udink ten Cate (L.H., Natuur- en Weerkunde) en mijzelf, later aangevuld met dr. ir. A.H.C.M. Schaapendonk (Cabo), vanuit de vakgebieden teeltkunde, plantenfysiologie, meet- en regeltechniek, systeemtechniek en natuurkunde, nauw samengewerkt. Juist vanuit deze interdisciplinaire samenwerking krijgt een proefschrift als dit zijn reliëf.

Het experimentele gedeelte van het onderzoek is gedeeltelijk uitgevoerd op het Proefstation voor Tuinbouw onder Glas te Naaldwijk en op het Instituut voor Mechanisatie, Arbeid en Gebouwen (Imag) te Wageningen.
Op het proefstation Naaldwijk werd nauw samengewerkt met dr. ir. J. van de Vooren. Door hem werden de experimenten ter plaatse voorbereid en gecoördineerd, waarbij vrijwel altijd met voor de praktijk buitennissige omstandigheden rekening moest worden gehouden. Jan, dit is eindelijk de gelegenheid om je voor je inbreng en je altijd flexibele instelling te bedanken.
De samenwerkingsovereenkomst tussen het Proefstation en de LH, Natuur- en Weerkunde bevestigde het gezamenlijke belang van het onderzoek. Ik wil het

Proefstation, in de persoon van haar directeur ir. E. Kooistra, graag bedanken voor de geboden mogelijkheden en voor de belangstelling en steun. Bij de voorbereiding en uitvoering van het onderzoek werd nooit vergeefs een beroep gedaan op de mensen van de Technische Dienst en de Tuindienst. Daarnaast zorgde Theo Strijbosch ervoor dat zeer veel praktische zaken werden geregeld.

Op het Imag werd de samenwerking gestimuleerd door ir. W.P. Mulder. Er werden gezamenlijke kasklimaatsmetingen opgezet voor zowel ons onderzoek naar het momentane kasklimaat, alsmede voor het onderzoek van drs. C. Stanghellini naar de relatie tussen de over langere tijd geïntegreerde verdamping en andere kasklimaatsgrootheden. Caecilia wil ik graag bedanken voor het vele praktische werk dat zij in deze op zich heeft genomen. Daarnaast werden faciliteiten geboden voor enkele afzonderlijke meetprojecten. Graag wil ik de directie van het Imag bedanken voor de geboden mogelijkheden.

Veel van de uitgevoerde experimenten konden worden uitgevoerd met behulp van apparatuur, aangeschaft met fondsen beschikbaar gesteld vanuit het zg. "Energiefonds". Graag wil ik de Energiebeleidscommissie, in de persoon van haar voorzitter ir. W.F.S. Duffhues, bedanken voor het in ons gestelde vertrouwen.

Met veel collega's heb ik bij verschillende gelegenheden mogen discussiëren over diverse aspecten van het kasklimaat. Juist deze discussies hebben bij mij het gevoel versterkt dat gezamenlijk aan een probleem met veel facetten wordt gewerkt zodat slechts door inspanning vanuit verschillende disciplines resultaten kunnen worden geboekt.

Binnen de vakgroep Natuur- en Weerkunde werd zeer nauw samengewerkt met dr. ir. A.J. Udink ten Cate. Alexander, onze discussies en samenwerking hebben veel bijgedragen aan mijn benadering van het kasklimaat. Ik wil je hiervoor zéér hartelijk bedanken.

In het onderzoek hebben veel studenten met grote inzet meegewerkt. Hierbij zijn bergen werk verzet. Graag wil ik alle hierbij betrokken studenten heel hartelijk bedanken. Jullie enthousiasme, werklust en inzet hebben een wezenlijke bijdrage aan dit proefschrift geleverd.

Zonder goede infrastructuur in de vakgroep kan geen onderzoek worden uitgevoerd. In onze vakgroep wordt de combinatie van verschillende elkaar aanvullende vakgebieden ondersteund door een instrumentmakerij, een elektronisch ontwikkellaboratorium en een algemene dienst. In de instrumentmakerij zorgden

Anton, Teun en Willy er altijd met veel vakmanschap voor dat extreme wensen werden vertaald in hanteerbare en betrouwbare meetinstrumenten. Voor de elektronische meetproblemen werd door Kees, Peter en Geerte altijd een adequate oplossing verwezenlijkt. Dimitri en Willem ontfermden zich over problemen rond gegevensverzameling en -verwerking. Bart en Dick losten veel problemen op rond het gebruik en de opstelling van meteorologische meetinstrumenten. Graag wil ik mijn dank voor jullie altijd bereidwillige inzet benadrukken.
Binnen de sectie Technische Natuurkunde werd ik vooral in de eindfase ontzien en namen Dane, Jaap en Rudi veel van mijn taken over. Corrie zorgde ervoor dat ik zo goed mogelijk werd afgeschermd. Ik wil jullie daarvoor graag bedanken.

Als eenmaal het manuscript is geschreven, moet hieraan een leesbare vorm worden gegeven. Paul heeft met het van hem bekende vakmanschap mijn schetsen omgezet in fraaie tekeningen. Ondanks het grote aantal, die je wel eens de vraag hebben ontlokt of we met een stripverhaal bezig waren, zijn ze ruim op tijd klaargekomen. Peter Schaap heeft het manuscript nagelezen en hieruit storende fouten in het Engels gezeefd. Len Weldring zette mijn manuscript, waarin veel doorhalingen en aanvullingen, snel en accuraat om in getypte tekst. Graag wil ik jullie hiervoor bedanken.

Tenslotte wil ik graag mijn gezin bedanken voor het geduld en de steun in de achter ons liggende periode. Lieve Vera, Ivo, Marjolein, Heroen en Gerwin, jullie zorgden voor het optimale binnenklimaat waarin dit proefschrift zich kon ontwikkelen. Ik draag daarom graag dit proefschrift aan jullie op.

Bennekom, 16 oktober 1983

Contents

LIST OF FREQUENTLY USED SYMBOLS

1. INTRODUCTION AND ORGANIZATION OF THE THESIS 1

2. GREENHOUSE CLIMATE AND PHYSICAL PROCESSES 6
   2.1. Introduction 6
   2.2. Greenhouse climate: quantities and physical processes 7

3. AIR EXCHANGE BY VENTILATION 13
   3.1. Introduction 13
   3.2. Literature review 14
   3.3. Ventilation mechanisms 16
      3.3.1. Flow characteristic of an opening 17
      3.3.2. Driving forces for ventilation 21
         3.3.2.a. Wind effects 21
         3.3.2.b. Temperature effects 22
      3.3.3. Resulting ventilation 25
         3.3.3.a. Ventilation due to wind effects 25
         3.3.3.b. Ventilation due to temperature effects 26
      3.3.4. Comparison of ventilation phenomena due to wind and temperature effects 32
   3.4. Experiments 34
      3.4.1. Experimental set-up 34
         3.4.1.a. Flow characteristic of a window opening 34
         3.4.1.b. Full scale ventilation 35
      3.4.2. Experimental results 37
         3.4.2.a. Flow characteristic of a window opening 37
         3.4.2.b. Full scale ventilation 43
   3.5. Discussion 49
      3.5.1. Ventilation due to wind effects 49
      3.5.2. Ventilation due to temperature effects 55

4. FLUCTUATING CHARACTER OF VENTILATION 58
4.1. Introduction 58
4.2. Experimental set-up 58
4.3. Experimental results 60
4.3.1. Fluctuating character 61
4.3.2. Window opening and frequency distribution 67
4.3.3. Fluctuating character and effective air exchange 68
4.3.4. Heat transfer through the window opening 71

5. RADIATION 76
5.1. Introduction
5.2. Shortwave radiation 77
5.2.1. Transmission for direct radiation 78
5.2.1.a. Reflectance, transmittance and absorption of a single transparent sheet 80
5.2.1.b. Geometry of direct light and glass cover 83
5.2.1.c. Interaction with the glass cover 86
5.2.1.d. Light interception by the opaque roof parts 93
5.2.1.e. Total transmission for direct radiation 100
5.2.2. Diffuse radiation 109
5.3. Longwave (thermal) radiation 120

6. CONVECTIVE EXCHANGE PROCESSES 122
6.1. Exchange with the cover 122
6.1.1. Introduction 122
6.1.2. Experimental situation 125
6.1.3. Experimental set-up 129
6.1.4. Experimental results 133
6.1.4.a. Heat exchange 133
6.1.4.b. Flow phenomena 137
6.2. Heat transfer from the heating pipes 141
6.2.1. Introduction 141
6.2.2. Experiments 143
6.2.3. Measuring results 148
6.3. Exchange with and transport in the soil 150

6.4. Exchange with the vegetation 152
    6.4.1. *Introduction 152*
    6.4.2. *Experimental conditions 154*
    6.4.3. *Experimental set-up 157*
    6.4.4. *Experimental results 160*

7. A DYNAMIC PHYSICAL MODEL OF GREENHOUSE CLIMATE 168
7.1. Introduction 168
7.2. Model considerations 170
7.3. Bond graphs and minicomputers in greenhouse climate control (reprint Eppo Bull. 9(3): 205-218 (1979)) 173
7.4. Outline of the present model 187
7.5. Experimental set-up 191
7.6. Simulation and experimental results 195
7.7. Commentary on the simulation result and procedure 204
7.8. Applicability of the model 207

8. FINAL DISCUSSION, CONCLUSIONS AND SUGGESTIONS 210

SUMMARY 216

SAMENVATTING 221

REFERENCES 226

CURICULUM VITAE 240

List of frequently used symbols

SYMBOLS

A	area (m^2)
a	constant (-)
b	constant (-)
c	constant (-)
Cap	capacity (JK^{-1})
Cl	cloudiness (-)
C_p	specific heat at constant pressure (Jkg^{-1}K^{-1})
c	concentration (kg m^{-3})
D	distance (m)
d	diameter (m)
E	emission coefficient (-)
Eu	Euler number (-)
e	vapour pressure (Nm^{-2})
F	aspect ratio factor (-)
f(.)	function of (.)(-)
G(.)	window function (-)
G	Gill anemometer
Gr	Grashof number (-)
g	gravitational acceleration (ms^{-2})
H	height (m)
h	height (m)
I	irradiation (Wm^{-2})
i	angle of incidence (deg.)
K	coefficient (-)
$\vec{k}$	normalized vector along a co-ordinate (-)
L	Leeward (in chapter 4 only), length (m)
Le	Lewis number (-)
l	length (m)
N	ratio (-)
$\vec{N}$	vector normal to a surface (m)
Nu	Nusselt number (-)

n	refractive index (-)
Pr	Prandtl number (-)
R	reflectivity (-)
Re	Reynolds number (-)
RMS	root mean square
r	window aperture (%) or (-)
Sc	Schmidt number (-)
SR	sunrise
SS	sunset
T	temperature (^{o}C or K)
TC	thermocouple
t	time (s)
u	outside wind speed (ms^{-1})
V	volume (m^{3})
v	velocity (ms^{-1})
W	windward (in chapter 4 only), width (m)
x, y, z	co-ordinates (m)
∠	angle

Greek symbols

α	orientation relative to north-south direction (in chapter 5 only) (deg.) heat transfer coefficient (Wm^{-2}K^{-1})
β	latitude (in chapter 5 only)(deg.), thermal expansion coefficient (K^{-1})
γ	altitude (deg.)
Δ	difference
δ	declination (deg.)
ζ	window opening angle (deg.)
υ	time angle (deg.)
λ	thermal conductivity (Wm^{-1}K^{-1})
ν	angle between y- and z-component (deg.)
ξ	angle between x- and z-component (deg.)
ρ	density (kg m^{-3})
Σ	sum
σ	Stephan-Boltzmann constant (Wm-$^{-2}$K^{-4})
τ	transmission (in chapter 5 only) (-), time constant (s^{-1}).

ϕ	flux (m^3s^{-1} or kg s^{-1})
χ	angle (deg.)
ψ	roof slope angle (deg.)
∇	gradient (m^{-1})

Subscripts

a	outside (ambient)
b	bar
c	convective
cs	circumsolar
d	diffuse
e	vapour pressure
eff	effective
f	fluctuation
fo	forced
fr	free
g	gutter (in section 5.2.1.d. only), glass cover
h	hydrostatic (in chapter 3 only), heat
i	incidence (in chapter 5 only), inside
l	lower (in chapter 5 only), leaves
m	mass
n	net
o	opening
p	heating pipes
r	ridge (in section 5.2.1.d. only), radiant
r2	reflected from pane 2
rg	ridge gutter combination
s	solar (in chapter 5 only), soil
t	time
tot	total
T	temperature
u	upper (in section 5.2.1.d. only), outside wind
v	volume
w	window
x, y, z	x, y, z direction
xr	screen

note: combined subscripts e.g. $\alpha_{g,a}$ = heat transfer coefficient between the glass cover and the outside air.

Superscripts

~	amplitude (in chapter 3 only), increment
—	average value
*	vapour pressure difference as "driving force"
"	normalized per unit area
→	vector
'	fluctuation (in chapter 4 only)

1. Introduction and organization of the thesis

Transparent shelters have been used to modify environmental conditions for plants ever since people have tried to grow plants at a location or in a season with a hostile natural climate for such plants. As early as the Middle Ages exotic plants were grown in Northern Europe and these plants had to winter in dark barns or cellars, which were kept frost free. When glass became a common material, the lack of light could be decreased by incorporating windows in one vertical wall but still the lack of light was the most important imperfection of this type of shelters. Improvements were therefore aimed at increasing the light transmission of this archetype greenhouse (Van de Muyzenberg, 1943, 1948). This was achieved by increasing the amount of glass in the wall and the portion of the construction that could be furnished with transparent materials. A great improvement was the construction of a transparent roof. So the early greenhouse was constructed with a transparent wall and roof facing south with a stone wall at the north side. This type was in use until the twentieth century especially for the commercial growing of grapes at northern latitudes. The step from one sided to two sided entrance of light could be made when better materials and construction techniques became available and the single span glasshouse was introduced. It was not until the early twentieth century before the first multispan glasshouse was introduced.

As glasshouses were economically exploitable notably in the neighbourhood of some restricted regions near markets with great purchasing-power there was a need to ameliorate the supply side. As a result a horticultural and technical evolution started to improve production and quality at a higher net outcome. As we have seen from the short historical sidelight the improvement of the growth conditions is an important item in the technical evolution. At first empirical knowledge, intuition and the trial and error principle together with the availability of better materials and construction methods were the main driving factors in this evolution. But at an early stage scientific research was focussed on this field. Businger (1963) reviewed the technical developments and the basic knowledge until that moment. Commercial greenhouses had turned from simple aids into complex facilities in which production factors were strongly improved. The empirical knowledge was supplemented by physical interpretation. The climate could be described in terms of coupled energy and water-vapour balances, though most terms in these balances could only be estimated coarsly. The more recent review by Seemann (1974) can be summarized in the same terms.

New facilities for improvement were made available by the introduction of automatic climate control, at first by simple on-off thermostats but very soon by electronic equipment. At the beginning, the main advantage was that it was labour saving because laborious hand control was taken over by automatic continuous control. The control algorithms implemented in these apparatus were based on the way the grower had performed hand control (Strijbosch and Van de Vooren, 1975). However, the continuous watching of the environmental factors allowed production to be increased and that the quality of the products could be improved. The extra capabilities of the equipment and more available knowledge of the plant physiology of greenhouse crops (Gaastra, 1959) were a challenge to develop methods to control plant growth directly (Takakura, 1974). It was also the starting point of directly applicable, plant oriented adaptations of control algorithms. Bowman et al. (1970) and Bokhorst et al. (1972) introduced the light dependent temperature control and Heyna (1975) presented an algorithm to control the water vapour deficit.

The introduction of computers for practical greenhouse climate control was again a new challenge to exploitation of the capabilities of this aid (Van de Vooren, 1975) and the application of horticultural and plantphysiological knowledge in control algorithms seemed a very nearby fact. However, this required an integration of knowledge of various fields together with a framework in which this knowledge could be implemented and applied. With the introduction of a system approach in this field (Bot et al., 1978, Udink ten Cate et al., 1978) such a framework was constructed. In this approach the growing of a crop to a desired yield in a controlled environment is described as a hierarchical system in which three levels can be distinguished. The first level is that of momentaneous growth; at this level an appropriate control algorithm has to realize desired levels (set points) of controllable environmental conditions in an accurate way. The second level is that of short term plant response in relation to the greenhouse climate; on this level the setpoints have to be established which must be realized on level one.

The third level is that of long term plant growth and development; this determines the long term strategy to guide the crop to its final yield. On the different levels possibilities for improvements were indicated and an inventary of missing knowledge was made. This missing knowledge was both of technical nature and of horticultural and plant physiological nature. Technically more operational knowledge was wanted about the dynamic response of the greenhouse climate to changing outside weather conditions and about the direct relation between the momentaneous greenhouse climate and the outside weather. In the field of horticulture and plantphysiology quantitative information was demanded about both the short- and longterm dynamic response of crop-growth and -development to changing environmental conditions.

Recently Udink ten Cate (1983) reported at length on the control aspects of the greenhouse climate. The dynamic response of the greenhouse climate on the outside weather conditions was reproduced by simple, though reliable, black box models. The reliability was obtained by subdividing the response into a high and low frequency part. Control algorithms were presented to control the greenhouse climate on the first level in an accurate way.

The present study will be dealing with the quantification of the fundamental physical processes in greenhouse climate and the combination of these processes into a dynamic physical model. It was performed parallel to the work of Udink ten Cate. If the relation between the greenhouse climate and changing outside weather conditions is established in a physical way, more detailed information is gathered on the dynamic behaviour of the inside climate. This explains how different environmental factors from outside and inside are related and how energy and vapour fluxes react in the complex system. Moreover, this information is indispensible if increased knowledge on dynamic short and long term plant behaviour will become available.

Besides the urgent need for quantitative, physical knowledge following from the systems approach, another development yet strengthened this need. The high energy demand of greenhouse production was a minor problem at the time energy costs were low. After the oil crises, however, these costs rapidly increased and the search for energy saving strategies became vital for greenhouse operation (Germing, 1978). From a technical point of view at first one of the strategies was to adapt greenhouse equipment and construction to a less energy consuming production facility. The main question that arises at any adaptation invariably is: what is the impact on the greenhouse climate conditions and consequently on the yield and quality of the crops. Greenhouse climate is a very complex, dynamic phenomenon so that predictions about this impact based on empirical knowledge only will not be accurate or sometimes even result in wrong conclusions. If the physical processes involved are defined and quantified in a proper way greenhouse climate conditions can be predicted as a function of greenhouse construction and outside weather conditions together with the achieved energy saving. With this technique a choice can be made between several possible adaptations before horticultural experiments have to uncover how crop yield and quality is affected.

Since an adequate description of the basic physical processes is the starting point for an improved quantitative approach of greenhouse climate, in this thesis close attention will be paid to these processes. After a general survey of the greenhouse climate, the climate quantities and the processes involved (chapter 2), the main processes are treated separately. Air exchange between the greenhouse interior and exterior is called ventilation and this process is determined in chapter 3 for different window geometries as a function of window-aperture, outside wind speed and wind direction and temperature difference between in- and outside air. The fluctuative nature of the ventilation process is evaluated in chapter 4. The interaction of the greenhouse cover with both direct and diffuse radiation is described in chapter 5 together with the longwave radiative exchange. In chapter 6 the essential convective exchange processes are treated quantitatively. These are transpiration (from crop to greenhouse air), exchange of sensible heat between crop and greenhouse air, heat transfer from the heating pipe system to the air, condensation to the glass cover, heat exchange between the soil surface and the inside air, between the inside air and the glass cover and between the glass cover and the outside air. In chapter 7 the various processes are combined into a dynamic physical model and the quantitative results of the previous chapters are combined with parameter estimation techniques to obtain reliable, accurate results. The model itself is composed of coupled energy and water vapour balances over various components of the system, so ultimately it leads to a set of differential equations. These equations are represented in a graphical way by using the bond graph notation. A reprint of a joint publication with prof. ir. J.J. Van Dixhoorn (Twente University of Technology) on this subject is added as part of chapter 7. Conclusions are presented in the final chapter 8.

2. Greenhouse climate and physical processes

2.1. INTRODUCTION

The term greenhouse climate is used to indicate the set of environmental quantities in a greenhouse as they affect crop growth and development. In meteorology the term climate is used to indicate a long term average (over a large number of years) of the environmental quantities to point out differences between various locations and various seasons. The momentaneous set of values of the outside environmental quantities is referred to as the outside weather. So for a greenhouse it would be consequent to introduce the term "greenhouse weather" related to the outside weather at any moment and to reserve the term "greenhouse climate" to the average condition of the "greenhouse weather". However, this distinction would be more academic than practical, so we will follow common practice and use the term greenhouse climate in the context of the first sentence of this paragraph.

The difference between greenhouse climate and outside weather is mainly caused by two mechanisms:

- The air in a greenhouse is stagnant due to the enclosure, so the air exchange with the surrounding (outside) air is strongly decreased compared with that of the air without envelope and the local air velocities are small compared to that in the open air. These smaller local air velocities affect the transfer processes between the greenhouse air and the greenhouse inventory while the reduction of the air exchange or ventilation directly affects the energy and mass balances of the greenhouse air.
- The inward shortwave irradiation is decreased due to the light interception by the opaque and transparent components of the greenhouse and the longwave radiative exchange between inside and outside the greenhouse is influenced by the radiative properties of the covering materials. With glass as covering material this mechanism leads to the mousetrap theory: glass is (partly) transparent for the incoming shortwave radiation and opaque for the longwave radiation emitted from within. As indicated by Businger (1963), it was proved already by Wood (1909) and Van Gulik (1910) that this effect

is of minor importance to an explanation of the increased air temperature in the greenhouse. The common name "greenhouse effect" for the mousetrap-theory is therefore misleading. Nevertheless the radiative effects are indispensible to a description of the greenhouse climate because they directly affect all energy balances.

The general mechanisms may be relatively simple, the impact on the greenhouse climate itself is of a more complex nature. Thereby it is important what aspects of greenhouse climate are taken into account. Udink ten Cate (1983) defined a terminology for different aspects of greenhouse climate, especially to define in a proper way the relation between control actions and greenhouse climate. In this thesis, as said before, greenhouse climate is considered as the set of environmental quantities in a greenhouse, since they affect crop growth and development either directly or indirectly. Due to the physical interaction with the crop, the physical parameters of the crop have to be taken into account.

2.2. GREENHOUSE CLIMATE; QUANTITIES AND PHYSICAL PROCESSES

In this section only a short qualitative overview of relevant quantities and physical processes will be given. A more detailed treatment with literature references is given in the following chapters that are devoted to specific topics.

As the greenhouse cover is the barrier between the in- and outside environment, the interaction of the cover will be considered first. The first kind of interaction is with the shortwave radiation. The outside global irradiation is an energy source independent of the greenhouse, so it can be considered as a boundary condition for the greenhouse climate. The cover will transmit, absorb or reflect parts of the direct and diffuse outside irradiation (figure 2.1.). The transmitted radiation is partly absorbed by the canopy and some part will reach the soil surface and be absorbed there. Of course there is interreflection between the canopy and the cover and between the soil and the canopy or cover. The result will be an effective absorption by the cover canopy and soil and a total reflection from the greenhouse. The primary interaction of the shortwave radiation with the cover is discussed in chapter 5. Apart from the interaction with the short wave radiation, long wave thermal

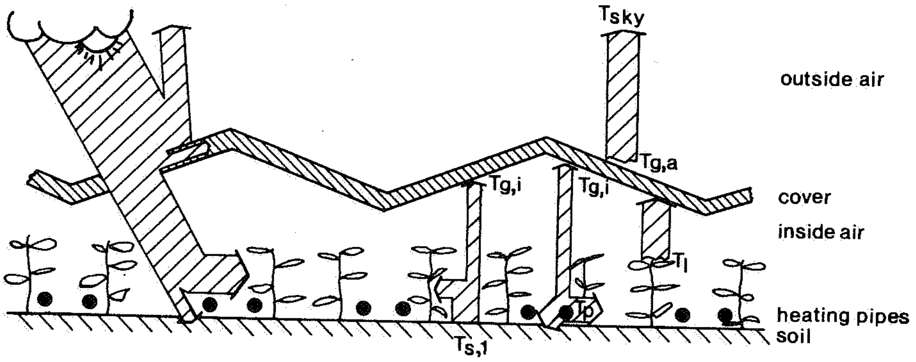

Fig. 2.1. Interaction of the shortwave radiation with the greenhouse components (left)and the radiative longwave exchange between the various greenhouse components and of the greenhouse cover with the outside environment (right).

radiation is exchanged between the cover and both outside and inside. The longwave radiation from the atmosphere is represented by the radiation from the sky vault with an effective temperature T_{sky} (chapter 5). This temperature is determined by the outside atmospheric conditions, so this, too, is a boundary condition for the greenhouse climate. The radiative exchange between cover and sky, then, can be calculated by the Stephan-Boltzmann equation. The same holds true for the exchange from the cover to the inside opaque greenhouse components like canopy, soil and heating system (figure 2.1.). The cover only partly interacts with each of these elements, which is accounted for by a view factor. The mutual interaction of the inside opaque elements, so heating-pipes and canopy, heating-pipes and soil surface and canopy and soil surface can be calculated according to the Stephan-Boltzmann equation too under consideration of view factors and emission factors.

The cover as a barrier between the inside and outside air also exchanges heat with both sides by convection (figure 2.2.). Heat transfer coefficients on both sides characterize these exchange processes while the temperature difference between cover and air on each side is the driving force for this exchange (chapter 6). It is not allowed to combine the convective heat transfer on the outside and the radiative longwave heat transfer on this side into one heat transfer coefficient because in general the outside air temperature does not equal the sky temperature. The combination of the heat transfer at both

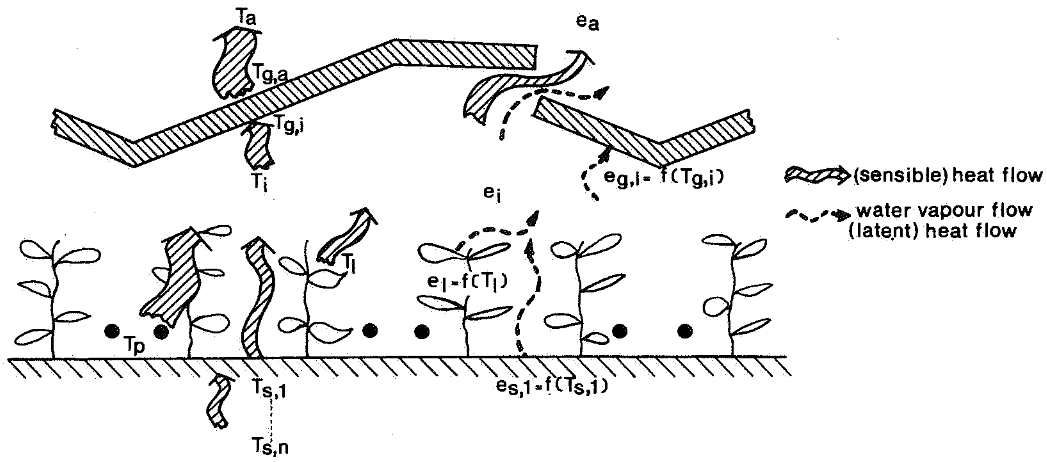

Fig. 2.2. Heat flows (sensible heat) and water vapour flows between the various greenhouse components and those leaving the greenhouse.

sides of the roof into one transmission coefficient for the cover would therefore also lead to wrong results. So the roof temperatures at both sides of the cover ($T_{g,i}$, $T_{g,a}$) have to be considered as greenhouse climate quantities. The outside air temperature T_a is an outside condition so a boundary condition for the greenhouse climate. The inside air temperature T_i of course is a climate quantity too.

The cover is not only a barrier for energy transfer, but also for transfer of water vapour and other gases (carbondioxide, ethene). If the inside cover temperature is lower than the dew point temperature of the inside air, condensation on the inner cover surface may occur. So a water vapour flow from the inside air to the cover is then generated. The driving force is the difference between the water vapour pressure of the inside air e_i and that at the cover e_{gi} (i.e. the saturation vapour pressure at inside cover temperature) and the transfer is characterized by a mass transfer coefficient. The convective mass transfer to and from the cover is also discussed in chapter 6.

Besides convective heat and mass transfer we should also consider direct heat and mass transfer through the cover. Air exchange between in- and outside via cracks and leaks or ventilation window openings transports sensible heat, water vapour and other gases. The amount of exchange is determined by the volumetric air exchange and the difference in in- and outside temperature water vapour pressure or gas concentration. The volumetric air exchange in its turn depends on outside conditions like wind velocity and direction, on greenhouse parameters like the leakiness of the cover, the type of ventilation windows and the window aperture and on climate conditions like the temperature difference between in- and outside air. This complex pattern is discussed in chapters 3 and 4.

Having qualitatively described the interaction with the cover, we can focus our attention to the vegetation, the final object of greenhouse activity. The short- and longwave radiative interactions with the canopy have been indicated earlier in this chapter. Besides this radiative exchange, convective exchange of sensible heat, water vapour and carbondioxide occurs. The sensible heat (figure 2.2.) is exchanged between both sides of the leaf and the surrounding air. The exchange can be characterized again by a heat transfer coefficient between leaf and air and the difference between leaf temperature T_l and inside air temperature T_i. Water vapour evaporates from the vacuola in the leaf, so it has to be transported first to the leaf surface and then from the surface to the greenhouse air. The transport from the vacuola to the leaf surface can take place through the stomata, mostly on one side of the leaf, and through the cuticula on both sides of the leaf. In general the resistance to water vapour transfer of the cuticula is much greater than that of the stomata. The stomatal opening, so the resistance of the stomata is regulated by plant physiological processes driven by external conditions. Due to the evaporation, the heat of evaporation has to be accounted for in the heat balance over the leaf. From the leaf surface the water vapour is transported to the surrounding air. This process is characterized by a mass transfer coefficient. The transport of carbondioxide can be described analogously.

Besides the input of energy by shortwave radiation, the energy input of the heating system affects the greenhouse climate. The radiative longwave heat exchange with the cover, canopy and soil surface is mentioned before; the convective exchange with the surrounding air (figure 2.2.) can again be characterized by a heat transfer coefficient. Though in general the heating pipe temperature is controlled to realize a desired inside air temperature, the heating pipe temperature is a boundary condition for the greenhouse climate. The temperature is imposed by the control system and not by the greenhouse climate directly.

The remaining greenhouse component, the soil, exchanges thermal radiation with the other opaque components and sensible heat and water vapour with the greenhouse air (figure 2.2.). The heat and water vapour exchanges are characterized again by a heat transfer and mass transfer coefficient between the soil surface and the greenhouse air. For a well-watered soil like in a greenhouse, the water vapour pressure at the soil surface is the saturation vapour pressure at the surface temperature. In the water saturated soil there is no need to account for the water transport, but the heat transport should be taken into account. It is conducted from high to low temperatures and must be calculated from the temperature gradient in the soil and the heat conductivity in the soil. So temperatures at various depts $T_{s,1}$.....$T_{s,n}$ define the heat transport. At a depth where no seasonal temperature fluctuations occur, the soil temperature has to be given as a boundary condition. The various convective heat transfer effects, the transpiration of the vegetation and the conduction in the soil are treated in chapter 6.

Summarizing the above, the following sets of greenhouse climate quantities are needed for a physical description of the greenhouse climate:

- For the absorption of shortwave irradiation in the various greenhouse components we need the outside shortwave radiation (boundary condition) to be separated in direct and diffuse irradiation (figure 2.1.).
- To determine the longwave radiation exchange between the various components of the greenhouse we need the sky temperature T_{sky} (boundary condition), the outside and inside cover temperature $T_{g,a}$, $T_{g,i}$ respectively, the leaf temperature T_l, the heating pipe temperature T_p (boundary condition) and the soil surface temperature $T_{s,1}$.
- To determine the convection and ventilation heat transfer we need the outside air temperature T_a (boundary condition), the outside and inside cover temperatures $T_{g,a}$,$T_{g,1}$ respectively, the inside air temperature T_i, the leaf temperature T_l, the heating pipe temperature T_p (boundary condition) and the soil surface temperature $T_{s,1}$. Also the air exchange between in- and outside has to be known from the outside wind velocity and direction, the temperature difference between in- and outside and the ventilation arrangement.
- For the mass transfer of water vapour we need the outside air vapour pressure e_a (boundary condition) and the inside air vapour pressure e_i. The va-

pour pressure in the leaf e_1, against the inner side of the cover $e_{g,i}$ and at the soil surface $e_{s,1}$ are found from the respective temperatures, so they are not considered as independent climate quantities.

- For the soil heat flux we need the soil surface temperature $T_{s,1}$ and the gradient of the soil temperature, so the soil temperature at various depths $T_{s,1} \ldots T_{s,n}$ up until the depth where no seasonal variations of the temperature occur (boundary condition).
- The carbon dioxide consumption of the plants at day and the release at night have to be described by a photosynthesis-assimilation-respiration model of the vegetation. This model is typically plant physiological, but for a description of the transport processes we need the outside carbon dioxide concentration $C_{co_2,a}$ (boundary condition) and the inside carbondioxide concentration $C_{co_2,i}$. Also the ventilation should be known as volumetric air exchange in the same way as for the ventilation heat and water vapour transfer. The carbondioxide supply in the greenhouse (e.g. from the exhaust gases of natural gas burners) is a boundary condition for the physical greenhouse climate.

In the survey up to now, no attention has been given to the homogeneity of the greenhouse climate. All phenomena described and all quantities mentioned may be different locally. Vertical as well as horizontal gradients in the various quantities may occur. Vertical gradients for a great deal originate from the vertical circulation pattern and horizontal gradients from the spatial circulation pattern. Horizontally no important gradient would occur if only a vertical circulation pattern were present. But due to leaks in the gables, air is coming in through the gable at the windside and leaving through the gable at the leeside. The effect is strongest at the upper half of the gables due to the wind profile. So an air flow from the windward to the leeward gable is generated in the greenhouse above the canopy. Thereby a circulation flow is induced which leads to a return flow over the soil surface and through the canopy. With low heating pipes, the windward side of the greenhouse will then be warmer than the leeside. The radiative conditions of the leaves are inhomogeneous too. Besides the distinction between sunlit and shaded leaves or part of leaves, the diffuse radiation is extinguished in the canopy. So for the characterization of the greenhouse climate not only the climate quantities itself have to be considered but also the local distribution of these quantities.

3. Air exchange by ventilation

3.1. INTRODUCTION

The exchange between the greenhouse interior and the air outside is a process which affects the greenhouse climate considerably. It has its impact not only on the energy balance and therefore on the air temperature, but also on the balance of the air components and so on the concentration of water vapour, carbondioxide and other gases. For a proper quantification of the climate factors therefore it is necessary to define the ventilation process adequately in terms of factors relevant to it. This is vital, not only in model studies, like the present one, but also in strategies for humidity control (Udink ten Cate, 1983) and in common greenhouse practice, where carbondioxide in the air is considered more and more as a fertilizer (Hey and Schaapendonk, 1983, Schaapendonk and Gaastra, 1983a, b).
In this chapter ventilation is considered as a static phenomenon, dependent on relevant factors like outside wind speed and temperature difference between in- and outside. Due to the fast fluctuations of the wind speed, the instantaneous ventilation will fluctuate too. Considering the static ventilation, we only look at the resulting effective mean air exchange between in- and outside. The fluctuative nature of the air exchange is discussed in the next chapter.

In literature (see section 3.2) and in greenhouse practice, ventilation is commonly characterized by the term ventilation rate, which indicates the amount of air replacement per hour. This term however cannot be applied to compare the ventilation in different greenhouses. With the equivalent air exchange and distint average heights, the ventilation rate will be different. Therefore in this work it is preferred to define the ventilation as the volumetric air flux per unit area of the ventilation window. This quantity can be used to compare the ventilation in different greenhouses with the same type of windows and is suitable for calculation of other quantities like ventilation rate.

The aim in this chapter is to establish a more detailed theoretical model for the ventilation of greenhouses affected by wind and temperature. Experiments with a greenhouse model as well as measurements in compartments of a large multispan greenhouse are carried out to evaluate our theoretical results.

3.2. LITERATURE REVIEW

Though ventilation in greenhouses is an important exchange mechanism, only few publications with quantitative data on this subject are known.
Morris and Neale (1954) reported on ventilation in a small and in a large single-span greenhouse, with both roof and side wall ventilation windows. They applied a tracer gas techniquê, using carbon-dioxyde as tracer gas, and carried out measurements during a whole year. The number of measurements, however was relatively small. As a result they were unable to establish a relationship for ventilation as a function of relevant factors. In their paper no theoretical treatment was given, only some figures representing an order of magnitude of ventilation were presented. Anyhow these data were the first ones ever published in this field. They measured ventilation rates of about 60 h^{-1} at low and 25 h^{-1} at very low wind speed. No numerical explanation about these "low" and "very low" wind speeds is given.
Whittle and Lawrence (1960) also applied a tracer gas technique using hydrogen as tracer gas. They were able to determine a relationship between ventilation rate and wind speed for ventilation through leaks only, in closed small single-span greenhouses. The relation showed a proportional increase of ventilation rate with wind speed. No theoretical consideration was given. The authors also carried out experiments with open windows which gave the same results as those of Morris and Neale: no relationship was developed but an order of magnitude for several situations was given.
Also Okada and Takakura (1973) determined the leakage ventilation of a small greenhouse. They expressed the ventilation per unit glass area since the glass area determines the extent of leakage whereas the volume of the glasshouse is irrelevant in this respect. Also their relation shows a linear proportionality between ventilation flux and wind speed. However their coefficient is about 35% lower than that found by Whittle and Lawrence. Apart from this they also established the dependency of ventilation flux on the temperature difference between in- and outside and found a proportionality with the square root of this temperature difference.

Gudehus (1977) also investigated the air exchange through leaks. He applied a fan to blow air from inside through the openings in the cover to outside and measured the excess pressure and the volume flux. This method was meant to compare the leakage of different greenhouses with a standard technique. Kozai and Sase (1978), Kozai, Sase and Nara (1980) and Sase, Kozai, Nara and Negishi (1980) were the first to present a model approach to greenhouse ventilation. They formulated basic relationships between ventilation rate, window opening, wind pressure and buoyancy for a single opening. The coefficients in these relationships were based in the first report on literature data and in the latter ones on wind tunnel experiments. The relations were applied in a computational scheme, executed on a computer. The ventilation rate was calculated for a single-span or a multi-span (with a maximum of four spans) greenhouse with both roof and side wall ventilation windows. Though the results could not be compared with full scale measurements, their model was the first quantitative approach to ventilation in greenhouses. It gave a very valuable insight in the sensitivity of ventilation to wind speed, window opening and temperature difference between in- and outside.

Also in other types of buildings natural ventilation plays an important role in the indoor climatic conditions. In livestock buildings, houses, schools, offices etc. it is an essential process contributing sensibly to the comfort of living in such a building. In livestock buildings, the natural ventilation mostly takes place through fixed openings and the research is focussed on finding optimal sizes and shapes of these openings (Dybwad et al., 1974, Froehlich, 1975, Edgan and Hellickson, 1978, Abeels, 1981, Freriks, 1981, v.d. Weerdhof, 1982). Generally one finds a linear proportionality between exchange rate and wind velocity. Attempts at decreasing the dependency on wind speed by the use of specially shaped wind screens in front of the opening (Smith and Hazen, 1968, Brandsma, 1977), did not change this tendency forwards a linear relationship.
In domestic buildings natural ventilation with windows closed, (leak) and variable openings, (windows and doors open), is of interest. The most common arrangement is a variable opening in a vertical wall. Ventilation through leaks was already investigated by von Pettenkofer (1858). He introduced the thumb's rule that for good comfort in a room the air has to be refreshed about once per hour. This publication was followed by a large number of pa-

pers on ventilation. Among which some classical ones stating relations between ventilation and relevant factors like outside windspeed and temperature difference between in and outside (Shaw, 1907, Dick, 1950, Georgii, 1954) and some others on more specific items. Brown and Salvason (1962) investigated natural convection through vertical openings in a wall. Later on Shaw (1971) combined this with forced air flow effects through these openings. Hitchin and Wilson (1967) reviewed experimental techniques for the investigation of natural convection in buildings. A simple theoretical model for ventilation through a single opening caused by wind effects was derived and experimentally checked by Cockroft and Robinson (1976). De Gids (1978) presented a junction model to calculate the natural ventilation in buildings. An extended bibliography was given by Ross and Grimsrud (1978).

In most papers a relation between volumetric airflux by ventilation and relevant parameters is given. As a rule this relation is validated by wind tunnel experiments. Warren (1977) reported on ventilation research that has some relation with our work. He investigated ventilation through side-mounted and centre pivoted windows due to wind and temperature effects and presented experimental results both on wind tunnel models and on a full scale model. His problem differs from ours, however, in that the openings in his case were in one vertical wall only, while the ventilation windows in a greenhouse usually are distributed over the roof.

3.3. VENTILATION MECHANISMS

In almost all publications on ventilation (section 3.2.) only empirical relations between ventilation rate and relevant factors have been applied. An exception is the paper of Brown and Solvason (1962) who provided a theoretical consideration of the relation between ventilation rate and temperature difference over the opening.

Okada and Takakura (1973) combined the resistance against flow of an opening with the wind pressure on the wall as driving force to present a general equation for leakage ventilation. They found that leakage ventilation is proportional to the wind velocity and to the square root of the temperature difference between in- and outside.

The same approach was also followed by Kozai, Sase and Nara (1978, 1980) in their study on ventilation through roof and side-wall windows of small greenhouses. They investigated the resistance of the window opening as a function of wind speed and -direction.

In the present investigation ventilation through roof windows of large multi-span greenhouses is explored. In the first part of this section the resistance to flow (flow characteristic) of a window opening is considered as a parameter which is only dependent on the geometry of the opening itself. In this way various opening geometries can be compared. The flow through the opening is caused by a pressure difference over the opening due to wind and temperature effects. This will be discussed in the second part of this section. In the third and concluding part, the results of the first two parts are brought together. The flow characteristic of the opening is linked up with the pressure difference due to wind and temperature effects, so that it is possible to predict the ventilation through differently shaped ventilation windows.

3.3.1. Flow characteristic of an opening

Before we can investigate the flow through the opening of a ventilation window, we should first discuss the characteristic of data available about the rectangular opening (figure 3.1.). Over the opening there is a pressure difference causing a flow through the opening with a mean volume flux ϕ_v, which is the product of the average velocity $\overline{v}$ through the opening and the area A_0 of the opening. The geometry of the opening is defined by its length L_0 and height H_0. As inertial forces amply dominate the viscous forces in this problem the viscosity will be of less importance and the flow is affected by the density ρ of the flowing medium and the shape of the opening only. On account of this it can be expected that for these rectangular openings:

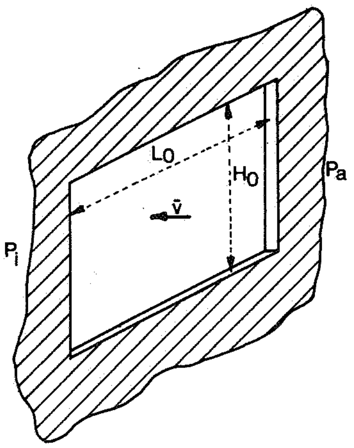

Fig. 3.1. Flow through a rectangular opening.

$$Eu = \frac{\Delta p}{\frac{1}{2}\rho\bar{v}^2} = f(\frac{L_o}{H_o}) = F_o \qquad (3.1)$$

So the Euler number Eu, being defined as the pressure difference over the kinetic energy per unit volume in the opening behaves as a function f of the geometry of the opening only. The function $f(L_o/H_o)$ is called the aspect ratio factor F_o of the opening. If also viscous effects were of importance, the Euler number would be a function of both the geometry and the Reynolds number. Experimental evidence must decide whether the Reynolds number (and so the frictional forces) has any effect.

In the case of ventilation we are mainly interested in the relation between the pressure difference over the opening and the volume flux ϕ_v through the opening. When the area A_o of the opening is substituted. relation 3.1 can be rewritten as:

$$\Delta p = F_o \tfrac{1}{2}\rho(\frac{\phi_v}{A_o})^2 \qquad (3.2)$$

With a ventilation window over the opening, mounted at the upper horizontal edge (fig. 3.2., the above approach can be followed too. For that purpose we introduce the effective opening area A_w of the window opening that is related to the original opening area A_o by a factor f_2 that depends on the opening angle ζ. Also the aspect ratio of the effective opening will vary with the opening angle, from a high ratio at small opening angles to the ratio L_o/H_o of the original opening at large opening angles. Consequently also the aspect ratio factor F_w of the effective opening is dependent on the opening angle ζ. In order to relate the area A_w and the aspect ratio F_w of the effective opening to the values A_o and F_o of the original opening without window we can state that:

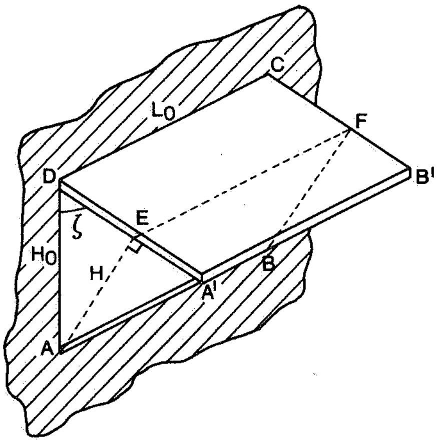

Fig. 3.2. Ventilation window over an opening.

$$F_w = F_o\ f_1(\zeta) \qquad (3.3a)$$

$$A_w = A_o\ f_2(\zeta) \qquad (3.3b)$$

with $f_1(\zeta)$ and $f_2(\zeta)$ functions of the opening angle.

The relation 3.2 is transformed into:

$$\Delta p = \frac{F_o}{f_w(\zeta)} \tfrac{1}{2}\rho\left(\frac{\phi_v}{A_o}\right)^2 \qquad (3.4)$$

with $f_w(\zeta) = (f_2(\zeta))^2/f_1(\zeta)$ (3.5)

The window function $f_w(\zeta)$ combines the two functions $f_1(\zeta)$ and $f_2(\zeta)$ and will have values between 1 at full and o at perfectly closed opening.

For a prediction of the function $f_1(\zeta)$ the aspects ratio factor's dependency on the aspect ratio and the aspect ratio's dependency on the opening angle have to be determined first. The second dependency could be estimated by stating that the effective opening area is more or less equal to the area AEFB in figure 3.2. Then the aspect ratio of the opening is H/L_o and thus equals $H_o \sin\zeta/L_o$. The first dependency however cannot be determined a priori.
For the function $f_2(\zeta)$ some estimations could be made. If the effective area were represented by the area AEFB (figure 3.2) then a very simple function for $f_2(\zeta)$ could be found

$$f_2(\zeta) = H_o \sin\zeta \; L_o/H_o L_o = \sin\zeta \qquad (3.6a)$$

The side areas DAE and CBF however will enlarge the effective area. If exactly these areas are added to the area AEFB then

$$f_2(\zeta) = \sin\,(1 + \frac{H_o}{L_o}\cos\zeta) \qquad (3.6.b)$$

However, some correction has to be made on the contribution of the side areas. It is obvious that the flow through the side areas is reduced by the flow through the front area (or vice versa). As a matter of fact $f_2(\zeta)$ cannot be larger than 1. So the term $H_o \cos\zeta/L_o$ in relation 3.6b needs special attention when experimental results will be evaluated.
After experimental results were available (section 3.4.2a) the following model was derived for the side area effect: If the side areas AED and BFC were closed (figure 3.2), air would pass through the effective exchange are ABFE.

If now the side areas are opened, some air, originally passing through the front area, will then pass through the side areas. However, this does not increase the effectiveness of the total area. Only that part of the side areas through which extra air is flowing, will increase the total exchange area. A very simple assumption for this shielding off of the side areas may be that the air flowing through the front area covers the areas AA'E and BB'F (figure 3.3) and that these parts of the side areas have a more or less circular shape with A and B as central points. The area of these circle sections can be substracted from the side areas. When the opening angle ζ increases, the area of the circular sections increases too and they cover the whole side area for $\zeta = 90^0$. In this way a correction on the side is made which depends on ζ. If the area of the circular section is substracted from the side area, relation 3.6b is transformed into:

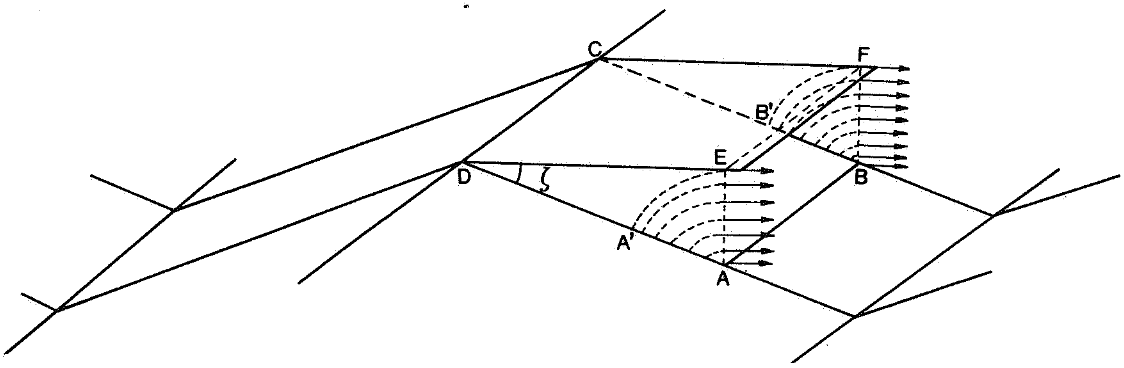

Fig. 3.3. Model to describe the effect of the side areas.

$$f_2(\zeta) = \sin\zeta\{1 + a \frac{H_0}{L_0}(\cos\zeta - b2\pi(\frac{90-\zeta}{360})\sin\zeta)\} \qquad (3.6.c)$$

where a and b are arbitrary constants to incorporate a correction on the shielding effect.

3.3.2. Driving forces for ventilation

3.3.2.a. Wind effects

The interaction of wind with a rough surface or with an object like a building will result in a very complex flow pattern. It can be characterized however in a very general way. At the up-wind side of an obstacle, like a building, the static pressure will be higher than the barometer pressure, whereas at the lee-side a wake is formed which results in general in a static pressure lower than the barometer pressure. Around an object the different positive and negative time average pressures (relative to barometric pressure) will result in a pressure distribution. This distribution is mostly experimentally determined on scale models in a wind tunnel.
The static pressure due to wind effects p_u is related to the mean wind speed $\overline{u}$ at reference level by defining a dimensionless pressure coefficient K_p:

$$p_u = K_p \tfrac{1}{2} \rho_a \overline{u}^2 \qquad (3.7)$$

ρ_a being the external (ambient) air density.
The pressure distribution around an abject then may be represented as a distribution of pressure coefficients. Turning to our specific problem of flow through an opening, we notice that in this static approach there will be an inward flow through an opening in the wall (or roof) if a positive coefficient K_p is found. If, on the contrary, K_p is negative the flow will be outward. This in- and outflow will be constant and the approach seems reasonable when different openings are located at places with different pressure coefficients. In greenhouses this is only applicable when the constructions are relatively small or when they have openings in both the side walls and the roof (Kozai, Nara and Sase, 1978, 1980).
Allmost all of the Dutch greenhouses, however, are built as large multispan blocks, surrounded by other greenhouses. Moreover their side walls are thermally insulated with the result that these are practically sealed. The ventilation openings are all situated in the roof and under normal weather conditions only the windows at the lee-side are opened. Due to the fact that the pressure distribution is identical around each span of a large block, the pressure coefficient K_p is the same at each opening so it would result in no

ventilation at all. So the static approach is not suited to explain the ventilation of a large greenhouse.

We have to keep in mind, however, that wind speed is not a static quantity, but varies continuously. This results in pressure fluctuations. So, if the mean pressure is the same at the outside of two distinct openings, the momentary pressure still may be different. This gives rise to momentary pressure differences outside different openings or a fluctuating pressure difference over one opening. Then the amplitude of these fluctuations $\tilde{p}_u$ is the driving force for ventilation. Analogously to the definition of the pressure coefficient K_p(rel.3.7) we define a pressure fluctuation coefficient K_f:

$$\tilde{p}_u = K_f.\tfrac{1}{2}\rho_a\tilde{u}^2 \tag{3.8}$$

So,similar to relation 3.7 the driving force for ventilation is stated to be proportional to the volumetric mean kinetic energy of the wind. It is not known a priori if K_f will be constant for the normal windspeed range. This can only be concluded from experiments. In this approach there is only one value of the coefficient for all different openings in the roof. This facilitates obtainment of one relation for the exchange through all window openings. There is still another factor which has to be mentioned in connection with relation 3.8. In the coefficient K_f the translation of the wind speed at reference level to the wind speed near the opening is incorporated. This local wind speed is affected by the open window itself, so it can be expected that K_f is affected by the open window. So in general K_f is a function of the opening angle ζ and we can incorporate this by writing $K_f(\zeta)$.

3.3.2.b. Temperature effects

An enclosed space is observed in which the air temperature T_i and the air density ρ_i are uniform. The hydrostatic pressure p_h in this enclosure varies with height z, according to:

$$p_h = p_r - \int_{z_r}^{h}\rho_i g dz \tag{3.9a}$$

with p_r pressure at reference level z_r
g gravitational acceleration

Also the hydrostatic pressure outside the enclosure, where the temperature T_a and density ρ_a are uniform, varies with height z, similar to relation 3.9a:

$$p_h = p_r - \int_{z_r}^{h} \rho_a g dz \qquad (3.9b)$$

So, as a rule, the hydrostatic pressure differs at the same level in- and outside the enclosure due to the difference in air density. If there is an opening in the enclosure, we may expect the pressure difference at each level in the opening to act as a driving force for air exchange between in- and outside. Some different opening geometries will be discussed now

- *one vertical opening in the enclosure*:

  In a greenhouse this would be one opening in the side walls or one vertical opening in the roof (or possible more identical vertical openings at the same height). As can be seen from figure 3.4 the front opening under a ventilation window in the roof can be regarded as a vertical opening and the side areas of this window as well. The pressure difference in the opening at each level between in and outside due to the density difference can be calculated if the variation of the hydrostatic pressure in- and outside is taken into account (fig. 3.5). According to Brown and Solvason (1962) the reference level is in the middle of the opening where the in- and outside pressure will be the same due to the fact that at this level no exchange occurs (in- and outflow are the same so each takes one half of the opening). For an outside density higher than the inside density (inside temperature higher than outside) and if both are homogeneous, the variation of the hydrostatic pressure inside and outside is given in figure 3.5. The driving force for the flow at each level is given by the pressure difference between in- and outside. So from relation 3.9:

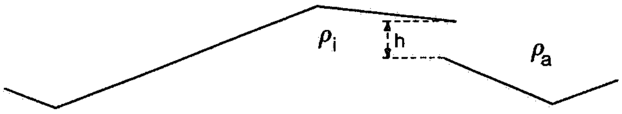

Fig. 3.4. Opening under a ventilation window in the roof.

$$p_i - p_a = -(\rho_i - \rho_a)gz \qquad (3.10)$$

For the lower half of the opening the outside pressure p_a is higher than the inside pressure p_i at each level and thus gives rise to an inflow. In the upper half p_i is higher at each level, so there an outflow takes place. As a result the colder outside air penetrates the enclosure through the lower half of the opening while the warmer inside air leaves through the upper half.

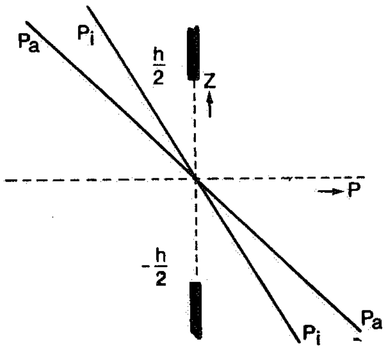

Fig. 3.5. Variation of the hydrostatic pressure with height at two sides of a vertical opening.

- *two equal vertical openings*

This situation occurs in a greenhouse if the ventilation windows in a side wall and the ventilation windows in the roof are opened and if their openings have equal heights. In figure 3.6 the variation of the hydrostatic pressure is given for this situation. This follows from figure 3.5 where the central part of the opening is covered symmetrically. Due to the symmetry, the reference level will still be in the centre and the variation of the hydrostatic pressure in- and outside will remain the same. So, relation 3.10 still holds true. This is also in agreement with the empirical fact that with higher outside density, i.e. lower outside temperature, the inflow is through the lower and the outflow through the higher opening.

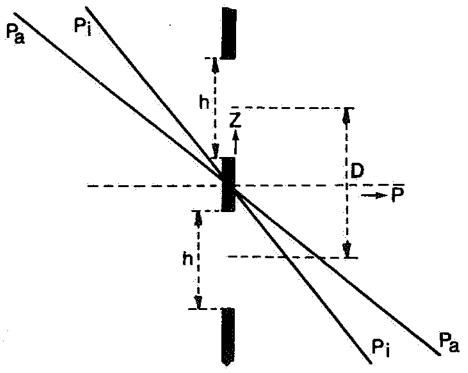

Fig. 3.6. Two vertical equal openings in an enclosure.

- *two unequal vertical openings*

This is a more general situation in a greenhouse because the side wall windows and roof windows do not always have the same height. Due to the continuity equation the inflow through the lower and the outflow through the upper opening have to be equal. When the lower opening is the smaller one (figure 3.7) the pressure difference over this opening has to be larger at each level to induce the same total flow over the opening. This means that the reference level is nearer the higher opening. The exact position can be found if a relation for the flow through the opening is derived first (section 3.3.3).

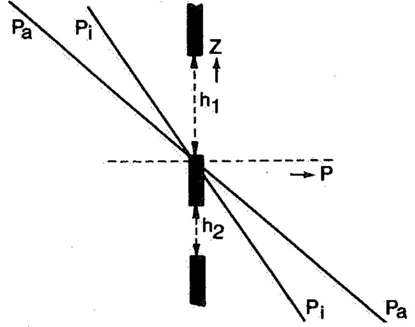

Fig. 3.7. Two unequal vertical openings in an enclosure.

3.3.3. *Resulting ventilation*

3.3.3.a. *Ventilation due to wind effects*

The driving force due to wind effects, as given by relation 3.8 can be combined with the resistance of the opening, defined by the flow characteristic (relation 3.4) of the window opening. If we take into account that half of the total exchange area can be made available for the inflow and the other half for the outflow, then the above results in:

$$K_f(\zeta)\tfrac{1}{2}\rho_a\bar{u}^2 = \frac{F_o}{f_w(\zeta)}\tfrac{1}{2}\bar{\rho}\left(\frac{\phi_v}{\tfrac{1}{2}A_o}\right)^2 \tag{3.11}$$

$$\text{so:}\quad \frac{\phi_v}{\bar{u}} = \tfrac{1}{2}A_o\sqrt{\frac{K_f(\zeta)f_w(\zeta)\rho_a}{F_o\bar{\rho}}} = A_oG(\zeta) \tag{3.12}$$

Relation 3.12 states that for any opening angle of the ventilation window, the air flow is linearly proportional to the wind speed, while the proportionality factor varies with the opening angle according to a function $G(\zeta)$. This function $G(\zeta)$ contains a combination of different window parameters, some of which are a function of the opening angle. The parameters $F_o, f_w(\zeta)$ can be determined experimentally by separate experiments. It will be very difficult to determine the pressure fluctuation coefficient $K_f(\zeta)$ because this coefficient not only defines how the pressure fluctuations near the window depend on the wind speed at reference level, but also how effectively these pressure fluctuations generate a mean ventilation flux. So it seems a better way to determine the ventilation flux at various wind speeds and to calculate the pressure fluctuation coefficient from the ventilation flux and the window parameters. This can be used then to determine the ventilation for other window geometries with known window parameters.

3.3.3.b. Ventilation due to temperature effects

The driving force for air exchange as given by relation 3.10, is a function of the height relative to the reference level. So at any height a flow is generated according to a combination of the driving force and the flow characteristic of the window. For the most simple case of one opening in a vertical wall this results in:

$$-(\rho_i - \rho_a)gz = F_0 \tfrac{1}{2}\rho v_z^2 \qquad (3.13a)$$

As we neglected friction effects for the flow through an opening, F_0 has the same value for any z.

The density difference can be expressed in the temperature difference between in- and outside:

$$-(\rho_i - \rho_a) = \rho\beta(T_i - T_a) = \rho\beta\Delta T \qquad (3.13b)$$

with β the thermal expansion coefficient

$$\text{so then: } v_z = \left(\frac{2g\beta\Delta T}{F_0}\right)^{\frac{1}{2}} |z|^{\frac{1}{2}} = m|z|^{\frac{1}{2}} \qquad (3.13c)$$

By calculating v_z from the kinetic energy, no information on the direction of v_z is available in relation 3.13c. This information was already given by relation 3.10. There it was already mentioned that the flow through the upper half is outward and through the lower half inward when the inside air has a higher temperature than the outside air. The volume flux ϕ_v through the opening with length L and height h can be found by integration of relation 3.13c over the upper or the lower half of the opening.

The flux through the upper half is:

$$\phi_{v,1} = \int_{0}^{\frac{1}{2}h} m\, L|z|^{\frac{1}{2}} dz \qquad (3.14a)$$

and the flux through the lower half:

$$\phi_{v,2} = \int_{-\frac{1}{2}h}^{0} m\, L|z|^{\frac{1}{2}} dz \qquad (3.14b)$$

so $$\phi_{v,1} = \frac{L}{3\sqrt{2}} m h^{3/2} = \frac{L}{3}\left(\frac{g\beta\Delta T}{F_o}\right)^{\frac{1}{2}} h^{3/2} \qquad (3.15a)$$

It was mentioned already that the flow through the upper half is outward. The flux through the lower half is:

$$\phi_{v,2} = -\frac{L}{3\sqrt{2}} m h^{3/2} = -\phi_{v,1} \qquad (3.15b)$$

Consequently this flow is inward.

Relations 3.15 define the ventilation of a greenhouse through the roof- or side-windows due to temperature effects only. The height h of the roof window opening is a function of the opening angle ζ (figure 3.8) according to

$$h = H_o\{\sin\psi - \sin(\psi - \zeta)\} \qquad (3.16)$$

with a maximum height of $H_o \sin\psi$ when the opening angle ζ equals the roof angle ψ (horizontal position of the window).

Special attention has to be paid to the effect of the ventilation through the side area (triangle ACD in figure 3.8). Especially at small opening

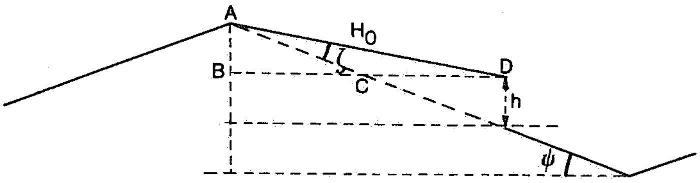

Fig. 3.8. Height of the opening of a roof window

angles this side area can be expected to have some effect because the height in the side area then is largest. An estimation of the ventilation flux both through the front area (relations 3.15 and 3.16) and that through the side areas can make clear how they compare. The triangle ACD has a base with length CD equal to $H_0 \sin\zeta/\sin\psi$ and a height AB equal to $H_0 \sin(\psi - \zeta)$ (fig.3.8). Over this triangle there is a density difference between in an outside. To calculate the pressure difference between in- and outside at each level in the triangle a reference level has to be chosen. Without any vertical symmetry in the triangle the reference level has to be chosen at an arbitrary level (figure 3.9), that will be defined later. Then the relation 3.14a and b can be applied with adapted boundary conditions. This leads to the following expressions:

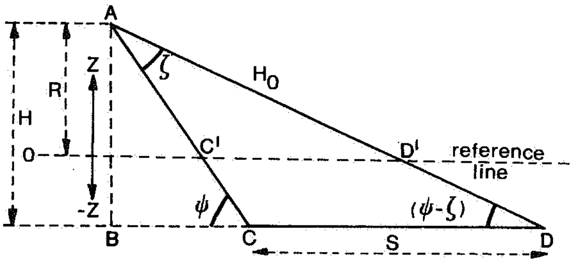

Fig. 3.9. Reference level in side area

The flux through the area above the reference level is:

$$\phi_{v,1} = \int_{o}^{R} ml|z|^{\frac{1}{2}} dz \tag{3.17a}$$

and below the reference level:

$$\phi_{v,2} = \int_{-(H-R)}^{o} ml|z|^{\frac{1}{2}} dz \tag{3.17b}$$

In these equations l is the length of the base at height z. This length is dependent on z, according to:

$$l = \frac{S}{H}(R - |z|), \ (z >= o) \tag{3.18a}$$

and $l = \frac{S}{H}(R + |z|), \ (z < o)$ (3.18b)

Combination of relations 3.17a and 3.18a results in

$$\phi_{v,1} = \int_{o}^{R} m\frac{S}{H}(R - |z|)|z|^{\frac{1}{2}} dz =$$

$$= \frac{4mSR^{5/2}}{15H} \qquad (3.19a)$$

and $$\phi_{v,2} = - \int_{o}^{-(H-R)} m\frac{S}{H}(R + |z|)|z|^{\frac{1}{2}} dz =$$

$$= - m\frac{B}{H}[\frac{2}{3}R(H-R)^{3/2} + \frac{2}{5}(H - R)]^{5/2} \qquad (3.19b)$$

The reference level is some part of H so

$$R = aH \qquad (3.20)$$

Due to the continuity equation:

$$\phi_{v,1} + \phi_{v,2} = o \qquad (3.21)$$

Combination of relations 3.19a, 3.19b, 3.20 and 3.21 yields:

$$\frac{4}{15}a^{5/2} - \frac{2}{3}a(1-a)^{3/2} - \frac{2}{5}(1-a)^{5/2} = 0 \qquad (3.22)$$

The solution of a can be obtained numerically and appears to be:

$$a = 0.6843$$

This means that the area above the reference line is smaller than that under this line due to the fact that the height above the line is greater.
The in- and outflux can be calculated according to relations 3.19 and 3.20

with $B = H_o \sin\zeta/\sin\psi$ and $H = H_o\sin(\psi - \zeta)$.

Then: $$\phi_{v,1} = 0.1033\ m\ \frac{\sin\zeta}{\sin\psi}.(\sin(\psi - \zeta))^{3/2}\ H_o^{5/2} \qquad (3.23)$$

Now the flow through the front area under the ventilation window can be compared with the flow through the two side areas:

$$\frac{\phi_{v,side}}{\phi_{v,front}} = 0.6198\,\frac{H_o}{L_o}\left\{\frac{\sin(\psi-\zeta)}{\sin\psi-\sin(\psi-\zeta)}\right\}^{3/2}\left(\frac{\sin\zeta}{\sin\psi}\right) \qquad (3.24)$$

The ratio of both fluxes is linearly proportional to the inverse aspect ratio of the window and to some complex intricate function of the opening angle ζ. In figure 3.10 the ratio of the fluxes as a function of the opening angle ζ is given for a window with aspect ratio equal to 1 and a roof angle of 26^o (Venlo type greenhouse). As was expected the flux from the side areas is dominant for small openings: its importance however decreases very fast for larger openings. So this side area flux only has to be considered for opening angles smaller than about 10 degrees. When the flow through the front area affects the flow through the side areas, the effect of the side areas is even smaller.

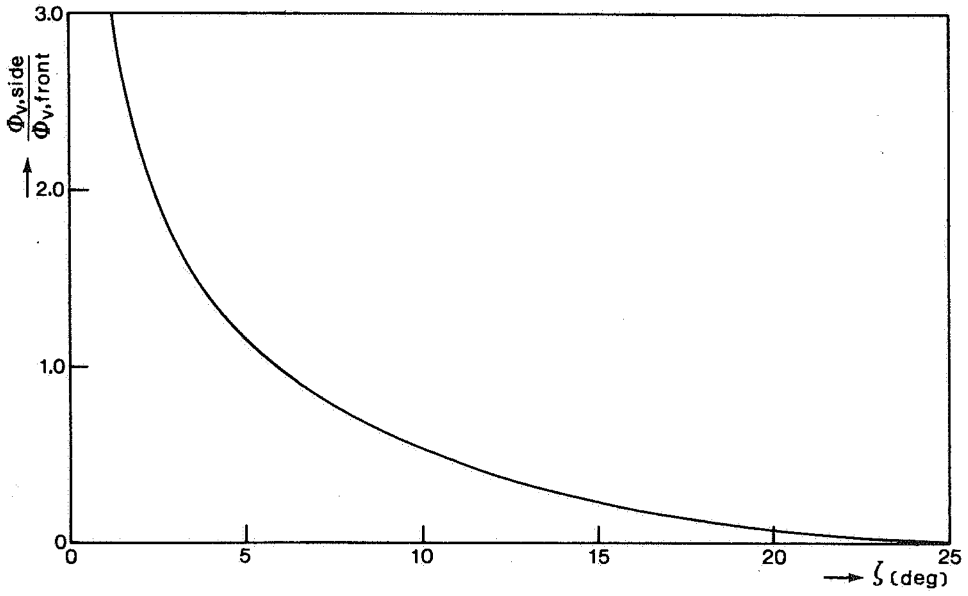

Fig. 3.10. Ratio of fluxes due to the temperature effect through side and front area of windows with aspect ratio 1 as function of opening angle ζ of the window.

a preliminary arbitrary reference level has to be chosen that will be fixed later. The roof window is open from z_1 to $z_1 + h$, and the side wall window from $-z_2$ to $-(z_2 + h_2)$. According to relations 3.14a and b the flux through the lower and upper window are respectively:

$$\phi_{v,2} = \int_{-(z_2+h_2)}^{-z_2} mL_2|z|^{\frac{1}{2}} dz \qquad (3.27a)$$

and
$$\phi_{v,1} = \int_{z_1}^{z_1+h_1} mL_1|z|dz \qquad (3.27b)$$

resulting in:

$$\phi_{v,2} = \frac{-2\ L_2}{3} m\{(z_2 + h_2)^{3/2} - (z_2)^{3/2}\} \qquad (3.28a)$$

and
$$\phi_{v,1} = \frac{2L_1}{3} m\{(z_1 + h_1)^{3/2} -(z_1)^{3/2}\} \qquad (3.28b)$$

z_1 and z_2 can be expressed in terms of each other i.e.:

$$z_2 = D - (z_1 + \tfrac{1}{2}h_1 + \tfrac{1}{2}h_2) \qquad (3.29)$$

together with the continuity equation ($\phi_{v,1} + \phi_{v,2} = 0$) this results in:

$$L_1\{(z_1 + h_1)^{3/2} - z_1^{3/2}\} = L_2\{(D - (z_1 + \tfrac{1}{2}h_1 - \tfrac{1}{2}h_2))^{3/2} - (D - (z_1 + \tfrac{1}{2}h_1 + \tfrac{1}{2}h_2))^{3/2}\} \qquad (3.30)$$

as a relation which defines the position of the reference level z_1 as a function of the geometrical factors (L_1, L_2, D, h_1, h_2). So for every arrangement of openings the position of the reference level can be calculated and thereby the ventilation flux according to relation 3.28.

3.3.4. Comparison of ventilation phenomena due to wind or temperature effects

To estimate under what kind of circumstances the ventilation will be mainly

For two identical vertical openings with vertical distance D (figure 36) the integration of relation 3.13c has to be performed between the boundaries $z = \frac{1}{2}(D - h)$ and $\frac{1}{2}(D + h)$. This results in:

$$\phi_{v,1} = \frac{L_o}{3}\left(\frac{g\beta\Delta T}{F_o}\right)^{\frac{1}{2}}\{(D + h)^{3/2} - (D - h)^{3/2}\} \qquad (3.25a)$$

If D>>h we may approximate:

$$\frac{1}{3}\{(D + h)^{3/2} - (D - h)^{3/2}\} = hD^{\frac{1}{2}} \qquad (3.25b)$$

So then:

$$\phi_v = \left(\frac{g\beta\Delta T}{F_o}\right)^{\frac{1}{2}} A.D^{\frac{1}{2}}\} \qquad (3.26)$$

The relation 3.26 with A: area of the opening $(hL_o)(m^2)$ is also valid for the exchange through two horizontal openings in the enclosure at a vertical distance D and an area A (Chimney effect). For the vertical openings, the integration over the openings results in relation 3.25a. The effect of the height of the openings decreases, however, when D>>h.

In a greenhouse the side wall windows can be opened in addition to the roof windows. In that case (summer conditions) the roof windows are completely opened. In general the two heights of both windows are not equal and the same holds for the lengths. In that case (fiqure 3.11), just as was earlier done

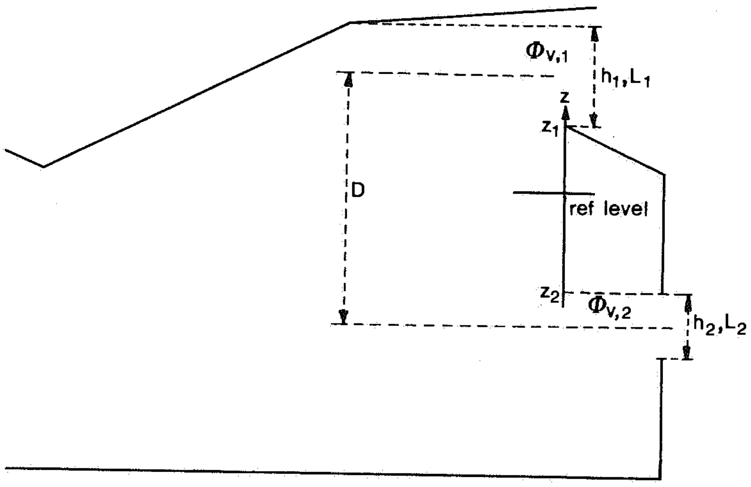

Fig. 3.11. Ventilation due to the temperature effect through roof and side wall windows of unequal height.

due to wind or temperature effects, a comparison of the ventilation fluxes will be made with windows completely open.

According to relation 3.12 with $f_w(\zeta) = 1$ and the difference between the outside and mean air density being neglected the ventilation due to wind effects through one window opening is:

$$\phi_{v,u} = \tfrac{1}{2}L_oH_o\left(\frac{K_f(\zeta)}{F_o}\right)^{\frac{1}{2}}\bar{u} \qquad (3.31)$$

and ventilation due to temperature effects (relations 3.15 and 3.16):

$$\phi_{v,T} = \frac{L_oH_o^{3/2}}{3}\left(\frac{g\beta}{F_o}\right)^{\frac{1}{2}}(\sin\psi)^{3/2}(\Delta T)^{\frac{1}{2}} \qquad (3.32)$$

The ratio of both ventilation fluxes is:

$$\frac{\phi_{v,u}}{\phi_{v,T}} = \frac{3}{2}\left(\frac{K_f(\zeta)}{g\beta}\right)^{\frac{1}{2}} \cdot \frac{1}{H_o^{\frac{1}{2}}(\sin\psi)^{3/2}} \cdot \frac{\bar{u}}{(\Delta T)^{\frac{1}{2}}} \qquad (3.33)$$

For a Venlo type greenhouse $\psi = 26$ and H_o is 0.8m for a common type of ventilation window. When we tentatively estimate $K_u(\psi)$ to be 0.01, while $g = 10\ ms^{-2}$ and $\beta = 3.6.10^{-3}K^{-1}$, we get

$$\frac{\phi_{v_1u}}{\phi_{v_1T}} = 3\,\frac{u}{(\Delta T)^{\frac{1}{2}}} \qquad (3.34)$$

The factor 3 is expressed in S.I. units, i.e. $K^{\frac{1}{2}}s.m^{-1}$.

So the ventilation due to wind effects will be dominant if:

$$3u > (\Delta T)^{\frac{1}{2}} \qquad (3.35)$$

An extreme value for the temperature difference between in- and outside the greenhouse is about 25 K. In this extreme situation the wind speed has to be higher than 1.67 ms^{-1} for a dominancy of the wind effect. The conclusion may be drawn that the ventilation due to temperature effects will be of importance at low wind speeds only.

The temperature effect is increasing with the square root of the temperature difference, while the wind effect is linearly proportional to wind speed. So with increasing wind speed the influence of the wind effect will increase very fast compared with that of the temperature effect; consequently the latter one can be neglected. Another effect still strengthens this conclusion. For increasing wind speed namely, the temperature difference will necessarily decrease as a consequence of increasing ventilation. Of course also the reverse is true: at low wind speed the wind effect decreases rapidly and the temperature effect will become dominant.

3.4. EXPERIMENTS

3.4.1. Experimental set up

In this section the experiments in real greenhouses as in scale models are described. The results are summarized and discussed in section 3.4.2.

3.4.1.a. Flow characteristic of a window opening

The flow characteristic, as defined by the relations 3.2 to 3.5 was to be determined for different opening geometries. If this would be done in a full scale greenhouse one would have to measure the very small pressure differences over the window opening as they occur at the current fluxes in a realistic environment. Under these conditions all kinds of disturbing pressure fluctuations due to wind and temperature effects may be expected. Therefore we did the experiments on scale models of window openings applying different values of the scale factor N to check the validity of the upscaling. The window openings were mounted on a model of a Venlo type greenhouse with the same scale factor. In this way we also avoid differences in the geometries of the model and the full scale enclosure.

In the experiment air was blown through the opening from inside to outside or in the opposite direction. For various flow velocities, the air volume flux and the pressure difference over the opening were measured. Air was brought into or sucked from the model via the floor, that was constructed as a perforated plate to improve the uniformity of the flow in the enclosure. The flux was chosen in such way that the flow through the model opening was similar to that through the full scale greenhouse opening. To obtain this the values of the Reynolds number in the model opening were taken as identical to those in the real glasshouse when the ventilation flux varies between low and high values.

3.4.1.b. Full scale ventilation

In agreement with section 3.3.3.a. we measured the full scale ventilation in a greenhouse applying CO_2 as a tracer gas and using the equilibrium concentration method (Hitchin and Wilson, 1967). The experiments were performed in the Naaldwijk multifactoral glasshouse situated at the Horticultural Experiment Station, Naaldwijk, The Netherlands. This glasshouse (Venlo type) contains 24 identical compartments (figure 3.12). A computer system controls the climate in each individual compartment and datalogs the in- and outside climate factors. An extensive description of the facilities is given by Van de Vooren and Koppe (1975) and Van de Vooren (1979).
Simultaneous measurements in seven compartments were carried out during three periods of about three weeks each. These compartments were selected in the block in such a way that the wind, when blowing from the West, approached them after having passed at least 16 spans. Only the windows in the leeward side of the roof were opened. No crop was present in the compartments. The

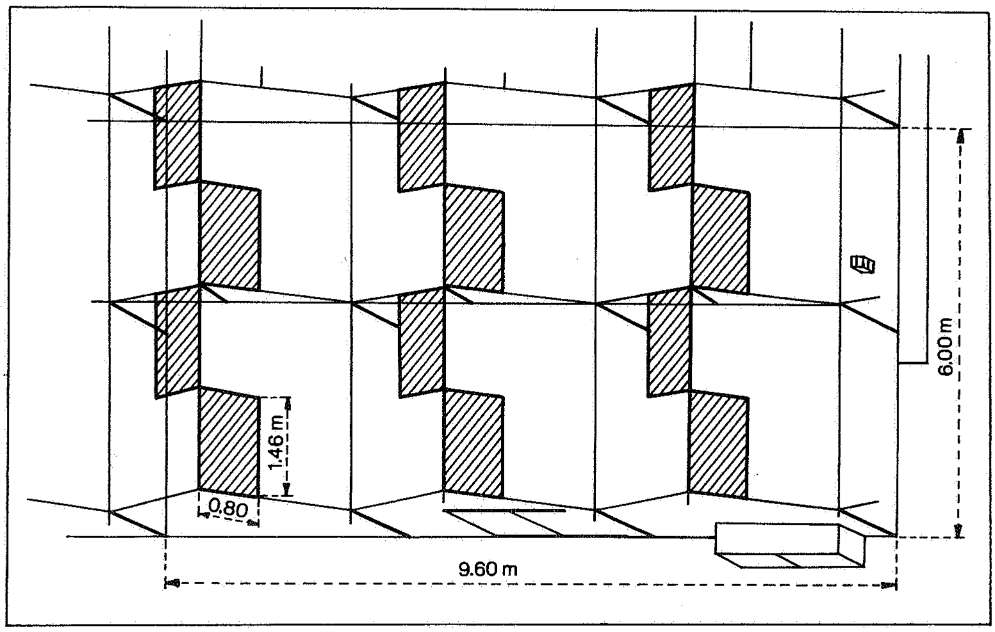

Fig. 3.12. Greenhouse compartment of the Naaldwijk complex in which the measurements were carried out.

tracer gas was distributed at soil level by a perforated tube system, the tubes were oriented parallel to the ridge at an equidistance of 1.6 m. CO_2 exchange with the soil was prevented by covering the soil with plastic sheet. Gas exchange through the side walls was prevented by sealing these walls in a gastight way.

The ventilation flux ϕ_v can be calculated from the CO_2 balance over the compartment, according to:

$$V\frac{dc_i}{dt} = \phi_v(c_i - c_a) + \phi_m \tag{3.36}$$

with V volume of the compartment - (m^3)
c CO_2 concentration (kgm^{-3})
and ϕ_m the influx of distributed CO_2 (kgs^{-1})

In the equilibrium concentration method, a stable situation has to occur without variation in carbondioxide concentration, so $dc_i/dt = o$. The ventilation flux can be calculated from the measured concentration difference between in- and outside and the influx of distributed CO_2 according to:

$$\phi_v = \phi_m/(c_i - c_a) \tag{3.37}$$

The advantage of this method is that uncertainties in the effective glasshouse volume do not count. Though relation 3.36 is based on a perfect mixing of the inside air, yet presumably there are some stagnant pockets of air in the compartment, particularly in the corners. This does not effect the results of the equilibrium concentration method. A disadvantage is that one has to wait for an equilibrium situation. When the ventilation fluxes are low, so the time constant τ (= $/\phi_v$) is large, the environmental factors like wind speed, have to remain constant for a long period. However, these factors can be averaged over a long period too. The averaging time was taken as about 1/3 to 1/2 of the estimated τ and the constant period had to be about 2 to 3 times τ. The amount of distributed pure CO_2 was measured by a rotameter while the in- and outside CO_2 concentrations were measured by infra-red gas analysers. The outputs of the analysers were logged by the central computer system, together with all relevant in- and outside climate conditions and the aperture of the window opening in the various compartments. In six compartments the CO_2 concentration was measured at one position in the centre of the space, while in the seventh compartment the CO_2 concentration was measured at seven different positions distributed evenly in the compartment. In this way we could check whether a perfect mixing of the inside air actually does take place.

3.4.2. Experimental results

3.4.2.a. Flow characteristic of a window opening

In the first set of measurements we determined the aspect ratio factor F_0 of a rectangular opening, as defined by relation 3.1. So for a number of aspect ratios (L_0/H_0), F_0 was measured according to section 3.4.1.a. as the slope of the Δp, $\frac{1}{2}\rho\bar{v}^2$ graph (relation 3.1). In figure 3.13 two of these graphs are given. The proportionality appeared to be linear in all cases. From this proportionality the conclusion can be drawn that for any aspect ratio the factor F_0 is constant, so the Euler number is not dependent on the Reynolds number but on the aspect ratio only. This is in perfect agreement with our assumption

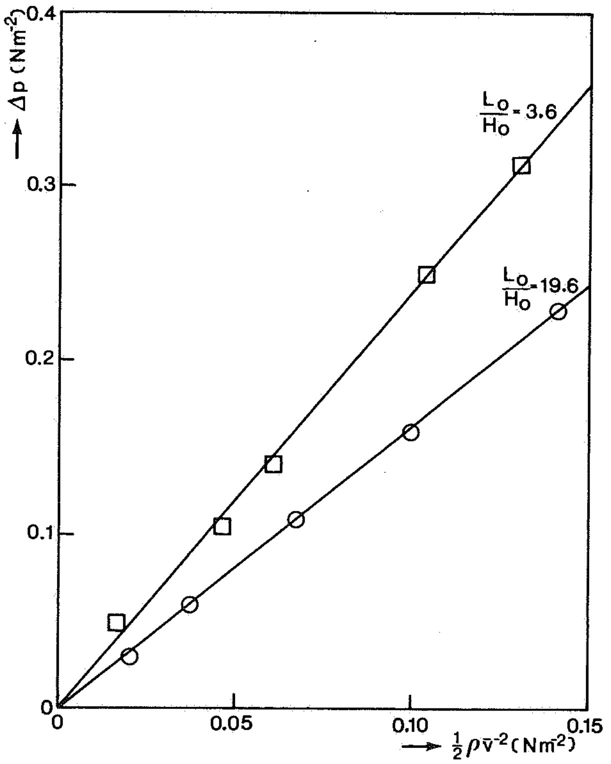

Fig. 3.13. Pressure difference over a rectangular opening as a function of the volumetric kinetic energy in the opening for two aspect ratios.

in section 3.3.1.

In figure 3.14 all measured factors F_0 are given as function of the aspect ratio L_0/H_0. They are ranging from 2.45 to 1.75 at small and large aspect ratios respectively and their course appears to be approximately exponential in between.

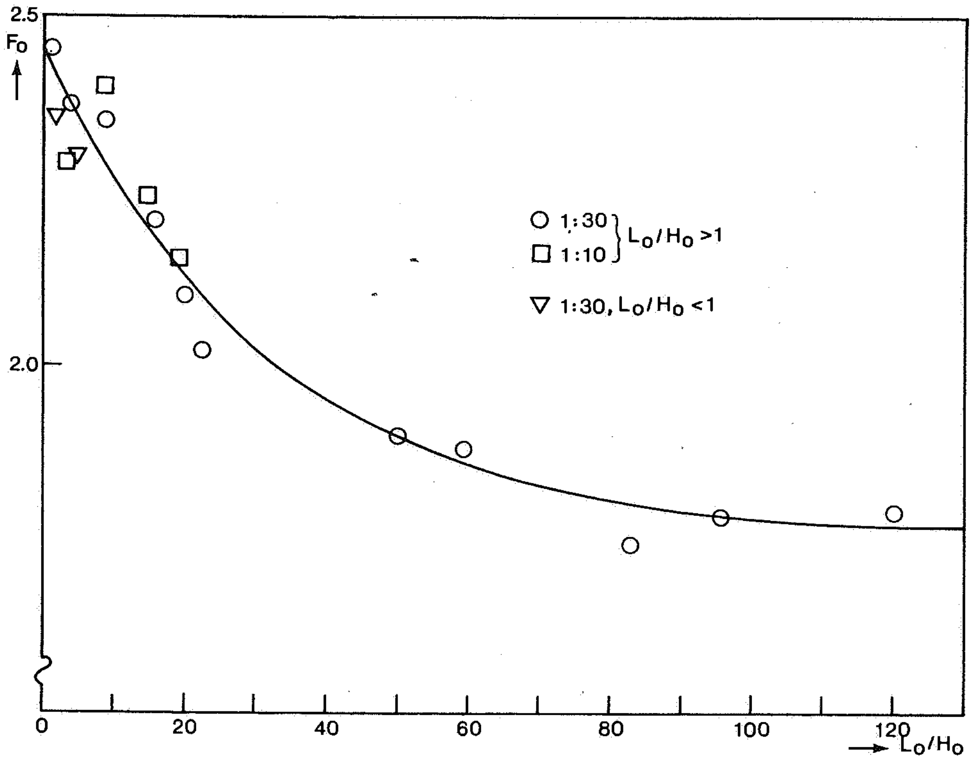

Fig. 3.14. Aspect ratio factor for a rectangular opening.
Full curve represents eq. 3.38.

The following function fits the measuring points in a satisfactory way:

$$F_0 = 1.75 + 0.7 \exp(-(L_0/H_0)/32.5) \qquad (3.38a)$$

for $L_0/H_0 > 1$.

This relation is represented in figure 3.11 as a full curve. For $L_0/H_0 < 1$, L_0 is no longer the larger dimension. Since it can be expected that $F_0 = f(L_0/H_0)$ is symmetrical with respect to $L_0/H_0 = 1$, for the region $L_0/H_0 < 1$ relation 3.38a will remain valid if only for L_0/H_0, the inverse is substituted:

$$F_0 = 1.75 + 0.7 \exp(-H_0/L_0)/32.5) \qquad (3.38b)$$

for $L_0/H_0 < 1$

Some experiments in this region (Δ in figure 3.14) seem to confirm this conclusion. Most of the experiments shown in figure 3.14 are performed in a model with scale factor 30. Also some measurements in the same L/H region are carried out in a model with scale factor 10. Though in the latter case the scatter of the measuring points is larger, due to the fact that the pressure differences over larger openings are smaller and therefore the pressure measurements less accurate, the points still fit in with relation 3.38. So from the similarity of the results of the two differently scaled models we may conclude that they will also be similar to the flow through the full scale opening.

In the second set of measurements we determined the characteristics of top mounted window openings with varying opening angle, as defined by the relations 3.3, 3.4 and 3.5. The window opening function $f_w(\zeta)$ then is (relation 3.4):

$$f_w(\zeta) = \frac{1}{2} \frac{\rho F_0 \phi_v^2}{A_0^2 \Delta p} \qquad (3.39)$$

in which F_0 and A_0 are the aspect ratio coefficient and the area of the rectangular opening without window respectively . $f_w(\zeta)$ is a combination of a function $f_1(\zeta)$ defining the ratio of the aspect ratios of the window opening F_w and the rectangular opening without F_0 (relation 3.3.a) and a function $f_2(\zeta)$, defining the ratio of the effective exchange area of the window opening A_w and the area of the rectangular opening without window A_0 (relation 3.3.b). By these definitions both of these quantities have a value of 1 at full opening ($\zeta = 90^0$)

The function $f_1(\zeta)$ can be estimated if the height H of the effective window opening can be substituted in relation 3.38. As can be seen from this relation, $f_1(\zeta)$ will vary from $1.75/F_0$ for very small opening angles, when the window opening has a very small height and so a very large aspect ratio, up to 1 at full opening. With a rough estimate of H we may already get an impression of the effect of the window opening on the function $f_1(\zeta)$. Such a first estimate of H was made in section 3.3.1 taking $H = H_o \sin\zeta$. Then substitution in relation 3.38 yields

$$f_1(\zeta) = \frac{F_w}{F_o} = \frac{1.75 + 0.7 \exp\{-(L_o/H_o \sin\zeta)/32.5\}}{1.75 + 0.7 \exp\{-(L_o/H_o)/32.5\}} \qquad (3.40)$$

In figure 3.15a a graph of $f_1(\zeta)$ is given for some illustrative values of the aspect ratio. For small aspect ratios $f_1(\zeta)$ increases very rapidly to the value 1, for larger aspect ratios it varies from 0.85 to 0.95 between opening

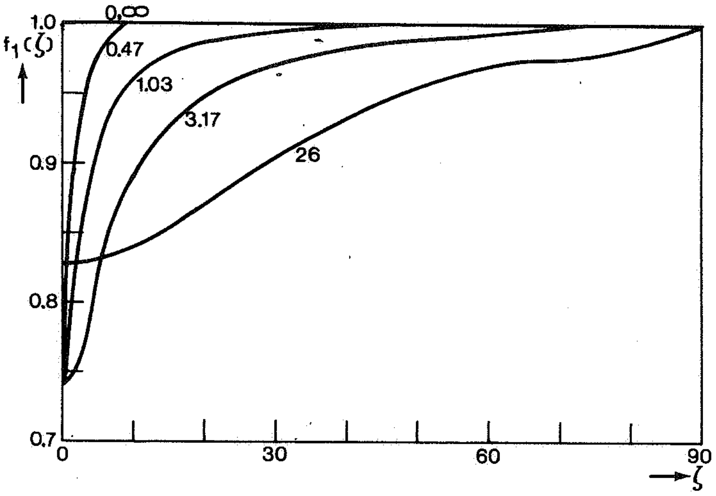

Fig. 3.15a. The function $f_1(\zeta)$ as function of the window opening for various aspect ratios.

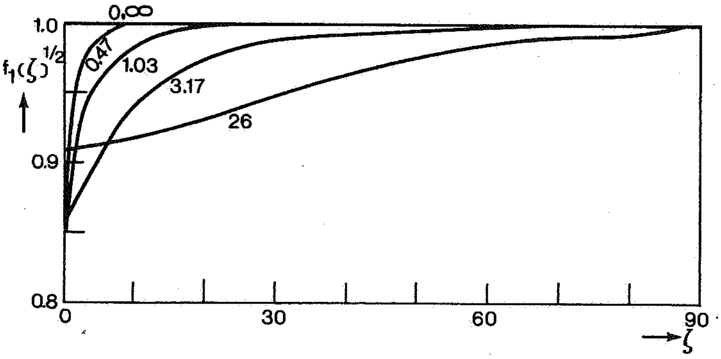

Fig. 3.15b. The square root of the function $f_1(\zeta)$ as function of the opening angle of the window for various aspect ratios.

angles of 0 to 50^0. For infinite and zero aspect ratios it equals 1 for all opening angles. The effect of $f_1(\zeta)$ on the window function $f_w(\zeta)$ has to be compared with the effect of the square of the function $f_2(\zeta)$. It can be expected that the function $f_2(\zeta)$ has the greater impact on the window function $f_w(\zeta)$. Some estimates of $f_2(\zeta)$ have been given already in section 3.3.1 (relations 3.6.a and b). For a determination of the function $f_2(\zeta)$, relation 3.39 and 3.5 are combined:

$$f_2(\zeta) = (\tfrac{1}{2}\rho f_1(\zeta)\frac{F_0}{A_0})^{\frac{1}{2}} \frac{\phi_V}{(\Delta p)^{\frac{1}{2}}} \tag{3.41}$$

To illustrate the small effect of the square root of the function $f_1(\zeta)$, in figure 3.15b this square root is given as a function of the opening angle of the window for the same aspect ratios as in figure 3.15a.

According to relation 3.41, experiments were carried out on models of the window opening with different aspect ratios at various opening angles. So for a range of opening angles of differently shaped windows, at each opening angle a series of ϕ_V and Δp values were measured. The quantity $f_2(\zeta)$ was determined for that particular opening angle of that particular window as the slope of the ϕ_V against $(\Delta p)^{\frac{1}{2}}$ graph with the known correction factor $(\tfrac{1}{2}\rho f_1(\zeta)F_0/A_0)^{\frac{1}{2}}$. In greenhouse practice the aspect ratios of the ventilation windows vary from about 0.4 (window from ridge to gutter, so for a Venlo type glasshouse H_0 = 1.7m; and length L_0, the length of one glass pane of 0.7m) to 2 (window with H_0 is half of gutter ridge distance and double length). For one small top mounted window over the whole length of the greenhouse the aspect ratio may become much larger still. For low aspect ratios it can be expected that the effect of the side areas of the windows is relatively large and for very high ratios the effect will be relatively small. So in the experiments the aspect ratio was varied from very low to high values and at any ratio $f_2(\zeta)$ was determined at various opening angles. The results of these measurements are presented in figure 3.16 as measuring points for the different aspect ratios. The full lines represent theoretical curves which will be discussed later. The positions of the points indicate that for low aspect ratio the increase of $f_2(\zeta)$ with increasing ζ is very strong but the value 1 is attained only at full opening ($\zeta = 90^0$). For higher aspect ratios, the increase is less steep.

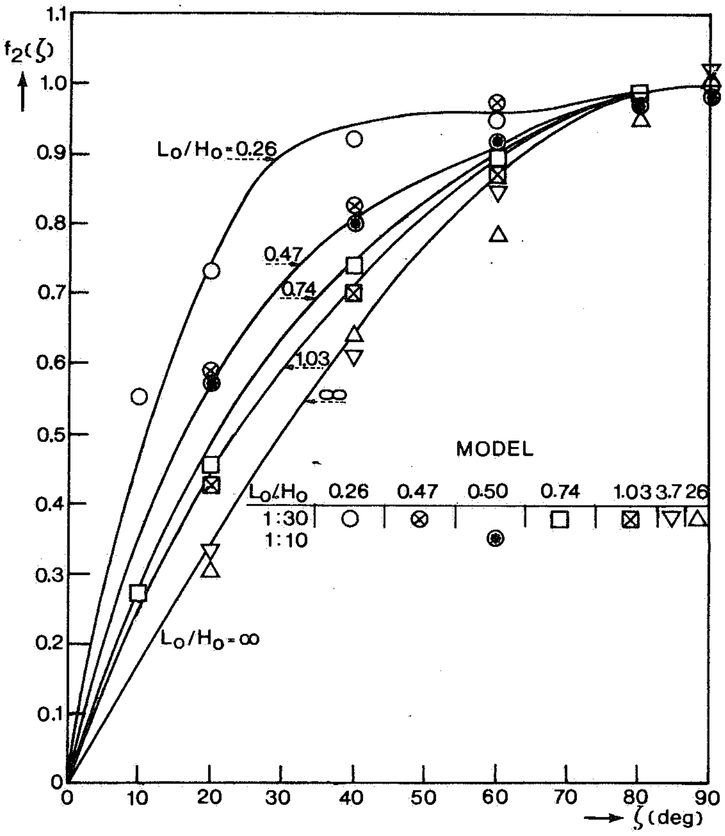

Fig. 3.16. Measurements of the function $f_2(\zeta)$ together with a theoretical model (full curves) related to the opening angle.

Earlier in this chapter the relations 3.6a, b and c were suggested to describe the function $f_2(\zeta)$. For high aspect ratios indeed, according to relation 3.6a, $f_2(\zeta) = \sin\zeta$ seems to cover the measurements reasonably well. This means that the effective exchange area under the window is represented by the perpendicular open area between roof and window (area ABFE in figure 3.2) when no side areas are involved. For lower aspect ratios an increasing influence of the side areas can be noted. The effect however is not covered by relation 3.6b. At low aspect ratios this function would have its maximum at small opening angles, but in the measurements the maximum is reached for all aspect ratios at full opening ($\zeta = 90$). It seems that the effect of the side areas decreases when ζ increases. To incorporate this effect we derived the model, represented by relation 3.6c. When the measuring points are fitted to this function we find b = 1 and a = 0.6. In figure 3.16 relation 3.6c with b = 1 and a = 0.6 is represented for the respective aspect ratios as full curves. The measuring points agree with the function in a satisfactory way for the various aspect ratios. For very high ratios, H_0/L_0 in relation 3.6c will be almost zero and the side area effect disappears, which results in $f_2(\zeta) = \sin\zeta$.

A very interesting aspect of relation 3.6c is that for low aspect ratios ($L_0/H_0 = 0.26$) it seems to show an inflection point near $\zeta = 55^o$. Though the precision of our measurements is not sufficient to confirm the existence of this inflection point, they certainly do not contradict it.

Most measurements represented in figure 3.16 have been performed on a scale model with scale factor 30. For one aspect ratio we also performed measurements on a scale model with scale factor 10. These measurements are in full agreement with the others. Again we may conclude from the similarity of the results of the two different scaled models that they will also be similar to the flow through the full scale opening.

3.4.2.b. Full scale ventilation

Continuous measurements of air temperatures and in- and outside CO_2 concentrations were performed.Simultaneously window apertures outside wind speed and wind direction were observed. From these results stable periods were selected. During such a stable period the mean values of wind speed and wind direction, in- and outside air temperature and the CO_2 concentration have to be constant to meet the requirements for the application of the equilibrium concentration method (relation 3.37). The averaging time of the quantities and the required length of the stable period was dependent on the expected ventilation rate, which was estimated from preliminary short measurements.

An example of the variation of some quantities measured during one day is given in figure 3.17. The correlation between the carbondioxide concentration and the wind speed at constant window aperture can be observed together with the response of the carbondioxide concentration on changes in the window aperture. During two periods an almost stable situation occurs marked in the figure with a symbol *. These periods however are relatively short. The window aperture was usually kept constant during longer periods to increase the probability of an equilibrium situation.

Due to the fact that continuous measurements were performed in seven compartments during three periods of about three weeks a number of stable periods could be selected in which a whole range of wind speeds and directions, win-

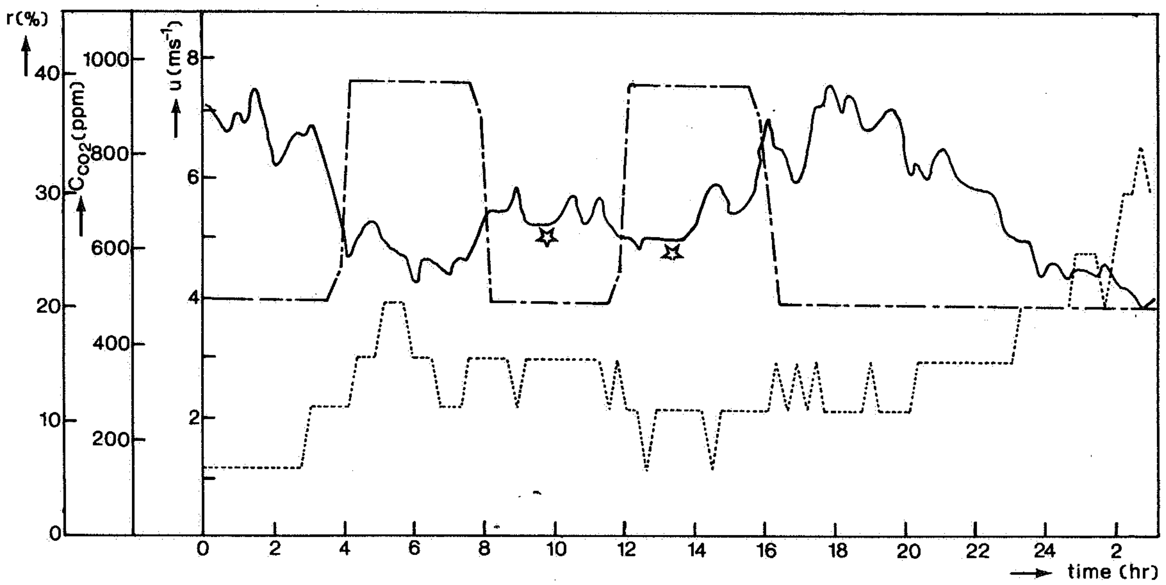

Fig. 3.17. Measured outside wind speed u (············), window aperture r (—·—·—) and carbondioxide concentration c_i (———) during a 24 h test period.

dow apertures and temperature differences occured. This set of data was analysed to find the separate effects of the different quantities mentioned above on the ventilation flux.

At every window opening that was applied, the relation between the measured ventilation flux and the wind speed as main variable was determined. Also the variation of this relation as a function of wind direction was investigated. Moreover the effect of the temperature difference between in- and outside air was considered. The result is shown in figure 3.18 for some of the window openings.

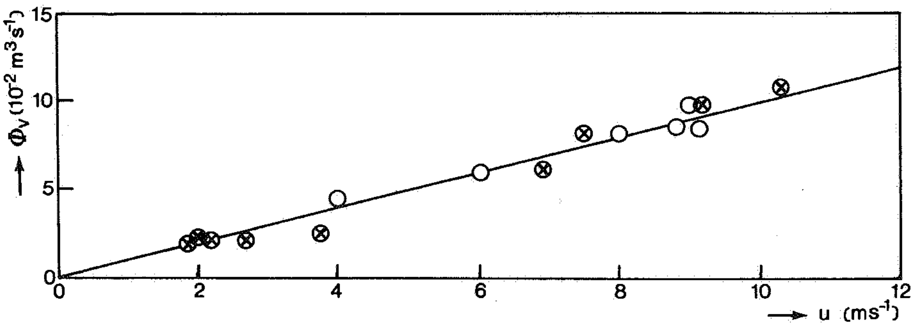

Fig. 3.18a
r = 2%
(ζ = 0.88^0)

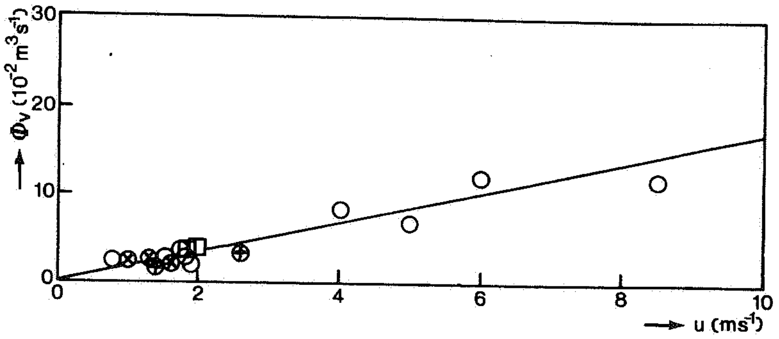

Fig.3.18b
$r = 4\%$
$(\zeta = 1.76^0)$

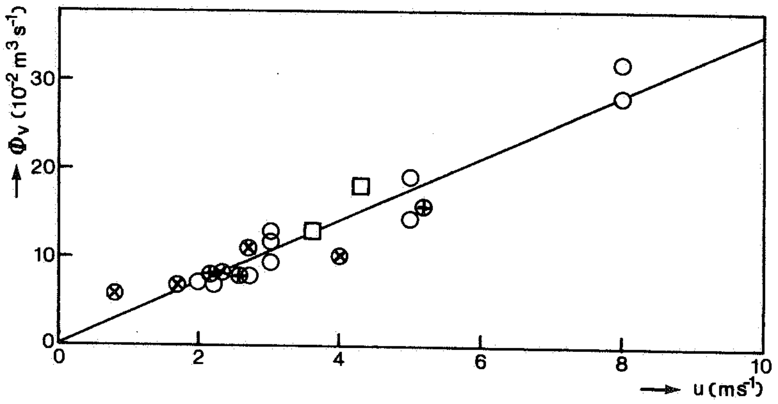

Fig.3.18c
$r = 10\%$
$(\zeta = 4.4^0)$

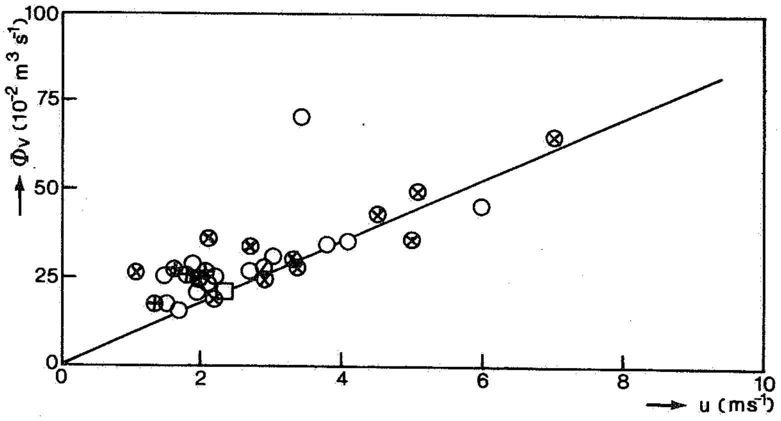

Fig.3.18d
$r = 40\%$
$(\zeta = 17.6\%$

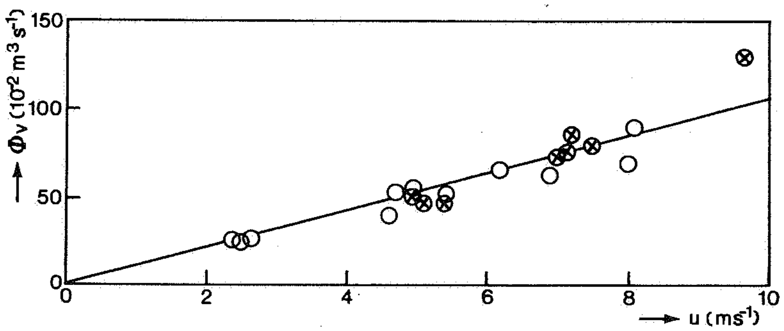

Fig.3.18e
r = 50%
(ζ = 22^0)

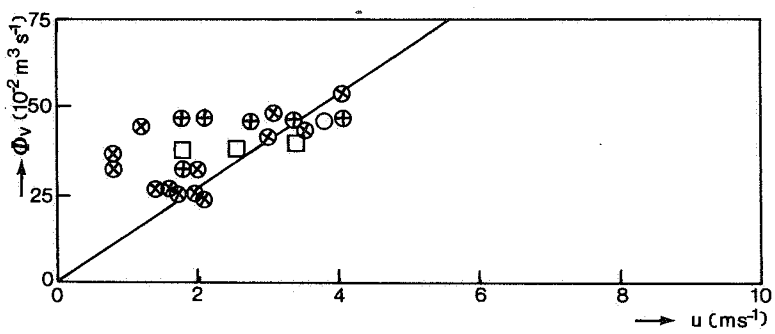

Fig.3.18f
r = 80%
(ζ = 35.2^0)

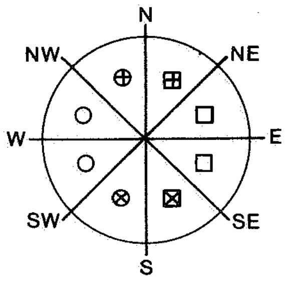

Fig.3.18g
symbols used to distinct
the wind directions

Fig. 3.18. Ventilation flux in one compartment (figure 3.12) as a function of wind speed u at some of the applied window apertures r. Wind direction is specified according to figure 3.18g.

At every window opening a linear relationship between ventilation flux and and wind speed can be observed, as was predicted by relation 3.12. The measurements were classified in some wind directions according to figure 3.18g. Each time only the leeside windows were opened. The orientation of the greenhouse is North-south; so with the wind from the west, the east windows were opened and conversely. Under these conditions no dominant effect of the wind direction could be observed. If there is any effect it will be smaller than the accuracy of the measurements, which is about 15%. Even in the scattering of the measuring points, no trend related to wind direction is apparent. The effect of the temperature difference could only be observed at wind speeds under about 1 ms^{-1}, as predicted in section 3.3.4. At a window aperture of 10% one measuring point at a wind speed lower than 1 ms^{-1} appears and at 40 and 80% aperture the scattering of the measuring points increases at low wind speeds. However only two measuring points at a wind speed lower than 1 ms^{-1} appear at a window opening of 80%. The temperature differences in the scattered measuring points between wind speed 1 and 2 ms^{-1} are rather small due to the fact that the ventilation rate is already relatively high at these window apertures and wind speed. The scattering must be caused by a high absolute inaccuracy of the measurements at the low wind speeds. The anemometer for instance was of a standard type with a poor response at low wind speeds. The trend of the measurements at high window apertures is illustrated by the measurements at apertures of 2 and of 50%. At these apertures neasurements over a wide range of wind speeds could be performed. This supports the interpretation of the measurements at apertures of 40 and 80%.
The conclusion concerning the temperature effect is that this effect is a small one. The amount of measurements at very low wind speeds was too low, however, to support a more quantitative statement. When new experiments relative to this effect have to be set up, then they are preferably carried out far from the windy coastal area. However, only in laboratory experiments the environmental conditions will probably be stable enough for this exacting kind of experiments.

In figure 3.19, the slope of the ventilation flux wind speed graphs (figure 3.18a-f) is plotted against the window aperture for all of the realised openings. At small window openings, up to about 20%, the relationship shows an almost linear proportionality. For these openings the best fit through the measuring points is:

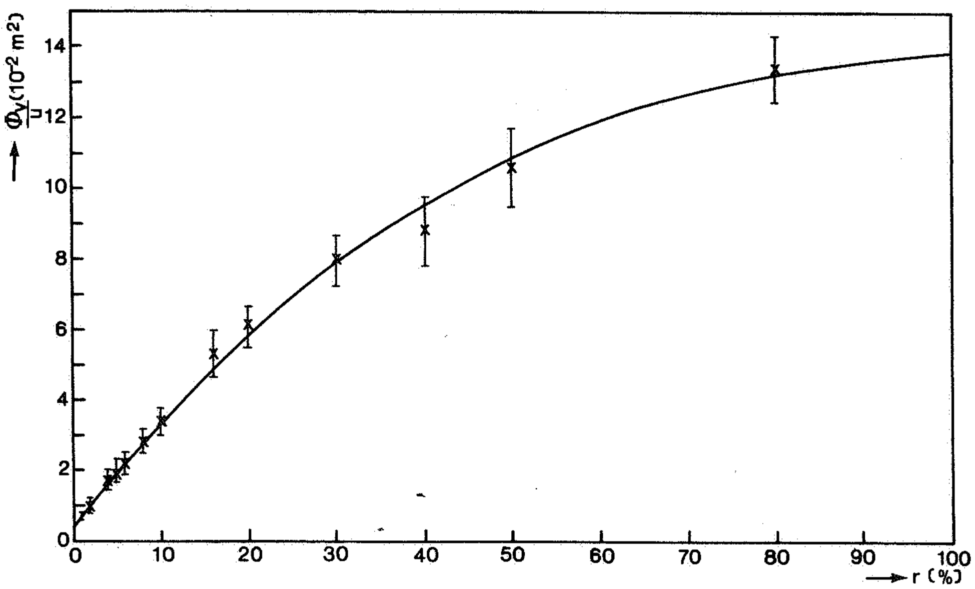

Fig. 3.19. Measurements and fit (full curve) of ventilation flux over wind speed as a function of window aperture.

$$\frac{\phi_v}{u} = 3.1\ 10^{-3}(r + 1)\ \Big\}\quad r < 20\% \tag{3.43}$$

At an aperture r = o, the leakage ventilation is found. For this particular greenhouse this is similar to the ventilation through a window opening with r = 1%. Relation 3.43 can be compared to measurements reported by Nederhoff et al. (1983) in which the authors applied another measuring method based on the decay rate of the CO_2 concentration from a high initial value without CO_2 addition. The measurements of Nederhoff et al. resulted in the same kind of relation as relation 3.43 but with a coefficient $2.9\ 10^{-3}$

Relation 3.43 holds in specific for the size of the compartments involved. To generalize it, the leakage will be normalized per unit area of the glass cover A_g, as suggested by Okada and Takakura (1973), and the ventilation through the window opening per unit area of the ventilation windows A_o, according to relation 3.12. In our case $A_g = 64\ m^2$ and $A_o = 7\ m^2$. Moreover the aperture r will be expressed in the opening angle ζ by $r = 2.27\ \zeta$. The relation 3.43 can be transformed into:

$$\frac{\phi_v}{u} = 1.0\ 10^{-3}\ A_o\zeta + 4.8\ 10^{-5}A_g\ \Big\}\quad \zeta < 9^o \tag{3.44}$$

The first right hand term of the equation states the ventilation through the ventilation windows; the second is the leakage ventilation. So for small opening angles the function $G(\zeta)$ (relation 3.12) is linear.
For the whole range of apertures the function $G(\zeta)$ can be fitted through the measuring points. This fit yields a relation holding in specific for this compartment:

$$\frac{\phi_v}{u} = 3.3\ 10^{-3} r\ \exp(-8.9\ 10^{-3} r) + 3.1\ 10^{-3} \qquad (3.45)$$

Transformation into the more general relation results in:

$$\frac{\phi_v}{u} = 1.07\ 10^{-3}\ A_o \zeta\ \exp(-\zeta/50) + 4.8\ 10^{-5}\ Ag \qquad (3.46)$$

Again the first right hand term represents the ventilation through the window openings, the second representing the leakage. So for the whole range of window apertures ($o < \zeta < 44^o$) the function $G(\zeta)$ for the observed type of window is found to be:

$$G(\zeta) = 1.07\ 10^{-3}\ \zeta\ \exp(-\zeta/50) \qquad (3.47)$$

The relation shows that the efficiency of larger openings decreases with increasing opening. This can also be seen directly from figure 3.17. $G(\zeta)$ would even have a maximum at $\zeta = 50^o$. This contradicts what follows from the flow characteristic of the opening, namely that the maximum flow always would occur at $\zeta = 90^o$. Consequently the pressure fluctuation coefficient also having its impact on $G(\zeta)$ (relation 3.12) has to be a function of the window aperture, as was already assumed in section 3.3.2.a.

3.5. DISCUSSION

3.5.1. Ventilation due to wind effects

As predicted by relation 3.12 for leeward side ventilation through roof windows a linear relation was found between the ventilation flux through a fixed opening and the wind velocity. The ventilation is presented as a static quantity, though the driving forces for this type of ventilation are the pressure

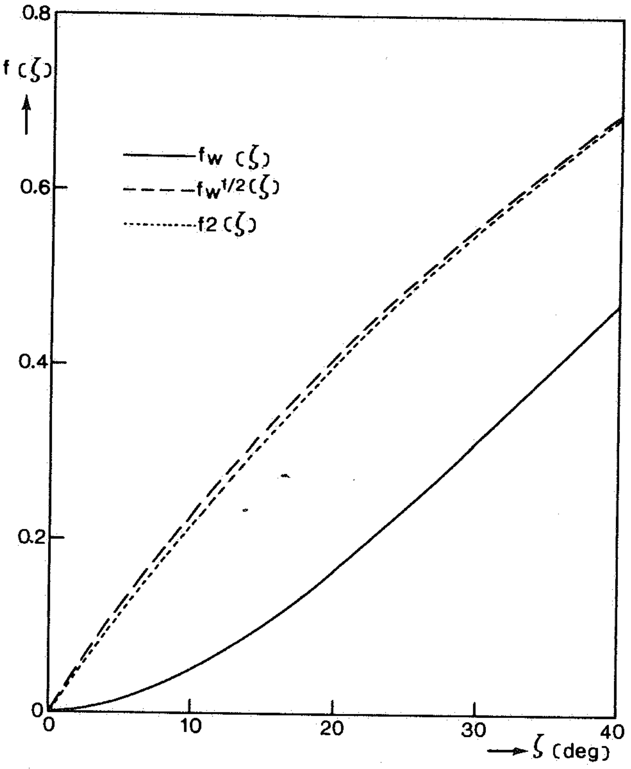

Fig. 3.20. Window function $f_w(\zeta)$ and the functions $f_1(\zeta)$ and $f_2(\zeta)$ of the ventilation windows of the Naaldwijk greenhouse.

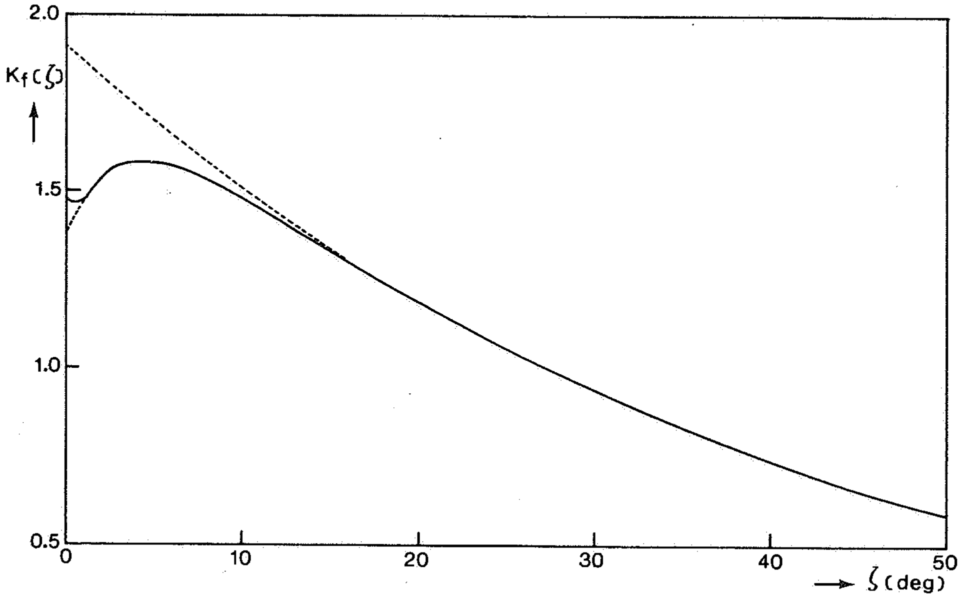

Fig. 3.21. The pressure fluctuation coefficient as function of the opening angle $K_f(\zeta)$ calculated from the experiments.

fluctuations due to the wind effect (section 3.3.2.a). The instantaneous ventilation, therefore is expected to vary as well. Nevertheless in the measurements an effective mean continuous ventilation is found. With varying window openings the proportionality factor $G(\zeta)$ could be expressed as a function of the opening angle. With the general relation 3.47 or 3.46 the ventilation flux through the openings of the observed type of ventilation window can be calculated at any wind speed in the range of 1 to 15 ms^{-1}. It was preferred to represent the ventilation flux per unit area of ventilation windows. In this form the results are also suited to calculate the ventilation in a greenhouse with the same type of ventilation windows, but with a different number of ventilation windows per unit of greenhouse area, or in a greenhouse with a different height. With the general equation 3.46 and the specific data of the greenhouse, we can for instance calculate the exchange rate, but exchange rate in itself however is not suited to compare the ventilation of different greenhouses.

From the measured functions $G(\zeta)$ and $f_w(\zeta)$ (flow characteristic) the pressure fluctuation coefficient can be calculated, according to relation 3.12. The window function $f_w(\zeta)$ is a combination of $f_1(\zeta)$ and $f_2(\zeta)$ (relation 3.5) which can be calculated from the window geometry according to the relations 3.40 and 3.42. The ventilation window considered in this chapter has an aspect ratio L_o/H_o = 1.46/0.8 = 1.825. The aspect ratio coefficient F_o of this window opening without window then is 2.41, according to relation (3.3.8.a). In figure 3.20 the calculated $f_w(\zeta)$ is given as full line. To show the effect of the function $f_2(\zeta)$ on $f_w(\zeta)$ also $f_2(\zeta)$ is given as a dotted line and $f_w^{\frac{1}{2}}(\zeta)$ as a broken line. As mentioned in section 3.42.a, $f_2(\zeta)$ is the major component of $f_w(\zeta)$ and $f_1(\zeta)$ gives rise to small corrections only.
With the flow characteristic and the ventilation function the pressure fluctuation coefficient is calculated numerically as a function of ζ, according to relation 3.12:

$$K_f(\zeta) = \frac{4F_o G^2(\zeta)}{f_w(\zeta)} \qquad 3.48$$

For the observed window the factor $4F_o$ is equal to 9.65.

The calculated pressure fluctuation coefficient is given in figure 3.21 as a full line. The coefficient behaves as a combination of two functions, one decreasing gently with increasing ζ and the other increasing fast at small opening angles. An almost perfect fit can be obtained by the following function:

$$K_f(\zeta) = 1.91\ 10^{-2}\exp(-\zeta/42)\{1 - 0.28\ \exp(-\zeta/35)\} \qquad (3.49)$$

Only at very small opening angles, lower than 1 degree, relation 3.49 does not agree with the $K_f(\zeta)$ calculated from our experiments. The coefficient calculated from experimental data is nearby constant at these small angles; relation 3.49 is indicated here as a dotted line. It is obvious that the calculations in this region are not reliable, probably because both functions $G(\zeta)$ and $f_w(\zeta)$ in relation 3.48 are approximating zero here.
The question arises which effects are responsible for the fast increase of the pressure fluctuation coefficient at small opening angles up to about 4 degrees and a slow decrease at large opening angles. The pressure fluctuation coefficient defines how effectively the pressure fluctuations drive the air exchange and how the wind speed at reference level is related to the pressure fluctuations near the window opening. It is hard to imagine that the effectivity of the pressure fluctuations decrease with increasing window opening, it is more probable that the reverse holds true, not only at small openings, but at large openings as well. Another aspect of the local pressure fluctuations and so air velocities related to the wind speed at reference height also deserves paying attention to. When the interaction between the wind and the saw tooth surface of the greenhouse roof is considered, very roughly three areas can be distincted: the boundary layer very near to the roof surface, the region in which the saw tooth shape has its impact on the air velocities and the region of the atmospheric boundary layer in which no direct effect of the saw tooth shape is present. When the moving window enters regions with higher air velocities the pressure fluctuation coefficient will increase. Starting from the closed position, the moving window first enters the boundary layer near the glass cover, which could explain the effect at small opening angles. This effect comes to an end at an opening angle of approximately 4-7 degrees which means a distance from the plane of the roof of about 5-10 cm. This could very well be the thickness of a boundary layer of a high turbulent flow like outside wind. The slight decrease at larger openings would indicate then that regions with lower air velocity are involved or that the window itself be-

comes an obstacle (leeward ventilation) and shields off the opening. Renard and Stein (1960) report on a visualization experiment of the flow over a saw tooth roof and describe, secondary eddies in the dips of the roof. No quantitative data were included in their paper. In our section 6.1 the flow field is investigated and this confirms the existence of secondary eddies. The isotachen pictures presented there indicate that the window itself acts as an obstacle at larger window openings and thereby cause the decrease of $K_f(\zeta)$.

The experimental relation between the pressure fluctuation coefficient $K_f(\zeta)$ and the opening angle can be applied to compute the ventilation flux through windows with different aspect ratios. Two common greenhouse types will be discussed, the first with aspect ratio 0.4 (ventilation window from ridge to gutter, with one glasspane; height H_0 is 1.7 m and length L_0 is 0.7 m) and the second with aspect ratio ∞ (ventilation window over the whole length of the greenhouse). For both aspect ratios the window function $f_w(\zeta)$ defining the flow characteristic can be calculated as was done above. With the pressure fluctuation coefficient, we can calculate $G(\zeta)$ for these types of ventilation windows, according to relation 3.12. In figure 3.22 the result is given, together with the directly measured $G(\zeta)$ of the ventilation window with aspect ratio 1.825.

As can be seen from figure 3.22, the ventilation of the window with aspect ratio 0.4 increases faster with increasing opening than the windows with greater aspect ratios, due to the greater effect of the side areas. The increase

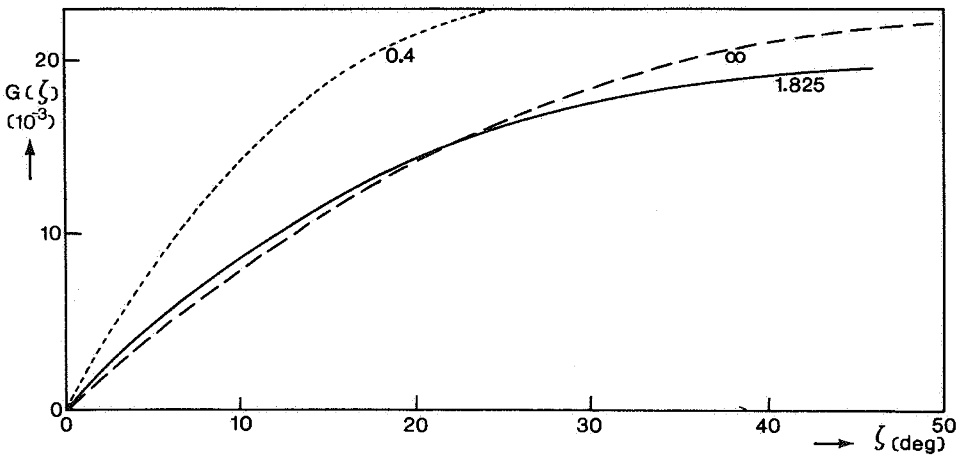

Fig. 3.22. $G(\zeta)$ of different types of ventilation windows as function of the opening angle. The aspect ratio of the window is given as parameter.

of $G(\zeta)$ for the aspect ratio 0.4 between closed position and an opening angle of 18 degrees is about the same as that of the window experimentally investigated between 0 and 44 degrees (full opening). The first window has to be opened then over a distance $D_{0,4}$ of 53 cm and the second over a distance $D_{1,825}$ of 60 cm, so the first one is a little bit more effective when it is opened over the same distance (figure 3.23).

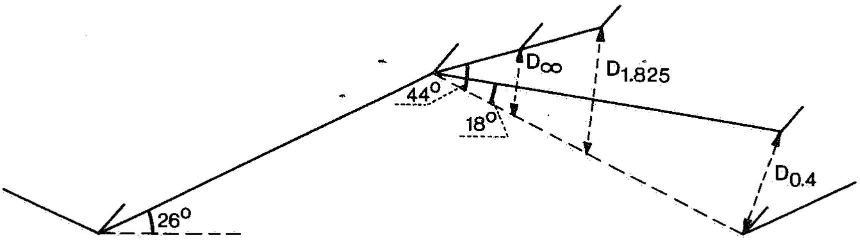

Fig. 3.23. Opening distances D of different shaped windows. The aspect ratio is given as an index to the distance D.

The difference between the functions $G(\zeta)$ of the two windows with aspect ratio 1.825 and ∞ is very small. Only for opening angles wider than 20 degrees the very long window has a somewhat higher ventilation and the maximum ventilation is at a wider opening angle. With the same ratio of ventilation window area A_0 to ground area, the opening distance D_∞ of the long window will be smaller than the other one. So in addition this window has to be opened over a smaller distance than the window with aspect ratio 1.825 (figure 3.23) to yield the same ventilation.

The calculated functions $G(\zeta)$ can be fitted by a relation similar to relation 3.47. With aspect ratio 0.4:

$$G(\zeta) = 1.9\ 10^{-3}\zeta \exp(-\zeta/35) \qquad (3.50)$$

and aspect ratio ∞:

$$G(\zeta) = 0.85\ 10^{-3}\ \zeta \exp(-\zeta/85) \qquad (3.51)$$

In the work of Warren (1977) some parallels to the present study is found.

His experimental results on the ventilation through a side mounted window in a vertical wall also show a maximum at opening angles smaller than at 90^{o}, namely at about 60^{o} for an aspect ratio of 1, at about 70^{o} for an aspect ratio of 1.6 and at about 80^{o} for an aspect ratio of 2.5. However, no explanation or theoretical consideration of this effect is given.

3.5.2. Ventilation due to temperature effects

In the full scale ventilation experiments, the temperature effect proved to be of minor importance. The only trace of the effect was found at large window openings and very low windspeed, which was in agreement with the theoretical prediction. However, the number of experimental data in this region was too small for quantitative conclusions. When the effect has to be quantified, new experiments especially pointed on this effect have to be set up either in a district with low average windspeed or in the laboratory.
The theoretical considerations can be applied to a quantitative prediction of the ventilation by the temperature effect. These predictions are supported by the agreement which was found to exist between the theory and the experiments of Brown and Solvason (1962) and Shaw (1971), who applied the same basic assumptions as were used in the present study.

When in practice there is a demand for ventilation in a greenhouse at very low windspeed, the ventilation windows will be opened completely due to the low ventilation flux. The estimation of the ventilation due to temperature effects will therefore be made at large window apertures. According to figure 3.10, the side area effect can then be neglected. With the help of relation 3.32 the ventilation per unit window area can be given:

$$\frac{\phi_{v,T}}{A_o} = \frac{1}{3}\left(\frac{g\beta H_o}{F_o}\right)^{\frac{1}{2}} (\sin\psi)^{3/2} (\Delta T)^{\frac{1}{2}} \qquad (3.52$$

For the Naaldwijk greenhouse (common Venlo-type), H_o= 0,8 m , F_o = 2.41, $\beta = 290^{-1}K^{-1}$, $g = 9.8\ ms^{-2}$ and $\psi = 26^{o}$. So relation 3.52 results in:

$$\frac{\phi_{v,T}}{A_o} = 10^{-2}(\Delta T)^{\frac{1}{2}} \qquad (3.53)$$

The numerical factor 10^{-2} is expressed in S.I. units i.e. $mK^{-\frac{1}{2}}s^{-1}$. When relation 3.53 is compared with the ventilation due to wind effects at full opening:

$$G(44^o) = \frac{\phi_v}{u.A_o} = 2.10^{-2} \quad (3.54)$$

then the wind effect will be dominant when

$$2u > (\Delta T)^{\frac{1}{2}} \quad (3.55)$$

This is of the order of magnitude as suggested in relation 3.34.
When the ventilation through the roof windows by the temperature effect only has to be estimated for other types of greenhouses the same approach (relations 3.15 and 3.16) can be adopted.

An interesting follow-up is the estimation of the effect on the ventilation when ventilation windows in the side walls are also opened. Nowadays most side walls of Dutch greenhouses are insulated and, as a result all side wall windows are sealed. In practice CO_2 deficiencies have been found when the conditions of high irradiation and low wind speed combine and the greenhouse crop is in its production stage(in the Netherlands mostly at spring time). An estimation of the effect of this sealing of the side wall windows on the ventilation at low windspeed is therefore very worthwhile.
Again the Naaldwijk greenhouse will be used as an example. The side wall ventilation windows are assumed to be located just under the gutter (figure 3.24). A first very simple estimation is made for a greenhouse in which the roof and side wall openings both have a vertical height h and length L. For the obser-

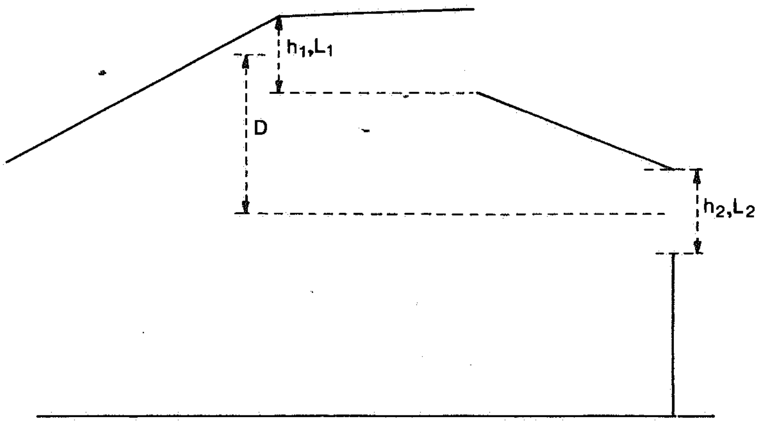

Fig. 24. Roof and side wall opening arrangement of the example discussed in the text.

ved greenhouse $h_1 = 0.35$ m, so $h_2 = 0.35$ m and D = 0.7 m. Now relation 3.25 can be applied, which results in:

$$\frac{\phi_{v,T}}{A_o} = 4.3\ 10^{-2}\ (\Delta T)^{\frac{1}{2}} \qquad (3.56)$$

This means an increase of more than 400% compared with the ventilation by roof windows only (relation 3.53). When the same approach is applied to a wide span, high greenhouse. D is much larger, so the increase is much higher still.

The condition that the vertical height and the length of the side wall windows equal that of the roof windows, can only be met in single- or twin-span greenhouses. For a multispan Venlo greenhouse this arrangement is not common. Therefore an estimation will be made for a multispan greenhouse, with side wall windows also just under the ridge. Here too we suppose the same vertical height in the roof and side wall windows, but the length of the side wall windows is just 0.1 of that of the roof windows. In that case relations 3.27 to 3.30 must be applied, to determine first the position of the reference level and after that the ventilation flux. From relation 3.30 the reference level in this case appears to be in the upper window opening, at a height of 14.1 cm, so 3.4 cm under the middle of the opening. This means that the influx does not only occur through the side wall windows, but also through the lower vertical 14.1 cm of the roof window while the outflux is through the upper vertical 20.9 cm of the roof window. The ventilation flux per unit roof ventilation window area can be calculated as

$$\frac{\phi_{v,T}}{A_o} = 1.66\ 10^{-2}(\Delta T)^{\frac{1}{2}} \qquad 3.57$$

So in this case, with only a relatively small amount of extra side wall windows, the ventilation is already increased with almost 70% comparing relation 3.57 with relation 3.53. This means that for large multispan greenhouses too, the sealing of the side wall windows has a serious impact on the ventilation at a very low windspeed.

4. Fluctuating character of ventilation

4.1. INTRODUCTION

In chapter 3 the exchange of air between inside and outside was assumed to be a continuous steady flow, mainly dependent on the outside windspeed as external factor and driven by the amplitude of the pressure fluctuations near the window opening. The contradiction between "steady flow" and "fluctuating driving force" was resolved by defining the steady flow as the time average of the effective air exchange due to the fluctuating flow. In summary some questions arise : is the instantaneous exchange indeed a fluctuating one; how can the fluctuations be characterized; how are the fluctuations related to the static representation?

The experiments described in this chapter were set up to answer these questions. An attempt was made to measure the fluctuations at several positions in one window opening at the same time and at one position in several different window openings too.

We are greatly indebted to prof. Ido Seginer of the Technion, Haifa (Israel) for his co-operation during the experiments.

4.2. EXPERIMENTAL SET-UP

In the window opening fluctuations of air movement were measured by a Gill anemometer (Holmes et al., 1964). Fluctuations of the temperature were observed by a, very thin, hot junction of a thermocouple. In a greenhouse, in general, the content is warmer than the outside air, so air going out has a higher temperature than air coming in. Temperature fluctuations in an opening are thus representative for air movement fluctuations.

The hot junction of the thermocouple was welded with 0.1 mm wire and, rolled out to a thickness of about 0.04 mm in order to obtain a fast response. Its dynamic behaviour was determined as a function of the windspeed in a wind tunnel by irradiating the hot junction with a chopped, high intensity light beam. At very low windspeed of about 0.5 ms^{-1}, the time constant proved to be 0.25 s and at higher windspeed (12 ms^{-1}) the time constant decreased to 0.05 s. The hot junction of the thermocouple was fixed in a supporting ring to facilitate easy mounting in the window opening. The reference junctions were placed in a Dewar vessel; the reference temperature was measured separately. Apart from these fluctuation measurements in the window opening the outside instantaneous windspeed, direction and azimuth were measured with a bivane Gill anemometer.

Eight signals were available: one inside Gill, four fast thermocouples and three signals of the outside Gill. Six of these eight signals could be handled automatically. They were amplified, filtered by a 4 H_z low-pass 12 db/oct Chebishev filter and then sampled 50 times per second each with a PDP 11/03 minicomputer controlled data logger system. The data could be averaged in clusters of adjustable size and then stored on a floppy disk in blocks of 2048 data per channel. The processing was done off-line on the DEC-10 Wageningen University computer applying standard Fast Fourier Transform techniques.

The experiments were carried out in one compartment of the Naaldwijk 24 compartment greenhouse (figure 3.12) to compare them with the static ventilation experiments carried out earlier (chapter 3). The ventilation windows of the middle span in the three span compartment (figure 4.1) were permanently closed. So if only ventilators at the leeside or the windwardside were opened, four windows were simultaneously open.

The fast thermocouples were arranged in the window openings in the plane of the roof. In the first part of the experiment the four thermocouples were fixed in one window opening (opening A_1 or A_2, figure 4.1) and in the second part they were each fixed in a different window opening (A_1, B_1, C_1, D_1 or A_2, B_2, C_2, D_2 in figure 4.1 respectively). The inside Gill was located in window A_1 or A_2 in the first part of the experiment and in window B_1 or B_2 in the second part, as close as possible to the plane of the roof with its axis perpendicular to the roof. The outside bivane Gill anemometer was located at position G_2 (figure 4.1) at a height of about 1.5 m above the ridge of the greenhouse.

Simultaneously with the fluctuation measurements, the Naaldwijk computer, on a one minute base, sampled the relevant outside weather conditions at the weather station, i.e. global solar irradiation, outside air temperature and windspeed and direction. Also the temperature of the reference junctions of the fast thermocouples, the inside air temperature in a vertical gradient of five spots at position E (figure 4.1) and the aperture of the ventilation windows were sampled in this way.

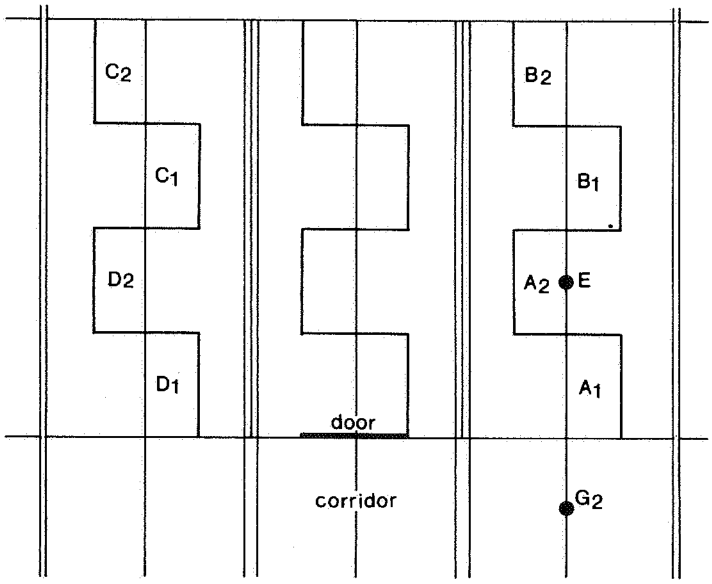

Fig. 4.1. Position of the open windows (A_1, B_1, C_1, D_1 or A_2, B_2, C_2, D_2) of the temperature gradient measurement (E) and of the outside bivane Gill anemometer (G_2).

During the experiments the window aperture was varied both for leeside and for windardside ventilation and the door between the compartment and the corridor was either closed or completely open (see figure 4.1). Due to the fact that the two opposite exit doors at both ends of the corridor were continuously open, a constant air flow was generated in the corridor. If the compartment door was opened a continuous flow was generated from the corridor to the compartment and therefore from the compartment through the window openings out. So by opening the door a static pressure difference was involved between the compartment and the outside, superposed on the fluctuating one. So in this way the relative effects of a static and a fluctuating pressure difference over the window openings could be investigated.

4.3. EXPERIMENTAL RESULTS

In the first runs an estimation was made of the frequency distribution of the various signals to determine how many samples had to be averaged in one set.

It turned out that a fair distribution over the high and low frequencies from 1 to 0.03 H_z could be obtained. For that goal 25 samples had to be averaged to one measuring point, resulting in 2 values per channel per second. the filtering properties of this averaging process are shown in e.g. Oppenheim and Schafer (1975).

Because 2048 values could be stored and processed per channel the measuring period covered about 17 minutes with 2 values per second. During 42 measuring periods data were collected. In the first 19 runs the fast thermocouples were located in one window opening; in the next 23 runs they were each located in a different window (see section 4.2).

4.3.1. Fluctuating character

Parallel to the automatic data logging, two of the channels were recorded on a two channel x-t recorder, to obtain an instantaneous estimation of the measurements as well. The fluctuating character can be demonstrated by some part of this recording (figure 4.2) of the inside Gill anemometer (lower record)

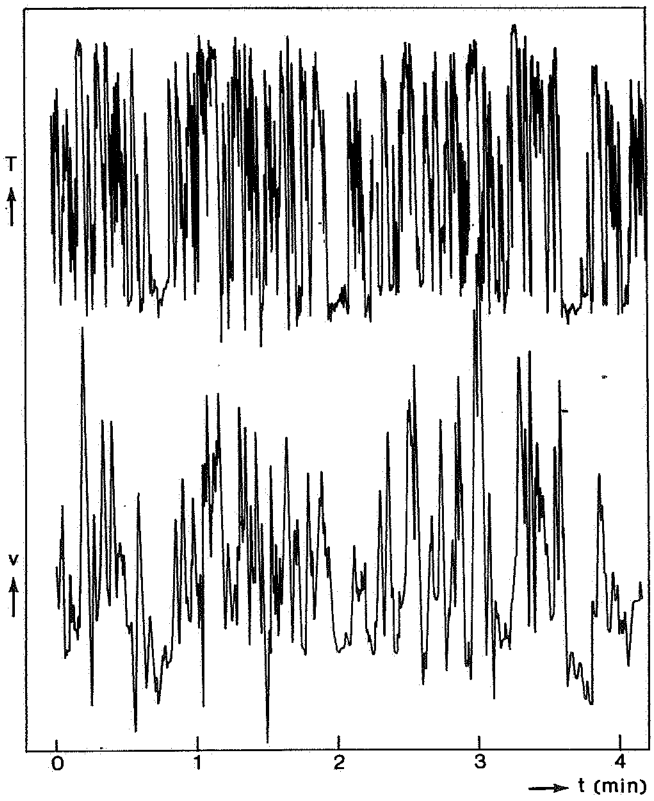

Fig. 4.2. Record of the measured fluctuating air temperature T and air velocity v in the window opening during some minutes.

and of the thermocouple located in the same window opening (upper record). The thermocouple signal is positive when the temperature is lower and the Gill signal is positive when the direction of the air flow is inward. At a first sight, both signals just fluctuate, but when they are studied in greater detail a characteristic correlation as well as a characteristic difference can be observed. Both signals tend to have the same sign and this is demonstrated very clearly when the thermocouple is uninterruptedly negative or positive during some time. Then the Gill record shows a remarkable correspondence. The characteristic difference between both signals is in their frequency response. The thermocouple signal contains higher frequencies than the Gill signal. This can be understood from the response characteristic of the Gill anemometer. Especially when the Gill is operating at low air velocities, the threshold sensitivity causes a loss of information, but also the (relatively) big dimension of the propellor smooths the fast components of the signal. The same phenomena can be observed when we compare the power spectra of the thermocouples and of the inside Gill anemometer. From chapter 3 we know that the volumetric exchange of air through the window opening, so the local air velocity in the window opening, decreases with decreasing window aperture. Besides it was observed (section 4.3.3) that the exchange for windwardside ventilation is higher than for leeside ventilation. Therefore it is interesting to compare the power spectra of the inside Gill anemometer with those of the fast thermocouples and those of the outside Gill anemometer at relatively high local air velocities (fully open window windwardside ventilation) and at lower local air velocities in the opening (half and quarterly open windows leeside ventilation), all situations at about the same outside windspeed. In figure 4.3 the power spectra are compared at a relatively high local air velocity in the window opening. A geometric similarity can be observed between the various spectra (no outside Gill anemometer signal was available during this run). To show especially the effect at high frequencies, in this run the samples were average in sets of 12, resulting in 4.17 measurements per second per channel to cover a range from 0.0625 to 2 Hz in the spectrum. In figures 4.4a and 4.4b the spectra are compared for lower local air velocities in the window. Again a geometric similarity can be observed between the thermocouple spectra but the spectrum of the inside Gill anemometer shows a much steeper decrease than the thermocouple spectra at the higher frequencies. The spectrum of the outside Gill is similar to that of the

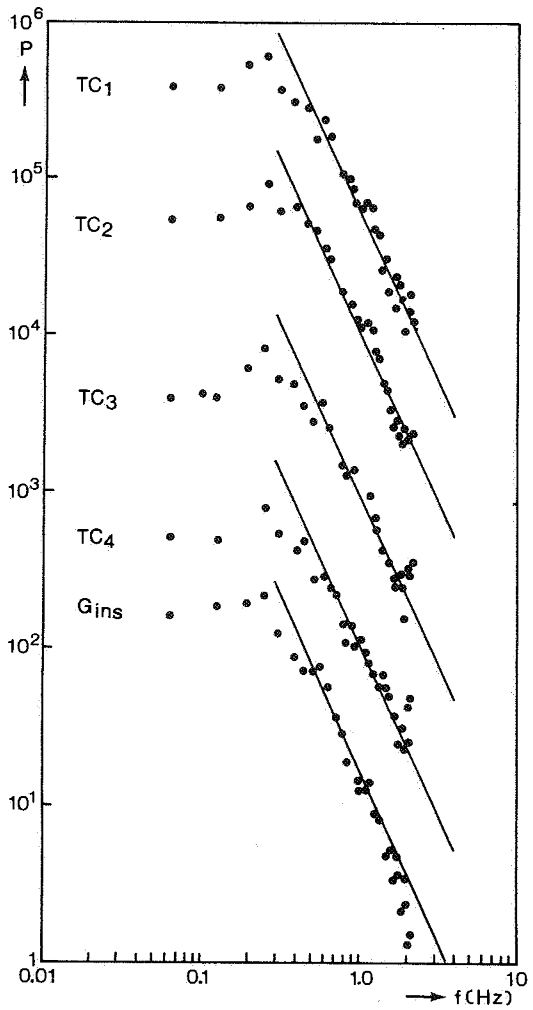

Fig. 4.3. Power spectra of four fast thermocouples and the Gill anemometer in the window opening for windward side ventilation at full opening (window aperture r = 1). Outside wind speed u = 7.2 ms^{-1}.

thermocouples at higher frequencies, the differences for lower frequencies are discussed in section 4.3.2.

The question arises how the high and low frequencies influence the effective exchange through the window opening. As mentioned before, air going out has a higher temperature than air going in. Near the opening there will be a region of mixing, so the mean temperature there will be between the in- and outside temperature. When air is coming from inside from beyond the mixing region it will have a temperature close to the inside temperature. So when it passes the opening with a high velocity it will come from far within: great fluctuations in air velocity will result in great air temperature fluctuations. On the other hand small air velocity fluctuations will give rise to small air temperature fluctuations. This effect was already demonstrated in figure 4.2, but it

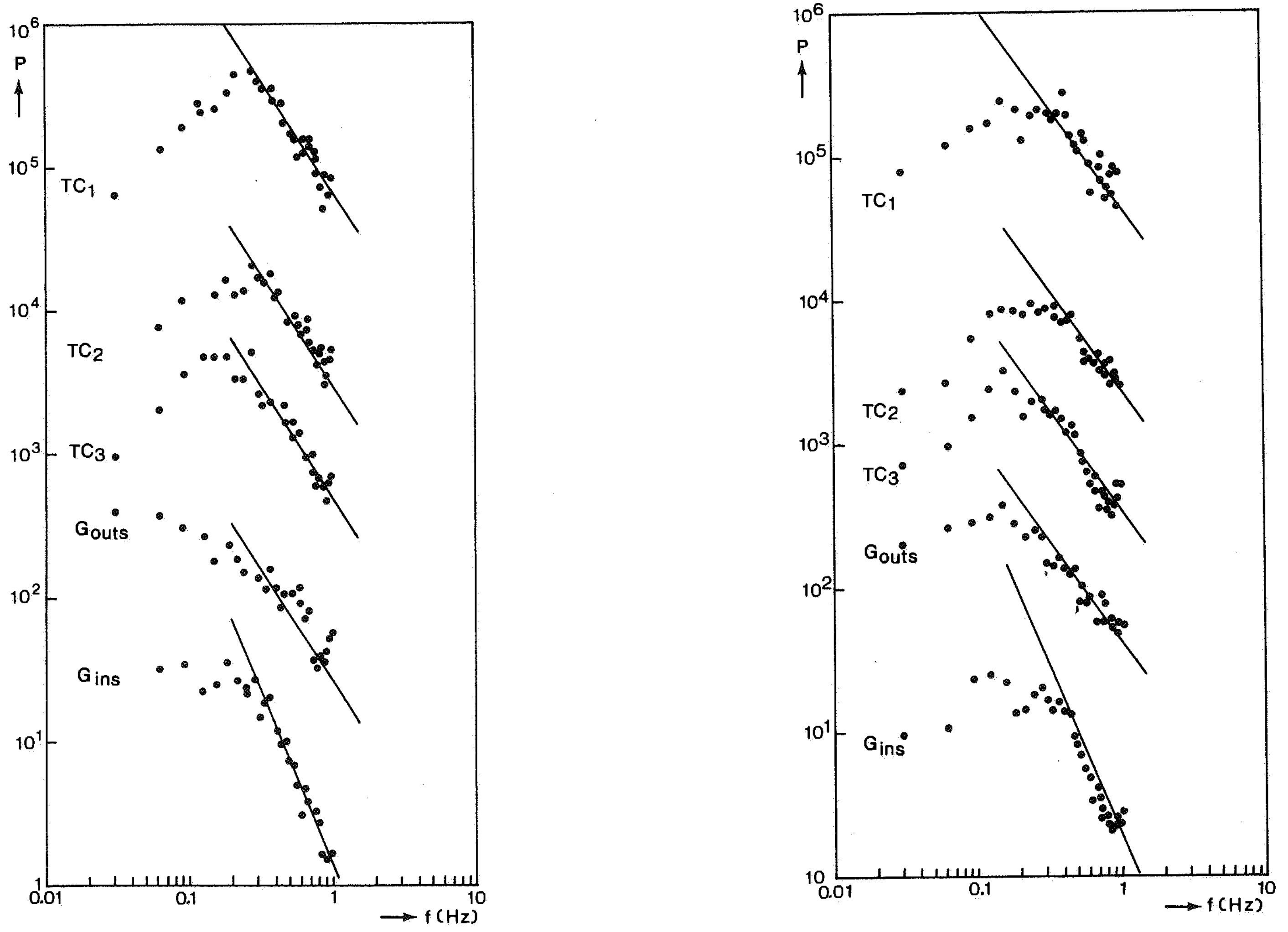

a. $r = 0.5$; $u = 7.0\ ms^{-1}$

b. $r = 0.25$; $u = 8\ ms^{-1}$

Fig. 4.4. Power spectra (vertical axis arbitrary) of three fast thermocouples and the Gill anemometer in the window opening and of the outside Gill anemometer for leeside ventilation at two window apertures r.

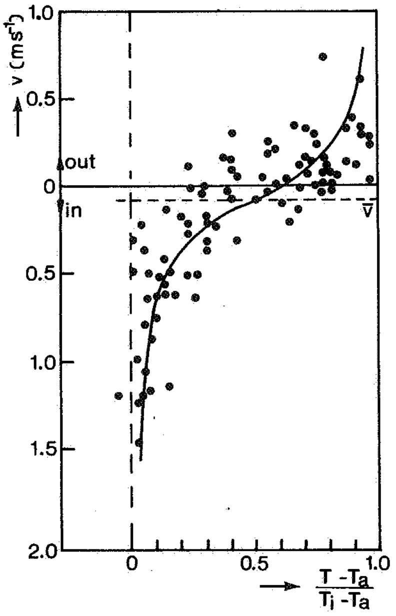

Fig. 4.5. Representation of air velocity v and temperature T in the window opening during one measuring period (correlation coefficient 0.8).

can be made clearer in figure 4.5 in which individual pairs of the local air velocity and temperature in the opening during one measuring period are shown as points in a velocity-temperature graph. If in this graph only small air velocity and temperature fluctuations were present, only the middle part of the graph would be occupied i.e. with a cloud of points. Due to the larger inward velocities at some moments also air temperatures near the outside temperature T_a are realized. Figure 4.5 is not symmetric with respect to the $v = 0$ axis, due to the fact that during this measuring period in this window opening a mean air velocity $\bar{v}$ was found. This average velocity was inward, so the left branch of the figur which is colder, is more pronounced.
An empirical curve that seems suitable to fit data of this kind is

$$v - \bar{v} = K \tan[\pi\{(\frac{T-T_a}{T_i-T_a}) - \tfrac{1}{2}\}] \qquad 4.1$$

with K an empirical constant (ms^{-1})

For the data of figure 4.5, $\bar{v} = 0.08\ ms^{-1}$ and $K = 0.2\ ms^{-1}$.
From figure 4.5 it can be concluded that the higher velocities and therefore the lower frequencies through the window contribute directly to the air exchange. The higher frequencies only transport the air across a smaller distance within the mixing region near the window, or are superposed on the lower frequencies. So considering the effective air exchange, the Gill anemometer is a useful instrument, but when the impact on the frequency distribu-

tion is considered use of the Gill anemometer leads to a loss of information at high frequencies, which makes it less useful.

The high degree of systematics in figure 4.5 indicates that the measurements of the air velocity and the temperature in the opening correlate very well. The correlation coefficient of these velocity-temperature measurements was 0.80, which is quite high. Especially the left and/or right branch of the figure contributes to this high correlation. When these branches are less pronounced lower correlation coefficients will be found. These branches will be less pronounced when the effective air exchange is lower. Therefore the correlation coefficient may be expected to be lower if the effective air exchange is lower. In chapter 3 it was indicated that the air exchange is a function of the product of the window aperture r and the outside wind velocity u, so the correlation coefficient of the local air velocity in the opening and the nearby air temperature will be dependent on r*u. This is demonstrated in figure 4.6 for both leeside and windwardside ventilation. For windwardside ventilation the effective air exchange is higher (section 4.3.3) and the dependency of the correlation coefficient on r*u is pronounced. For the leeside ventilation it is less pronounced, but the dependency can still be traced. It must also be clear that if the air velocity in one window opening is matched to the air temperature in another opening, a figure like figure 4.5 will result in a much less systematic picture. So the correlation coefficient of two signals in different window openings will be very low. Actually this is what we did observe during the experiments with the thermocouples in different window openings.

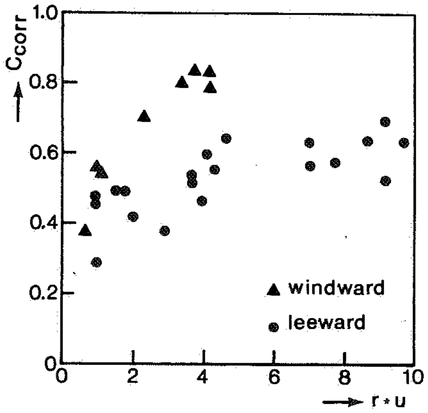

Fig. 4.6. Correlation coefficient C_{corr} between inside Gill anemometer and nearby thermocouple as a function of the product of window aperture r (completely open is 1) and outside windspeed u.

4.3.2. Window opening and frequency distribution

In fig. 4.4a,b are also given the power spectra of the outside Gill anemometer. When these are compared with spectra of the thermocouples it can be observed that the decrease at high frequencies is similar, but that there are deviations at low frequencies. A direct comparison of the different spectra at different window openings for both windward- and leeside ventilation

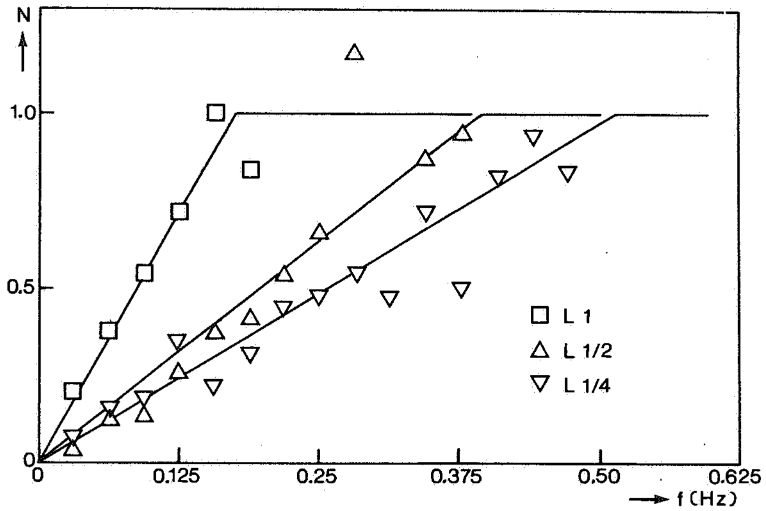

a. leeside ventilation

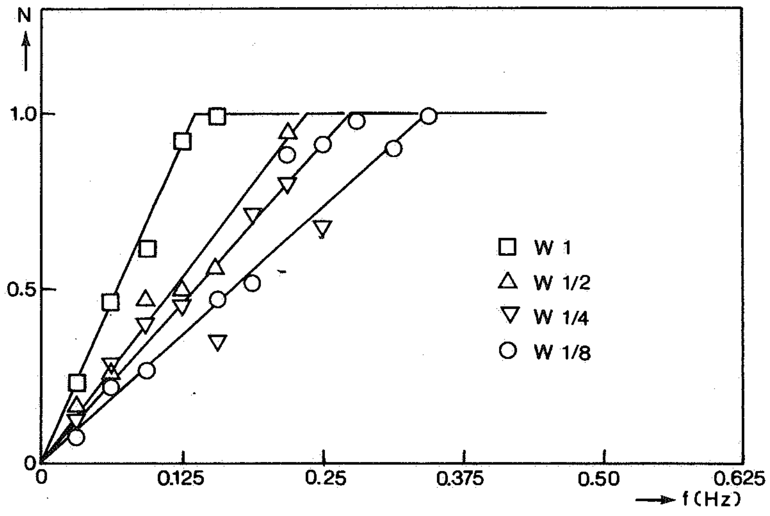

b. windwardside ventilation

Fig. 4.7. Normalized ratio N of the power spectra of the outside Gill Anemometer and a fast thermocouple in the window opening with indicated aperture both for leeside and windwardside ventilation.

is confusing, because the spectra of the outside wind velocity differ for different measuring periods. Therefore an attempt was made to establish a normalized parameter from the spectra suitable to compare the various spectra. In the spectra the power in frequency intervals is given. The ratio of the power of two spectra in the same frequency interval was calculated as a parameter and this was normalized by this ratio at high frequencies, of course for the spectra under consideration. Due to the fact that the spectra are similar at high frequencies (figure 4.4a and b), the ratio is constant there. The result of these calculations is shown in figures 4.7a and b.
Though there is, of course, some scattering in the calculated points for each window opening, the general trend is quite unique: low frequencies are depressed and the depression decreases more or less linearly for each window opening up to a frequency where the ratio equals 1. The depression increases when the window opening decreases. The effect is stronger for leeside ventilation. So the window openings act as tunable high pass filters.

4.3.3 Fluctuating character and effective air exchange

As well known the effective exchange resulting from a fluctuating flow is characterized by the root mean square (RMS) of the momentaneous flow velocity. As shown already, the low frequency components comprise the more important part of the spectrum, so the RMS of the inside Gill anemometer can be used as a measure of the effective exchange.
The effective exchange is a function of mainly the outside wind velocity and the window aperture (chapter 3), so the RMS of the inside Gill anemometer can be examined for its dependency on these variables. In figure 4.8 this Gill RMS is represented as a function of the outside wind velocity for different window apertures (aperture 1 means completely open window) for both leeside (4.8a) and windwardside ventilation (4.8b). The filled symbols represent measuring periods with open door between compartment and corridor. Though the number of measuring periods, i.e. the amount of measuring points in figure 4.8, is only small for each window opening, there is this noticeable trend. When lines are plotted through the points for different window openings, the slope of the line increases when the window opening increases. For the windwardside ventilation the slopes are steeper than for leewardside ventilation.

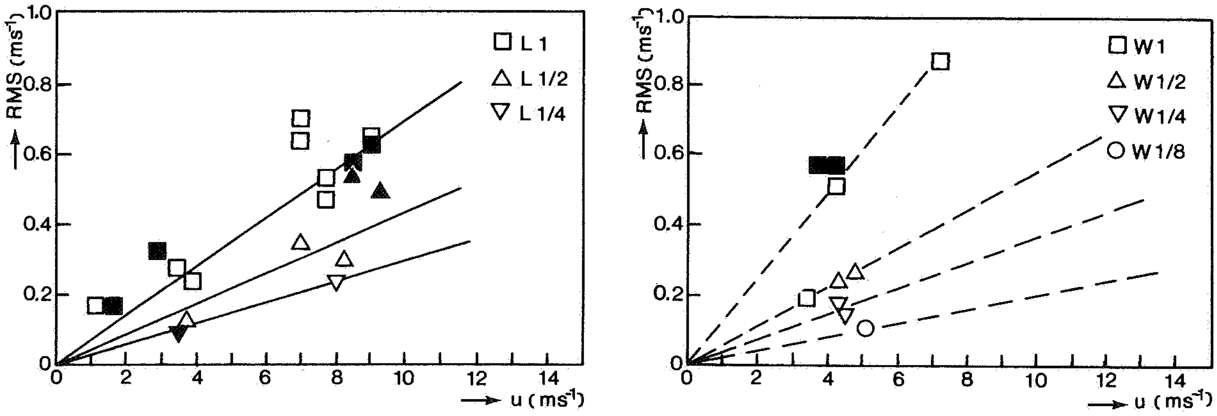

a. Leeside ventilation

b. Windwardside ventilation

Fig. 4.8. The RMS of the Gill anemometer in the window opening related to the outside wind velocity u for various window apertures both for leeside and windwardside ventilation.

As the next step the slopes of the lines, i.e. RMS/u can be plotted against the window opening. This leads to figure 4.9, where both windwardside and leeside ventilation are represented.

To discuss the results of figure 4.9 we turn to the static approach of chapter 3. There the effective flow was characterized by the volumetric air exchange per unit area of the window opening. So the quotient of the effective flow over the wind velocity equals to the function G(ς), according to relation 3.12. It is interesting to compare the RMS/u values calculated from the fluctuation experiments with the function G(ς) determined from the tracer gas

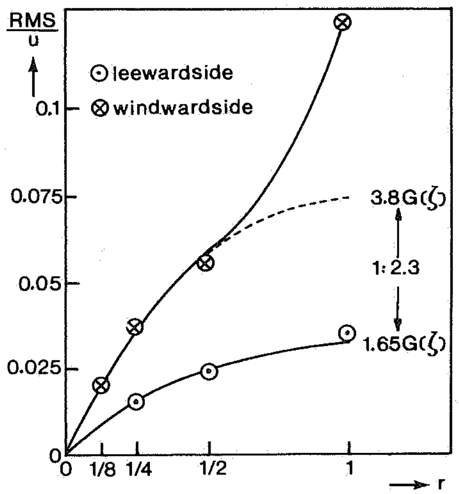

Fig. 4.9. The slope of the plotted lines in fig. 4.8a and b as a function of window aperture r (measuring points). Compared with the function G(ς) (Chapter 3).

experiments. When $G(\zeta)$ is calculated according to relation 3.47 and will be combined with a scaling factor, a good fit will be obtained with a scaling factor of 1.65 for leeside and 3.8 for windwardside ventilation (curves in figure 4.9). So for leeside ventilation:

$$\frac{RMS}{u} = 1.65 \ G(\zeta) = 1.65 \ \frac{\phi_v}{uA_o} \qquad (4.2)$$

The term $\phi_v/(\frac{1}{2}A_o)$ may be called the effective air velocity v_{eff} in the window (in relation 3.12 half of the exchange area A_o is utilized for the inward flux and the other half for the outward flux), so from relation 4.2:

$$v_{eff} = 1.2 \ RMS \qquad (4.3)$$

So the effective air velocity calculated according to the empirical relation for the air exchange (relation 3.47) is found to be 1.2 times the RMS calculated from the fluctuation experiments. The empirical factor 1.2 and the theoretical factor 1 are of the same order of magnitude, which again demonstrates the fluctuating character of the air exchange.
The agreement with the curves in figure 4.9 is clear for all observed slopes except for that at full opening measured with windwardside ventilation. The slope at this opening (figure 4.8b) is based on 5 measuring periods and 4 of them are highly coherent, so the RMS/u value cannot be a deflective point. The much higher RMS/u value can be understood when the geometry of the ventilation window in the roof is considered. At a window aperture of 0.59, the opening angle is 26°, which equals the roof angle, so the window is in horizontal position. If the aperture increases then, some part of the window opening will be above the ridge level and thus intercepts directly some part of the main air flow above the roof.

From the scaling factors 1.65 and 3.8 between the function $G(\zeta)$ and RMS/u for leeside and windward ventilation side respectively, it can be stated that:

$$\left.\begin{array}{l}\phi_{v,windwardside} = 2.3 \ \phi_{v,leeside} \\ \qquad\qquad r < 0.6\end{array}\right\} \qquad (4.4)$$

At full opening, the windwardside RMS/u value is 3.7 times the value for leeside ventilation. Between aperture values of 0.6 and 1 unfortunately no measuring points are available. Since the measuring point at full opening is based on a set of 4 coherent measuring periods, this point is quite reliable. If the ratio of RMS/u is linearized in the interval a statement on the windwardside ventilation can be made:

$$\phi_{v,\mathrm{windwardside}} = (3.5\ r + 0.2)\ \phi_{v,\mathrm{leeside}} \Big\} \quad 0.6 < r < 1 \qquad (4.5)$$

The linearization will only cause a relatively small error in this range. The leeside ventilation can be calculated according to chapter 3, so with relation 4.4 and 4.5, also the air exchange at windwardside ventilation can be calculated.

4.3.4. Heat transfer through the window opening

The heat flux density through the window opening ϕ_H'' (W_m^{-2}) can now be calculated following two different approaches:

a) an effective continuous air flow with an effective air velocity v_{eff} continuously transports heat through the opening. According to this approach the heat flux density is:

$$\phi_H'' = \rho C_p v_{eff}(T_i - T_a) \qquad (4.6)$$

with:

ρC_p the volumetric heat capacity ($Jm^{-3}K^{-1}$) and $(T_i - T_a)$ the temperature difference between in- and outside (K).

As we have seen, the effective velocity is in the same order of magnitude as the RMS of the momentaneous velocity so

$$\phi_H'' = \rho C_p \mathrm{RMS}(T_i - T_a) \qquad (4.7)$$

(It should be noted that the heat flux is normalized per unit area of A_o (ventilation window area), because the local air velocity and temperature were measured in the window opening in the plane of the roof).

The heat flux density calculated according to this approach will be called the effective heat flux density.

b) a turbulent air flow with fluctuations of the air velocity v' and of the temperature T' and a mean velocity and temperature $\overline{v}$ and $\overline{T}$ respectively in the opening, transports heat through the opening. The transport is the sum of a turbulent term due to fluctuations and a convective term due to the steady flow with mean velocity $\overline{v}$:

$$\phi'' = \rho c_p(\overline{v'.T'} + \overline{v}.\overline{T}) \tag{4.8}$$

so: $\overline{v'.T'}$, the average of the product of the momentaneous fluctuations of the air velocity v' and of the temperature T', is the term due to turbulent transport

and $\overline{v}.\overline{T}$, the product of the averages of air velocity $\overline{v}$ and temperature $\overline{T}$, is the convective term.

If only transport due to fluctuations occured, the convective term would be zero because the mean velocity is zero. The mean temperature $\overline{T}_m$, as measured in the opening, would then equal $(T_i + T_a)/2$. So the mean temperature $\overline{T}$ in relation 4.8 is the actual difference between the measured mean temperature $\overline{T}_m$ and the reference temperature in the opening $(T_i + T_a)/2$:

$$\overline{T} = \overline{T}_m - (T_i + T_a)/2 \tag{4.9}$$

During the runs the momentaneous temperatures and velocities were measured, so all terms formulated before could be calculated. A comparison was drawn between the effective heat flux density and the term due both to turbulent transport and the total transport according to relation 4.8. As mentioned before (section 4.2), during some measuring periods an attempt was made to establish the static term of relation 4.8 by opening the door between the compartment and the corridor.

In figure 4.10 the term $\overline{v'.T'}$ is compared to RMS $(T_i - T_a)$. Because the vertical axis is arbitrary, no quantitative comparison can be made. Only the proportionality can be checked. The open symbols represent measuring periods with door between compartment and corridor closed and filled symbols refer to periods with open door. There is no significant difference between the measurements with open and closed door and there is a reasonable correlation between the effective and the turbulent flow. There is only one measuring point in both 4.10a and b marked with an arrow, which does not fit to the other mea-

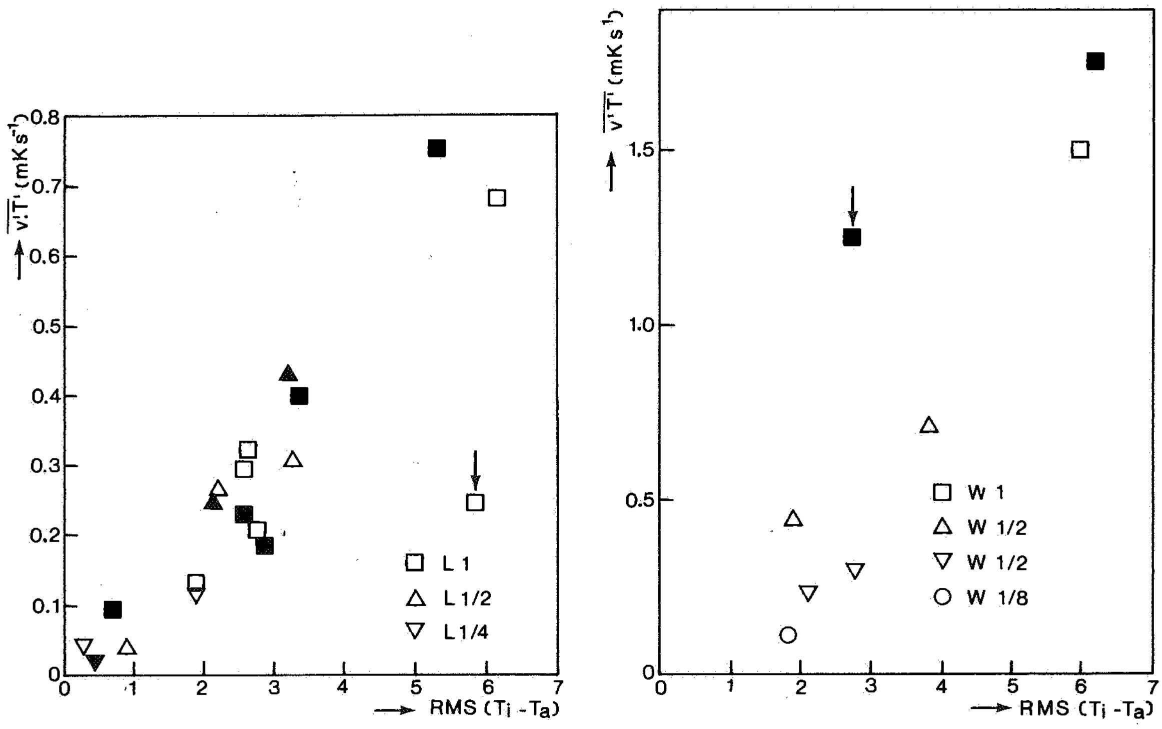

a. leeside ventilation b. windwardside ventilation

Fig. 4.10. The real fluctuative term ($\overline{v'.T'}$) related to the effective exchange term (RMS (T_i - T_a)) both for leeside and windwardside ventilation. Vertical scale is arbitrary.(Filled and open symbols represent measurements with door of compartment open and closed respectively).

surements. From figure 4.10 it may be concluded that the possible presence of a static pressure difference during the measuring periods with the door opened, does not significantly influence the fluctuative exchange through the window opening.

In figure 4.11, the sum of the fluctuative and the convective contribution is compared with the effective exchange, again the vertical axis is arbitrary. Because the term $\overline{v'.T'}$ will be always positive, the absolute value of $\overline{v}.\overline{T}$ is added to it. The number of measuring periods in figure 4.11 is somewhat smaller than that in figure 4.10 because $\overline{T}_m$ and so $\overline{T}$ (relation 4.9) could not be determined during some measuring periods. In figure 4.11a some of the measurements with the door open (filled symbols), do not deviate significantly from those with the door closed. In these points the ratio of the terms $\overline{v}.\overline{T}$, and $\overline{v'.T'}$ i.e. of the convective and fluctuative term, varies between 0.08 and 0.9, with

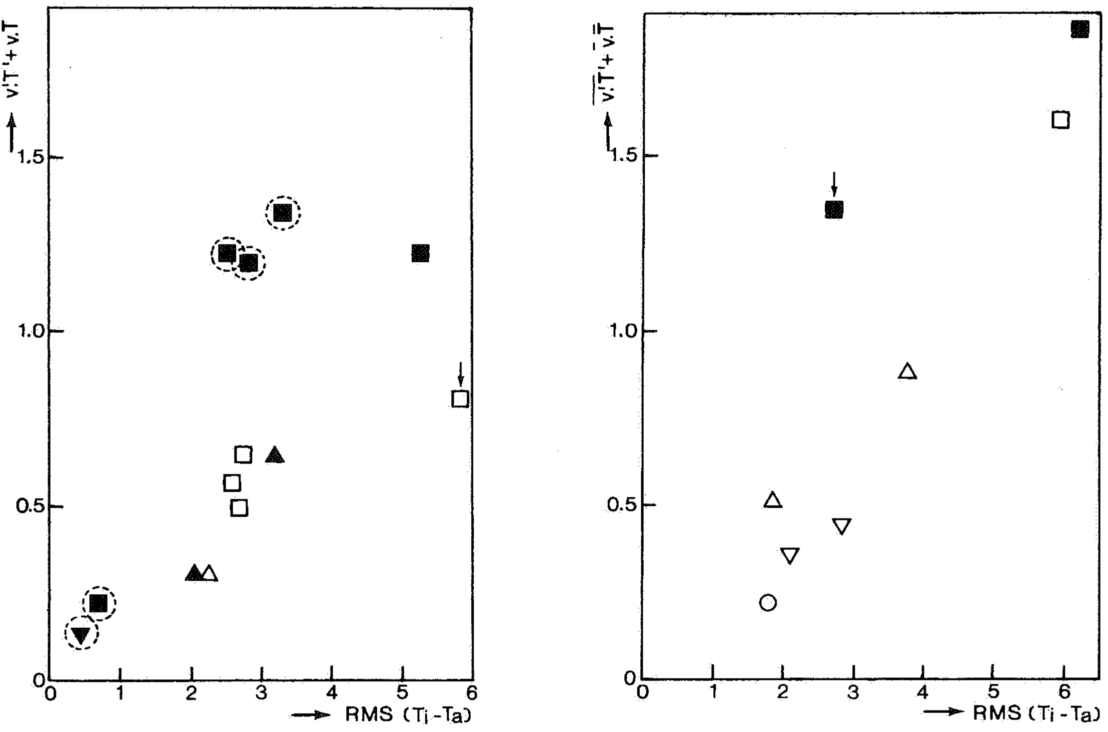

a. leeside ventilation b. windwardside ventilation

Fig. 4.11. The sum of the fluctuative and static exchange ($\overline{v'.T'} + \overline{v}.\overline{T}$) related to the effective exchange term (RMS(T_i - T_a)) both for leeside and windwardside ventilation.
Vertical scale is arbitrary.
(Filled and open symbols as indicated in fig. 4.10).

an average of 0.4. Again there is a good correlation with the effective exchange RMS(T_i - T_a). The conclusion may be, then, that the exchange is never ideally fluctuating in these measuring points (door closed and some points door open), but it is the sum of a major fluctuative and a minor convective term. This convective term varies randomly during the measuring periods. The other measurements with open door (measuring points marked by encircling them) have a significantly higher ratio of $\overline{v}.\overline{T}$ and $\overline{v'.T'}$. The ratios in these points vary from about 2. up to about 5. The ratio of the increased total exchange $\overline{v'.T'} + \overline{v}.\overline{T}$ in the encircled measuring points and the other points is about 2. So, when there is a static pressure difference over the window opening the exchange due to pressure fluctuations and the exchange due to the static pressure difference (difference between encircled and non encircled points) are in

the same order of magnitude.
The addition of the convective term is of less importance for windwardside ventilation (figure 4.11b) as it was for leeside ventilation (figure 4.11a). The ratio of $\overline{v}.\overline{T}$ and $\overline{v'.T'}$ is much lower, it is only 0.07 for the fully open window and somewhat higher for smaller window openings. No difference can be observed between the measurements with open or closed door. The exchange due to fluctuations (figure 4.10b) is much higher than that for leeside ventilation (figure 4.10b), which confirms the conclusions of section 4.3.3. The extra exchange due to convective exchange is much lower than it was for leeside ventilation and it seems as if the exchange due to a static pressure difference is also of less importance.

5. Radiation

5.1. INTRODUCTION

The term radiation is commonly used to indicate energy transfer by electromagnetic waves. In a description of greenhouse climate, two wave length regions are of interest: first the shortwave, solar irradiation with wavelengths between about 0.2 and 5 μm and second that of the longwave, thermal radiation with wavelengths between about 5 and 60 μm. General aspects of the radiation in these regions have already been investigated extensively; they are described in various handbooks (Robinson, 1966, Kondratyev, 1969, Coulson, 1975).

The shortwave irradiation is the primary driving force for fotosynthesis and the main incoming energy flow available at no cost in the greenhouse. Due to the fact that the greenhouse cover is not completely transparent, the shortwave radiation is always reduced. This is a disadvantage for a greenhouse in periods when there is a shortage of light or when the greenhouse has to be heated during the day. In moderate climates, like the Dutch climate these periods mostly coincide during winter.

The interaction of the shortwave radiation with the greenhouse cover is of importance for greenhouse production and for greenhouse climate. The transmission factor determines which amount of the incoming radiation is available for plant growth. The same amount also contributes directly to the energy balance of the canopy. The radiation absorbed by the greenhouse cover contributes directly to the energy balance of the cover.

In the first part of this chapter the interaction of the shortwave radiation and the greenhouse cover is discussed. The contribution to the energy balances is discussed in chapter 7. Longwave thermal radiation exchange takes place between the surfaces of all bodies that are opaque for this kind of radiation. In the Netherlands glass is the most common covering material for greenhouses. Since glass is opaque for radiation in the wavelength region higher than 3 μm, the glass cover acts as a radiation shield between the greenhouse interior and its environment. So the interaction with the cover is an important part of the longwave radiative exchange, which in his turn is a part of the energy balances. Therefore the longwave radiative exchange will be discussed in the second part of this chapter, while again the contribution to the energy balances is discussed in chapter 7.

5.2. SHORTWAVE RADIATION

Shortwave radiation originating from the sun, reaches the earth surface as direct radiation and as diffuse radiation. The direct radiation comes from the unobscured sun's disc and the diffuse radiation from the sky. Both types of shortwave radiation are geometrically and spectrally different (Taylor, 1941, Hull, 1954). For a description of the transmission through the greenhouse cover, especially the geometrical differences are of interest. The spectral differences are not significant in the interaction with the cover, because the spectral properties of the glass and most transparant materials do not vary very much in the region where the spectra of the direct and diffuse radiation differ.

The geometry of the direct radiation can be characterized by means of the position of the sun, which is a function of the time and date. From the sun's position and the greenhouse geometry the transmission of the greenhouse cover for direct radiation can be calculated if the optical properties of the glass are known.

Diffuse radiation is omnidirectional and the distribution of the radiation over the sky very strongly depends on the atmospheric conditions. The two most pronounced instances are a clear sky and an overcast one and for both conditions several distributions are suggested in literature (section 3.2.2). The variation of the distribution due to the variation in atmospheric conditions is a complicating effect if the transmission for diffuse radiation is to be determined for any time. For the two ideal conditions the transmission can be calculated and the difference in transmissivity for the clear sky and the completely overcast situation yields the variation of the diffuse transmissivity on days which are partly clouded.

5.2.1. *Transmission for direct radiation*

In the Netherlands as in most countries with moderate climates, direct radiation is only a small part of the global radiation, especially in winter. The climatological irradiation at De Bilt (The Netherlands) for both diffuse and direct radiation is given by Slob (1982) (averaged over a measuring period of 10 years). From his data figure 5.1 was constructed, showing the average ratio of the diffuse and the global radiation for each month. In the months November through January, which are the most critical ones for greenhouse crops due to the light conditions, the diffuse radiation covers almost 75 percent of the global radiation. These figures, as mentioned before, are climatological averages. At any moment they may vary very fast and over a wide range. Especially on partly clouded days these variations may be very strong. So, though the transmission for direct radiation seems to be of minor importance to the average situation, it is of vital importance to the situation from moment to moment.

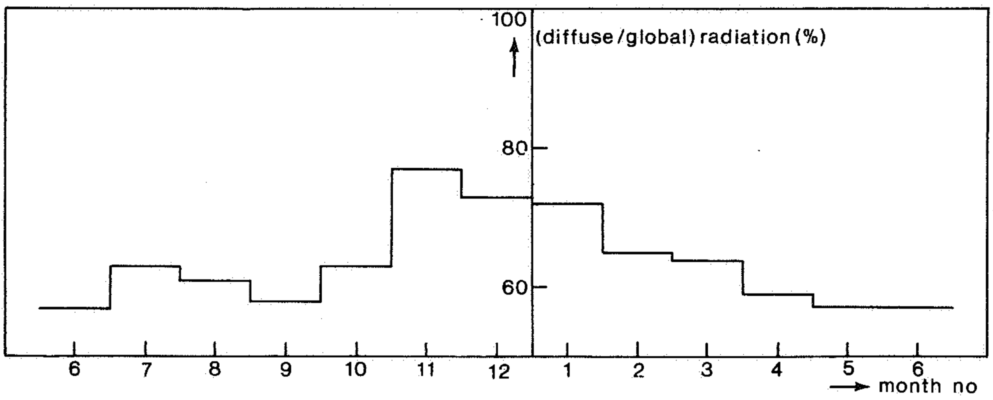

Fig. 5.1. The climatological ratio of diffuse and global radiation at De Bilt (The Netherlands) (after Slob, 1982).

In the literature, the transmission of the greenhouse cover for direct radiation has been discussed for many years. As early as in 1812 MacKenzie studied the optimal shape of a glasshouse. He concluded that a hemisphere would give maximum light transmission. Only for winter gardens, as used in the 18th and 19th century, this shape can be realized. For commercial greenhouses it is not practicable. The shape and orientation of a greenhouse, however, considerably affects the light transmission and this problem has been explored by several authors.

Seemann (1952) used the measurements of the transmission through differently sloped single glass panes to calculate the transmission of differently oriented single span greenhouses.

Whittle and Lawrence (1959) and Lawrence (1963) showed that the transmission of single span greenhouses depends on the type of greenhouse and the orientation. They concluded that for all types under winter conditions an East-west orientation of the greenhouse ridge was advantageous.

Los (1962) reported on measurements of the average transmission factor in the case of four different multispan greenhouses. The solarimeters in the greenhouse were moved over a rail system to integrate the irradiation in space. Only some final numerical results of the transmissivity were presented.

Nissen (1962) built a transmission model for differently shaped single span greenhouses without constructive parts. The impact of the optical properties on the transmission factor, especially that of diffusing materials, were also investigated by Nisen and coworkers (Deltour and Nisen, 1970, Baseaux, Deltour and Nisen, 1973).

Edwards (1963) and Edwards and Lake (1964, 1965), just like Whittle and Lawrence (1959), reported measurements of the transmission of single span glasshouses. Contrary to the earlier authors they observed the transmission during a period of several years. They showed the variation of the transmission during the year at some different locations in England. A distinction was made between the direct and diffuse component of the radiation.

Manbeck and Aldrich (1967) tried to determine the transmission of differently shaped greenhouses in an analytical way.

Stoffers (1967) was the first to develop a complete transmission model for a multispan greenhouse for both direct and diffuse light. He combined the transmissivity of the glass panes with the shadowing of the constructive parts and calculated the transmission factor for various roof slopes and greenhouse orientations as a function of time and season.

Bowman (1970) concentrated on the transmission factor for diffuse light and calculated it by an analytical method.

Smith and Kingham (1970) and Kingham and Smith (1971) in the first paper presented transmission measurements of two differently oriented single span greenhouses and in the second one a calculation method.

Kirsten (1973) examined the transmission of a large number of differently shaped single span greenhouses together with some multispan types by means of a transmission model.

Harnett (1973, 1974) confirmed the conclusions of previous authors by measurements of the transmission of some different types of greenhouses.

Kozai (1977), Kozai and Kimura (1977) and Kozai, Goudriaan and Kimura (1978) presented an extensive transmission model for both direct and diffuse radiation for different types of greenhouses. In their model, the transmissivity could be calculated as a place dependent factor that is also a function of time and season. This factor was used to calculate the photosynthesis in the greenhouse.

Recently, Critten (1983) presented a transmission model, related to that of Kozai et al (1978).

In the present study we are interested in the transmission of large multispan greenhouses at any moment for direct and diffuse radiation. Both the transmission through the glass cover with constructive parts and the absorption in the glass have to be determined, because these amounts of energy are terms in the energy balances of glasshouse components. Because none of the models mentioned before exactly meets the requirements, and because these models were not accessible to easy adaptation, a completely new model was developed. In the following sections this model will be constructed.

5.2.1.a. *Reflectance, transmittance and absorption of a single transparent sheet.*

The reflectance, transmittance and absorption of a single plan parallel glass pane (thickness D, index of refraction n) can be calculated applying the well known Fresnel equations.

The incident beam of radiation $\vec{I}_i$ can be considered as composed of two components: one polarized parallel ($\vec{I}_{pa}$) and another polarized perpendicular ($\vec{I}_{pe}$) to the plane of incidence. (The plane of incidence is the plane containing the incident ray $\vec{I}_i$ and the normal $\vec{N}$ to the surface). For the two components single surface reflectivities $R_{pa,pe}$ are given by the Fresnel equations (e.g. Corson and Lorraine, 1962, Jefimenko, 1969):

$$R_{pa} = \{\frac{\sin(i - i')}{\sin(i + i')}\}^2 \qquad (5.1.a)$$

$$R_{pe} = \{\frac{\tan(i - i')}{\tan(i + i')}\}^2 \qquad (5.1.b)$$

with

i angle of incidence with respect to the normal $\vec{N}$
i' angle in the glass with respect to the normal $\vec{N}$
(sin i/sin i' = n)

If we write

$$C = n\cos i' = (n^2 - \sin^2 i)^{\frac{1}{2}} \qquad (5.2)$$

then 5.1a and b can be rewritten:

$$R_{pa} = \{\frac{\cos i - c}{\cos i + c}\}^2 \qquad (5.3.a)$$

$$R_{pe} = \{\frac{n^2\cos i - c}{n^2\cos i + c}\}^2 \qquad 5.3.b)$$

In a planparallel glaspane two surfaces have to be considered. Moreover multiple reflection between the two surfaces will have its impact on the reflection and transmission. The single surface reflectivities 5.3.a and b can be corrected to encounter for this effect using the method described by e.g. Chamberlain et al. (1966):

$$R'_{pa} = R_{pa} + R_{pa}(1 - R_{pa})^2.Q/(1 - R^2_{pa}Q) \qquad (5.4.a)$$

$$R_{pe} = R_{pe} + R_{pe}(1 - R_{pe})^2Q/(1 - R^2_{pe}Q) \qquad (5.4.b)$$

Q is a factor which accounts for the absorption by the glas:

$$Q = \exp\{ - 2C_{abs}D'\}$$

with

C_{abs}: the power absorption coefficient (m^{-1})
D' the optical pathlength in the glass (m)

D' equals to:

$$D' = D/\{1-(\sin i/n)^2\}^{\frac{1}{2}} \qquad (5.6)$$

The total reflection R from the glasspane depends on the polarization of the radiation. For the most simple case of unpolarized light:

$$R = (R'_{pa} + R'_{pe})/2 \qquad (5.7)$$

In figure 5.2 this R is given as function of the angle of incidence i.
The transmission τ of the glaspane follows from:

$$\tau_{pa} = (1 - R'_{pa})^2 Q^{\frac{1}{2}}/(1 - R'_{pa}Q) \qquad (5.8.a)$$

$$\tau_{pe} = (1 - R'_{pe})^2 Q^{\frac{1}{2}}/(1 - R'_{pe}Q) \qquad (5.8.b)$$

τ can be composed from τ_{pa} and τ_{pe}. Again for the most simple case of unpolarized light:

$$\tau = (\tau_{pa} + \tau_{pe})/2 \qquad (5.9)$$

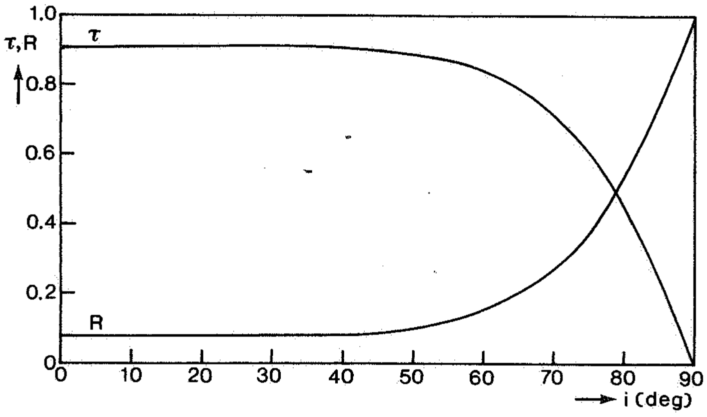

Fig. 5.2. Transmittance τ and reflectance R for a single transparent plan-parallel sheet as function of the angle of incidence i.
Thickness 0.004 m, refrective index 1.5, power absorption coef.2.5m^{-1})

In figure 5.2 this τ is given as function of the angle of incidence i. The total absorption a of the flass follows from:

$$a = 1 - \tau - R \qquad (5.10)$$

5.2.1.b. Geometry of direct light and glass cover

The geometry of the direct light is given by the position of the sun which is defined by its azimuth α_s relative to the North-south direction and its altitude γ (figure 5.3). These quantities are both functions of the time t and the angle δ between the axis of the earth and the connection line between sun and earth. The position on the earth is given by the latitude β. The altitude and the azimuth can be deducted from the solar time t_s, the declination δ and the latitude β according to the well-known relations (e.g. Robinson, 1966):

$$\upsilon = (t_s - 12)\ 360/24 \qquad (5.11)$$

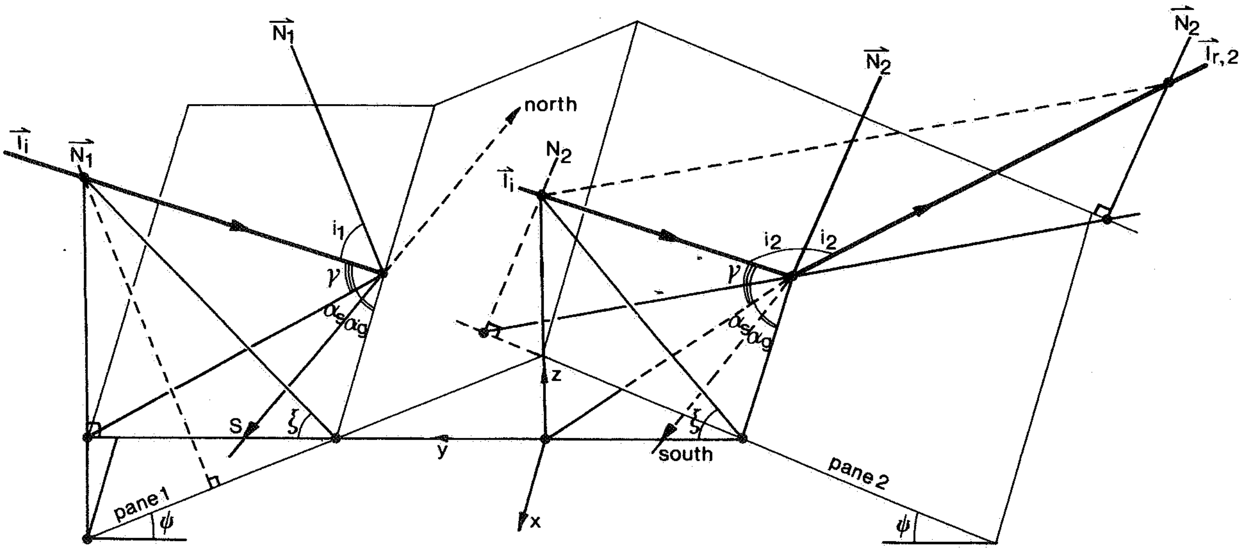
$\vec{N}_1$
$\vec{I}_i$
$\vec{N}_1$
north
N_2
$\vec{I}_i$
$\vec{N}_2$
$\vec{N}_2$
$\vec{I}_{r,2}$
i_1
γ
α_s α_g
i_2
i_2
γ
α_s α_g
z
S
ξ
y
ξ
south
pane 2
pane1
ψ
x
ψ

Fig. 5.3. Solar azimuth α_s, altitude γ and greenhouse orientation α_g, and angles of incidence $i_1 = i(\vec{I}_i,\vec{N}_1)$ and $i_2 = i(\vec{I}_i,\vec{N}_2)$

which translates the solar time t_s to a time angle υ relative to noon time,

$$\sin\gamma = \sin\beta\sin\delta + \cos\beta\cos\delta\cos\upsilon \tag{5.12}$$

and

$$\sin\alpha_s = \cos\delta\sin\upsilon/\cos\gamma \tag{5.13}$$

If the earth arbit around the sun is assumed to be a perfect circle then the declination can be approximated by:

$$\delta = 23.45\ \sin\{(D - 81)\ 360/365\} \tag{5.14}$$

with

D: serial number of the year of the considered day.

From relation 5.12 and 5.11 the sunset and sunrise can be found by substituting $\sin\gamma = 0$ for these moments:

$$\text{sunrise: } t = 12 - (24/360)\cos^{-1}(-\tan\beta\tan\delta) \tag{5.15a}$$

$$\text{sunset : } t = 12 + (24/360)\cos^{-1}(-\tan\beta\tan\delta) \tag{5.15b}$$

The geometry of the glass cover of a large multispan greenhouse is given by the roof slope ψ, the span width W and the orientation α_g of the greenhouse to the North-south direction (figure 5.13). We assume that the ridges of the greenhouse are in a horizontal plane. With an easy adaptation also a slope between the ridges and the horizontal plane can be introduced but this would be of small practical importance.

For the calculation of the incident angles on the glasspanes a co-ordination system has to be chosen. The most convenient choice is a system with the x-axis along the ridge, the xy-plane horizontally and so the z-axis vertically. Then the incident direct light $\vec{I}_i$ can be considered as a vector in this co-ordinate system:

$$\vec{I}_i = I_o(\vec{k}_x I_x + \vec{k}_y I_y + \vec{k}_z I_z)$$

$$= I_o(\vec{k}_x\cos\gamma\cos(\alpha_s + \alpha_g) + \vec{k}_y\cos\gamma\sin(\alpha_s + \alpha_g) + \vec{k}_z\sin\gamma) \tag{5.16}$$

The normals $\vec{N}$ on the two glasspanes can also be given:

$$\vec{N}_1 = N_o(\vec{k}_y \sin\psi + \vec{k}_z \cos\psi) \qquad (5.17a)$$

$$\vec{N}_2 = N_o(-\vec{k}_y \sin\psi + \vec{k}_z \cos\psi) \qquad (5.17b)$$

according to:

$$\vec{I}.\vec{N} = |I||N|\cos i(\vec{I},\vec{N}) \qquad (5.18)$$

the angles of incidence i on the two glasspanes can be calculated:

$$i_1 = i(\vec{I}_i,\vec{N}_1) = \cos^{-1}\{\cos\gamma\sin(\alpha_s + \alpha_g)\sin\psi + \sin\gamma\cos\psi\} \qquad (5.19a)$$

$$i_2 = i(\vec{I}_i,\vec{N}_2) = \cos^{-1}\{-\cos\gamma\sin(\alpha_s + \alpha_g)\sin\psi + \sin\gamma\cos\psi\} \qquad (5.19b)$$

Not only the angle of incidence of the incident light is of interest, also the angle of incidence of the reflected light may be important (section 5.2.1.c.). If we consider the reflection on glasspane 2 the direction of the reflected light $\vec{I}_{r,2}$ will have to be found first. Therefore a x,p,q co-ordinate system is introduced with the q axis along the normal $\vec{N}_2$:

$$p = y\cos\psi + z\sin\psi \qquad (5.20a)$$

$$q = -y\sin\psi + z\sin\psi \qquad (5.20b)$$

The components of the incident light along this co-ordinate system can be expressed as:

$$\vec{I}_i = I_o[\vec{k}_x\{\cos\gamma\cos(\alpha_s + \alpha_g)\} + \vec{k}_p\{\cos\gamma\sin(\alpha_s + \alpha_g)(\cos\psi + \sin\gamma\sin\psi)\} + \\ + \vec{k}_q\{-\cos\gamma\sin(\alpha_s + \alpha_g)(\sin\psi + \sin\gamma\cos\psi)\}] \qquad (5.21)$$

The reflected light then is:

$$\vec{I}_{r,2} = I_o[\vec{k}_x\{-\cos\gamma\cos(\alpha_s + \alpha_g)\} + \vec{k}_p\{-\cos\gamma\sin(\alpha_s + \alpha_g)(\cos\psi + \sin\gamma\sin\psi)\} + \\ + \vec{k}_q\{-\cos\gamma\sin(\alpha_s + \alpha_g)(\sin\psi + \sin\gamma\cos\psi)\}] \qquad (5.22)$$

Which in the x,y,z system is:

$$\vec{I}_{r,2} = I_o[\vec{k}_x\{ - \cos\gamma\cos(\alpha_s + \alpha_g)\} + \vec{k}_y \{ - \cos\gamma\sin(\alpha_s + \alpha_g)(\cos2\psi - \sin\gamma\sin2\psi)\}$$

$$+ \vec{k}_z\{ - \cos\gamma\sin(\alpha_s + \alpha_g)(\sin2\psi - \sin\gamma\cos2\psi)\}] \qquad (5.23)$$

The angles of incidence of this reflected light with the wo glasspanes can again be calculated from the vectorial product (relation 5.18):

$$i(\vec{I}_{r,2},\vec{N}_1) = \cos^{-1}\{\cos\gamma\sin(\alpha_s + \alpha_g)(- \sin\psi\cos2\psi - \cos\psi\sin2\psi) +$$

$$+ \sin\gamma(\cos\psi\cos2\psi - \sin\psi\sin2\psi)\} \qquad (5.24a)$$

and

$$i(\vec{I}_{r,2},\vec{N}_2) = \cos^{-1}\{\cos\gamma\sin(\alpha_s + \alpha_g)(\sin\psi\cos2\psi - \cos\psi\sin2\psi) +$$

$$+ \sin\gamma(\cos2\psi\cos\psi + \sin\psi\sin2\psi) \qquad (5.24b)$$

Since (see relations 5.19b and 5.24b):

$$\sin\psi\cos2\psi - \cos\psi\sin2\psi = - \sin\psi \qquad (5.25a)$$

and

$$\cos2\psi\cos\psi + \sin\psi\sin2\psi = \cos\psi \qquad (5.25b)$$

the angles of incidence $i(\vec{I}_1,\vec{N}_2)$ and $i(\vec{I}_{r,2},\vec{N}_2)$ are equal. This is in full accordance with the fact that all glasspanes 2 are parallel!
The angles of incidence between the reflected light by surface 1 and surface 1,2 can be found in an analogous way.

5.2.1.c. Interaction with the glass cover

Though the reflection and transmission through the glasspanes has to be considered in the x,y,z co-ordinate system, the projection in the y-z plane may show what kind of interactions are taking place. The angle determining this interaction is the angle ξ in the y-z plane between the incident ray and the y-axis (figure 5.3):

$$\xi = \tan^{-1}(\vec{I}_z/\vec{I}_y) \qquad (5.26)$$

We have to distinguish between two kinds of interactions between the incident radiation and the glasspanes. The first kind of interaction takes place if the angle ξ is smaller than ψ (roof slope). The the light enters through e.g. pane 1 and penetrates the greenhouse through several roof surfaces before reaching the ground. Following the interaction, the reflection against pane 2 also contributes to the transmission.

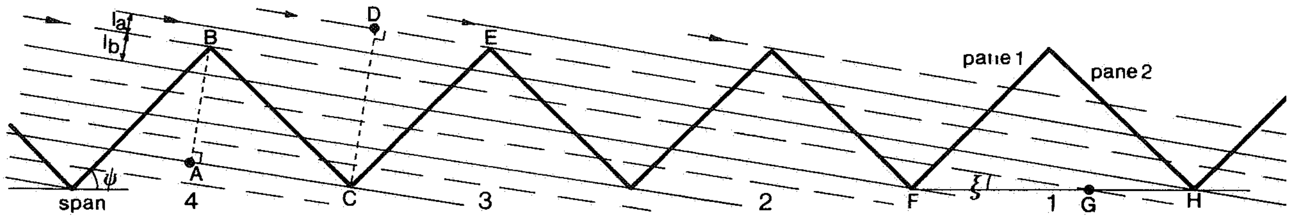

Fig. 5.4. Light transmission for the region $\xi < \psi$.

In figure 5.4 an example of this situation has been given. The light entering the greenhouse definitely via the horizontal plane through the gutters over one span FH (figure 5.4) is divided by ridge B in two parts l_a and l_b. The parts l_a and l_b can be calculated in the triangles ABC and DEC. Since angle ACB equals to $\psi - \xi$, angle DEC equals $\psi + \xi$, the length BA to $2(l_a + l_b) + l_b$ and the length DC to $3(l_a + l_b) + l_b$, l_a and l_b can be calculated:

$$l_a = l_o\{3\sin(\psi + \xi) - 4\sin(\psi - \xi)\} \qquad (5.27a)$$

$$l_b = l_o\{-2\sin(\psi + \xi) + 3\sin(\psi - \xi)\} \qquad (5.27b)$$

with l_o equals the length BC (or EC).

It is clear that the numerical factors in relation 5.27 depend on the number of intercepting spans. In the example 3 spans are involved. The number of interacting spans m can be found from the angles ψ and ξ according to

$$m = \mathrm{Int}\{\tfrac{1}{2}(1 + \tan\psi/\tan\xi)\} \qquad (5.28)$$

which means that m is the smallest integer of the expression between the brackets. The general expressions for l_a and l_b are:

$$l_a = l_o\{m\sin(\psi + \xi) - (m + 1)\sin(\psi - \xi)\} \tag{5.29a}$$

$$l_b = l_o\{(1 - m)\sin(\psi + \xi) + m\sin(\psi - \xi)\} \tag{5.29b}$$

The total transmission of the glass τ_g is composed from the contributions of l_a and l_b. In the example (figure 5.4):

$$\begin{aligned}\tau_g = \{ & l_a(\tau_{i,1}(R_{i,2} + \tau_{i,1} \cdot \tau_{i,2} \cdot R_{i,2} + (\tau_{i,1} \cdot \tau_{i,2})^2) + \\ & + l_b(\tau_{i,1}(R_{i,2} + \tau_{i,1} \cdot \tau_{i,2} \cdot R_{i,2} + (\tau_{i,1} \cdot \tau_{i,2})^2 R_{i,2} + \\ & + (\tau_{i,1} \cdot \tau_{i,2})^3))\}/(l_a + l_b)\end{aligned} \tag{5.30}$$

The number of spans affects the contribution of the reflection against pane 2 and the final transmission through the panes.
In general the transmission through m spans (m given by relation 5.28) can be written as:

$$\begin{aligned}\tau_g = \{ & l_a \tau_{i,1}(R_{i,2} \sum_{s=0}^{m-2} (\tau_{i,1} \cdot \tau_{i,2})^s + (\tau_{i,1} \cdot \tau_{i,2})^{m-1}) \\ & + l_b \cdot \tau_{i,1}(R_{i,2} \sum_{s=0}^{m-1} (\tau_{i,1} \cdot \tau_{i,2})^s + (\tau_{i,1} \cdot \tau_{i,2})^m)\}/(l_a + l_b)\end{aligned} \tag{5.31}$$

with l_a and l_b given by relation 5.29a and b respectively.

Analogous to the transmission, the absorption A in glass pane 1 and 2 can be found:

$$A_1 = a_1\{l_a \sum_{s=0}^{m-1} (\tau_{i,1} \cdot \tau_{i,2})^s + l_b \sum_{s=0}^{m} (\tau_{i,1} \cdot \tau_{i,2})^s\}/(l_a + l_b) \tag{5.32a}$$

$$A_2 = a_2\{l_a \sum_{s=0}^{m-2} (\tau_{i,1} \cdot \tau_{i,2})^s + l_b \sum_{s=0}^{m-1} (\tau_{i,1} \cdot \tau_{i,2})^s\}/(l_a + l_b) \tag{5.32b}$$

If the angle ξ becomes larger than the angle ψ (roof slope) the light enters the greenhouse through both glasspanes (figure 5.5).

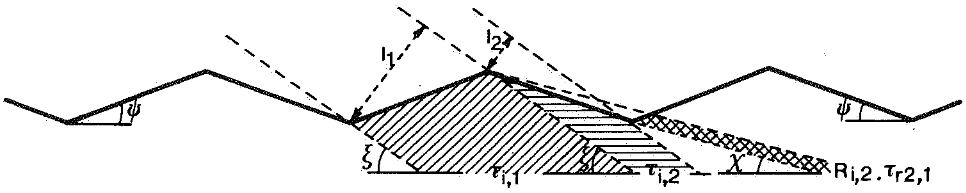

Fig. 5.5. Light transmission for the region $\xi > \psi$.

Not only the light transmitted directly through the glasspane, but some light reflected by glasspane 2 (figure 5.5) too will contribute to the incoming energy. If ξ increases this reflected beam becomes more and more horizontal, and will interact with an increasing number of spans. This continues until the reflected beam will be exactly horizontal, so theoretically it interacts with an infinite number of pans. In this case the angle ξ will equal 2ψ. If ξ increases further, the reflected beam will be directed upwards and will interact with a decreasing amount of spans until the moment of zero interaction for ξ equals 3ψ. The regions $\psi<\xi<2\psi$ and $2\psi<\xi<3\psi$ will be discussed separately.

In the region $\psi<\xi<2\psi$ (figure 5.6) the reflected beam is directed downwards and intersects an increasing amount of spans when ξ increases. The light

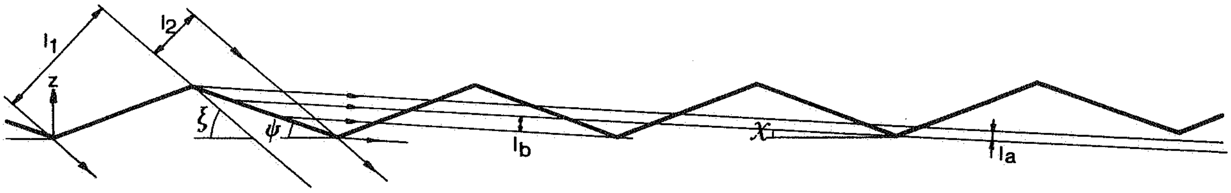

Fig. 5.6. Light transmission for the region $\psi<\xi<2\psi$.

penetrating one span is divided into a part l_1, primarily falling on pane 1 and l_2 primarily falling on pane 2. The light transmitted directly ($\tau_{i,1,2}$) is easily found:

$$\tau_{i,1,2} = (l_1\tau_{i,1} + l_2\tau_{i,2})/(l_1 + l_2) \tag{5.33}$$

The contribution to this transmission by the light, reflected by pane 2 is more complex. Parts l_b (figure 5.6) of the reflected beam fall through one span and a part l_a only falls through some part of a spanwidth. The number m of spans involved is determined by the angle χ between the reflected light and the y-axis. This angle χ equals:

$$\chi = |2\psi - \xi| \tag{5.34}$$

The number of spans can be found analogous to relation 5.18:

$$m = \mathrm{Int}\{\tfrac{1}{2}(1 + \tan\psi/\tan\chi)\} \tag{5.35}$$

The dimensions l_1 and l_2 are found to be:

$$l_1 = l_o\sin(\xi + \psi) \tag{5.36a}$$

$$l_2 = l_o\sin(\xi - \psi) \tag{5.36b}$$

l_a and l_b can be found analogous to relation 5.29a and b:

$$l_a = l_o\{m\sin(\xi - \psi) - (m - 1)\sin(3\psi - \xi)\} \tag{5.37a}$$

$$l_b = l_o\{-\sin(\xi - \psi) + \sin(3\psi - \xi)\}$$

The transmission of the reflected light $\tau_{r2,1,2}$ from pane 2 can be found analogous to relation 5.31, if we take into consideration that the part l_b has to be counted for an increasing amount of spans:

$$\tau_{r2,1,2} = \{l_aR_{i,2} \cdot \tau_{r2,1}(R_{r2,2}\sum_{s=0}^{m-2}(\tau_{r2,1} \cdot \tau_{r2,2})^s + (\tau_{r2,1} \cdot \tau_{r2,2})^{m-1}) +$$

$$+ l_b R_{i,2} \cdot \tau_{r2,1}(R_{r2,2} \sum_{s=o}^{m-3} (\sum_{n=o}^{s} (\tau_{r2,1} \cdot \tau_{r2,2})^n) +$$

$$+ \sum_{s=o}^{m-2} (\tau_{r2,1} \cdot \tau_{r2,2})^s)\}/(l_1 + l_2) \qquad (5.38)$$

The total transmission of the glass τ_g then equals:

$$\tau_g = \tau_{i,1,2} + \tau_{r2,1,2} \qquad (5.39)$$

Theoretically, the absorption by the panes 1 and 2 has to be considered as the sum of the absorption of the light transmitted directly and the absorption of the light reflected by pane 2. In practice the energy absorbed from the reflected beam will be so sparse that it can be neglected. So the absorption in the panes 1 and 2 practically equals a_1 and a_2 (section 5.20.1a) respectively.

In the region $2\psi<\xi<3\psi$, the reflected beam is directed upwards and with increasing ξ, the number of intersecting spans decreases. The angle χ is still captured by relation 5.34 and the number of intersecting spans by relation 5.35. The parts l_a and l_b have to be reconsidered (figure 5.7), but l_1 and l_2 are still captured by relations 5.36a and b respectively.

$$l_a = l_o\{ -(m - 1)\sin(\xi - \psi) + m\sin(3\psi - \xi)\} \qquad (5.40a)$$

$$l_b = l_o\{\sin(\xi - \psi) - \sin(3\psi - \xi)\} \qquad (5.40b)$$

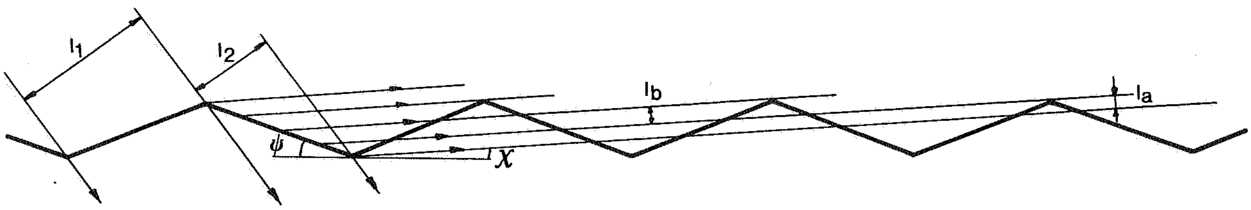

Fig. 5.7. Light transmission for the region $2\psi<\xi<3\psi$.

The transmission of the light reflected from pane 2 is only contributed by the reflection from pane 2 downwards:

$$\tau_{r2,1,2} = \{l_a R_{i,2} \cdot \tau_{r2,1} \cdot R_{r2,2} \cdot \sum_{s=0}^{m-1} (\tau_{r2,1} \cdot \tau_{r2,2})^s +$$

$$+ l_b R_{i,2} \cdot \tau_{r2,1} \cdot R_{r2,2} \sum_{s=0}^{m-2} (\sum_{n=0}^{s} (\tau_{r2,1} \cdot \tau_{r2,2})^s)\}/(l_1 + l_2) \quad (5.41)$$

The directly transmitted part of the light is still given by relation 5.33 and the total transmission by relation 5.39. For the absorption the results mentioned in the foregoing ξ region still hold true.

The last region that has to be mentioned is the region between 3ψ and 90^0. Here the reflection on pane 2 does not account for the total transmission any more, so $\tau_{r2,1,2}$ is equal to zero and the total transmission is equal to $\tau_{i,1,2}$ as given by relation 5.33.

If the roof slope ψ were larger than 30^0, it could be that the reflected light from pane 1 intersects the neighbouring spans. From figure 5.8 it can be seen that for the light reflected by pane 1 the angle with the y-axis equals to $180^0 - 2\psi - \xi$. If this angle becomes smaller than ψ then intersection of this light with the neighbouring span occurs. So if $\xi > 180 - 3\psi$ light reflected from pane 1 has to be considered for the total transmission. Multi-

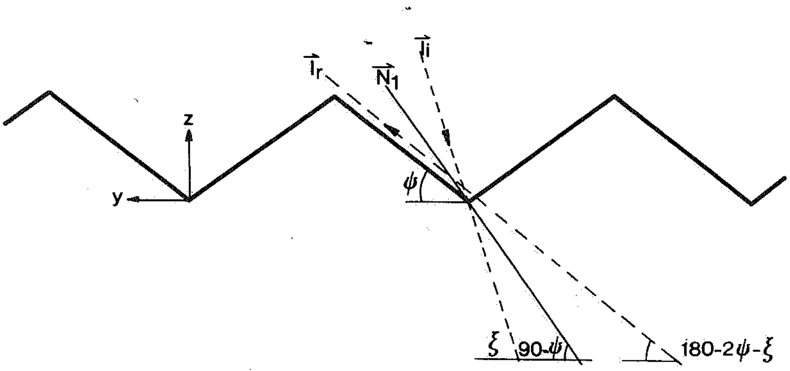

Fig. 5.8. Light transmission if $\psi > 30^0$.

span greenhouses however very rarely have roof slopes larger than 30°. And if so the interaction would only be with one span which results in a very low contribution to the total light transmission. So the contribution of this reflection to the light transmission can be neglected and the possible occurrence of this case does not require our further attention.

5.2.1.d. Light interception by the opaque roof parts

The opaque roof parts act as shadowing bodies. In consequence they will have their impact on the total transmission of the greenhouse cover. When a Venlo type multispan greenhouse cover is considered we can distinguish the shadowing bodies in ridges, gutters and glazing bars. The ridges and gutters are parallel to the x-axis (figure 5.3) so the light interception is determined by the angle ξ only. The glazing bars have a component along the y- and z-axis so their impact has to be discussed separately.

The ridges and gutters are considered together because of their parallel arrangement. Moreover there are situations in which their shadows coincide and a combined approach facilitates a description of these situations. The geometry of the ridges and gutters is defined by their heights H_r and H_g and their widths W_g and W_r respectively together with the spanwidth W_s. Only symmetrical spans are taken into account. To define their position relative to the glasspanes, the height of the gutter or ridges is given according to figure 5.9 above and below the intersection line of the glass. To approximate their geometry more precisely, also their width at the lower and upper side is defined as well.

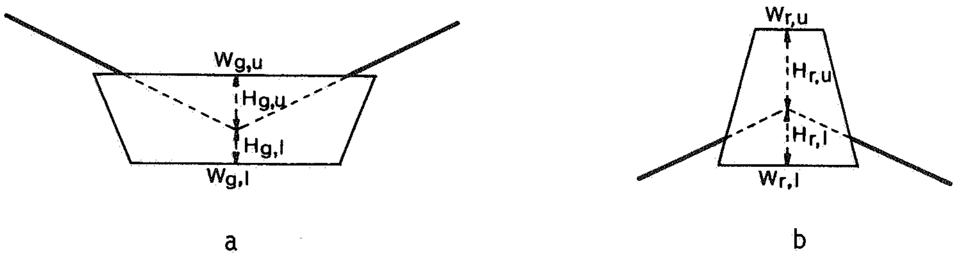

Fig. 5.9. Geometry of the gutter (a) and the ridge (b)

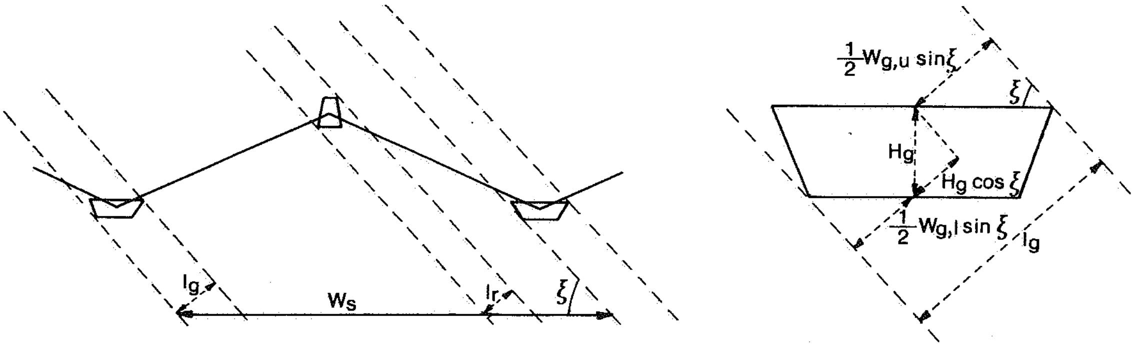

a. interception by the gutter-ridge system b. interception by the gutter

Fig. 5.10. Light interception by the gutter and ridge.

The light interception will be calculated according to figure 5.10, in analogy with the calculations in section 5.2.1.c. The part of the lightbeam intercepted by the ridge l_r and the gutter l_g is found to be:

$$l_r = H_r\cos\xi + \tfrac{1}{2}(W_{r,l} + W_{r,u})\sin\xi \qquad (5.42a)$$

$$l_g = H_g\cos\xi + \tfrac{1}{2}(W_{g,l} + W_{g,u})\sin\xi \qquad (5.42b)$$

If the angle ξ is wider than the slope of the side of the gutter given by $\tan^{-1}\{H_g/(\tfrac{1}{2}(W_{g,u} - W_{g,l})\}$ then:

$$l_g = H_g\cos\xi + W_{g,u}\sin\xi \qquad (5.42a)$$

or for the ridge

$$l_r = H_r\cos\xi + W_{r,l}\sin\xi \qquad (5.43b)$$

if $\xi > \tan^{-1}\{H_r/(\tfrac{1}{2}(W_{r,l} - W_{r,u}))\}$.

The transmission of the ridge gutter system τ_{rg} equals:

$$\tau_{rg} = 1 - (l_g + l_r - l_c)/(W_s\sin\xi) \qquad (5.44)$$

with l_c a correction on the sum of l_g and l_r if the shadows of the gutter and the ridge coincide.

The coincidence of the shadows of the ridge and the adjacent gutter for increasing ξ will start at some angle ξ_1 indicated by the situation at the left side in figure 5.11 and will be finished at the angle ξ_2 indicated by the situation at the right side. The coincidence of the shadows of the non-adjacent ridges and gutters can be treated in an analogous way.

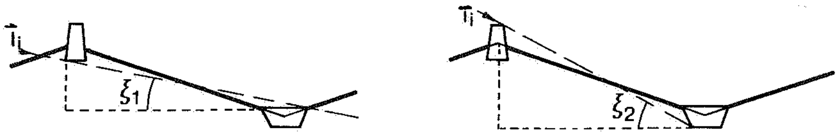

Fig. 5.11. Starting and finishing point of the coincidence of the ridge and gutter shadows for a neighbouring ridge and gutter.

The angles ξ_1 and ξ_2 can easily be found:

$$\xi_1 = \tan^{-1}\{(W_s\tan\psi - 2H_{r,l} - 2H_{g,u})/(2m - 1)W_s + W_{r,l} + W_{g,u})\} \qquad (5.45a)$$

and

$$\xi_2 = \tan^{-1}\{(W_s\tan\psi + 2H_{r,u} + 2H_{g,l})/((2m - 1)W_s - W_{r,u} - W_{g,l})\} \qquad (5.45b)$$

with m = 1 for the adjacent ridge gutter. For non-adjacent ridge gutters, m is the number of spans inbetween given by

$$m = 1 + \mathrm{Int}\{\tfrac{1}{2}(\tan\psi/\tan\xi)\} \qquad (5.46)$$

The shadows will coincide completely in the ξ region indicated by figure 5.12. The angles ξ_3 and ξ_4 are found in the manner of ξ_1 and ξ_2.

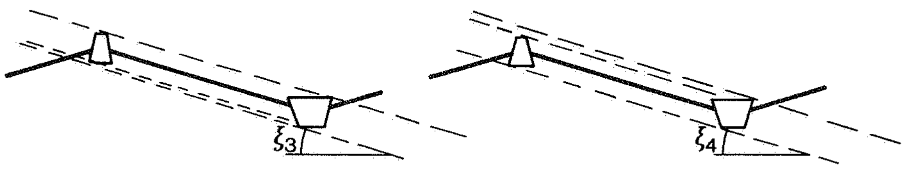

Fig. 5.12. Region of complete coincidence of the ridge gutter shadow.

$$\xi_3 = \tan^{-1}\{(W_s\tan\psi + 2H_{r,u} - 2H_{g,u})/((2m - 1)W_s - W_{r,u} + W_{g,u})\} \qquad (5.47a)$$

and

$$\xi_4 = \tan^{-1}\{(W_s\tan\psi - 2H_{r,l} + 2H_{g,l})/((2m - 1)W_s + W_{r,l} - W_{g,l})\} \qquad (5.47b)$$

It is assumed that the shadow of the ridge is smaller than that of the gutter, which will be true for normal type greenhouses. From the above it follows that three regions of the angle ξ have to be considered for the coincidence of the shadows. The most simple one is the region

$$\xi_3<\xi<\xi_4 \qquad (5.48a)$$

then

$$l_c = l_r \qquad (5.48b)$$

In the regions $\xi_1<\xi<\xi_3$ and $\xi_4<\xi<\xi_2$ there is only partial coincidence. The correction factor l_c can be found from figure 5.13 in both regions:

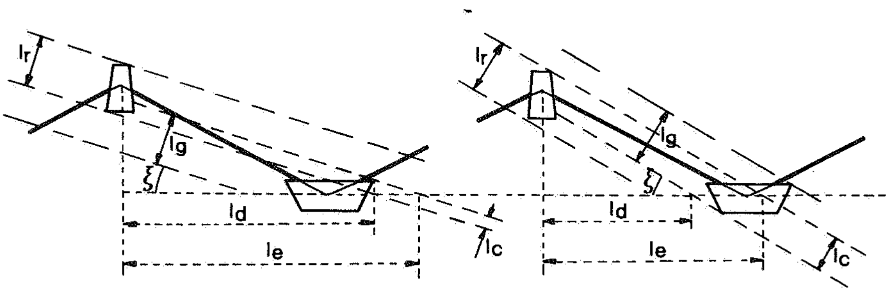

$\xi_1<\xi<\xi_3$ $\xi_4<\xi<\xi_2$

Fig. 5.13. Partial coincidence of the ridge gutter shadows.

For the region $\xi_1<\xi<\xi_3$: (5.49a)

$$l_c = (l_e - l_d)\sin\xi \qquad (5.49b)$$

with:

$$l_e = \tfrac{1}{2}((2m - 1)W_s + W_{g,u}) + H_{g,u}/\tan\xi \qquad (5.49c)$$

and

$$l_d = (\tfrac{1}{2}W_s\tan\psi - H_{r,l})/\tan\xi - \tfrac{1}{2}W_{r,l} \qquad (5.49d)$$

For the region $\xi_4<\xi<\xi_2$: (5.50a)

$$l_c = (l_e - l_d)\sin\xi \qquad (5.50b)$$

with:

$$l_e = (\tfrac{1}{2}W_s\tan\psi + H_{r,u})/\tan\xi + \tfrac{1}{2}W_{r,u} \qquad (5.50c)$$

and

$$l_d = \tfrac{1}{2}((2m - 1)W_s - W_{g,l}) - H_{g,l}/\tan\xi \qquad (5.50d)$$

Here m has the same meaning as in relation 5.45 and 5.46. Its value is 1 for the adjacent ridge gutter and equals the number of spans inbetween for non-adjacent ridge gutters as given by relation 5.46.

The light interception by the glazing bars (only bars in the plane of the roof perpendicular to the ridge gutter are taken into account) is not only affected by the angle ξ, but also by the angle in the x-z plane, between the light and the x-axis:

$$\nu = \tan^{-1}(\vec{I}_z/\vec{I}_x) \qquad (5.51)$$

This is illustrated in figure 5.14 showing the projection of a bar on a horizontal plane and the matching shadow pattern for the situation in which the angle ξ is wider than the roofslope ψ.
The light interception can be calculated from the area of ADEFCB which is the sum of the area ADCB and DEFC. The areas are determined by the distances between the parallel lines and their lengths and these quantities can be determined from the geometry. The length L_1 of area ADCB equals:

$$L_1 = \{(\tfrac{1}{2}W_s + H_s/\tan\xi)^2 + (H_s/\tan\nu)^2\}^{\frac{1}{2}} \qquad (5.52a)$$

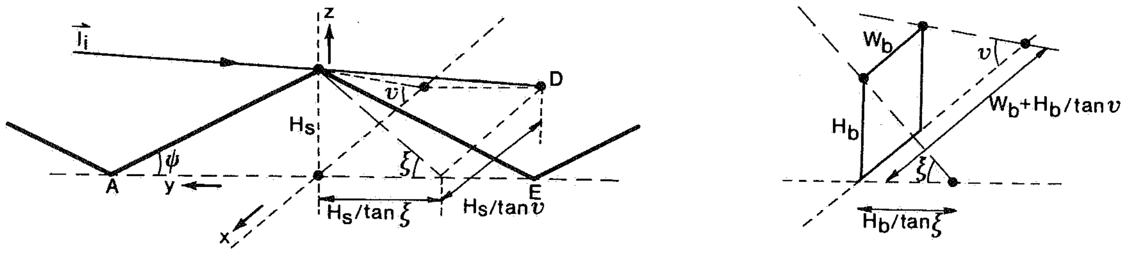
$\vec{I}_i$
z
D
v
Hs
ψ
A
y
ξ
E
x
Hs/tan ξ
Hs/tan v
Wb
v
Hb
Wb+Hb/tan v
ξ
Hb/tan ξ

a) projection of a bar on
a horizontal plane

b) dimensions of the shadow
of a bar with height H_b
and width W_b

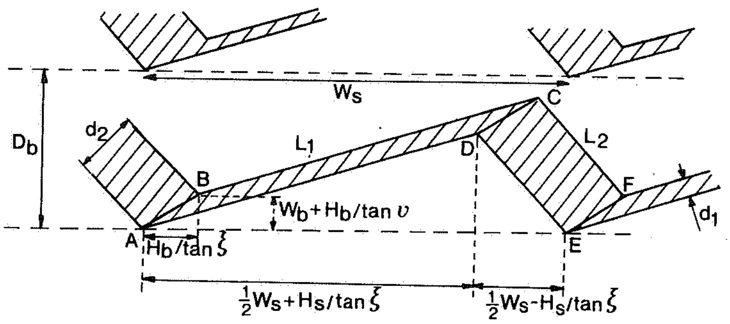
Ws
Db
d2
L1
C
L2
B
D
F
Wb+Hb/tan v
d1
A
Hb/tan ξ
E
½Ws+Hs/tan ξ
½Ws-Hs/tan ξ

c) Shadow pattern of the bars on the ground of the situation under a) and b)

Fig. 5.14. Light interception by a bar for $\xi>\psi$.

and of DECF

$$L_2 = \{(\tfrac{1}{2}W_s - H_s/\tan\xi)^2 + (H_s/\tan\nu)^2\}^{\frac{1}{2}} \qquad (5.52b)$$

The distance d_1 equals

$$d_1 = AB \ . \ \sin(\angle BAD) \qquad (5.53a)$$

with

$$AB = \{(H_b/\tan\xi)^2 + (W_b + H_b/\tan\nu)^2\}^{\frac{1}{2}} \qquad (5.53b)$$

and

$$\angle BAD = \tan^{-1}\{\frac{W_b + H_b/\tan\nu}{H_b/\tan\xi}\} - \tan^{-1}\{\frac{H_s/\tan\nu}{\frac{1}{2}W_s + H_s/\tan\xi}\} \qquad (5.53c)$$

The distance d_2 can be found in an analogous way:

$$d_2 = EF\sin\angle(FED) \tag{5.54a}$$

with

$$EF = \{(H_b/\tan\xi)^2 + (W_b + H_b/\tan\nu)^2\}^{\frac{1}{2}} = AB \tag{5.44b}$$

and

$$\angle FED = 180 - \tan^{-1}\{\frac{W_b + H_b/\tan\nu}{H_b/\tan\xi}\} - \tan^{-1}\{\frac{H_s/\tan\nu}{\frac{1}{2}W_s - H_s/\tan\xi}\} \tag{5.54c}$$

The light transmission of the bars τ_b for this situation ($\xi>\psi$) is:

$$\tau_b = 1 - (L_1d_1 + L_2d_2)/(D_b.W_s) \tag{5.55}$$

If the angle ξ is smaller than ψ then the shadow of the ridge point of the bars exceeds one span. A shadow pattern for this situation is given in figure 5.15. The widths of the shadow and the projection measures are still given by the angle ξ and ν as indicated by figure 5.14.
In this ξ-region, the shadows of the bars in the two sides of the roof interfere, since they cross each other. This means that the transmission of the bars τ_b is the product of the transmission for the bars at each side of the roof:

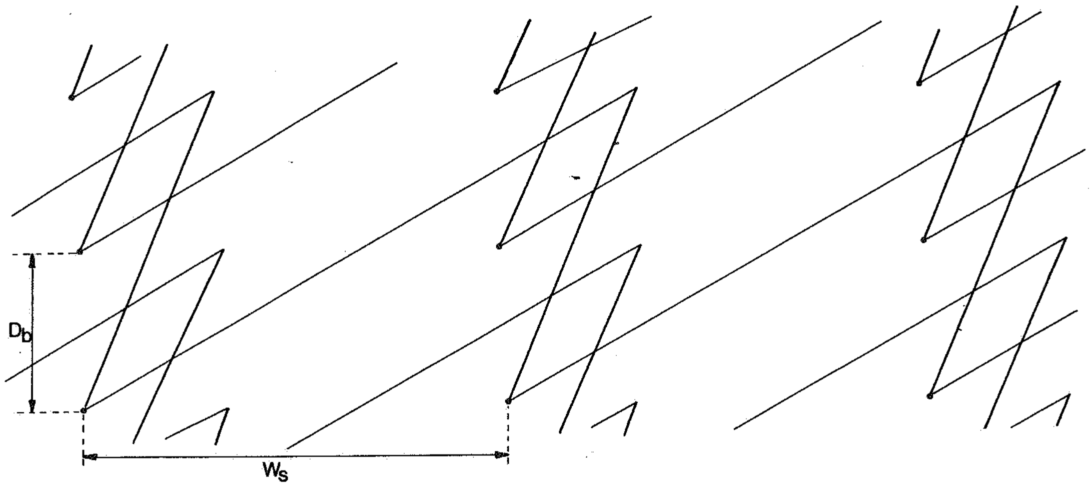

Fig. 5.15. Shadow pattern of the bars on the horizontal plane for $\xi<\psi$.

$$\tau_b = (1 - L_1.d_1/D_b.W_s) \; . \; (1 - L_2.d_2/D_b.W_s) \qquad (\xi<\psi) \tag{5.56}$$

with

L_1, d_1, L_2 and d_2 defined by relations 5.52 to 5.54.

5.2.1.e. Total transmission for direct radiation

The total transmission τ_{tot} of a large multispan greenhouse can now be composed by combination of the transmission of the glass cover τ_g, that of the ridge gutter system τ_{rg} and that of the glazing bars τ_b:

$$\tau_{tot} = \tau_g \tau_{rg} \tau_b \tag{5.57}$$

So for direct light the total transmission can be calculated from relation 5.57 as a function of the solar position, the greenhouse location and geometry. This complex task was performed by combining the calculations from section 5.2.1.a to d in a computer program. This program was fed into the small computer that served as the controller of the data logging system that we used for the energy balance experiments (chapters 6 and 7). So in an easy way a set of transmission data could be generated previous to the experiments which could be handled together with the measurements.

Some results of the computations will be discussed, following a visualization of the apparent solar orbit in figure 5.16 for an observer at a location with latitude β. The observer is in the origin 0 and the apparent solar orbit is a circle with its centre moving along a line with an angle β towards the north-south axis. The time angle ν is defined by the position of the sun on its circular orbit, the solar orientation α_s is the projection of this angle on the horizontal plane. Only on the equinox, the observer is in the centre of the circular orbit and the sunrise-sunset are exactly on the east-west line. So the altitude at noon γ_n on this day equals 90-β; the solar orientation or azimuth varies between - 90 to + 90^o. This range of the azimuth decreases from the equinox to the winter solstice and increases from the equinox to the summer solstice.

The greenhouse is situated in the origin 0; when its orientation is 0^o, the ridges and gutters are directed north-south and when the orientation is 90^o or - 90^o the greenhouse is oriented east-west. The x,y,z co-ordinate system

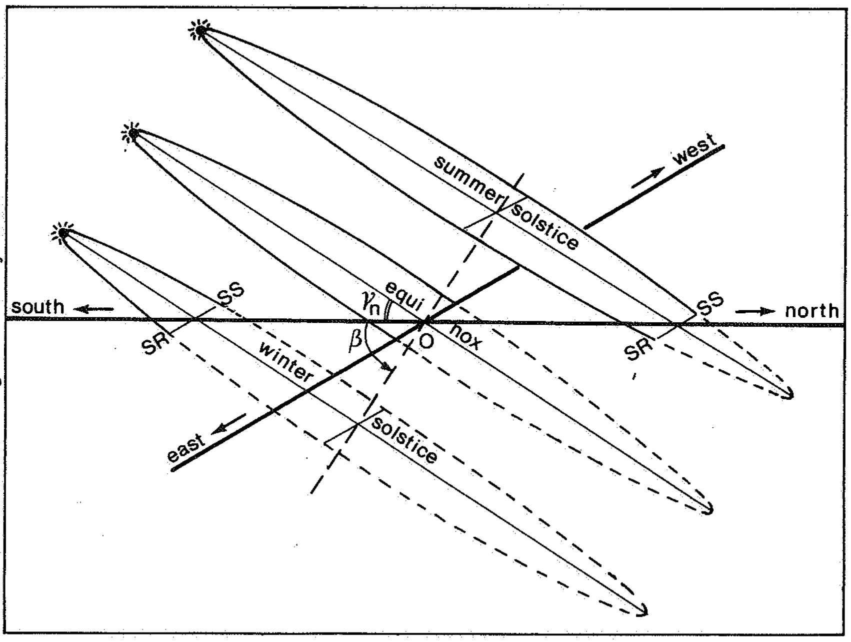

Fig. 5.16. Apparent solar orbit for an observer at a place with latitude β.

and the angle ξ are chosen according to figure 5.3.

When first the transmission of the glass for some day, e.g. the equinox, is observed, some characteristics are evident. This transmission is represented in figure 5.17a for glass with a refraction index of 1.5, a power absorption coefficient of 2.5 m^{-1} and a thickness of 0.004 m. The roof slope of the observed glass cover is 22^0 and its orientation is north-south.
From sunrise (SR) until the moment the angle ξ equals the roof slope ψ (figure 5.4), the light enters the greenhouse through the east-facing glasspane only. The glasspane facing west receives irradiation when $\xi>\psi$ (figure 5.5), some of which is transmitted directly and some after reflection. In figure 5.17b the angle ξ is equal to ψ at 8.20 a.m. and as can be seen, from this moment onwards, the pane facing west, or pane 2, contributes to the light transmission. The reflected light gives a contribution $\tau_{r2,1,2}$ (dotted area in figure 5.17a). The reflected light covers just one span if ξ equals $2\psi - \tan^{-1}(\frac{1}{3}\tan\psi)$, which is 36.3^0 in this case. This occurs at 9.20 a.m. and the contribution of the reflected light $\tau_{r2,1,2}$ is maximal at this moment. When it is in interaction with more and more spans, $\tau_{r2,1,2}$ decreases and it is directed horizontally when $\xi = 2\psi$ at 9.80 a.m. Then a very small contribution of $\tau_{r2,1,2}$ is left and this decreases still more when the reflected light

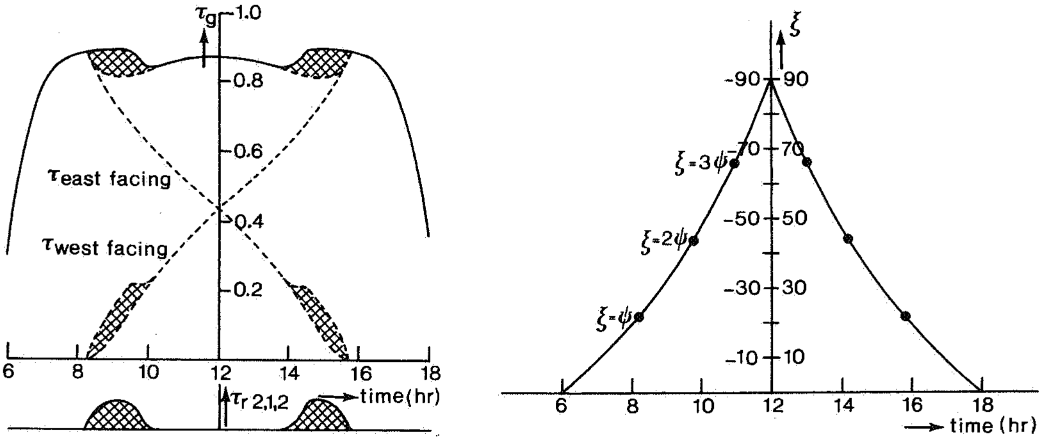

a. Course of the various components of the glass transmission during the day.

b. Course of the angle ξ during the day.

Fig. 5.17. Glass transmission τ_g and angle ξ as function of time at 22 March (equinox) for a north-south oriented multispan glasshouse with a roof slope of 22^0, located at a latitude of 52^0 (north) (glass thickness 0.04 m, refraction index 1.5, power absorption coefficient 2.5m^{-1}).

directed upward (figure 5.7) interacts with a decreasing number of spans. It covers one span again when $\xi = 2\psi + \tan^{-1}\{\frac{1}{3}\tan\psi\}$, which is 51.6^0 at 10.25 a.m. and $\tau_{r2,1,2}$ disappears until the moment ξ equals 3ψ at 10.90 a.m. In figure 5.17 the contribution of $\tau_{r2,1,2}$ to τ_g is dotted. In the afternoon the above repeats itself for the reflected light from the east facing pane.

The transmission of the ridge-gutter combination τ_{rg} shows the characteristics as described in section 5.2.1.d. In figure 5.18 this transmission is given for a north-south oriented glasshouse at winter solstice. It is calculated with a very small time step (0.01 hr) to detect small details. At 10.06 a.m. the angle ξ equals the roof slope $\psi(22^0)$. As can be seen there is a bump on the transmission line, showing that the ridge shadow coincides with that of the gutter. From 9.84 a.m. to 9.97 a.m. the shadow of the ridge partly coincides and gently moves into that of the gutter, then from 9.97 to 10.15 a.m. the ridge shadow completely coincides with that of the gutter and finally from 10.15 to 10.27 a.m. the ridge shadow gently moves out. The shadow of the gutter is greater than that of the ridge which is visible at 10.00 a.m.

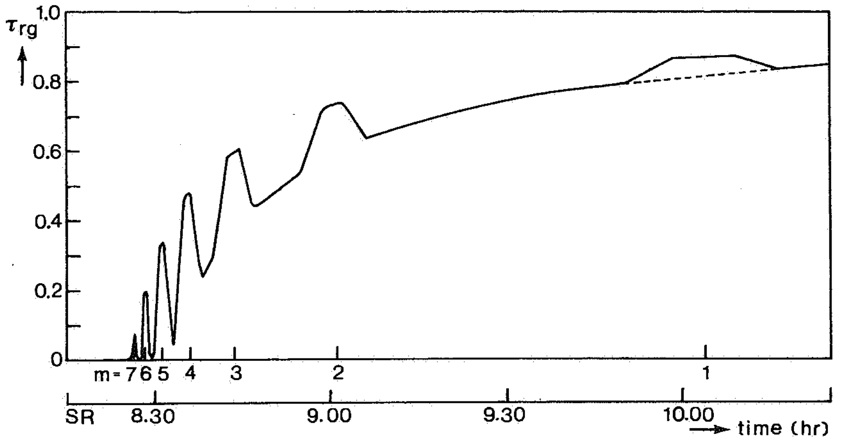

Fig. 5.18. Transmission of the ridge gutter combination for a north-south oriented glasshouse on 21 december.
Dimensions of the ridge and gutter:
height ridge : lower side 0.03 m
upper side 0.029 m
width ridge : lower side 0.02 m
upper side 0.02 m
height gutter: lower side 0.04 m
upper side 0.045 m
width gutter : lower side 0.22 m
upper side 0.22 m
span width : 3.2 m
roof slope : 22^0

The gutter shadow is $1-\tau_{r,g}$ at this moment which is 0.135 and the combination shadow would be 0.2. Not only the coincidence of the shadows of the adjacent ridge and gutter can be observed (m = 1) but also that of ridge gutter combinations with more spans inbetween, even up to 7. Before the moment the first small peak can be observed, the angle ξ is so small that the ground area is completely in the shadow. (When gutter and ridge shadows do not coincide in this period anyhow they cover the ground area completely).

For some characteristic days the transmission of the glass τ_g, the ridge gutter combination τ_{rg} and the bars τ_b is combined into the total transmission τ_{tot}. They are given both for a north-south and for an east-west oriented glasshouse with the measures given in figure 5.17. Because of the symmetry of these two orientations in the morning and afternoon, only the transmissions

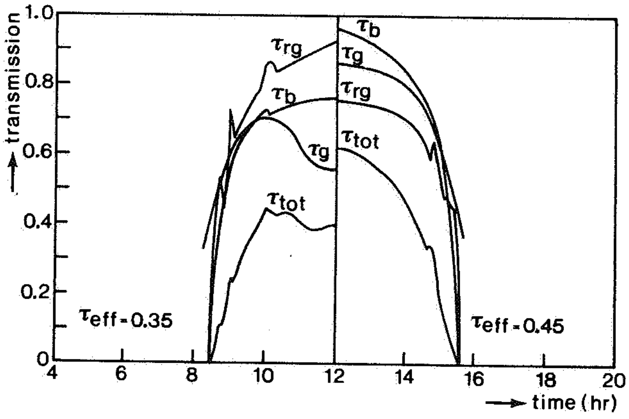

Fig. 5.19a. Transmission at 21 December (winter solstice)

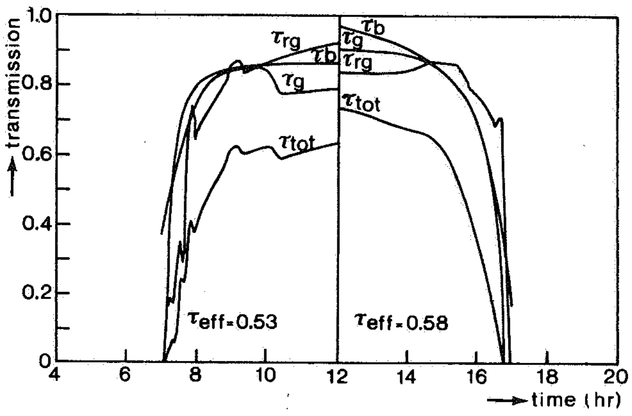

Fig. 19b. Transmission at 21 February

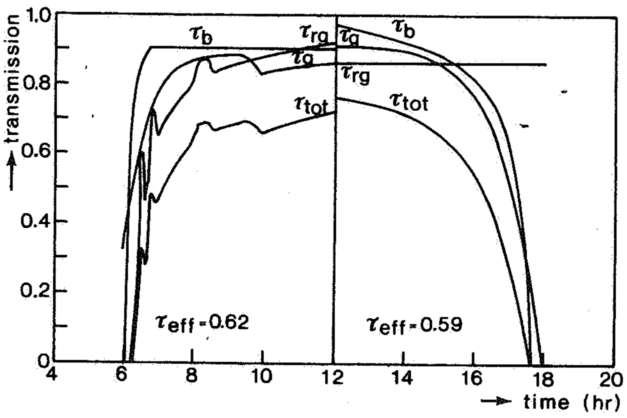

Fig. 5.19c. Transmission at 22 March (equinox)

Fig. 5.19d. Transmission at 21 April

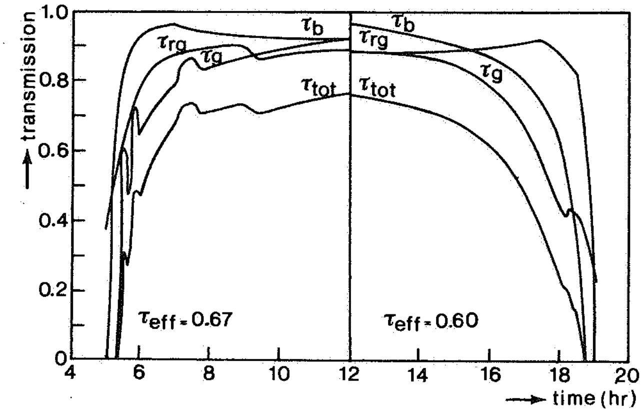

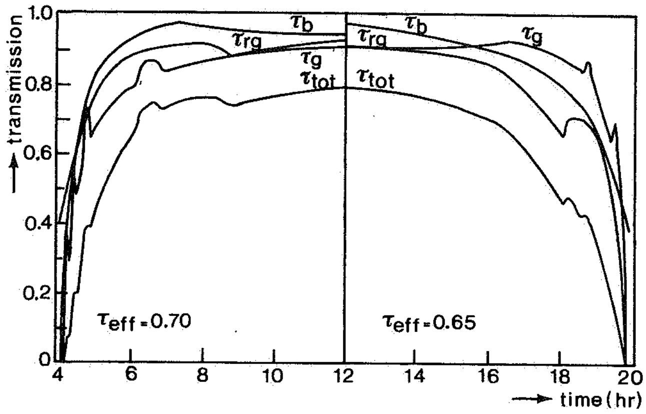

Fig. 5.19e. Transmission at 21 June (summer solstice)

Fig. 5.19. Transmission of the glass (τ_g), the ridge gutter system (τ_{rg}), the bar system (τ_b) and the total transmission (τ_{tot}) of a multispan Venlo greenhouse with roofslope $\psi = 22^0$, at a latitude β of 52^0 (north) for both a north-south (at left) and an east-west orientation (at right) at various dates. Dimensions of the constructive parts are given in figure 5.7, the glass properties are given in figure 5.16.

during half a day are given.
At winter solstice (figure 5.19a), the total transmission for direct light of the north-south oriented glasshouse is rather small, only about 0.4 during about half a day. In the east-west house the transmission is higher during most of the day. The difference in the transmission for both orientations can be quantified by defining an effective time average transmission τ_{eff} as the quotient of the integrated radiation flux density ϕ''_r during one day inside and outside the greenhouse:

$$\tau_{eff} = \frac{\int_{sunrise}^{sunset} \tau_{tot}(t)\phi''_r(t)dt}{\int_{sunrise}^{sunset} \phi''_r(t)dt} \qquad (5.58)$$

The radiation flux density ϕ''_r (Wm^{-2}) of the direct radiation was assumed to be a function of time according to a half-sine between sunrise and sunset. In winter time, the effective transmission of an east-west oriented glasshouse is higher than that of a north-south oriented one and this is reverse during the equinox and later on. This conclusion is confirmed by other publications (see section 5.2.1). The characteristics of the glass transmission for the north-south oriented glasshouse as shown in figure 5.17 and those of the transmission of the ridge gutter combination (figure 5.18) can be found again for the different days, though less detailed because of the greater time step (0.1 hr). For the east-west oriented glasshouse the same kind of characteristics can be observed. At winter solstice the highest solar altitude is about 15^o for the latitude of 52^o. So the angle ξ has a maximum value of 15^o at noon and the irradiation never hits the north facing glass pane directly for this orientation. Some peaks in $\tau_{r,g}$ of non-adjacent ridge gutters can be observed. At 21 February for the east-west orientation, ξ will rise up to about 27^o and it can be seen that the coincidence of the ridge gutter shadows takes quite some time. Also the contribution of $\tau_{r2,1,2}$ will begin to be important to this orientation.
At the equinox the ridge gutter transmission is constant for the east west oriented glasshouse during the whole day. The plane of the solar orbit is just going through the gutter on this day (figure 5.16) so the angle ξ is constant during the whole day and equal to $90-\beta$. Inbetween the equinox and summer solstice the sun passes over the east-west line with increasing alti-

tude. For the north-south oriented glasshouse this causes a maximum of the transmission of the barsystem and, for the east west orientation, a maximum of the transmission of the ridge gutter.

Experimental verification of the calculated transmission for direct light is very difficult. The transmission for direct light is a quantity composed by the sun-lit and shadow regions in the greenhouse. So in an experimental determination the factor has to be integrated over a large area at every moment and at the same time a very good separation in the direct and diffuse component of the radiation has to be achieved inside as well as outside the greenhouse. Moreover, some of the direct light will be scattered on the cover and detected as diffuse light inside, though it has to be counted as a contribution by the direct light. However the model for the calculation of the transmission for direct light can be applied to calculate the transmission for diffuse light (section 5.2.2) and this latter result can be related to measurements of the transmission for diffuse light.

Although there is no adequate way to compare the results of the present model with experiments, they can be compared with the results of some transmission models from the literature. The two models that can be considered as relevant to our purpose are that of Stoffers (1967, 1971) and that of Kozai et al. (1978).

Stoffers presents his results in some tables of the glass transmission on several days and tables of the transmission of the construction (ridge gutter system and bars) on one day, the 2^o of January. All results are calculated at hourly intervals. The dimension of his opaque elements, in his model represented as cylinders, and the properties of the glass, were used as input to the present model. The results are reproduced in figure 5.20a for the glass transmission τ_g on some days and in figure 5.20b for the transmission of the ridge gutter combination τ_{rg} and of the bars τ_b. The various transmission values are in close agreement with each other.

In the publication of Kozai et al. (1978), there is one graph i.e. representation of the space averaged transmission of a multispan greenhouse located in Osaka (latitude 34, 65^o) on 22 December. Unfortunately only total transmission values were provided. In the present model the data of the greenhouse investigated by Kozai et al. were fed together with measures of opaque elements of a standardized Venlo greenhouse. In figure 5.21 the calculations of the present model for two orientations together with the results of Kozai

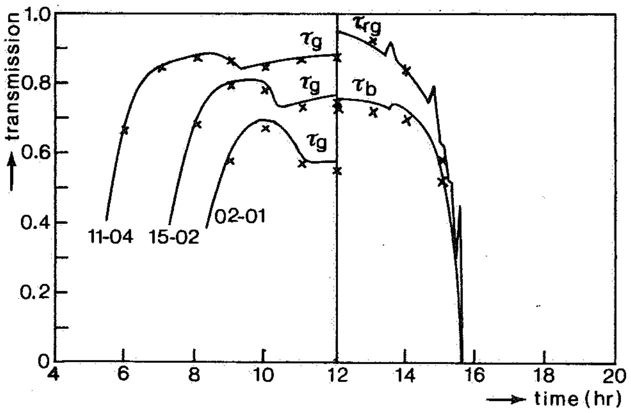

a. Glass transmission τ_g at various dates

b. Transmission of the ridge gutter system τ_{rg} and the bar system τ_b at January 2

Fig. 5.20. Comparison of results of the present model (solid lines) with that of Stoffers (1967) (crosses). Roof slope 20^0, orientation north-south, latitude 52^0 north.

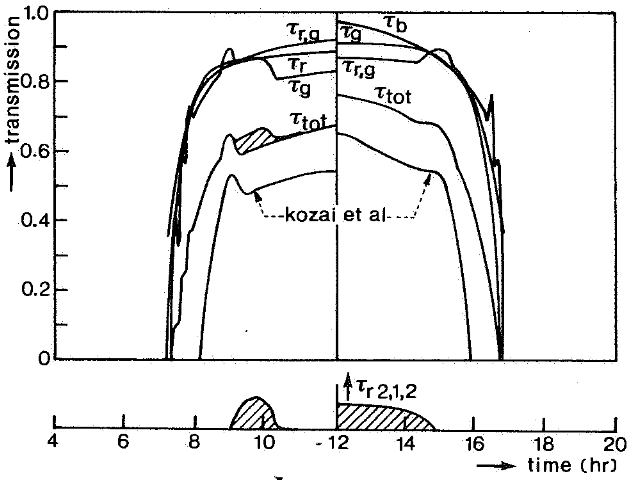

Fig. 5.21. Comparison of results of the present model with that of Kozai et al. (1978). Roof slope 24.6^0, orientation north-south (left) and east-west (right), latitude 34.65^0 north (Osaka), date 22 December.

et al. are given. Probably the opaque elements in the model of Kozai et al. are very extensive because during a long period from sunrise to about 8.15 a.m. no light penetrates into the north-south greenhouse and the transmission is significantly lower during the day for both orientations. The small peak of the transmission at 9.00 a.m. is identical for both models which means that the calculation of the angles of incidence agree fairly well. The relatively large decrease of the transmission of the Kozai model just after the peak at 9.00 a.m. however might be caused by the neglection of the contribution of the reflected light by the west facing pane ($\tau_{r2,1,2}$). If this contribution is neglected in the present model (dotted area) then the shapes of the transmission curves are similar.
Though the results of the present model agree with that of models reported in literature, it is not identical to these models. It differs in the description of the light penetration in the greenhouse. In our model detailed information is obtained on the time dependent course of the various components of the light transmission which is needed for the description of the momentaneous greenhouse climate.

5.2.2. *Diffuse radiation*

The diffuse or sky radiation is the radiant energy in the short wave region that is received from the complete hemisphere, except for the direct solar irradiation. The main mechanism for the sky radiation is scattering of light on molecules and aerosols. If the scattering is on molecules and extremely small particles with a size smaller than the incident wavelength, it will scatter in the small wavelength region of the spectrum and it is called "Rayleigh scattering". The scattering on larger particles with a size larger than the wavelength will be in the whole wavelength region of the spectrum; this is called "Mie scattering". Which scattering mechanism predominates in the diffuse radiation is dependent on the atmospheric conditions. In general it can be stated that for a clear sky Rayleigh scattering is predominant, while for a heavy clouded sky Mie scattering predominates. For conditions inbetween, like a hazy sky, both mechanisms contribute to the same extent.

In general, two kinds of papers on sky radiation may be distinguished in the literature. One analyses the scattering process from a theoretical point of view and the other presents correlations between experimental data. In the first kind of studies, the theoretical analysis can be based on a description of the scattering process in the non-homogeneous atmosphere by approaching the regarding as being composed of homogeneous layers in which the scattering can be represented by a radiative transfer equation (e.g. Chandrasekhar, 1960, Liu et al., 1978, Stamnes and Swanson, 1980). The analytical-numerical solution of this type of models is aimed at determining the atmospheric absorption at different heights. The results are used in atmospheric circulation models and in determining the diffuse irradiation at the earth's surface dependent on the atmospheric conditions. In another type of theoretical analysis the scattering in the atmosphere is considered as an over-all phenomenon which can be described as a function of measurable optical properties (e.g. Buckius and King, 1978, Dave, 1979, Hatfield et al., 1981). Both types of theoretical analysis have the advantage of general applicability. The disadvantages are the complexity, especially for the first type, and the requirement that a variety of atmospheric conditions and optical properties should to be investigated to obtain a reasonable idea of what may happen.

The correlation of experimental data has been reported for a great number of different locations. In most studies a correlation is made between hourly or daily sums of global and diffuse irradiation (e.g. Liu and Jordan, 1960, (Massachusetts), Stanhill, 1966, (Israel), Ruth and Chant, 1976, (various locations in Canada), Kasten and Czeplak, 1980, (Hamburg, Germany), Goldberg and Klein, 1980, (Alaska, Maryland and Panama), Iqbal, 1980, (various locations in Canada)). In some of these papers meteorological parameters like cloudiness are also taken into account as variables. From the locations mentioned that of Kasten and Cseplak comes most closely to the conditions found in the Netherlands. These authors analysed the hourly sums of global and diffuse irradiation, collected during a 10 year measuring period, to establish the dependency of these quantities on solar elevation and cloudiness. For the diffuse radiation they expressed the quotient of this irradiation at a certain cloudiness and that at clear sky as a function of cloudiness for varying solar elevations. For solar elevations higher than 30^o the quotient was independent of this elevation. It was constant (value 1) up to a cloudiness Cl of 2/8, then increased linearly to 1.5 at Cl = 5.5/8, kept up this value until Cl = 7/8 and then decreased linearly down to 0.75 at Cl = 8/8. For lower solar elevations the shape of the curves is similar, but the maximum is less pronounced; it has a value of 1.25. Also at Cl = 8/8 the quotient is lower, for small elevations it decreases to 0.6. Especially during the months November through February almost exclusively these low elevations occur.

Besides papers in which global and diffuse irradiation are correlated there are also studies in which the isotropy of diffuse radiation for different conditions is established from measurements (e.g. Pokrowsky (1929), Moon and Spencer, 1942, Morris and Lawrence, 1971, Coulson, 1975). Three different kinds of intensity distributions can be distinguished: distribution from the clear sky, from a so-called standard overcast sky and from a so-called uniform overcast sky.

For the clear sky condition it is observed that the diffuse radiation consits of two components. Due to the fact that the sun is the ultimate source of diffuse radiation, the scattering will take place on the one side along the direct light beam and on the other side on the total air mass. The scattering along the direct light beam causes diffuse radiation from a region adjacent to the position of the sun, increasing when nearing closer to the sun. It is called the circumsolar diffuse radiation. The scattering on the total air mass originates in the entire sky vault and it will have its maximum from the direction in which the total air mass appears to be maximal. So, theoretically, the distribution of this so-called hemispherical diffuse radiation would be proportional to $1/\sin \gamma$ with γ the altitude.

Pokrofsky (1929) suggests one intensity distribution in which both components are included, while Morris and Lawrence (1971) suggest separate distributions for both components. They express the intensity of the circumsolar diffuse radiation as an exponential function of the angular distance from the sun, which has its 1/e value at an angular distance of 22.5°. For the hemispherical diffuse radiation they suggest a polynomial equation for the intensity with a maximum at lower altitudes. The authors suggest that the difference with the $1/\sin \gamma$ distribution postulated earlier is due to the fact that the concentration of scattering particles is higher at lower heights. The hemispherical component contributes 43% and the circumsolar component 57% to the diffuse radiation.

For an overcast sky the uniform overcast sky with an isotropic intensity is suggested the most simple distribution. This distribution is often incorporated in modeling studies of the light distribution in canopies (e.g. De Wit, 1965), though it is a purely hypothetical distribution, unsupported by measurements. The other overcast sky distribution is the standard overcast sky approximation as suggested by Moon and Spencer (1942) and confirmed by Coulson (1975). In this distribution the maximal intensity appears in the zenith and is dependent on the altitude γ according to $(1 + C\sin\gamma)/(1 + C)$. For C Moon and Spencer suggest a value of 2 while Coulson suggests a value of 3, but basically the distribution is characterized in similar terms. The distribution results from measurements but it only appears for an overcast sky, so for a cloudiness of 8/8.

The important question now arises what are the most common conditions and what kind of intensity distribution for the diffuse radiation can be expected. In their paper, Kasten and Cseplak (1980) also represent tables in which the number of hours are given for every season with a defined cloudiness at a defined solar elevation. The relative number of daily hours with a defined cloudiness is given in figure 5.22. The figures are an average over a 10-year measuring period, so they are not predictive of a forthcoming period, but indicate what kind of diffuse radiation appears most of the time. During all periods hours with a heavy cloudiness (7/8 and 8/8) are predominant by far. In the winter period this is most striking. Then these two classes of cloudiness cover 80% of the time whereas in spring and autumn they only cover 62 and 64% respectively. The ratio of the diffuse and the global irradiation was observed to be constant for a cloudiness of 0 to 2/8 at a certain altitude and the hours with these classes cover 12, 19 and 18% in winter, spring and autumn respectively.
From the histograms of figure 5.22 and from the above mentioned variation of

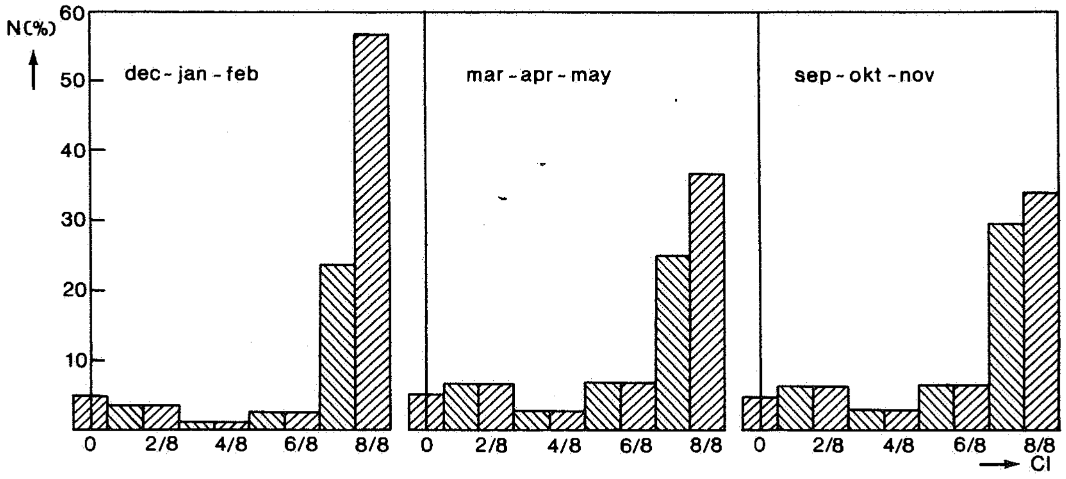

Fig. 5.22. The relative amount of hours with the defined cloudiness as observed by Kasten and Czeplak (1980) in Hamburg (Germany).

the diffuse irradiation with cloudiness, we may conclude that especially for the winter period, most of the diffuse radiation is caused by an overcast sky. So if the transmission of the greenhouse for overcast sky conditions is known, the situation occurring most often is accessible to a quantitative approach. However our main interest is not in the transmissivity during an average situation but in the transmissivity at any time during varying conditions. So it is also necessary to investigate the transmission for the clear sky diffuse radiation and the dependency of the transmissivity on variable conditions.

The transmissivity of the greenhouse for diffuse radiation τ_{dif} is the quotient of the irradiation on a horizontal surface (Wm^{-2}) inside and outside the greenhouse. This irradiation is the integrated intensity from the whole sky vault and the intensity I ($Wm^{-2}sterad^{-1}$) can be a function of the altitude γ and azimuth α as mentioned before. Also the light transmission of the greenhouse τ_{tot} is dependent on the altitude and azimuth of the incoming light ray, so ultimately:

$$\tau_{dif} = \frac{\int\limits_{\alpha=o}^{2\pi} \int\limits_{\gamma=o}^{\pi/2} \tau_{tot}(\gamma,\alpha) I(\gamma,\alpha) \sin\gamma \cos\gamma d\gamma d\alpha}{\int\limits_{\alpha=o}^{2\pi} \int\limits_{\gamma=o}^{\pi/2} I(\gamma,\alpha) \sin\gamma \cos\gamma d\gamma d\alpha} \qquad (5.59)$$

with α and γ defined according to the co-ordinate system as given in figure 5.23.

The transmission for each direction can be calculated according to the transmission model, as described in section 5.2.1. In figure 5.23c this transmission is given as a function of the azimuth at various altitudes for the above mentioned Venlo greenhouse. To understand the variations of the transmission, first the transmission of the glasscover $\tau_g(\gamma,\alpha)$ and that of the construction $\tau_{constr}(\gamma,\alpha)(= \tau_{rg}.\tau_b)$ are given in figure 5.23 a and b respectively. The most striking effect in figure 5.23a is the large variation of τ_g with increasing azimuth for constant altitudes up to the represented 32.5^o. This is mainly due to the increasing part of the radiation falling on the light facing pane and the decreasing angle of incidence on this pane with increasing azimuth. Both effects co-operate. For higher altitudes both glass panes are almost equally oriented relative to the radiation vector and hardly any varia-

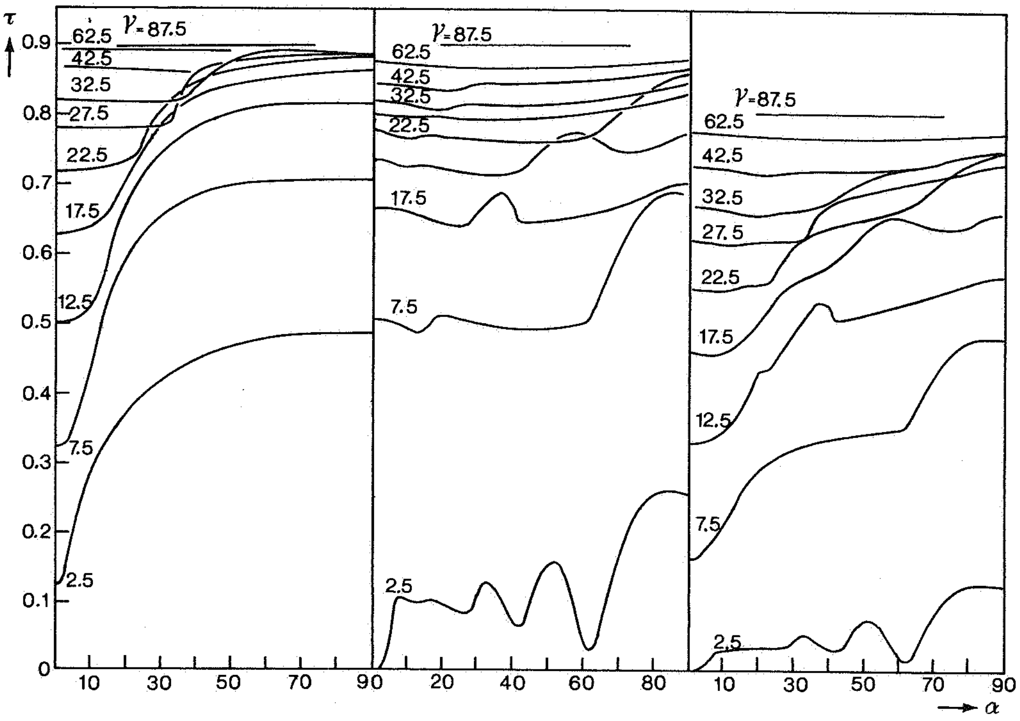

a. $\tau_g(\alpha,\gamma)$ b. $\tau_{constr}(\alpha,\gamma)$ c. $\tau_{tot}(\alpha,\gamma)$

Fig. 5.23. The transmission of the glasscover (τ_g), the construction (τ_{constr}) and the total transmission τ_{tot} as function of the azimuth α for various altitudes γ. The dimensions and properties of the greenhouse concerned are given in fig. 5.19.

tion with azimuth is observed. Therefore τ_g is only partly given for altitudes of 42.5 and 62.5^0. In the transmission of the construction both the transmission of the ridge gutter system and of the bars co-operate. Because of the roof slope of 22^0 it can be observed that for an altitude of 22.5^0 and at an azimuth of 90^0 the ridge gutter shadows coincide, so the transmission is increased. The variations at lower altitudes are also due to the coincidence of these shadows of the adjacent or non-adjacent spans. In the total transmission τ_{tot} the variations in τ_g and τ_{constr} are superposed. For lower altitudes up to the presented 32.5 τ_{tot} increases with increasing azimuth. This also explains the variation in effective transmission (relation 5.58) for direct light from winter to summer. In winter the solar altitude is low during the whole day and the variations in azimuth are under ± 90^0. So for the north-south oriented greenhouse the transmissions for lower altitudes of the left side of figure 5.23c are realized, while for the east-west oriented house those of the right side take place. In summertime the low solar elevations occur in the morning and in the evening when the sun passes the east-west line. Then for the north-south oriented house the favourable transmissions of the right side of figure 5.23c are realized, while at noon with higher solar elevation the high transmissions at the left side take place. For the east-west oriented house the converse holds true, so its effective transmission will be lower then.

The transmission for diffuse radiation is calculated according to relation 5.59 for various distributions of the radiation intensity along the sky vault. The most simple cases are those of the overcast sky and the hemispherical distribution of the clear sky which are only dependent on the altitude γ. The distribution of the circumsolar diffuse radiation is dependent on both the altitude γ and the azimuth α and differs for any solar position (α_s, γ_s). The variation in the transmissions for the above mentioned distributions is given in table 5.1 while for the circumsolar radiation it is given in figure 5.24 as a function of the solar altitude γ_s and azimuth α_s. So for any of the

$I(\gamma,\alpha)$ =		transmission
constant	(uniform overcast sky)	0.70
$(1 + 2 \sin\gamma)/3$	(standard overcast sky) (Moon and Spencer, 1942)	0.72
$(1 + 3 \sin\gamma)/4$	(standard overcast sky) (Coulson, 1975)	0.72
$(1/\sin\gamma)$	(air mass function)	0.60
$(4.319 - 0.101\gamma + 7.125.10^{-4}\gamma^{2})$	(hemispherical radiation) (Morris and Lawrence, 1971)	0.65
$\exp(- \omega/22.5)$	(circumsolar radiation) (Morris and Lawrence, 1971)	see fig. 5.24

with:

$\omega = f(\gamma, \gamma_s, \alpha, \alpha_s)$ is angular distance of a point at α, γ to the sun at α_s, γ_s

Table 5.1. Calculated transmission factor τ_{dif} for diffuse radiation with various intensity distributions $I(\gamma,\alpha)$.

represented solar azimuth-altitude combinations τ_{dif} was calculated according to relation 5.59 with the circumsolar intensity distribution.

The transmissions for the diffuse light of the overcast conditions do not vary very much for the various intensity distributions. The transmission of the standard overcast sky distribution is gradually higher than that of the uniform overcast sky, but the difference is in the same order of magnitude as the accuracy of the calculations. With an overcast sky, the direct radiation will be small, so the transmission of the greenhouse for all radiation is determined by the transmission for diffuse radiation.

Under clear sky conditions the diffuse radiation is only about 30 to 40% of the direct radiation. About half of the diffuse radiation is hemispherical; the other half is circumsolar radiation. So a variation of about 5 to 6 percent in the transmission for circumsolar or hemispherical radiation yields a variation of 1% in the summed transmission of direct and diffuse radiation. Each of them therefore should be estimated with an accuracy of about 2.5 to 3% if an eventual accuracy of 1% is wanted.

It could be expected that the transmission for hemispherical diffuse radiation is smaller than that for the two overcast types because in the latter cases the maximal intensity is at the low altitudes and for these directions the transmission of the greenhouse is poor. The intensity distribution according to the air mass function is an extreme and the calculated transmission for the hemispherical intensity distribution according to the polynome is just inbetween the value of the overcast condition and the extreme condition with the air mass function. The polynome is just a regression of existing situations; these situations are never found very near the intensities according to the overcast or the air mass function distribution but they are always inbetween. So it seems that the calculated transmission of 0.65 for the hemispherical component of the diffuse radiation approximates the existing fluctuating conditions the the required accuracy.

The transmission of the circumsolar component of the diffuse radiation $\tau_{d,cs}$ (figure 5.24) tends to have the same trend as the transmission for the direct light (figure 5.23c). However due to the fact that for any solar elevation-azimuth combinations an integration over the entire sky vault was performed (relation 5.59), the fluctuations are smoothed and the range of the transmission factor is decreased relative to that for direct radiation. The represented transmissions of figure 5.24 are symmetrical with respect to the azimuth 0^o and 90^o and of course also with respect to 180^o and 270^o.

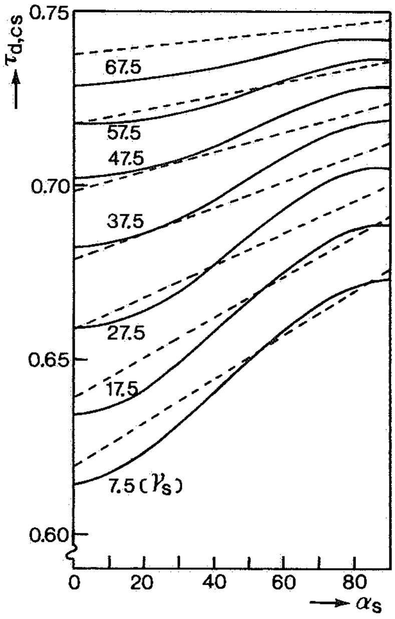

Fig. 5.24.
The transmission for the circumsolar component of the diffuse radiation $\tau_{d,cs}$ as a function of solar azimuth α_s for various solar elevations γ_s according to relation 5.59 (solid curves) together with the approximation according to relation 5.60 (broken curves).

For a period with lower solar elevations (wintertime) the transmission for circumsolar radiation varies between 0.60 and 0.69 and this changes to values between 0.60 and 0.74 in summertime. Hence the introduction of an average transmission factor for the circumsolar component of the diffuse radiation is not permitted. Furthermore the addition of this component to the direct radiation and hence the calculation of its transmissivity according to the transmission of the direct radiation will introduce a considerable error most of the time.

The calculation of $\tau_{d,cs}$ is quite cumbersome and time consuming so it is not possible on line on the computer of a computer controlled data logger system. On the other hand it has to be carried out only once and the results can be stored to determine $\tau_{d,cs}$ afterwards at any time. It is easy to store them as a set of numerical tables but it is also possible to linearise the results and to combine the dependency on the elevation and the azimuth in a linearized relation. For the greenhouse concerned the best fit was made by:

$$\tau_{d,cs} = 0.762 - 8.75\ 10^{-6}(\gamma_s - 80)(\alpha_s - 225) \quad (0<\alpha_s<90) \qquad (5.60)$$

The transmission factor according to this relation is represented in figure 5.24 as dotted curves for the same solar elevations as the ones originally calculated by means of relation 5.49 (the full curves). The difference never exceeds 0.01 which is far within the required accuracy. Relation 5.60 is only valid for a solar azimuth between 0 and 90^o, for the other azimuth values the symmetry has to be taken into account for this value and a corresponding one between 0 and 90^o. For other greenhouses the same approach can be followed, just calculating $\tau_{d,cs}$ once and storing the results or linearising them.

The difference between the transmission factors for both components of the diffuse radiation necessitates the determination of two independent values. These values however are always so close that only a rough estimate is needed of the magnitude of the circumsolar or hemispherical part of the diffuse radiation. Morris and Lawrence (1971) reported 57% for the circumsolar component and 43% for the hemispherical component as contributing to the total diffuse radiation. In wintertime the transmissions for both components are nearly almost equal and a positive variation of 20% in the contributions mentioned only yields a variation in the total transmission for diffuse radiation of less than $\pm$ 0.01. In summertime the transmissions for both components differ more greatly and the variation in that of the circumsolar component is larger. Yet the variation in the total transmission is smaller than 0.02 when there is again a variation in the contributions by both components of $\pm$ 20%. So it is permitted to fix the contribution of the circumsolar component at 57% of the total diffuse radiation and that of the hemispherical component at 43%.

The transmission of the extreme situations of clear sky and overcast sky is defined now. The clear sky situation will be valid up to a cloudiness of 2/8 since Kasten and Czeplak (1980) indicate that up to this value the global G(N) and diffuse radiation D(N) about equal that at cloudiness 0 (G(0) and D(0) respectively).With increasing cloudiness (G(N)/G(0) decreases and D(N)/D(0) increases which indicates that the diffuse component of the global radiation rapidly increases. This increase is due to the increase of the scattering on clouds especially on the sides. At low altitudes the cloudiness seems to increase and the scattering on the sides is shielded by the other clouds. So with increasing cloudiness the hemispherical radiation distribution is blocked. Due to the decreasing contribution of the direct radiation, also the circumsolar component of the diffuse radiation will decrease. The clouds are distributed at random along the sky, so, though the diffuse radiation will not be isotropic it will be distributed at random except for the lower altitudes. Therefore the transmission of the diffuse radiation can be calculated according to the overcast sky condition for a cloudiness > = 3/8. The cloudiness itself can be estimated from simultaneous measurements of the diffuse and global radiation but it has to be based on at least hourly sums of these measurements. Therefore it can only be determined afterwards and not on line.

In the greenhouse under consideration the transmission for diffuse radiation from an overcast sky was measured. Nine equally spaced solarimeters were used to measure the irradiation inside the greenhouse and one solarimeter outside the greenhouse. The inside measurements were performed in the centre of the greenhouse at an height of 1.5 m, on a line perpendicular to the ridge, in between two gutters. The measuring method was developed by Van de Kieboom and Stoffers (1982) to compare the transmissivity for diffuse radiation of commercial greenhouses. The results of the measurements are given in figure 5.25 (Van de Kieboom 1983). Due to the influence of the gutters there is a variation in transmission in the measuring points.

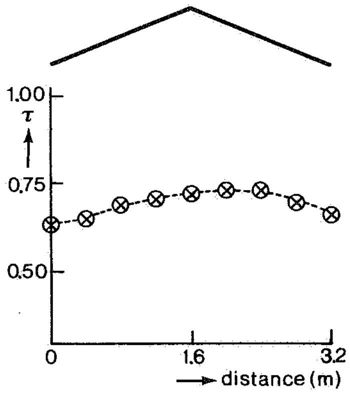

Fig. 5.25.
Transmission for diffuse radiation τ_d from an overcast sky, as measured in the considered Venlo type greenhouse (Van de Kieboom, 1983).

The average transmission is 0.70, which is in very good agreement with the calculated transmission for diffuse radiation under an overcast sky. So the conclusion may be that the developed transmission model yields reliable results.

5.3. LONGWAVE (THERMAL) RADIATION

The total radiant energy exchange between the surfaces of two opaque bodies can be calculated, applying the Stephan-Boltzmann equation with a view factor to incorporate what spatial angle is enclosed between the two bodies and taking into account the emission and reflection factors of the surfaces (e.g. Sparrow, 1973, Kreith, 1976). Inside the greenhouse this leads to straight forward relations for the radiant energy exchange between the surfaces of the observed opaque components (heating pipes, plants, soil, glass cover) which will be discussed in chapter 7. Outside the greenhouse the radiant energy exchange occurs between the glass cover and the atmosphere. Here the difficulty arises that the radiation from the atmosphere is the resultant of the radiation at different heights with different temperatures and composition.
In several papers this problem is tackled by defining an effective sky temperature, which can be used in the Stephan-Boltzmann equation. This temperature is a function of measurable meteorological parameters. In principle the same approach is to determine the thermal irradiation directly from the atmosphere as a function of the meteorological parameters. The latter can be used to calculate an effective sky temperature. Ångström (1915) and Brunt (1932) proposed equations for the atmospheric thermal irradiation as a function of the air temperature and vapour pressure at standard height, while Swinbank (1964). Idso and Jackson (1969) and Monteith (1973) proposed equations in which only the air temperature is needed. In the proposed equations coefficients have to be derived from measurements and in general these coefficients are strongly dependent on the location and the atmospheric conditions. Wartena et al. (1973) compared several modifications of the Brunt and Swinbank equations with measurements at Deelen (the Netherlands) for clear sky conditions. They found large variations of the coefficients for various conditions and concluded that the Brunt type of equation fitted best to their data. Idso (1974) compared the Ångström and Brunt equation with the Swinbank and the Idso-Jackson formula. In his case the Ångström and Brunt equation gave identical results and this was also true for the Swinbank and Idso-Jackson formula for air temperatures higher than 0^oC. There was no equation with an accurate prediction under all measuring conditions.

The conclusion may be that it is very difficult to find a reliable relation for the atmospheric thermal radiation even at equal welldefined atmospheric conditions e.g. clear sky. For cloudy conditions this is even harder than for a clear sky. Kondretyev (1965) summarizes several corrections proposed in the literature. Due to the above mentioned difficulties we decided to measure the atmospheric thermal radiation continuously during measuring periods in the greenhouse. The suggestion by Idso (1971) was investigated first, to blacken the downward dome of a net radiometer and to measure the temperature of this dome as a reference temperature. For practical reasons finally a normal net radiometer was used, positioned above a surface with a defined temperature. The reliability of these measurements was checked by also measuring the net radiation above the glass cover of the greenhouse together with the glass temperature. In chapter 7 these measurements will be discussed together with the other results.

6. Convective exchange processes

In this chapter the various non-radiant exchange processes in the greenhouse are described. These are the heat and water vapour flow (with simultaneous condensation) from the greenhouse air to the cover, the heat flow from the cover to the outside air, the heat flow from the heating pipes to the greenhouse air, the heat and vapour flow (evaporation) from the soil surface to the greenhouse air and the heat and vapour flow (transpiration) from the plant leaves to the greenhouse air. All of these exchange processes can be characterized as convection. Nevertheless transpiration is a combination of diffusion through the stomata and cuticula and convection from the leaf surface to the air.

6.1. EXCHANGE WITH THE COVER

6.1.1. Introduction

The extent of the heat transfer to and from the cover determines the efficiency of the cover as a barrier between the in- and outside air. Therefore, if the relation between the greenhouse climate and the outside weather has to be determined, it is extremely important to characterize these exchanges as functions of relevant factors. In most greenhouse climate model studies this is done by distinguishing long-wave thermal radiation exchange and convection at the in- and outside of the cover. The outside weather conditions also play an important role in the energy expenditure of the greenhouse. As the proper calculation of the energy consumption under varying conditions is the starting point for the design of the heating system and other equipment, one would expect great effort to be made in this field. Considering this it is a bit disappointing to find that in literature the energy consumption of a greenhouse is simply characterized by the heat loss coefficient. This coefficient is defined as the quotient of the energy consumption and the temperature difference between in- and outside; so the longwave radiation and the convection in- and outside are brought together into one coefficient jointly with the heat loss due to leakage ventilation (Bailey, 1978, 1981, O'Flaherty and Maher, 1978, Okada and Hayashim, 1978, Schockert and Von Zabeltitz, 1978, 1980, Tantau, 1978, Sebesta and Reierson, 1981). The heat loss coefficient is then expressed as a function of outside wind speed only. As a rule the resulting graphs show a large scattering due to the interference of the convection and radiation effects. For locations with different weather types e.g. coastal areas with high average wind speed and high cloudiness and inland areas with low average wind speed and low cloudiness to compare the energy consumption in this way is risky. As indicated by Bot (1981) the convection and radiation effects can be simply separated by incorporating the net radiation above the greenhouse in the definition of the heat loss coefficient.

The convective heat exchange processes at the in- and outside of the cover according to literature on heat transfer can be formulated in terms of a relation between the Nusselt number (Nu) and the Reynolds (Re) and Prandtl (Pr) numbers for the case of forced convection and a relation between the Nusselt number and the Grashof (Gr) and Prandtl numbers in the case of natural or free convection. Usually these relations have the form:

$$Nu_{fo} = C_{fo}Re^{n}Pr^{m} + D_{fo} \qquad (6.1.a)$$

for forced convection
and

$$Nu_{fr} = C_{fr}Gr^{a}Pr^{b} + D_{fr} \qquad (6.1.b)$$

for free convection.
The coefficients C_{fo} and C_{fr}, the exponents n,m,a and b and the terms D_{fo} and D_{fr} are dependent on the geometry of the surface under consideration and on the flow characteristics over the surface indicated by Re or Gr. Mostly D_{fo} and D_{fr} equal zero and C_{fo} and C_{fr} are constants for a defined range of Re or Gr.
As far as known to the author, the only study aiming at determining convective heat transfer at the outside of the greenhouse directly is that of Iqbal and Khatry (1977). These authors investigated the convective heat exchange at the outside of a small model of a single span greenhouse in a windtunnel. An average heat transfer coefficient over the entire greenhouse was presented as a function of wind velocity. Their model size was about 1/200 and their highest wind velocity in the tunnel about 20 ms^{-1}. So after upsca-

ling via the Reynolds number their results are only valid in the same Reynolds region, i.e. for extremely low wind velocities.

Without any quantitative data on the heat transfer due to convection to or from a saw-tooth surface like the cover of a multispan greenhouse, an estimation of the order of magnitude may be derived from the convective exchange with a horizontal or slightly inclined flat plate. The inside of the cover can then be considered as a cold plate facing downwards and the free convection of this surface equals that of a hot plate facing upwards. The outside of the cover is generally warmer than the outside air, so it may also be considered as a hot plate facing upwards. Knowledge of the free convection of this arrangement is well established in literature. The Grashof number will have an order of magnitude of 10^9-10^{10} if the gutter ridge distance (1.7 for a Venlo-greenhouse) is chosen as characteristic length. For this range of Gr the exponents a and b in e.g. 6.1.b are unanimously reported as being 1/3. The coefficient C_{fr} is reported as varying from 0.13 to 0.14 (Mac Adams, 1954 , Bovy and Woelk, 1971, Raithby and Hollands, reviewing literature, 1975). Recently Wang (1982) suggested a value of 0.156, while Youssef et al. (1982) suggested 0.162 .
The effect of the slope is investigated by Pera and Gebhart 1973 (a,b) with an arrangement of two ridged inclined plates. This arrangement is similar to two panes of a saw tooth roof but still a difference in flow will occur in the entrance region of the plates. Unfortunately their experiments were performed in the Gr region up to about 10^6 so in the laminar flow region. They reported an increase of the heat exchange with increasing inclination due to a decrease of the boundary layer thickness, Raithby and Hollands (1975) reviewing the literature, suggested a decrease of the heat exchange with increasing inclination in the turbulent region due to a stabilizing effect on the flow. For the slope of the greenhouse roof panes (22-26^0) the latter reference claims a decrease of only 2.5 to 3.5% relative to the exchange from a horizontal plate.
The forced convection heat exchange from a horizontal flat plate is also investigated and reported extensively. In handbooks the values of n, m and C_{fo} are found to be 1/2, 1/3 and 0.66 respectively in the laminar flow region ($Re < 10^5$) and 0.8, 1/3 and 0.036 respectively in the turbulent region ($10^5 < Re < 10^7$). In the recent study by Wang (1982) these values were confirmed. The exchange with a horizontal or slightly inclined flat plate may indicate

the order of magnitude of the exchange with the saw-tooth roof of the multi-span greenhouse, the difference in geometry will probably cause substantial differences. Therefore an experiment was set up to determine the exchanges due to convection at the in- and outside of the cover in a direct way.

6.1.2. Experimental situation

The heat transfer to and from the cover is schematically represented in figure 6.1. From the inside air energy is transported to the cover by convection and long wave radiation and water vapour is transported to the cover by convection too. While condensing against the cover the heat of condensation is released to the cover.
The convective heat flux density $\phi''_{h,i,g}$ (Wm^{-2}) to the inside of the cover is characterized by a convective heat transfer coefficient $\alpha_{c,i,g}$ ($Wm^{-2}K^{-1}$) according to:

$$\phi''_{h,i,g} = \alpha_{c,i,g}(T_i - T_{g,i}) \tag{6.2}$$

The coefficient $\alpha_{c,i,g}$ is determined by the heat transfer mechanism and the geometry of the surface involved and in general the dependency on relevant

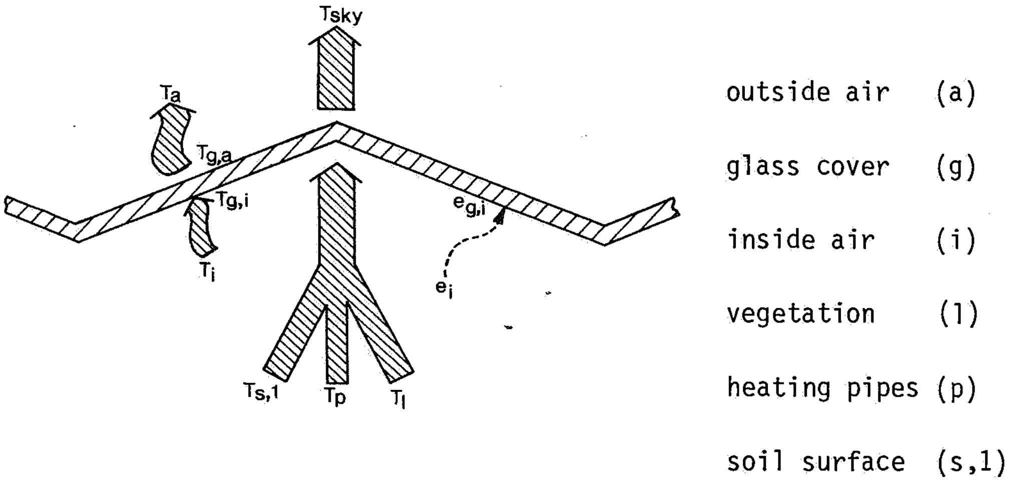

Fig. 6.1. Heat and water vapour fluxes to and from the cover.
(for heat and vapour flow symbols see figures 2.1 and 2.2).

parameters is formulated according to relation 6.1.a and b. The mechanism originates from free and/or forced convection and the role of each depends on the Reynolds and Grashof numbers. The order of magnitude of the Grashof number has already geen given at 10^9-10^{10}. The Reynolds number will be about $(1\text{-}2)10^4$ because local air velocities are measured at 0.1-0.2 ms^{-1} and the characteristic length can also be assumed to be at 1.7 m. For the criterion to decide whether the exchange will be due to free or forced convection or a combination of both (transition region), various combinations of Re and Gr have been suggested in literature. In several theoretical studies (Hieber, 1973, Chen et al., 1977, Ramachandran et al., 1983) pure free convection is suggested if $Gr/Re^{5/2} > 10$. Wang (1982), in an experimental study, suggests that the exchange can be assumed to be due to pure free convection if $Gr/Re^{5/3} > 50$. If the Nusselt relations (6.1.a and b) for the forced and free convection exchange are equated to compute an equivalent Reynolds number for free convection (Morgan, 1975 in an overview, citing various authors), then the criterion can be concluded to be $Gr/Re^{3/2} > 3.10^3$ (the exponents of Gr and Re are 1/3 and 1/2 respectively as indicated by their flow regions). It may be mentioned that the theoretical studies only include laminar free convection, so the criterion from these studies can be disregarded in our case. So the order of magnitude of Gr and Re point out that $Gr/Re^{5/3} \approx 70\text{-}2000$ which indicates pure free convection and $Gr/Re^{3/2} \approx 350\text{-}10^4$ which indicates that the exchange may sometimes be in the transition region.

The water vapour transport to the cover (with simultaneous condensation on the cover) is due to the same mechanism as the heat transport. It can be characterized by a mass transfer coefficient $k_{c,i,g}(ms^{-1})$, so the mass flux density $\phi''_{m,i,g}(kg\ m^{-2}s^{-1})$ is:

$$\phi''_{m,i,g} = k_{c,i,g}(C_i - C_{g,i}) \qquad (6.3.a)$$

with

C_i the water vapour concentration of the inside air (kg m^{-3})
$C_{g,i}$ the water vapour concentration at the inside of the cover (kg m^{-3})

With the ideal gas law the water vapour concentration C can be expressed in the water vapour pressure $e(Nm^{-2})$ so then:

$$\phi''_{m,i,g} = \frac{M}{R\overline{T}} k_{c,i,g}(e_i - e_{g,i})$$

$$= k^*_{c,i,g}(e_i - e_{g,i}) \qquad (6.3.b)$$

with

M : molecular weight of water (kg $kmol^{-1}$)

R : molar gas constant (J $kmol^{-1}K^{-1}$)

$\overline{T}$: average of Kelvin temperatures of inside air and inside of the cover

$k^*_{c,i,g}$: the mass transfer coefficient with pressure difference as driving force (sm^{-1}).

With simultaneous heat and mass transfer, interference between the free convection due to temperature-induced density differences and the free convection due to concentration-induced density differences depends on the Prandtl (Pr) and Schmidt (Sc) numbers. Schenk et al. (1976) indicate that for equal Pr and Sc values the heat and mass transfer do not mutually interfere. This conclusion remains valid in fair approximation if Pr = 0.71 and Sc = 0.63. So for the water vapour air system the mass transfer coefficient $k_{c,i,g}$ can be derived from the heat transfer coefficient $\alpha_{c,i,g}$ according to:

$$k_{c,i,g} = \frac{\alpha_{c,i,g}}{\rho C_p}(Le)^{1-b} \qquad (6.4)$$

with

ρC_p: volumetric heat capacity ($Jm^{-3}K^{-1}$)

Le : Lewis number (= Sc/Pr)

b : power of Pr and Sc in Nu = f(Gr,Pr) and Sh = f(Gr,Sc)

With the mass flux density $\phi''_{m,i,g}$ a latent heat flux density flows to the inside of the cover due to the heat of condensation.

The remaining heat transfer mechanism that must be taken into account in this connection is the long-wave radiation exchange between the inside of the cover and the canopy, heating pipes and soil surface respectively. These fluxes $\phi''_{r,1,2}$(Wm^{-2}) can be calculated according to the Stephan Boltzmann equation:

$$\phi''_{r,1,2} = F_{1,2}.E_{1,2}.\sigma(T_1^4 - T_2^4) \tag{6.5.a}$$

with

$F_{1,2}$: view factor between surface 1(cover) and 2(e.g. canopy)
$E_{1,2}$: combined emission factor between surface 1 and 2
τ : Stephan Boltzmann constant ($Wm^{-2}K^{-4}$)
T : Kelvin temperature (K)

As the radiating surfaces do not differ very much from parallel surfaces, the combined emission factor $E_{1,2}$ can be approximated by:

$$E_{12} = (E_1^{-1} + E_2^{-1} - 1)^{-1} \tag{6.5.b}$$

with

$E_{1,2}$: emission coefficient of surface 1,2.

So at the inside of the cover the convective heat flux appears together with a latent heat flux due to condensation and with some long-wave radiation fluxes.

At the outside (figure 6.1) heat is transported by convection to the outside air and by long-wave radiation to the sky. The convective heat flux can be represented analogously by a heat transfer coefficient at the outside $\alpha_{c,g,a}$ thus

$$\phi''_{h,g,a} = \alpha_{c,g,a}(T_{g,a} - T_a) \tag{6.6}$$

Here the convection mechanism is determined by Re and Gr. The Grashof number will be in the same order of magnitude as that at the inside, the Reynolds number will be about 10^5 at low wind velocities of about $1ms^{-1}$ to 10^6 at higher wind velocities. This means that the Nusselt relations for the turbulent region of both the free and forced convection have to be equated to find the criterion to decide whether the exchange is due to forced convection, to free convection or to a combination of both. This yields the criterion $Re^{2.4}/Gr > 700$ for pure forced convection. Wang (1982) suggests the criterion

$Re^{2.2}/Gr > 15$. The first criterion indicates that the exchange will be due to pure forced convection for $Gr = 10^{10}$ if $Re > 2\ 10^5$, i.e. at wind velocities larger than $2ms^{-1}$. The second yields the same for $Re > 10^5$, i.e. at wind velocities larger than $1ms^{-1}$. Only at low wind velocities the exchange may be expected to be in the transition region between free and forced convection; at higher wind velocities forced convection will predominate.
The long-wave heat exchange at the outside can be represented by relation 6.5. Surface 1 is the outside cover surface and surface 2 is the sky vault with sky temperature T_{sky} (section 5.3).

From the above it follows that the convective heat transfer at the in- and outside of the cover is only a part of the total heat transfer through the cover. Attempts at determining the convection terms from the total heat consumption of the greenhouse must include a determination of the long-wave heat fluxes, the heat flux due to condensation and the heat flux due to leakage ventilation. This method will lead to a cumulation of inaccuracies resulting in a very inexact determination of the convection terms. Therefore we decided to set up an experiment by which the convection exchange could be measured in a direct way and in which the other heat transfer mechanisms would be suppressed as much as possible. Inaccuracies in the determination of the radiation and convection terms will then cause a small error in the final result because these fluxes should be introduced as small corrections only.

6.1.3. Experimental set up

The heat flux through the cover was measured by two heat flow sensors. These sensors are constructed as solid discs with a diameter of 110 mm and a thickness of 5 mm in which the heat flow is measured as a temperature difference between the upper and lower surface. Because the resistance to heat flow of the disc is nearby constant in the temperature range in the cover, the temperature difference can be calibrated against the heat flux density. The temperature difference is measured very accurately and sensitively because a large number of thermocouples are embedded in the disc between upper and lower surface in a serial way. The effective thermal conductivity of the discs applied was about 0.45 $Wm^{-1}K^{-1}$. The sensors were embedded in a plate of polyethylene with a 5 mm thickness. The material of the plate was chosen in such a way that the thermal conductivity equalled that of the heat flow sensors as much as

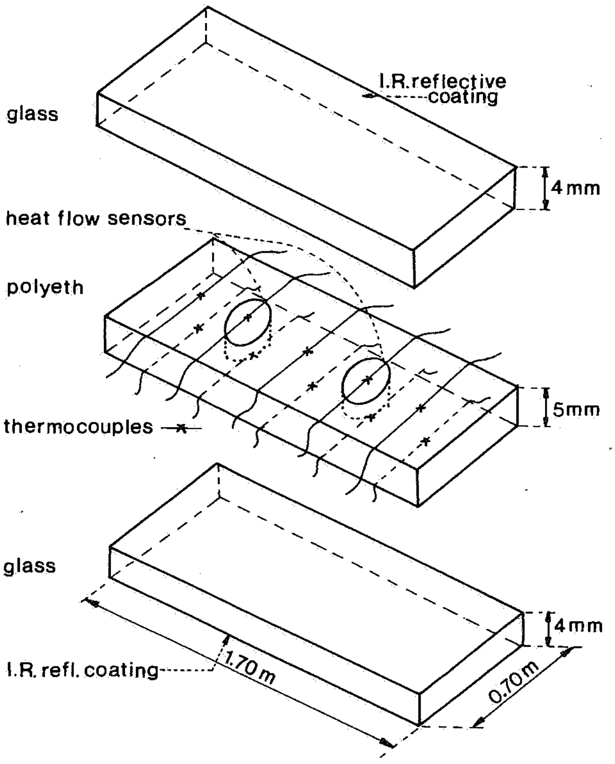

Fig. 6.2. Components of the measuring device for the convective heat flux at the in- and outside of the cover.

possible, namely 0.42 $Wm^{-1}K^{-1}$. 5 rolled thermocouples were fixed on each side of the plate. Then the plate was embedded between two 4 mm glass panes. One surface of each glass pane was coated (figure 6.2) with an I.R. reflective coating, so that this side had a low emission coefficient. The effective emission coefficient was measured from a similar sample and was found to be 0.1 (measured inbetween the wavelengths 5-40 μm). The sandwich combination was framed in an aluminium frame for an easy fixing in the greenhouse roof. The length and width of the measuring pane were chosen as equivalent to that of a glass pane in a normal multispan Venlo greenhouse, so that it could just replace an ordinary glass pane.

Before the measuring device was fixed in the roof, laboratory experiments were carried out to check whether the heat flux measured by the heat flow sensors really represented the actual heat flux through the pane. Therefore the pane was laid horizontally on an electrically heated thin foil (figure 6.3) with a

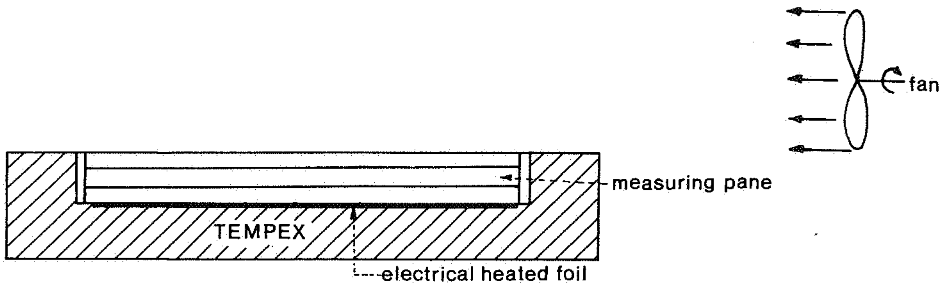

Fig. 6.3. Laboratory test set-up for the measuring pane.

width of 0.65 m and a length of 1.60 m, which in its turn was laid on a block of tempex provided with some extra thermocouples on both sides.
The combination of measuring pane, heating foil and tempex block was placed in front of a large fan (diameter about 1 m), so that air flow over the measuring pane could be generated. The heat flux sensors proved to indicate the electrically generated heat flux (with a small correction for the downward heat flux through the tempex) with an error never exceeding 5%. To attain this accuracy the system had to come into a thermal equilibrium first. The time constant of the measuring pane in front of the fan proved to be in the order of magnitude of half an hour. A numerical estimate (the square of the thickness, divided by the thermal diffusivity) leads to about 10 minutes. In the greenhouse it will also be in this order of magnitude; hence the effect of fast fluctuations in the environmental conditions (especially wind speed) on the heat flux through the pane is damped out effectively. As a consequence our experiment indeed leads to a reliable steady state relation between the heat transfer coefficients on both sides and the average environmental conditions.

After the laboratory measurements the measuring pane was attached in the roof of a 570 m^2, 8 span Venlo greenhouse, sited at the Institute of Agricultural Engineering (IMAG), Wageningen. In the greenhouse tomatoes were grown. The location of the pane in the roof was as well in the centre of the greenhouse as possible. The greenhouse orientation was east-west, so that wind from the north or the south, is perpendicular to the ridges. Together with the measu-

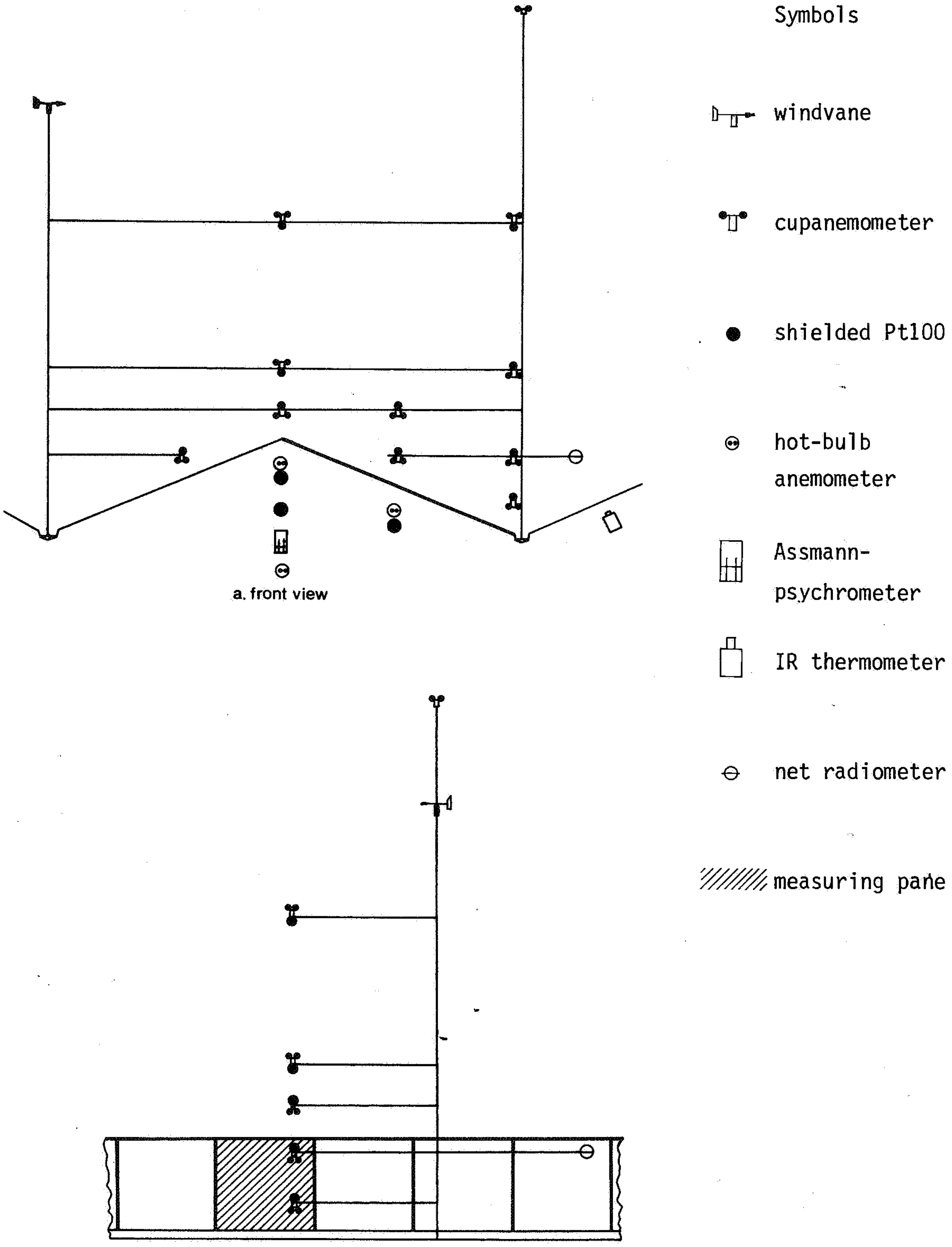
Symbols
windvane
cupanemometer
shielded Pt100
hot-bulb anemometer
Assmann-psychrometer
IR thermometer
net radiometer
measuring pane
a. front view
b side view

Fig. 6.4. Schematic overview of the experimental set up for the determination of the convective exchange with the cover.

ring pane, sensors were installed (figure 6.4) to measure:

- the inside air temperature at several positions near the pane (with Pt100's)
- the dry and wet bulb temperature of the inside air near the pane, and of the outside air (with Pt100's)
- the temperature of an ordinary glass pane (with an I.R. thermometer)
- the heating pipe temperature at several positions (with thermocouples)
- the inside air velocity at 4 positions near the measuring pane (with hot bulb anemometers)
- the outside wind velocity at 10 positions near the greenhouse roof (with small cup-anemometers)
- also at these 10 positions the outside air temperature (with Pt100's)
- the outside wind velocity at a height of 3 meter above the ridge level (with a small cup-anemometer)
- the outside wind direction at a height of 2.5 m. above the ridge level (with a wind-vane)
- the net radiation above the greenhouse roof and above a surface with a known temperature (for the determination of the sky temperature) (with net-radiometers).

The sensors were scanned by a computer controlled data-logging system once per minute, except for the 10 outside wind sensors near the greenhouse roof. These sensors were small cup-anemometers, with a low threshold sensitivity of about 0.2 ms^{-1}. To achieve this low threshold sensitivity the anemometer was equipped with a light chopper instead of a generator, so the output is an amount of pulses per second instead of an electrical voltage. Only two pulse counters were available in the datalogging system. Therefore one was used for the continuous counting and integration of the reference cup-anemometer once per minute whereas the other pulse counter was connected during one minute to each of the other cup-anemometers successively. So every 10 minutes each of these anemometers was counted during one minute.

6.1.4. *Experimental results*

6.1.4.a. *Heat exchange*

The measuring periods were restricted to the night period in order to exclude the effects of short-wave radiation on the measurements. The data were processed to calculate the heat flux through the pane and all other quantities as an average over a one hour period. At the outside the heat flux due to radiation proved to be small. As a result only a small correction on the measured heat flux densities had to be made to calculate the heat transfer coefficient due to convection at this side.

At the inside unfortunately, condensation appeared and this seriously affected the emission coefficient of the inside surface. Nevertheless an attempt was made to calculate the heat fluxes due to condensation and radiation from the measuring data to determine the heat flux due to convection at the inside. Due to the accumulation of the inaccuracies in the various terms in these calculations, the resulting heat transfer coefficient due to convection at the inside showed considerable variations. Its value varied between about 2 and 4$Wm^{-2}K^{-1}$, without any significant correlations with the temperature difference between the inside glass surface and the greenhouse air. The order of magnitude fairly agrees with what is generally accepted for free convection exchange from an horizontal surface, but these exchange relations could neither be confirmed nor adapted. For a proper determination at the inside, condensation has to be excluded so measurements must be repeated in a greenhouse without canopy.

At the outside the measuring results were much more consistent. Measuring results were selected from steady state periods in which no rain occurred. In figure 6.5a the heat transfer coefficient due to convection at the outside is given as a function of outside wind speed at reference level (3 m above the ridge). The outside wind direction is indicated by the use of different symbols for each defined range of wind directions. The graph demonstrates that no correlation is found with outside wind direction. During the measurements the wind speed only exceeded 4ms^{-1} in rainy periods. Of course these measuring results were discarded. For the observed wind speed range a linear relation between the coefficient and the wind speed satisfactorily covers the measuring results:

$$\alpha_{c,g,a} = 2.8 + 1.2\ u \qquad (6.7)$$

The heat transfer coefficient is expressed in $Wm^{-2}K^{-1}$ per unit roof area, the wind speed u is in ms^{-1}.

This linear relation is drawn as a full curve in figure 6.5.

Though the agreement with the measuring points is quite well, the puzzling question remains whether the exchange is by free or forced convection. The

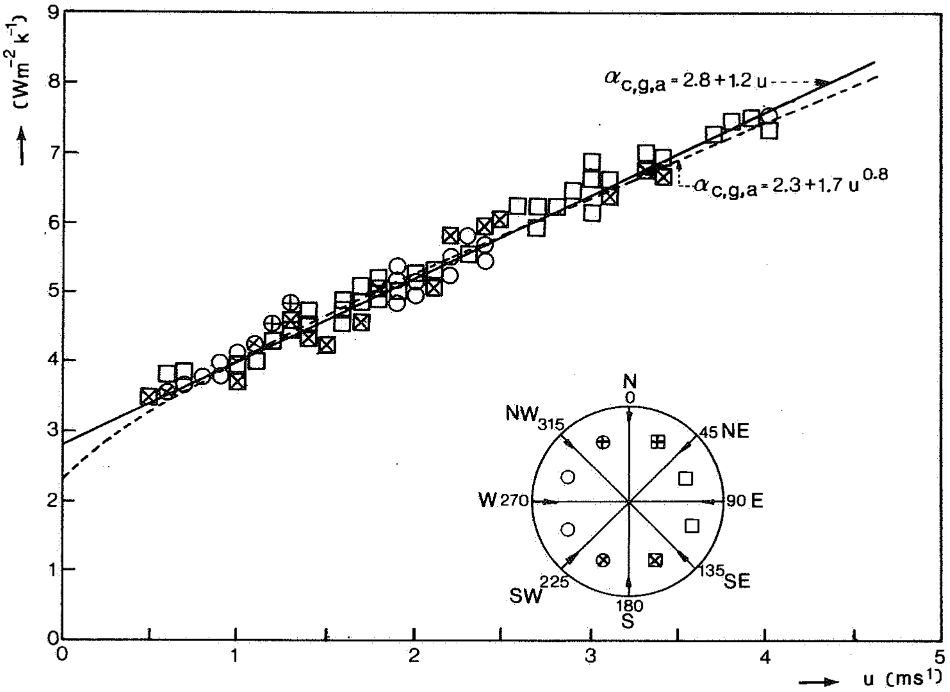

Fig. 6.5a. Heat transfer coefficient between cover and outside air as a function of outside wind speed at reference height for various wind directions as indicated by the compas card.

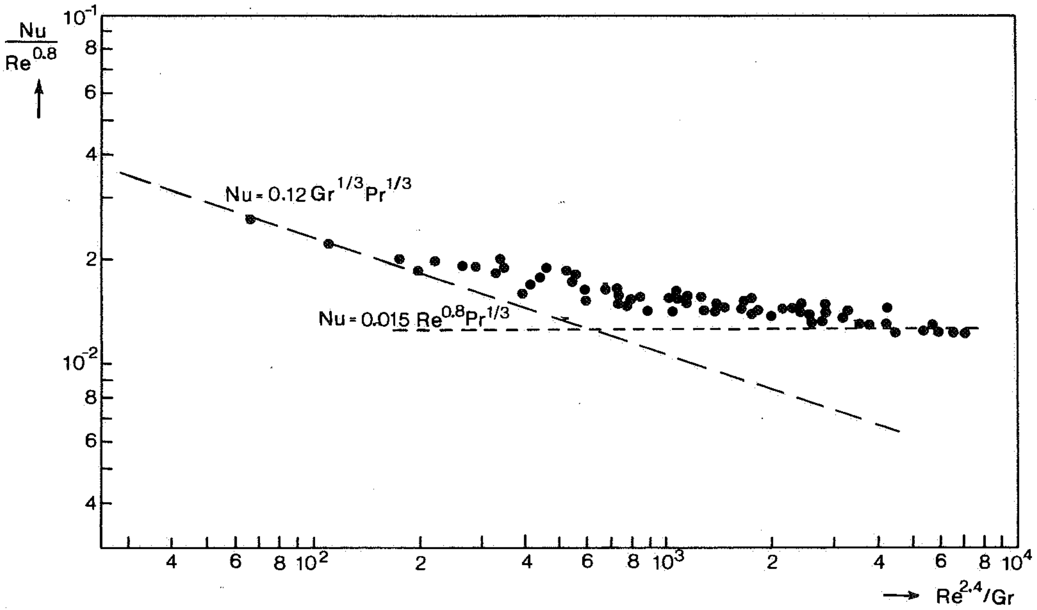

Fig. 6.5b. The ratio of $Nu/Re^{0.8}$ (proportionality between realized and expected forced convection exchange) as a function of $Re^{2.4}/Gr$.

extrapolated value of $\alpha_{c,g,a}$ at wind speed u = o and the linear increase with wind speed suggests that free convection takes a substantial part of the exchange. This can be investigated best by calculating the ratio between the realized exchange and the expected forced convection exchange. The observed exchange can be characterized by the Nusselt number. The forced convection exchange is expected to be proportional to $Re^{0.8}$ so the ratio of $Nu/Re^{0.8}$ is expected to be constant for pure forced convection. If we establish the relation of $Nu/Re^{0.8}$ with the criterion $Re^{2.4}/Gr$ mentioned earlier the domains of pure free and pure forced convection together with the transition region can be recognized. In figure 6.5b the measurements are represented in this way. The measuring points demonstrate at the right an almost constant value of $Nu/Re^{0.8}$ at large values of the criterion $Re^{2.4}/Gr$. For definite conclusions measurements have to be performed at even larger $Re^{2.4}/Gr$ so at wind speeds in the region of 4 to about $12 ms^{-1}$, or at very small temperature differences between the outside cover surface and the outside air. The right side of figure 6.5b tends to a constant value of $Nu/Re^{0.8}$ of 0.0125 which leads to a coefficient C_{gr} (relation 6.1b) of 0.015. This suggested pure forced convection exchange relation is added to the figure to demonstrate how this is represented. As mentioned before definite conclusions may only be drawn if measurements are performed at higher values of $Re^{2.4}/Gr$. However, the suggested coefficient 0.015 indicates that the definite coefficient will be much smaller than the value 0.036 found in literature on forced convection exchange with flat plates. One reason may be the choice of the characteristic length, which of course has to be the same for the Nusselt, Reynolds and Grashof numbers and dictated by the Grashof number at 1.7 m (distance ridge gutter). Another reason may be the difference between the flow above a saw-tooth roof and the flow above a flat plate. The flow phenomena will be discussed at the end of this section.
At the left side of the figure pure free convection is expected. For Gr an exponent of 1/3 in relation 6.1b will lead to a line with a negative slope of 1/3 in figure 6.5b. Some points at the left side of the figure indeed indicate this slope, but, again, definite conclusions may only be drawn if more measurements are available, in this region at lower wind speeds or larger temperature differences between the outside of the cover and the outside air.
To demonstrate the representation of pure free convection at the left side of the figure a line with a negative slope of 1/3 has been drawn which gives the best fit with the scarce points in this region. This line would result in a coefficient of 0.12 in the Nu, Gr, Pr relation which is only slightly lower

than that found for pure free convection from a horizontal plate. Again, the suggested coefficient is only an estimate of the order of magnitude. The precise value has to be established from much more measurements in this specific range.

Figure 6.5b clearly indicates that most measurements are performed in the transition region between free and forced convection. The first estimate of the forced convection at $Re^{2.4}/Gr > 700$ was based on the exchange from a horizontal plate. From our present data we can repeat this calculation. Figure 6.5b indicates that the pure forced convection from the saw-tooth surface is represented by a Nu, Re, Pr relation with a much lower coefficient than that from the horizontal plate. If this lower coefficient is used to estimate again where pure forced convection can be expected, then the criterion will be $Re^{2.4}/Gr > 6.10^3$. This is in agreement with figure 6.5b and indicates that pure forced convection can be expected if measurements are performed at larger wind speeds.

6.1.4.b. Flow phenomena

The flow phenomena can be analyzed from the local wind speed measurements. With the small cup-anemometers only the magnitude of the wind velocity, but no wind direction, can be detected. From the measurements lines with equal velocity (isotaches) can be constructed for different wind velocities and directions at the reference height. The local wind velocities used for the drawing of the isotaches are averaged over one hour, so average situations will be shown. The isotaches are given as dimensionless ratios of the wind velocity at reference height (3 m above ridge level).

The two most pronounced wind directions are those perpendicular to the ridge and those parallel to the ridge. With the wind perpendicular to the ridge (figure 6.6a and b) two kinds of phenomena can be observed. At very low wind velocities (figure 6.6a, $u = 0.7\ ms^{-1}$) the isotaches are more or less similar to the shape of the roof surface, which seems to indicate that the flow is more or less parallel to the roof surface. At higher wind velocities (figure 6.6b, $u_1 = 2ms^{-1}$) the isotaches are no longer similar to the roof surface but instead they show a divergency and convergency between the ridges. This might indicate the existence of a large secondary eddy in the roof dale. If the wind is parallel to the ridge (figure 6.6c and d) the same picture is observed. The isotaches parallel to the roof surface were found to appear at higher

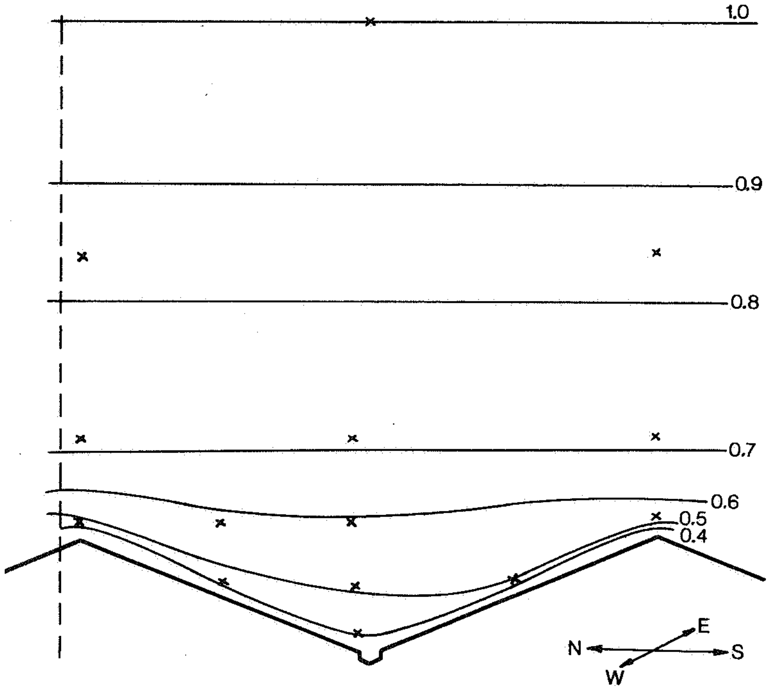
1.0
0.9
0.8
0.7
0.6
0.5
0.4
E
N
S
W

Fig. 6.6a
u_1 = 0.7ms^{-1}
ω = 180^{0}(S)

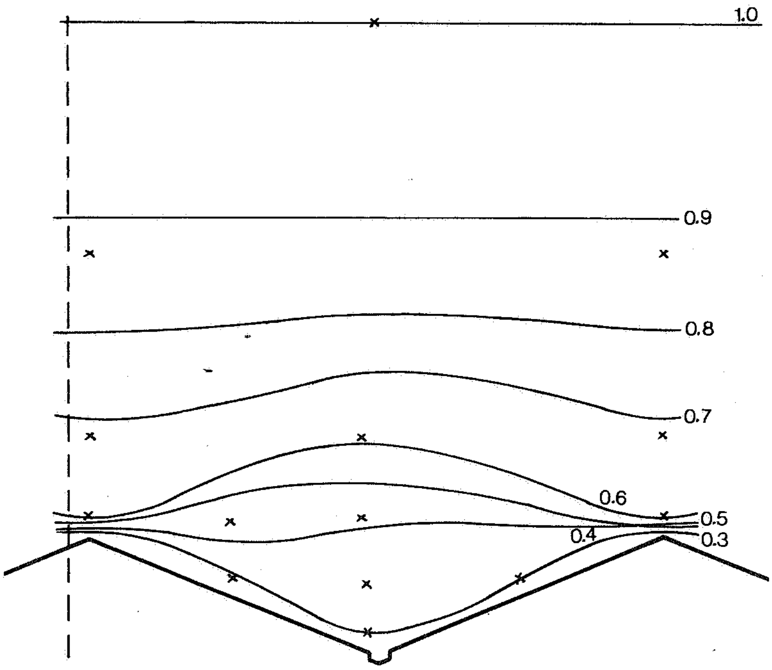
1.0
0.9
0.8
0.7
0.6
0.5
0.4
0.3

Fig. 6.6b
u_1 = 2.0ms^{-1}
ω = 190^{0}(S)

Fig. 6.6c
$u_1 = 2.4ms^{-1}$
$\omega = 84^{o}(E)$

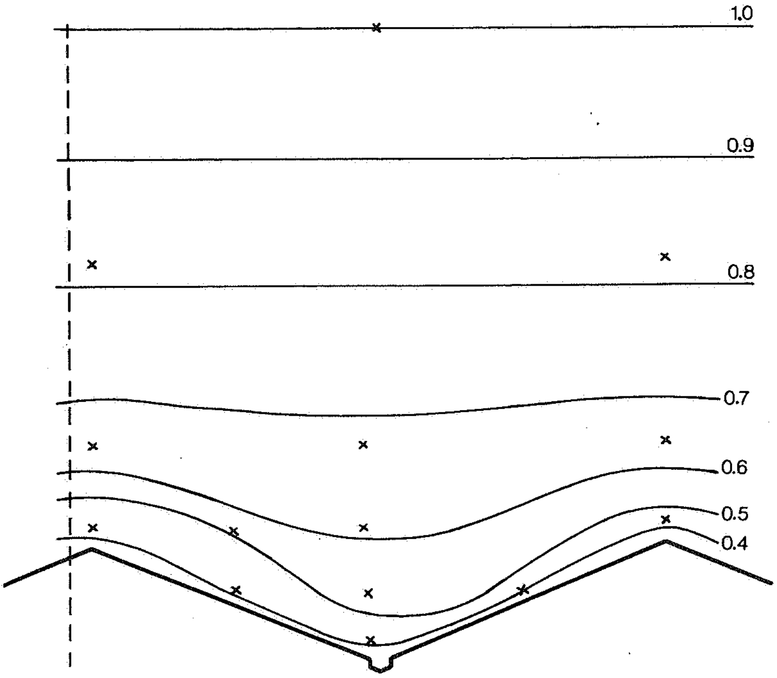

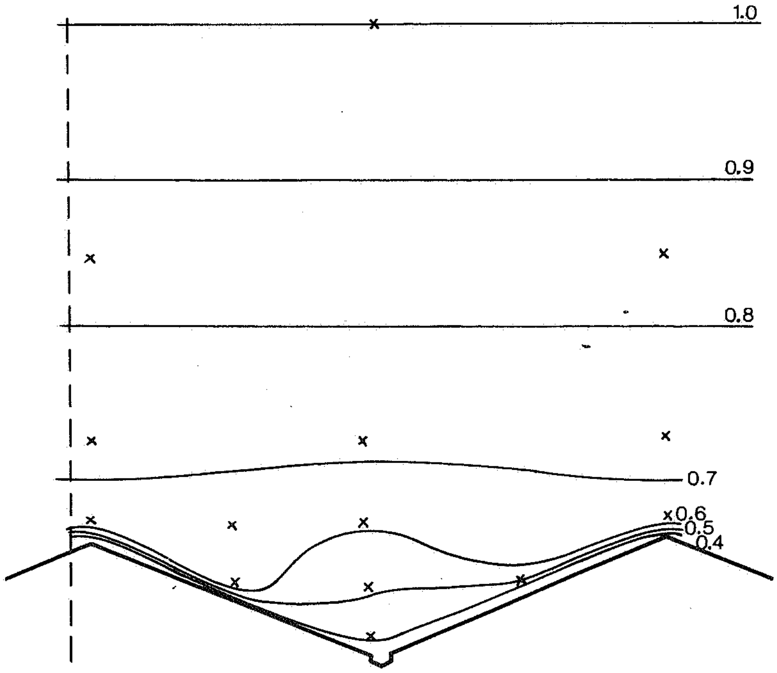

Fig. 6.6d
$u_1 = 3.4ms^{-1}$
$\omega = 269^{o}(W)$

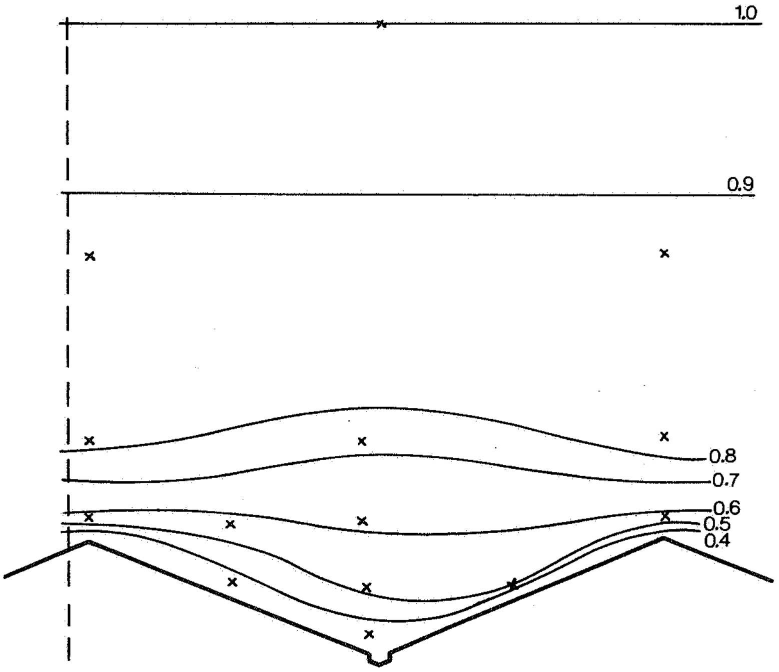

Fig. 6.6e
$u_1 = 2.2ms^{-1}$
$\omega = 135^{0}(SE)$

-Fig.6.6. Isotachen pictures above an East-West oriented multispan greenhouse at various outside wind speeds at reference level (u_1) and wind directions (ω).

wind velocities (figure 6.6c, $u = 2.4ms^{-1}$) than if the wind was perpendicular to the ridge, but with increasing wind velocity (figure 6.6d, $u = 3.4ms^{-1}$) the same kind of pattern as in figure 6.6b was found. The wind direction may be almost exactly from the West, but this is an average over an hour. The wind direction is a fluctuative quantity too, so at any moment the wind has a component perpendicular to the ridge. With the wind inbetween the two before mentioned directions (figure 6.6e) the same picture is seen again.
The observations of the wind field above the greenhouse roof were supplemented by flow visualization. This was accomplished by releasing smoke in the gutter and by observing how the smoke was carried away by the air flow. We could observe very clearly that secondary eddies developed in the roof dales, but also that the flow pattern was very fluctuative. So very dominant eddies appeared and vanished, but no real stable eddies established. The isotaches of figure 6.6. represent average situations because the local wind velocities were averaged over one hour. Therefore in an interpretation of the isotachen pictures the fluctuative nature of wind should be kept in mind. Also the number of measuring points is restricted so that our isotachen pictures contain

a lot of interpolation.
From figure 6.6 it can be seen that two flow regions above the roof can be distinguished: first the local boundary layer just above the roof surface and second the (more or less) mixing region above the roof. We found that the heat transfer coefficient was not significantly dependent on the wind direction. From figure 6.6. it can be seen that for all wind directions the boundary layer above the roof exists but that the mixing region is different depending on the wind direction. So the local boundary layer obviously determines the heat transfer coefficient and this coefficient is not significantly affected by the mixing region or the flow pattern outside the boundary layer.

6.2. HEAT TRANSFER FROM THE HEATING PIPES

6.2.1. Introduction

If the temperature in the greenhouse is only determined by the environmental conditions outside the greenhouse, the inside temperature may drop below the values demanded by the greenhouse crop. In that case extra heat has to be supplied to the greenhouse by a heating system. The most common way to do so is using a central boiler for a greenhouse complex and distributing the heat by a hot water pipe system in the greenhouse compartments. A large number of different pipe arrangements are in use, dependent on the character of the crop that is grown in the greenhouse (Von Zabeltitz, 1978). In our work we focussed on a system in which the pipes are installed at a height below that of the canopy. This system is widely used, since it has been proved that low heating pipes are energy saving compared to other systems (Meyer, 1977, Winspear, 1977, Heyna and Van Holsteijn, 1981). The height above the soil surface is about 5-10 cm for the low pipe system; it can also be used then as the rails of a transport system in the greenhouse by which labour saving may be achieved (Van Weel, 1981).

In the literature, the convective heat transfer from the heating pipes is usually derived from equations for the pure free convection exchange from horizontal cylinders. Especially in model studies of the greenhouse climate (Ch7) this is a common practice. However, as was mentioned already in section 6.1 too, some problems will have to be kept in mind if such equations are simply applied in the greenhouse.

The first problem is that of the similarity of the experimental conditions. The free convection heat transfer from a body is experimentally determined in a room where the walls, floor and ceiling do not have any significant effect on the flow around the body. For that reason they are at a great distance from the body and do not produce convective flows of themselves. In a greenhouse the situation is completely different. When the heating system is used, there is always a temperature difference between the greenhouse cover and the inside air, which also causes air flows. Moreover the distance from the low pipes to the soil surface is so small that this distance certainly will have an effect on the flow around the pipes. We still leave aside the influence of the surrounding vegetation.

The second problem is encountered in the exchange equation itself: great variety is found in the literature for this equation. In general the exchange is expressed as a relation between the dimensionless Nusselt, Grashof and Prandtl numbers according to equation 6.1.b. If the characteristic length equals the diameter of the heating pipes, then the order of magnitude of Gr will be 10^5-10^6 (diameter about 5 cm). In this range of Gr various values of C_{fr} are reported while a and b are reported unanimously at 1/4. The most classical reports are that of King (1932) and of Jodlbauer (1933) who suggested a value for C_{fr} of 0.55 and 0.45 respectively. The extended literature is reviewed by several authors to derive a general exchange formula by correlation of reported data over a wide range of Gr Pr. Churchill and Chu (1975) suggested an equation in which C_{fr} was a function of Pr. For our case (Pr = 0.71) the result was a C_{fr} value of 0.39. Morgan (1975) considered separate ranges of Gr Pr. In our range he suggested a C_{fr} value of 0.48. Raithby and Hollands (1976) proposed a very complicated relation between Nu, Gr and Pr. Recently Fand and Brucker (1983) suggested a relation in which the amount of dimensionless numbers was increased to 4 by the incorporation of a dimensionless parameter for the viscous dissipation.

From the above considerations we may infer that no general equation for the convective heat transfer from the heating pipes in a greenhouse to the greenhouse air can be formulated. Every arrangement of heating pipes has to be considered separately especially if a combination of heating pipes in a vertical or horizontal array is applied as is done in general. For the pure free convection exchange from a combination of pipes Farouk and Güçeri (1983) report considerable deviations from the exchange from a single cylinder. Stoffers

(1977) reports the convective exchange from a combination of a vertical row of 4 horizontal pipes in a greenhouse. He suggests a C_{fr} value of 0.60. Okada (1980) investigated the effect of various heating pipe arrangements on the gradients of inside air temperature and on the heat transfer coefficients inside the greenhouse. No results were presented for the heat transfer coefficient from the pipes but from the available data it may be concluded that this coefficient is highly dependent on the heating pipe arrangement.

In view of the lack of information on the convective heat exchange from low pipe systems we decided to set up an experiment to determine this exchange as a function of relevant parameters for our type of greenhouse (Venlo multispan).

6.2.2. Experiments

The heat exchange from the heating pipes to the greenhouse interior is due to convection to the greenhouse air and to radiation to the soil surface, the vegetation and the cover (figure 6.7.).
The heat flux density due to convection $\phi''_{h,p,i}$ (Wm^{-2}) per unit pipe area can be characterized by a heat transfer coefficient $\alpha_{c,p,i}$:

$$\phi''_{h,p,i} = \alpha_{c,p,i}(T_p - T_i) \qquad (6.8)$$

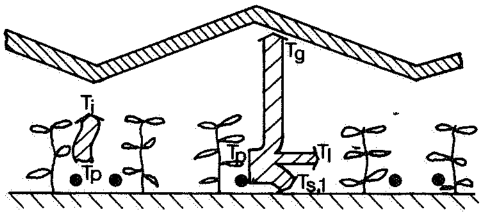

Fig. 6.7. Heat flows from the heating pipes (for indices see figure 6.1)

The mutual relation between Gr and Re again indicates what kind of convection can be expected. The order of magnitude of Gr was already mentioned as being 10^5-10^6. Local air velocities are observed to be about $0.1 ms^{-1}$ which results in a Re value of about 350. Fand and Keswani (1973) suggested that the exchange from a cylinder is due to pure free convection if $Gr/Re^2 > 40$. If the Nusselt relations for forced and free convection in the appropriate ranges of Re and Gr are equated, (Morgan (1975)) then the implication is that pure free convection will occur at $Gr/Re^{1.884} > 14$. The first criterion ranges from $0.8 < Gr/Re^2 < 8$ and indicates that the exchange will be in the transition region between free and forced convection. The second criterion ranges from $1.6 < Gr/Re^{1.884} < 16$ which indicates that the exchange will be due to pure free convection at large temperature differences only. The radiative heat transfer can be calculated by relation 6.4 with 1 the heating pipes surface and 2 the soil, vegetation and cover surface respectively. A small view factor accounts for the (zero) exchange with the adjacent pipe.

For a proper determination of the convection term it is preferable to lower the radiative heat exchange. The search for a proper paint to reduce the emission coefficient of the heating pipes was of no avail. To glue aluminium foil on the surface of the heating pipes seems inappropriate because the foil will crease and therefore change the surface roughness. In addition it seems very difficult to completely avoid air inclusions between foil and pipe wall. These inclusions will increase the thermal resistance. The replacement of some heating pipes by pipes with a polished surface was not practicable since they become filthy very soon. Moreover these polished pipes have a much smoother surface than the normal heating pipes, which also affects the heat transfer by convection.

In our experiment another approach was chosen. We tried to correct the radiant heat transfer by the calculation of the various radiation terms. The biggest problem with this correction is the radiant exchange with the soil surface. The view factor to this surface is about 0.5 for a low pipe system and the soil surface temperature is a quantity which is difficult to measure. Moreover the soil surface temperature may show large differences. The radiative heat exchange with the vegetation can be determined in a more accurate way. A fully grown crop will only transmit a small part of the radiation energy from the pipes and the leaves are almost at air temperature, particularly at night. As a result the radiative exchange between the heating pipes and the vegetation can be calculated from the heating pipe and air temperatures (re-

lation 6.4). The radiative exchange between pipes and cover will be small with a fully grown crop. It can be determined from measurements of the pipe and glass temperature and an estimation of the small view factor.
On account of these considerations we decided to eliminate as far as possible the radiative exchange between the soil surface and the heating pipes. Therefore the soil surface was covered with aluminium foil with a low emission coefficient (measured to be 0.15 in the wave length region of 5-40 μm). By the high reflection of the foil both the upward and the downward side of the pipes exchange radiative energy mainly with the vegetation and the glass cover. For these terms a reliable correction can be made.

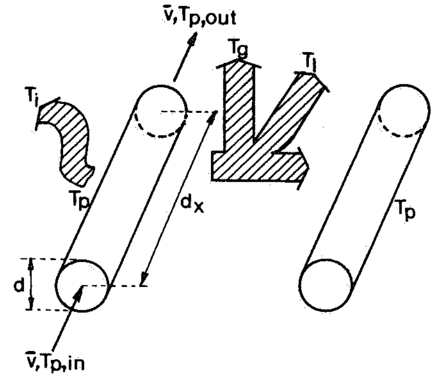

Fig. 6.8. Heat balance over a pipe segment.

The convective heat exchange is a term in the energy balance over a part of the heating pipes with length d_X (figure 6.8) from which we can derive:

$$\rho C_p \frac{dT_p}{dt} = - \frac{4}{d}\{\alpha_{c,p,i}(T_p - T_i) + \sum_{2=}^{1,p,g} F_{p,2}E_{p,2}\tau(T_p^4 - T_2^4)\} - \bar{v}\rho C_p \frac{dT_p}{dX} \qquad (6.9)$$

Thus two different measuring methods of the convection term can be distinguished:

- the sum of the convection and radiation terms can be determined in the steady state from the mean fluid velocity $\bar{v}$ through the pipe and the temperature difference between the in- and outlet of the pipe. Due to the high volumetric heat capacity of the fluid (water) an accurately detectable temperature difference between inlet and outlet only appears if the pipe length

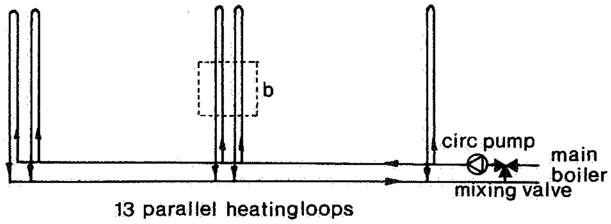
b
circ pump
main boiler
mixing valve
13 parallel heatingloops

a. Lay out of the heating system (see also fig. 7.5).

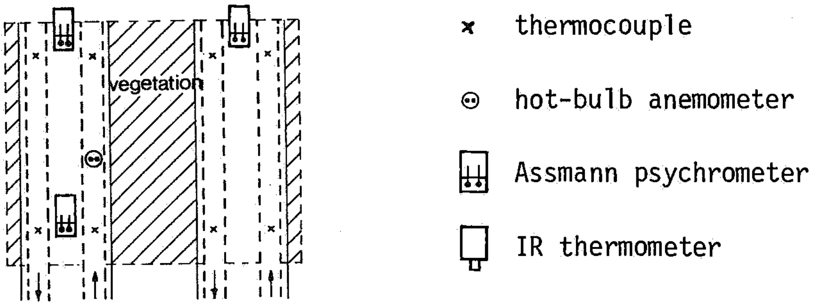
vegetation
thermocouple
hot-bulb anemometer
Assmann psychrometer
IR thermometer

b. Top view of the sensor arrangement

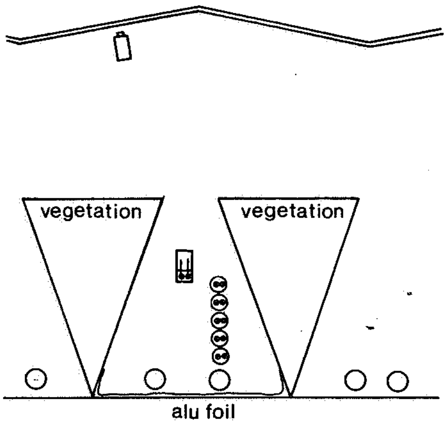
vegetation
vegetation
alu foil

c. Front view of the sensor arrangement

Fig. 6.9. Schematic overview of the sensor arrangement of the exchange from the heating pipes.

between inlet and outlet is large. This means a long residence time in the pipe. Small fluctuations at the inlet due to the variations of the mixing valve then disturb the steady state for a long period. Moreover a steady state situation in the greenhouse is hard to achieve: with a constant fluid flow the pipe temperature will gently vary due to the fact that greenhouse conditions vary. The storage term in relation 6.9 then contributes substantially to the heat balance. Reliable measurements can be made with this method only if the equation 6.9 is integrated over a long period (e.g. one day). During this period the sum of the convection and radiation terms can be considered to be large compared to the storage term. But then an average convection term and a radiation term are determined and only their relation to an average situation can be determined. While we expect a non-linear relation, the relation for average situations cannot provide definite answers.

- the sum of the radiative and convective terms can be measured from the cooling-down curve when no heat is supplied at the inlet. This means that the inlet flow has to be zero so that the three-way mixing valve at the inlet of the greenhouse heating system (figure 6.9) has to be closed completely. From the temperature decrease during a relatively small period, the sum of the convective and radiative heat transfer during this period can be determined. The difference between the initial and final temperature of each period has to be small compared to the temperature difference between pipe and surrounding air. This means that during one cooling-down curve a set of heat fluxes and temperature differences is measured.

In view of the above considerations we chose for the second measuring method. During some night periods at various positions the temperatures of the pipe, the greenhouse air and the cover were measured together with the local air velocities (figure 6.9). As mentioned before the soil surface was covered with aluminium foil. At about 10.00 p.m. the mixing valve was closed at a pipe temperature of about 70^{o}C. To make sure that no leakage through the mixing valve occurred, the circulation pomp of the heating system was switched off. The ratio between the internal resistance and the external resistance in the case of pure conduction (fluid perfectly at rest) is about 0.2, but this will be much smaller due to internal free convection flows.
The sensors were scanned every minute by a computer controlled data logging system during a measuring period of 6 hours per night.

6.2.3. Measuring results

Measurements as discussed in the foregoing section were carried out during 6 nights in a Venlo greenhouse with low heating pipes. The measuring data were filtered (moving average filter, time constant about 5 minutes) to smooth small fluctuations and then analyzed.

The local air velocities above the heating pipes varied from about 0.1-0.2ms^{-1}. They also fluctuated during one measuring period, but did not correlate significantly with the heating pipe temperature or the temperature difference between heating pipes and greenhouse air. During the various measuring periods the pipe temperature dropped from about 60 to 20^{o}C and the greenhouse air temperature dropped from about 25 to 15^{o}C. The cover temperature varied in a different way during the measuring periods. One night for instance it remained almost constant at 11-12^{o}C and another night it dropped from 16 to 11^{o}C. The difference between the heating pipe temperatures at different places on one pipe were small. The same holds true for the air temperature. Therefore the pipe and air temperatures were averaged to one pipe temperature and one air temperature. For these data the convective heat transfer was calculated. The results of the measuring periods were consistent. In figure 6.10 the convective heat transfer coefficient is given as a function of the temperature difference between the heating pipes and the greenhouse air as it is calculated for two of the nights during which the cover temperature showed the most pronounced difference.

The log-log graph is fairly linear over the whole range of temperature differences (about 4-40^{o}C). The results of the two nights with different conditions are mutually consistent, which indicates that the correction for the radiant exchange with the cover is in the right order of magnitude. For small temperature differences (about $<$ 10^{o}C) the scattering in the measuring points increases, but it does not lead to deflection of the linear proportionality. This indicates that the convective heat transfer is due to free convection over the whole range of temperature differences observed. Our first estimate was that the exchange was in the transition region (section 6.2.2). This estimate was based on measurements of the local air velocity. This local air velocity originates partly from free convection from the heating pipes, from free convection from the inside of the cover (section 6.1.1) and from leakage ventilation. Therefore the forced convection devaluates.

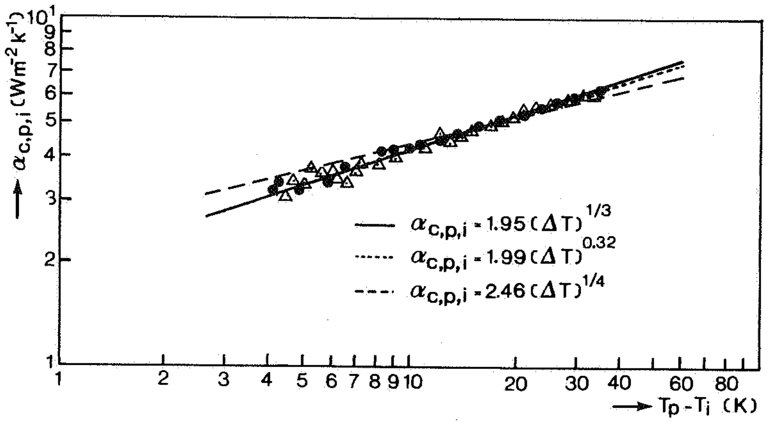

Fig. 6.10. The measured heat transfer coefficient due to convection between heating pipes and air as a function of the temperature difference between heating pipes and greenhouse air.

The linear behaviour in figure 6.10 demonstrates that the relation between $\alpha_{c,p,i}$ and $T_p - T_i$ is exponential:

$$\alpha_{c,p,i} = C_c(\Delta T_{p,i})^a \qquad 6.10)$$

The best fit of the measuring points is obtained with $C_c = 1.99$ and $a = 0.32$. This is indicated in figure 6.10 as a dotted line. For the range of Grashof numbers involved (10^5-10^6) the exponent a was expected to be 1/4 as unanimously reported in literature on free convection exchange from horizontal cylinders (section 6.2.1). If this exponent is applied, the coefficient C_c would become 2.46 (broken line in figure 6.10). The difference between the 1/4 power fit and the measurements is small in the temperature difference range from 10-40 K but it becomes relatively great for small temperature differences. For Grashof numbers > 10^8 an exponent a of 1/3 is found in literature, which is very near to our result of 0.32. For an exponent of 1/3, the best fit of our measurements is obtained for a coefficient $C_c = 1.95$ (solid line in figure 6.10). So we find a discrepancy between the exponent of Gr and the range of Gr.

As mentioned before, the air movement around the pipe originates not only from the free convection from the pipe but also from the free convection from the cover. The cover temperature is more or less correlated with the pipe temperature, so the free convection from the cover is expected to correlate with the free convection from the heating pipes. It may therefore be probable that the exchange is based on apparently much higher Grashof number than that calculated from the diameter of the heating pipes and the temperature difference between pipes and air.

If we compare our results to those of the literature on free convection from horizontal cylinders (section 6.2.1) we have to express equation 6.10 as a relation between Nu, Gr and Pr (equation 6.1b). Our 1/4 power fit then yields $C_{fr} = 0.55$ and the 1/3 power fit yields $C_{fr} = 0.19$. Both values are substantially higher than those from the literature. According to Morgan (1975), who reviewed the literature, an exponent 1/4 is found for $10^4 < \mathrm{Gr\ Pr} < 10^7$ together with a C_{fr} of 0.48 and an exponent 1/3 is found for $10^7 < \mathrm{Gr\ Pr} < 10^{12}$ with C_{fr} is 0.125. Our best fits yield higher coefficients, but this is caused by the different experimental conditions as discussed before.

To generalize from our results is not too easy. Our results were obtained for a heating pipe system of two parallel horizontal pipes at a distance of 20 cm with a small distance between the soil surface and the heating pipes. Obviously with another distance the relation will be different. So new experiments will have to throw light on how the convection exchange is affected. These experiments will be relatively simple if performed according to the method described in this section.

6.3. EXCHANGE WITH AND TRANSPORT IN THE SOIL

The soil is a greenhouse component which interacts with the greenhouse climate in several respects:

- the heat and moisture regime in the soil directly affects plant growth as it determines the climate in the root zone,
- the exchange on the surface also occurs in the heat balances of the other greenhouse components; therefore this phenomenon has an important effect on the plant growth conditions,
- due to the important heat capacity the soil stores energy at day time and releases it at night; therefore it has a long-term stabilizing effect on

the greenhouse climate.

At the soil surface various energy fluxes have to be distinguished; the short wave radiation that effectively penetrates the canopy is absorbed, heat and water vapour are exchanged with the greenhouse air and longwave radiant heat is exchanged with the other opaque greenhouse components. Thus heat is transported in the soil to or from the surface. The temperature of the soil surface is of vital importance in the interactions. Together with the concept of heat and mass transfer coefficients on the surface it determines the convective heat flow and the evaporation from the soil to the air and, last but not least, it determines the radiant exchange to the other opaque elements. So a proper determination of the soil surface temperature is crucial.
Looking at the various energy fluxes at the surface we notice that: the absorbed shortwave radiation is a boundary condition dependent on the transmissivity of the greenhouse cover and the canopy; the convective terms are dependent on the transfer coefficients; the radiant heat can be calculated according to Stephan-Boltzmann (relation 6.4, 6.5) and the soil fluxes are dependent on the thermal proporties of the soil. The transfer coefficients at the soil surface can be estimated, but under ordinary greenhouse conditions the contribution of the convective terms appears to be small. So the emphasis has to be laid on a proper determination of the soil fluxes. Therefore no special experiments were performed to establish the transfer coefficients but our experimental effort was directed towards the determination of soil fluxes during the measurements of the greenhouse climate.

The soil fluxes are due to conduction and can be calculated according to Fourier's law:

$$\phi_s'' = - \lambda \nabla T \tag{6.11}$$

with

ϕ_s'': heat flux density in the soil ($Wm^{-2}K^{-1}$)
λ : the thermal conductivity of the soil at the depth concerned ($Wm^{-1}K^{-1}$)
∇T: the gradient of the soil temperature at this depth (Km^{-1})

In general we are interested in the vertical fluxes to and from the surface.

In that case only the vertical term of the gradient needs to be considered. The values of the thermal conductivity of the soil in the greenhouse, used for our climate research, were measured in situ using the non-stationary needle method as recently improved by Van Haneghem (1981). These measurements were performed at two depths (5 and 20 cm) and at one depth in two extra positions to check the horizontal homogeneity. The vertical gradient was measured at four depths (5, 10, 20, 40 sm) at three locations (one under the low heating pipes, one under the plant rows and one inbetween). Apart from these measurements the heat flux density was measured at two depths (5, 20 cm) in two positions with heat flow sensors, as described in section 6.1. In this way the soil heat flows and temperatures as calculated in chapter 7 could be experimentally checked.

6.4. EXCHANGE WITH THE VEGETATION

6.4.1. Introduction

All greenhouse activities are aimed at an optimal growth and development of the crop as the supplier of greenhouse products. In this study the impact of the greenhouse climate on crop growth and development is out of the scope; the vegetation is approached as a well-defined body that exchanges heat, water vapour and carbon dioxide with the greenhouse air. The climate and the plants interact in this respect. Generally speaking, the greenhouse climate without plants can be marked as a desert climate. With plants it is transformed into a humid, hot climate. Study of the physical interaction between plants and environment must explain how this transformation is accomplished. The formulation of the exchange processes is the starting point of this study. Great effort has already been invested in the general understanding of the physical interaction between plants and environment, notably under outdoor conditions. The results have been reported extensively in literature and reviewed in handbooks: Van Wijk (1963), Rose(1966), Slatyer (1967), Slavik (1974), Rosenberg (1974), Monteith (1975, 1980). Only Van Wijk devotes a special chapter to greenhouse climate (Businger, 1963), while the other authors emphasize on the climate in the open. However the general physical concepts of the exchange with the vegetation can be easily applied to the exchange in a greenhouse.

In this approach the exchange of heat and water vapour at the outside of the leaf is defined in the same way as the heat and mass transfer from other surfaces. The description of the water transport from the inside of the leaf to the surface is based on the morphology of the leaf: the water evaporates in the internal cavities and has to penetrate the skin (cuticula) and the pores (stomata) of the leaf to the outside surface. So the water evaporates in the intracavities at the saturation pressure at leaf temperature and the vapour flow meets the resistance by the cavity, the cuticula or the stomata of the leaf and that of the boundary layer at the leaf surface, before it arrives at the greenhouse air. In this way the well-known resistance network of figure 6.11 is composed.

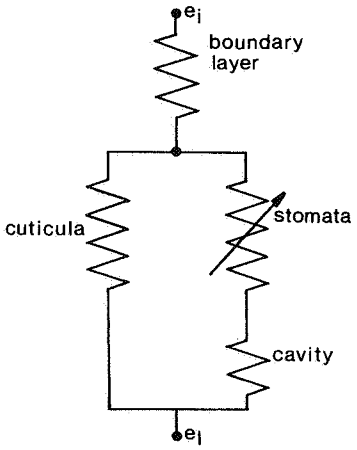

Fig. 6.11
Resistances to water vapour transfer from the inside of the leaf to the air (under greenhouse conditions).

The analogy of the network representation with the leaf morphology is very attractive, especially to describe the transpiration in the open. There the boundary layer resistance as well as the leaf resistance are variable, the first one due to variation of the local wind speed and the second due to variation of the stomatal opening. In a greenhouse the local air velocities are generally observed to be fairly constant. So there it is to be expected that only the leaf resistance will vary.

The boundary layer resistance is in general determined experimentally on model leafs (Parkhurst et al., 1968, Vogel, 1970, Iqbal and Stoffers, 1975, Cannon et al., 1979, Morrison and Barfield, 1981). For leaves with a smooth surface this approach can lead to reliable results but it is doubtful for hairy, rough leafs like that of tomato or cucumber leaves. For a leaf in an environment with low local air velocities a boundary larger resistance for mass transport is reported of about 2 - 4 s cm^{-1}. The heat transfer coefficient found by the analogy between heat and mass transfer is then 3 - 6 $Wm^{-2}K^{-1}$.

The total resistance in the leaf is mainly dependent on the stomatal resistance (Stigter, 1972). The resistance of the substomatal cavity is small and that of the cuticula is very high compared to that of the stomata. The opening itself is controlled by the plant in a plant physiological feedback loop (Raschke, 1975). Very elaborate models are presented in literature to describe stomatal resistance under all kind of environmental conditions (e.g. Penning de Vries, 1972). The two main factors directly or indirectly affecting the stomatal resistance are shortwave irradiation and water supply. So for a well-watered greenhouse crop it can be expected that mainly shortwave irradiation will affect stomatal resistance (Kuiper, 1961, Kanemasu and Tanner, 1969 a, b).

In the literature on greenhouse crop transpiration, the emphasis is on the total transpiration during a period varying from one week to one day (Morris et al., 1957, Rothwell and Jones, 1961, Lake et al., 1965, Hand et al., 1980, de Graaf, 1978, 1981). Transpiration sums are considered as an overall quantity and the relation to the environmental factors (especially sums of the global irradiance) is investigated by statistical correlation. Stanghellini (1981 a, b) in connection with this investigated a Penman type of formula for greenhouse evapotranspiration.

Our interest is in the momentaneous transpiration in mutual interaction with the momentaneous greenhouse climate. The transpiration concept offers a suitable approach to this problem. Therefore experiments were set up to evaluate the various resistances (leaf and boundary layer resistance). The integrated transpiration over a period of e.g. one day can be compared to literature data on greenhouse evapotranspiration.

6.4.2. Experimental conditions

The various terms in the energy balance over a single leaf are schematically represented in figure 6.12. The shortwave irradiation I_l on the leaf is not only dependent on the outside irradiation and the transmittancy of the cover (chapter 5), but also on the light penetration in the canopy, i.e. on the position of the observed leaf in the canopy. Also the longwave exchange with the other opaque greenhouse components is dependent on the "shadowing" of the

$$\phi''_{m,l,i} = k^*_{tot} LAI(e_l - e_i)$$

$$= k^*_{tot} LAI\ C_{p,T}(T_l - T_i) \qquad (6.12)$$

with:

k^*_{tot} : the combination of the conductivities of the leaf and the boundary layer for water vapour transport (sm^{-1})(compare eq. 6.3b).

LAI : the leaf area per unit ground area (Leaf Area Index)

$C_{p,T}$: the proportionality factor in the water vapour pressure-temperature relation at the average of the leaf and air temperature ($Nm^{-2}K^{-1}$).

The leaves of most plants of greenhouse crops have their stomata at one leaf-side only. Because of the high resistance of the cuticula, only the leaf side with stomata is supposed to transpire. The combined leaf conductivity k^*_{tot} is composed from:

$$k^*_{tot} = ({k^*_{l,stom}}^{-1} + {k^*_{c,l,i}}^{-1})^{-1} \qquad (6.13)$$

with

$k^*_{l,stom}$: the water vapour conductivity from the inside to the surface of the leaf; this quantity is mainly determined by the conductivity of the stomatal openings.

$k^*_{c,l,i}$: the mass transfer coefficient from the leaf surface to the greenhouse air.

The conductivity within the leaves, $k^*_{l,stom}$, is an average of that at various parts of the vegetation and it is supposed to be approximately dependent on the average environmental conditions. Therefore the experiments should be aimed at a direct determination of the effective stomatal conductivity.
The energy balance over the canopy per unit ground area reads:

$$Cap''_l \frac{dT_l}{dt} = \phi''_n - \alpha_{c,l,i}\ 2.LAI(T_l - T_i) - \Delta H\phi''_{m,l,i} \qquad (6.14)$$

with:

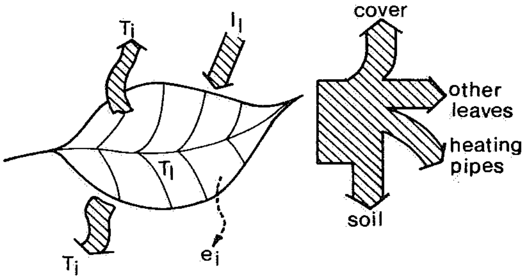

Fig. 6.12
Energy fluxes from a single leaf. Compare figure 6.7 for explanation of symbols.

observed leaf by other leaves. It is the local irradiance that mainly determines the stomatal resistance.

If the energy balance over a single leaf, or an ensemble of leaves with the same environmental conditions, is the base of a transpiration model then the vegetation has to be divided into regions with the same conditions. In model descriptions of photosynthesis (e.g. De Wit, 1965, Goudriaan, 1977) the vegetation is divided into different layers in which the shortwave irradiance can be described by light penetration models (also Lemeur and Blad, 1974, Stoffers, 1975). For photosynthesis this is needed, due to the strong non-linear dependency on the irradiation. For the description of the transpiration this is not necessary because the irradiation is not more than a term in the energy balance over a leaf. The radiation intensity determines for a great deal the stomatal resistance. The stomatal conductivity (converse of resistance) is found to be approximately linearly proportional to the light intensity (Kuiper, 1961, Behboudian, 1977). Although a non-linearity could be introduced by the temperature dependency of the saturation vapour pressure in the leaves, the differences in leaf temperature between various leaves in the greenhouse canopy are not so large as to introduce great errors by a linearization of the vapour pressure curve around an intermediate leaf temperature. So having only linear dependencies for the description of the transpiration, an averaging over the whole canopy is allowable. Therefore we decided to base the exchange of the vegetation on the energy balance over the whole canopy per unit ground area. By doing so cumbersome models of the short- and longwave radiation distribution are avoided.

The transpiration of the canopy per unit ground area $\phi''_{m,l,i}$ (kgm^{-2}s^{-1}) is then:

Cap''_l : the volume heat capacity of the leaves per unit ground area ($Jm^{-2}K^{-1}$)
ϕ''_n : the net radiation to the canopy (Wm^{-2})
$\alpha_{c,l,i}$: the heat transfer coefficient between leaf surface and air ($Wm^{-2}K^{-1}$)
ΔH : heat of evaporation (Jkg^{-1}).

Again the mutual relation between the Reynolds and Grashof numbers indicate what kind of convection around the leaves can be expected. Our experiments were performed with tomatoplants in the greenhouse. These plants have large composed leaves, the largest parts having a width of about 5-10 cm. With the local air velocities of 0.1 - 0.2 ms^{-1} Re will be 350 - 1400 and Gr will range between 2.10^4 - 2.10^5 per degree in temperature difference between leaf and air. If we apply the exchange with a flat plate as an estimate in the order of magnitude (section 6.12) than $Re^{2.4}/Gr$ ranges from 6 - 1800 and $Re^{2.2}/Gr$ from 2 - 400. Both criteria indicate that the exchange can be expected in the transition region for some Re - Gr combinations or in the region of pure forced convection for other combinations.

6.4.3. Experimental set-up

Measurements of the exchange with the vegetation have to be performed on a non disturbed canopy with undamaged leaves. To obtain representative results we aimed at the direct measurement of heat and water vapour flows at maximally different positions, together with the relevant climate quantities about the vegetation. A crucial accessory in this kind of measurements is a device to detect the momentaneous canopy transpiration. At the Technical University of Twente (The Netherlands) a very sensitive weighing lysimeter was developed which detects a change in weight of about 0.1 g at a total weight of 100 kg. This means that the transpiration at night of about 6 - 8 full grown tomato- or cucumberplants can be detected on a minute base. The construction, operation and application in greenhouse climate research has recently been reported elsewhere (Meyers et al., 1983).
Together with the transpiration measurements detailed climate measurements were performed to record the outside weather as a boundary condition for the greenhouse climate. A brief description of the complete set-up is given in chapter 7. Only that part which is relevant to the validation of the transpi-

ration concept is described here. In the test greenhouse, sited at the Institute of Agricultural Engineering (IMAG), Wageningen, tomatoes were grown on rockwool. The soil in the greenhous was covered with a thick white plastic sheet to prevent evaporation from the soil surface. Eight or six of the plants were placed on the lysimeter, located in the centre of the greenhouse, in a normal canopy row. With a plant density of $2m^{-2}$ this means the measurement of the transpiration of a ground area of 3 or $4m^2$.
The plants on the lysimeter were supported by a frame which, of course, also rested on the lysimeter. During the experiments no difference in growth and development, between the plants on the lysimeter and the other plants in the greenhouse could be observed.
Two types of experiments were performed:

- the transpiration was scanned together with the greenhouse climate quantities around the lysimeter to determine the effective vapour conductivity k^*_{tot} (relation 6.12) from the vegetation to the greenhouse air as a function of environmental factors
- during some nights a fluctuating energy flow was applied to the plants on the lysimeter to determine the heat transfer coefficient $\alpha_{c,l,i}$ from the leaf surface to the air. This fluctuating energy flow was obtained by switching infra-red heating lamps (I.R lamps) on and off above the lysimeter plants (figure 6.13).

With the I.R. lamps off, relation 6.12 and 6.14 in the steady state yield:

$$\phi''_{n,o} - K_{tot}(T_l - T_i) = 0 \qquad (6.15a)$$

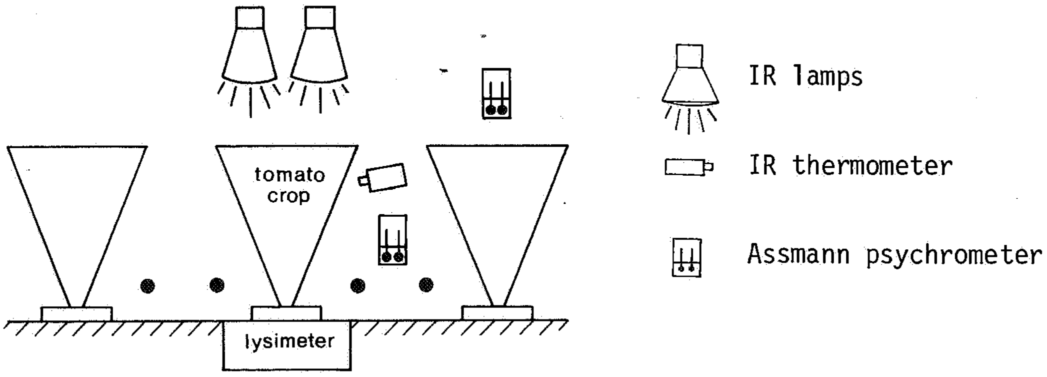

Fig. 6.13. Lysimeter and test arrangement with infra red heating lamps.

with

$$K_{tot} = \alpha_{c,l,i}\ 2LAI + \Delta H\ k^{*}_{tot}LAI\ C_{p,T} \qquad (6.15b)$$

When at t = o the lamps are switched on almost immediately an increment in the net radiation is achieved of $\tilde{\Phi}''_{n}$. This generates an increment of the leaf temperature $\tilde{T}_{l}(t)$. In formula this (after substraction of 6.15a) can be described by relation 6.14:

$$Cap''_{l}\ \frac{d\tilde{T}_{l}(t)}{dt} = \tilde{\Phi}''_{n} - K_{tot}\tilde{T}_{l}(t) \qquad (6.16)$$

The temperature of the air in the greenhouse is supposed to remain unchanged. The solution of (6.16) is:

$$\frac{\tilde{T}_{l}(t)}{\tilde{T}_{l,t=\infty}} = (1 - e^{-\frac{t}{\tau_{l}}}) \qquad (6.17)$$

with

$$\tilde{T}_{l,t=\infty} = \tilde{\Phi}''_{n}/K_{tot} \qquad (6.18a)$$

and

$$\tau_{l} = Cap''_{l}/K_{tot} \qquad (6.18b)$$

The net radiation is measured in the vegetation, but the result will not equal the effectively absorbed net radiation. However only the increment is relevant. The increment of the measured net radiation will be proportional to the increment of the effectively absorbed net radiation with a proportionality factor C_{n}, only if the other environmental conditions are constant. The same holds true for the increment of the leaf temperature: the increment of the measured leaf temperature will be proportional to the increment of the effective leaf temperature with a proportionality factor C_{T}. So then at t = ∞:

$$\text{rel}(6.18):\ \tilde{T}_{l,mes,t=\infty} = C_{n}\tilde{\Phi}''_{n,mes}/C_{T}K_{tot} \qquad (6.19a)$$

$$\text{rel}(6.12):\ \tilde{\Phi}''_{m,l,i,mes} = k^{*}_{tot}LAI\ C_{p,T}C_{T}\tilde{T}_{l,mes,t=\infty} \qquad (6.19b)$$

with

$\tilde{T}_{l,mes}$ and $\tilde{\phi}''_{m,l,i,mes}$ the measured increments of leaf temperature and transpiration respectively.

The measurement in the steady state (relation 6.12) produces k^*_{tot} if the vapour pressure difference between the vegetation and the air can be determined sufficiently accurately. Measurement of the time constant (relation 6.18b) yields K_{tot}. So from the combination of K_{tot} and k^*_{tot} the heat transfer coefficient can be found via (6.15b). In the relations used the leaf area index (LAI) should be known as well. This quantity can be found by measurements of the length of the leaves together with the amount of leaves per plant (Van der Vorst and Postel, 1972). The measurement of the steady state increments of the leaf temperature and transpiration with lamps switched on yields the proportionality factors C_T and C_n. These values may uncover how representative the leaf temperature and net radiation were that we have directly measured.

6.4.4. *Experimental results*

With the lysimeter reliable measurements of the transpiration on a small time scale could be performed. Due to the laboriousness of operating the lysimeter only a limited amount of measuring periods became available. From the night transpiration k^*_{tot} (relation 6.12) can be determined with small stomatal openings if the saturation pressure in the leaf e_l and the vapour pressure in the air e_i are known. The saturation pressure in the leaf is found from the leaf temperature. It is not a priori known to what extent the measured value is representative for that goal. If the increment is small then the difference between measured and effective leaf temperature will be small too. From that point of view accurate measurements require a leaf temperature that practically equals the air temperature. In that case only small vapour pressure differences will occur which means that a great relative error may be expected. So it is only possible to determine the order of magnitude of the total vapour conductivity k^*_{tot} in this way. Simulation afterwards (chapter 7) may show whether the measured conductivity matches all other measured climate quantities.

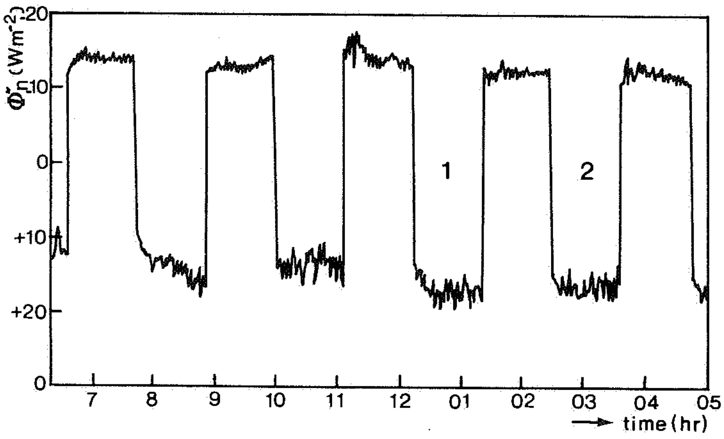

a. net radiation

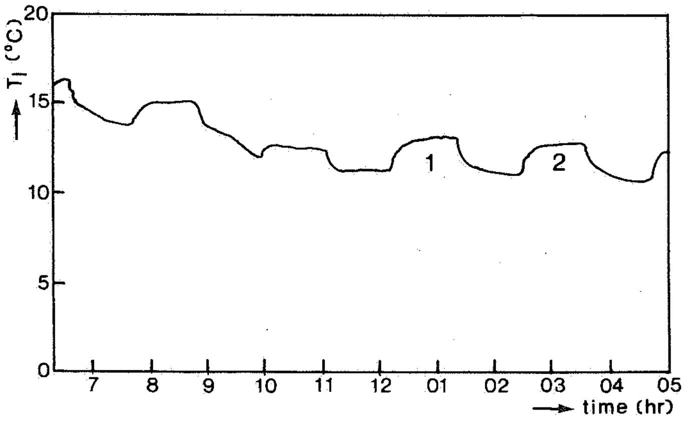

b. leaf temperature

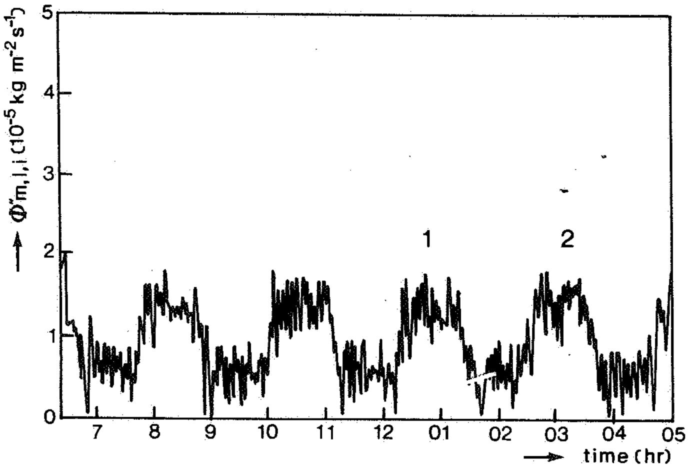

c. transpiration

Fig. 6.14. Measured net radiation, leaf temperature and transpiration during step response measurements.

From measurements during some night periods a total conductivity k^*_{tot} = 1.25 $10^{-8}sm^{-1}$ was found with an estimated error 0.5 $10^{-8}sm^{-1}$. After simulation runs (chapter 7) this error proved to be much smaller than what would follow from the measurements.

The heat transfer coefficient $\alpha_{c,l,i}$ can be found from the response of the leaf temperature on a step-wise change in the net radiation. In figure 6.14 measurements of the net radiation, the leaf temperature and the transpiration are given during a night with step-response measurements. After about 6 hours from the start of the scans (at 01.00 am), the successive values of the net radiation, leaf temperature and transpiration found with the I.R. lamps switched off, remain the same. The scattering of the transpiration is caused by the air movement around the leaves.

During the two "lamp on" periods at the end of the night we measured an increment of $30Wm^{-2}$ for the net radiation,of 1.7K for the leaf temperature and of 0.80 $10^{-5}kgm^{-2}s^{-1}$ for the transpiration. The measured leaf temperature curves are almost perfectly identical to the response curve of a first order system (figure 6.15). This means that relation 6.23 is valid and therefore that K_{tot} is constant during the measurement. This leads to the conclusion that the stomatal resistance is not affected by the step-wise irradiation of the I.R. lamps.

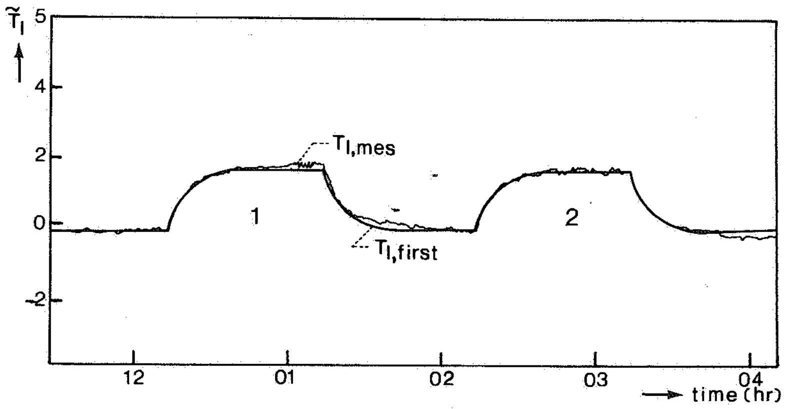

Fig. 6.15. The measured leaf temperature during the step response measurements ($T_{l,mes}$) compared to the step response of a first order system ($T_{l,first}$).

The calculated time constant τ_l is 325 s. To find K_{tot} from the time constant via (6.18b) we need the heat capacity of the leaves. In the measuring period concerned the leaf weight was 0.78 kg per m^2 of leaf area. This is in agreement with Acock et al. (1979) who proposed a relation for the specific leaf area as a function of the daily sum of photosynthetic active irradiation (Jcm^{-2}) and the mean daily temperature at which the tomato crop has been grown (daily sum of outside global irradiation was about $1250Jcm^{-2}$, which results in $440Jcm^{-2}$ of photosynthetic irradiation inside the greenhouse, and the mean daily temperature was about 16^oC). The LAI was determined at 2.0 and with the specific heat equalling that of water ($4.2\ 10^3JKg^{-1}K^{-1}$) this results in a heat capacity per m^2 ground area Cap''_l of $6.55\ 10^3Jm^{-2}K^{-1}$. So relation 6.18b yields $K_{tot} = 20.2Wm^{-2}K^{-1}$. Then relation 6.15b yields (with $\Delta H = 2.510^6Jkg^{-1}$ and $C_{p,T} = 90Nm^{-2}$ at 12^oC):

$$\alpha_{c,l,i} = (20.2/4) - (2.5 * 10^6 * 1.25\ 10^{-8} * 90/2) = 3.6Wm^{-2}K^{-1}.$$

From this heat transfer coefficient a mass transfer coefficient $k^*_{c,l,i}$ is found (relation 6.4 and 6.3b) of $2.2\ 10^{-8}sm^{-1}$ (the equivalent $k_{c,l,i}$ (relation 6.3a) is $2.9\ 10^{-3}ms^{-1}$ which again is equivalent to a boundary layer resistance of $3.4scm^{-1}$).
From the total conductivity k^*_{tot} (found to be $1.25\ 10^{-8}sm^{-1}$) and the conductivity of the boundary layer $k^*_{c,l,i}$ of $2.2\ 10^{-8}sm^{-1}$, the stomatal conductivity can be calculated, according to relation 6.13. The result is $k^*_{l,stom} = 2.9\ 10^{-8}sm^{-1}$. This is equivalent to a stomatal resistance of $2.6scm^{-1}$. The calculated boundary layer resistance shows a fair agreement with values found in practice under comparable conditions (section 6.4.1) while the stomatal resistance is low for night conditions (no light, closed stomata). However also Behboudian (1977) and De Graaf (1978, 1981), report greenhouse night transpiration values which are much higher than what could be expected from a resistance model with literature data. It might be possible that the resistance of the cuticula is much smaller for greenhouse plants than for plants in the open.

The transpiration at daytime will be much higher due to the shortwave irradiation. In figure 6.16 a daily course of transpiration, outside global irradiation and leaf temperature is given. After the steady transpiration during the night period a dynamic behaviour of the transpiration can be observed in

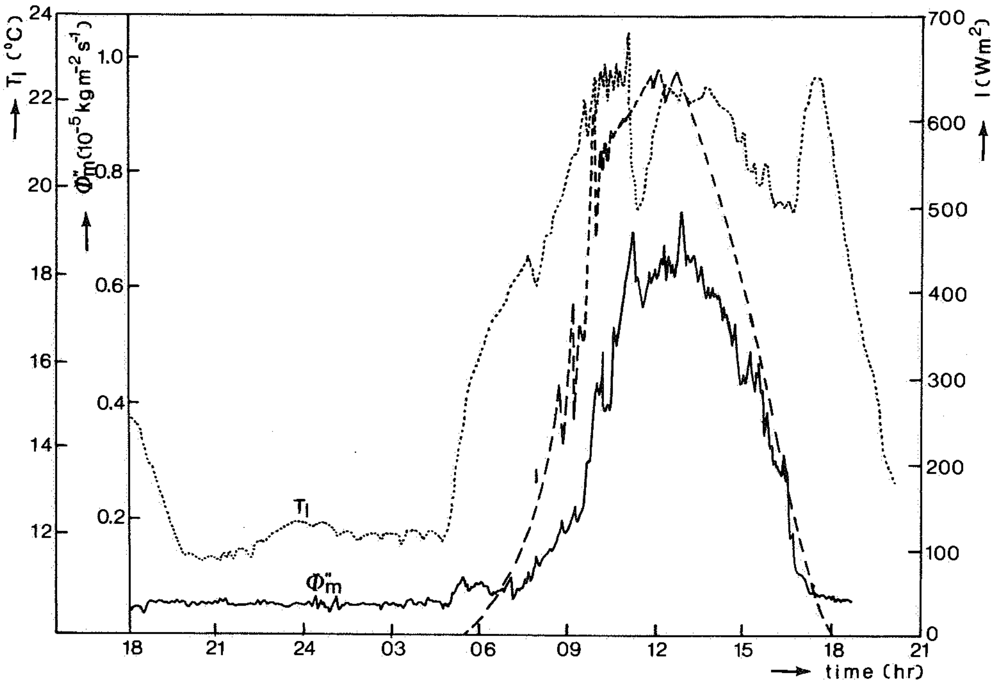

Fig. 6.16. Transpiration (ϕ''_m), outside global irradiation (I) and leaf temperature (T_l) during a 24 h. test period.

the daytime. First the irradiation affects the transpiration as a term in the energy balance over the leaves and so affects the leaf temperature. Secondly it affects the stomatal resistance directly or indirectly. However, irradiation is not the only phenomenon affecting transpiration. We found that for nearly equal irradiation the transpiration during the day represented in figure 6.16 is higher in the afternoon than in the morning. In figure 6.17 the transpiration during this day is given as a function of the irradiation. Very clearly some kind of hysteresis can be observed. This is not imperatively due to a difference in stomatal response on the light intensity between morning and afternoon but most probably to an effect of the greenhouse climate control. In the morning the ventilation windows are closed until the moment when the last peak can be observed in the leaf temperature (about 11.20 am). Before this moment in the greenhouse the vapour pressure is high and so the vapour pressure difference between leaf and air as the driving force for the transpiration is depressed. In the afternoon, until the windows are completely closed again (sudden raise in temperature at 16.15 am), transpiration is amplified by the decreased vapour pressure in the greenhouse air.

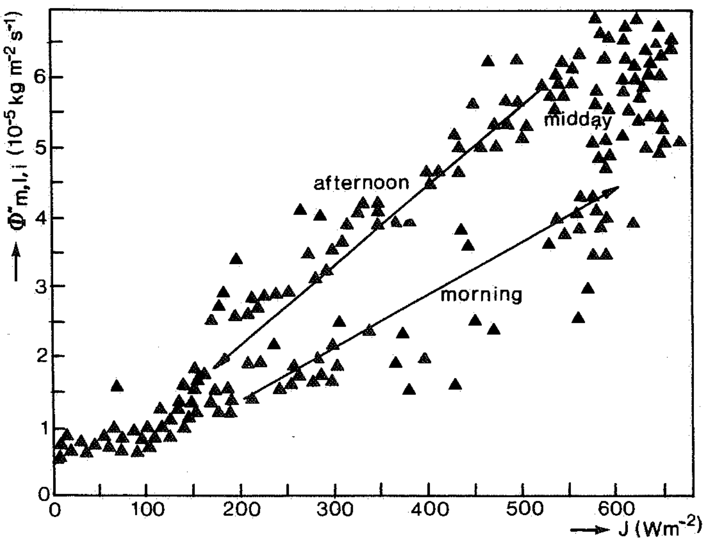

Fig. 6.17 Transpiration as function of outside global irradiation for the measurements represented in figure 6.16.

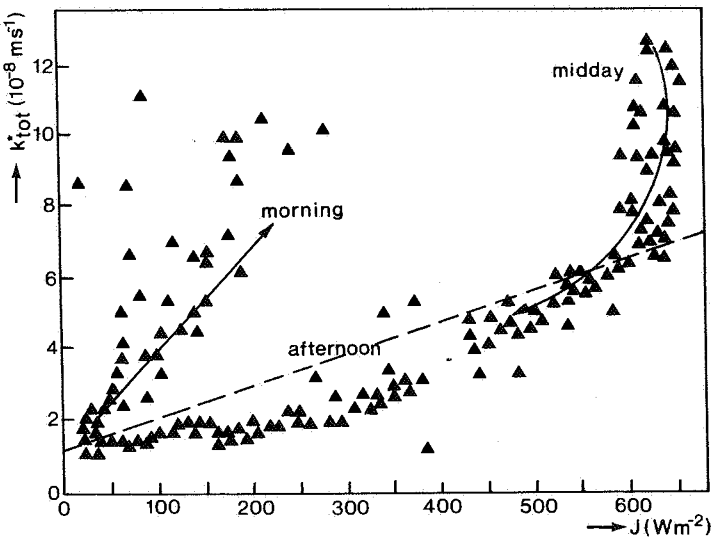

Fig. 6.18. The total conductivity k^*_{tot} plotted against outside global irradiation for the measurements represented in figure 6.16. (Most of the morning measuring points range out of the figure or are even negative).

In the daytime the total conductivity k^*_{tot} will not be constant as it was during the night. It will vary due to the varying stomatal conductivity $k^*_{l,stom}$. The total conductivity k^*_{tot} can be calculated during the day from the observed transpiration and vapour pressure difference between leaf and air (relation 6.12). In figure 6.18 the calculated k^*_{tot} is plotted against the outside global irradiation. The result shows large variations but some qualitative conclusions may be drawn. In the morning the total conductivity shows higher values than that in the afternoon but the scattering is so large in the morning that the quantitative results of this period do not seem reliable. The great scattering is caused by technical imperfections of the dry- and wetbulb psychrometers which were used to determine the air vapour pressure. Added to the inaccuracies in the saturation pressure inside the leaf, because of inaccuracies in the leaf temperature measurements, this resulted in vapour pressure differences that showed great variations between negative and positive values.

From about noon, much more consistency exists in the data. At high irradiation values it is noticeable in the figure that there is some evidence of a closure of the stomata. This phenomenon is known in literature as "midday depression" (Slavik, 1974) and is reported to be caused by waterstress. For well watered greenhouse plants no water stress will appear. However also Behboudian (1977) gives some evidence for a higher stomatal resistance in the afternoon for greenhouse tomatoes and Challa (1977) reports the same phenomenon for young well-watered cucumber plants. Whether it is caused by water stress due to the high transpiration, saturation with primary products of the photosynthesis or internal plant-physiological processes cannot be decided here.

Because of the scarceness of data speculation about the possible existence of hysteresis in the total conductivity k^*_{tot} as function of irradiance seems to be premature. Therefore a relation was assumed which linearizes the dependency of k^*_{tot} on the shortwave radiation I:

$$k^*_{tot} = (1.25 + 1.25\ 10^{-2}\tau_{tot}I)10^{-8}(sm^{-1}) \qquad (6.20)$$

with

τ_{tot} : total transmission of the greenhouse (chapter 5)

I outside global irradiation (Wm^{-2}).

Relation 6.20 is represented in figure 6.18 as a broken curve. The total transmission was about 0.7 during the measuring day. The preliminary relation 6.20 probably underestimates the transpiration in the morning and overestimates that in the afternoon. Further plant oriented research has to decide whether water-stress or other quantities have to be incorporated in relation 6.20.

The separation of the total conductivity into a leaf and a boundary layer conductivity during the day seems to be unnecessary in the greenhouse. The variations in the average local air velocities are measured as small and range from 0.1 - 0.2ms^{-1}. Therefore the conductivity of the boundary layer has been incorporated in the total conductivity as a nearby constant contribution.

7. A dynamic physical model of greenhouse climate

7.1. INTRODUCTION

The analysis of the energy budget of a greenhouse by Businger (1963) has lead to the consideration of various exchange processes in steady state energy and water vapour balances over various parts of the greenhouse. This approach has been adopted by many authors as a base for a calculation scheme simulating the effect of various factors on greenhouse climate.

Walker (1965) calculated the effect of ventilation on the temperature in the greenhouse using steady state equations.

Koppe and Stoffers (1967) applied the non-stationary energy balance over the greenhouse air with constant boundary conditions and an idealized daily sinus shaped shortwave radiation course to calculate the difference in response of greenhouses of different heights at various ventilation rates.

Takakura (1967, 1968) also calculated the response of the greenhouse air temperature from the over-all energy balance, applying Laplace transform. In the first paper the outside conditions varied according to a step function and in the second paper measured curves of the outside conditions were developed in a Fourier series for the same kind of calculation. In a further development (Takakura et al., 1971) latent heat was incorporated in the analysis and convective and radiant heat transfer were considered separately. Balances were set up for the soil (introduced as a two-dimensional medium) the vegetation, the greenhouse air and the greenhouse roof. The results were shown as a diurnal course of various greenhouse climate factors.

Seginer and Levav (1971) presented a detailed analysis of the physical modelling of greenhouse climate. The greenhouse was introduced as a one-dimensional system subdivided into the soil (varous layers), the vegetation, the greenhouse air and the cover. Energy and vapour balances were set up over these components. Results of the simulation were compared with measurements in a scale model of a greenhouse.

Selçuk (1973) used the steady state energy balances to calculate the climate in refrigerated, plastic covered, tube greenhouses.

Soribe and Curry (1973) combined a greenhouse climate model with a longterm plant growth model of lettuce. They presented a schematic diagram of a computer controlled greenhouse in which plant growth models had to be applied.

Maher and O'Flaherty (1973) calculated the effect of the solar irradiation, the ventilation rate, different covering materials and evaporative cooling on the leaf temperature using steady state energy balances over the vegetation, the greenhouse air and the greenhouse cover.

Kimbal (1973) based his model of the greenhouse climate on the steady state energy and vapour balances over the one dimensional compartmented greenhouse.

Garzoli and Blackwell (1973, 1981) in the first publication compared the measured response of a greenhouse under summer conditions from one steady state energy balance over the complete greenhouse. In the second publication, they compared the measured cover temperature to that calculated from the steady state energy balance over the cover.

Breuer (1976, 1983) applied the over-all steady state energy balance to calculate the energy demand for various crops under various growing conditions during one year, using weather records as boundary condition.

Froehlich et al. (1979) developed a closed-form analytical solution for the steady-periodic behaviour of the greenhouse climate using Fourier series as boundary conditions.

Kindelan (1980) presented a simulation model based on the non-stationary energy and vapour balances in a one dimensional compartmented greenhouse. Simulation results were presented but not compared with experimental data of real greenhouse experiments.

Van de Braak (1980) applied electrical network theory to simplify steady state energy balances over the greenhouse components. He gave an outline for easy hand calculations to make a quick evaluation.

Chiapale et al. (1981) computed the energy consumption during a defined period from the over-all steady state energy balance to estimate the regional distribution of the energy demand in France for various seasons.

Damagnez et al. (1979), Van Bavel et al. (1981) and Chiapale et al. (1982) applied a dynamic model based on the non-stationary energy and vapour balances in the one dimensional compartmented greenhouse to compare the behaviour of a fluid-roof greenhouse with that of a common glasshouse.

Ahmadi and Glockner (1982) and Ahmadi et al. (1982) numerically simulated the climate in a plastic-covered greenhouse. Their simulation results were compared with measurements in a small-scale greenhouse model.

Von Elsner (1982) based his simulation model on partly steady and partly unsteady heat and vapour balances. He divided the greenhouse into 10 horizontal air layers 6 vegetation layers and 7 soil layers to calculate the dynamical behaviour of the greenhouse climate. His test greenhouse was equipped with a heating system with high heating pipes and a chrysantemum crop was grown in the greenhouse.

Besides the differences in complexity and capability, there are also some striking similarities between the various simulation models. They are all built for single-span greenhouses but assume infinite horizontal dimensions by compartmenting the greenhouse in only one-dimension. All models were calculated for daily courses of the climate quantities regardless of fast fluctuations. In all cases literature data about the heat- and mass-transfer coefficients have been applied in order to calculate the energy and mass fluxes in the balances. The coefficients are neither validated nor adapted in greenhouse climate measurements. When there are differences between calculations and measurements (which, generally speaking, is always the case) then no attempt is made to minimize these differences afterwards.

In our work the emphasis is on the relation between the momentaneous greenhouse climate and the outside weather. In the Netherlands, especially in the coastal regions where most greenhouses are located, the weather conditions in general fluctuate very fast and very strongly. So the calculation of a smooth daily course of greenhouse climate quantities will hardly never correspond with reality. Therefore we decided to build up a model of greenhouse climate with the ability to calculate the greenhouse climate on a very short time scale. To achieve a high reliability we built up the model step by step. In the first set-up literature data were applied (Bot et al. 1977, Bot and Van Dixhoorn, 1978) and a first inventory of apparent problems could be made. The main problem was in the applicability of literature data to exchange processes. Much attention had to be paid to in-situ measurements on the various physical processes. These investigations were performed parallel to the development of the simulation model. Therefore in the present most recent model not all results of this research could be incorporated yet. However its stage of development is such that the main characteristics can be presented.

7.2. MODEL CONSIDERATIONS

To simulate the relation between the outside weather and the greenhouse climate, we have to consider first how the greenhouse climate can be represented. In chapter 2 the greenhouse climate quantities were defined. In general these quantities are distributed vertically as well as horizontally. It depends on the magnitude of their gradients whether they have to be considered as spatially distributed or as uniform quantities. We focussed our attention on the climate in a multispan greenhouse, in which tomatoes or cucumbers are grown, which is heated by hot-water heating pipes that are located at a small distance from the soil surface (low heating pipes).

The vertical gradients of the air temperature in a greenhouse with low heating pipes are reported to be small, while large gradients are reported in greenhouses with heating pipes located above the canopy (high heating pipes) (Winspear, 1977a,b, Okada, 1980). A tomato or cucumber crop is very open so that it does not introduce a vertical gradient. Other crops with a very closed canopy like most flower crops can be expected to introduce large gradients within the vegetation. Large horizontal gradients can be expected in greenhouses with leaky gables. Then a spatial circulation pattern is introduced by wind effects (Businger, 1963). The gables of our test greenhouses and of most greenhouses in practice are insulated and thereby sealed. In this case horizontal gradients can be expected to be small, as was confirmed by observations. This leads to the conclusion that in our case the greenhouse air can be assumed to be homogeneous. If a thermal screen is installed this still holds true if the screen is open. If it is closed then two homogeneous air compartments have to be considered, one below and one above the screen.

In section 6.4.2. the considerations for the vegetation were given. Due to the non uniform distribution of the net-radiation in the canopy, differences in leaf temperature can be expected. However, the assumption of an average leaf temperature and, therefore, a linearization of the transpiration and convection, does not introduce great errors. So the leaf temperature can be considered homogeneous. If photosynthesis has to be taken into account as well, then the canopy has to be divided into regions with uniform irradiation.

In the soil large gradients can be expected. In a large multispan greenhouse with a homogeneous soil, the soil heat fluxes will be mainly vertical, though with low heating pipes also horizontal fluxes will appear in the upper soil layers. The heat fluxes from the soil to the air are relatively small, so a homogenisation of the temperature in one horizontal soil layer will not introduce great errors. Therefore the soil can be divided into horizontal layers each of which having a homogeneous temperature.

The cover of the greenhouse is composed from one or more parallel sheets of transparent material (single or double glass etc.). In one sheet the difference between the temperatures at the inner and outer surface can be neglected. So for a cover with a single sheet the in- and outside cover temperatures are equal and one homogeneous cover temperature can be assumed. For a cover with more than one sheet a homogeneous temperature in each sheet has to be considered.

For each component defined above the energy and water vapour balance has to be set up. As we want to incorporate the effect of fast fluctuations in the outside weather conditions, the storage of energy or water vapour in the observed component has to be accounted for in the balances. This leads to a first order differential equation in time for each balance, so the complete model consists of a set of coupled first order differential equations. The notation of this set in normal mathematical formulas does not result in a clear picture of the physical interactions between the various equations. The differential equations can also be represented graphically; to do so we applied the bond graph notation. This leads to a very transparent scheme for the equations in which the coupling between the equations and therefore the various heat- and vapour-flows can be recognized. Besides having this advantage of transparancy the bond graph can be fed directly in the computer for an easy execution of the simulation.
In the next section the use of bond graphs for the representation of a dynamical physical model is explained and the first version of the greenhouse climate model is outlined. This first version is the framework which still supports the present model.

EPPO Bull. 9 (3) : 205-218 (1979)

7.3 Bond Graphs and Minicomputers in Greenhouse Climate Control[1] *

by G.P.A. BOT and J.J. VAN DIXHOORN

Laboratory of Physics and Meteorology, Agricultural University, Wageningen (Netherlands)

ABSTRACT

This paper is concerned with the modelling and simulation method used in greenhouse climate control. A bond graph is a topological diagram, clearly representing any kind of physical network. In this case, the bond graph models the heat and vapour flows between compartmented components and the coupling between heat and vapour flow.

The bond graph can easily be converted into a differential equation model to be solved, for example, by CSMP. In the present case, however, the bond graph was used as a direct input to an interactive simulation program on a minicomputer. The method was applied to model an experimental greenhouse described by STANHILL *et al.* (1973).

Introduction

In the department of Physics and Meteorology of the Agricultural University, Wageningen, research is aimed at developing better climate control strategies for implementation in computer-controlled greenhouses. The computer program will contain a simple model of the climate and of the behaviour of the plant.

The model makes it possible to estimate variables such as condensation of moisture on leaves. The control strategy can be adapted to prevent such conditions while optimizing biomass production and energy consumption. The accuracy of the model is restricted by the requirement that it has to be implemented using the cheap minicomputers that are nowadays used in greenhouse control.

This paper is concerned with the relatively new methods used for description and simulation of the climate model. Characteristic of these methods are :

— the easy representation of the model by a graph technique, in which the physical structure of the model is retained ;

— the conversational simulation of the model on a minicomputer which, after a parameter or structure change, shows the response of the model on a display scope or XY-plotter ;

— if needed, the differential equations can be simply extracted from the graph and can be simulated with a general simulation language like CSMP, using a large digital computer.

Additionally, these so-called bond graph models have the advantage that they are a uniform, topological description, applicable to thermodynamic, chemical, mechanical, hydraulic and electrical systems and the connections between such systems. The notation emphasizes the systems aspect of the problem and, at the same time, stimulates insight

---

[1] Paper presented at the Joint EPPO/IOBC Conference on Systems Modelling in Modern Crop Protection, Paris, 12-14 October, 1976.

* Reprinted with kind permission of the publisher

into its physical structure. Historically, bond graphs are a generalization of electrical analog networks of physical systems. They were developed in the 1960's by H.M. Paynter, D.C. Karnopp and R.C. Rosenberg (KARNOPP and ROSENBERG, 1975, OSTER *et al.*, 1973, VAN DIXHOORN and EVANS, 1974).

In the bond graph symbolism, a distinction is made between ideal components, like (heat) capacity, (thermal) resistance, or energy convertors, and power bonds, which are the energy-exchange connections between the components. The components are represented by letters or figures, while the bonds are depicted by a line with a half arrow.

$$C \;\longrightharpoonup\; R$$

Fig. 1
Two components connected by an oriented bond.

The orientation half-arrow shows the positive direction of energy flow.

Associated with every energy transfer at a power bond is a pair of physical variables, like force and velocity, voltage and current, temperature and entropy flow, chemical potential and molar mass flow. In bond graph terminology, they are called

symbol	generalised name	relation
$\xrightharpoonup[f]{e} R$	resistance	$e = R.f.$
$\xrightharpoonup[f]{e} G$	conductance	$f = G.e.$
$\xrightharpoonup[f]{e} C$	capacitance	$e(t) = e(0) + \frac{1}{c}\int_0^t f\,dt$ or $f = C\,\frac{de}{dt}$
$\xrightharpoonup[f]{e} J$	inertance	$f(t) = f(0) + \frac{1}{I}\int_0^t e\,dt$ or $e = I\,\frac{df}{dt}$
$\xrightharpoonup[f_1]{e_1} \underset{m}{TF} \xrightharpoonup[f_2]{e_2}$	transformer	$e_1 = m\,e_2$ $f_2 = m\,f_1$
$\xrightharpoonup[f_1]{e_1} \underset{r}{GY} \xrightharpoonup[f_2]{e_2}$	gyrator	$e_1 = r\,f_2$ $e_2 = r\,f_1$
$u(t) \longrightarrow SE \xrightharpoonup{e}$	e-source	$e = u(t)$ (externally specified)
$u(t) \longrightarrow SF \xrightharpoonup[f]{}$	f-source	$f = u(t)$ (" ")
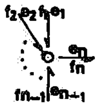	common-effort junction (parallel connection)	$e_1 = e_2 = \ldots = e_n$ $f_1 + f_2 + \ldots f_{n-1} = f_n$ (addition according to half arrows)
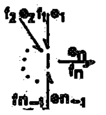	common-flow junction (series connection)	$e_1 + e_2 + \ldots e_{n-1} = e_n$ $f_1 = f_2 = \ldots = f_n$

Table 1
Definitions of bond graph components.

effort and flow variables, indicated by the letters e and f. In principle, these variables are chosen in such a way that their product has the dimension of power. The choice of the e- and f-variables partly corresponds with affinity and flux variables in irreversible thermodynamics.

Every component is defined to state a relation between the e- and f-variables at its connected bond(s), as indicated in table 1 for the most common linearized components.

It follows from the definitions that the bond graph of figure 1 is equivalent to equations (1) and (2), resulting in the well-known first order differential equation (3) :

$$e = Rf \tag{1}$$

$$f = -C \frac{de}{dt} \tag{2}$$

$$RC \frac{de}{dt} + e = 0 \tag{3}$$

The negative sign in equation (2) corresponds with the orientation half-arrow in figure 1 which, for C, is opposite to the defined direction.

The use of bond graphs is restricted to systems with lumped elements. Distributed systems, in which the variables are gradients and which are described by partial differential equations in space and time, can be approximated by concentrating variables and properties in discrete points of space. This is also done in the greenhouse model.

A Simplified Greenhouse Model

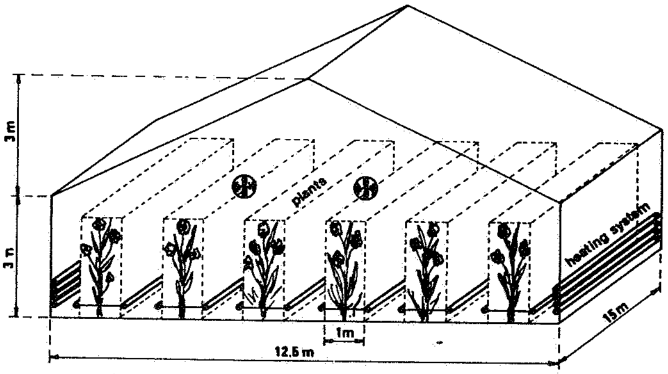

Fig. 2
The experimental greenhouse of Stanhill *et al.* (1973).

The model described here shows how bond graphs are used in our department. The experimental greenhouse of STANHILL *et al.* (1973) (fig. 2) was chosen to provide input data, because it gave the most complete list of data, especially radiation data. The glasshouse is aluminum-structured, glazed with diffusing glass and orientated N-S. The dimensions are given in figure 2. The plants, which covered 45 % of the greenhouse floor area, were roses cv. Baccara. Forced ventilation (25 times/h) was provided by cooled and humidified outside air, distributed throughout the length of the house by two perforated tubes of transparent plastic, 60 cm in diameter. This started working when the temperature in the greenhouse exceeded 28 °C. Natural ventilation was constant, about two times an hour. The heating system only worked at night, preventing low temperatures in the greenhouse.

In the model, some simplifications have first to be made: the inside air, the vegetation and the glass roof are considered to be internally homogeneous. For the air and the glass, this approximation is permissible, but for the vegetation, it is a much coarser approximation. It is accepted in this paper because the accent is not on accuracy but on demonstration. Finally, the soil is divided into four homogeneous layers. In the soil, sufficient water supply is assumed, so no restrictions have to be made for plant transpiration and soil evaporation due to water supply. The opening of the stomata is calculated according to the measurements of STANHILL *et al.* (1973).

From the simplifications, it follows that only thermal and water vapour models are needed. For the thermal model, the temperature T is the effort variable, expressed in °K (Kelvin) or °C; for the water vapour model, the vapour pressure (e) is expressed in N/m^2 (Newton per m^2). In figure 3, the effort variables, representing the states of all compartments, are indicated with an 0. These 0's will be the common effort or 0-junctions in the bond graphs in the figures which follow. No other temperatures and vapour pressures occur in the model. The flow variable in the thermal model would be entropy flow. A more practical choice, however, is heat flow (∅), expressed in W (Watt). In the water vapour model, this will be mass flow (f), expressed in kg/s.

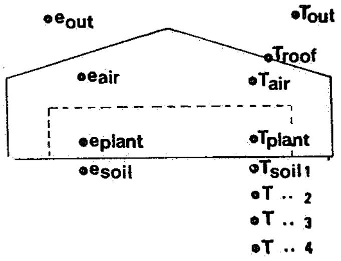

Fig. 3
The compartmented greenhouse.

Variables and Components in the Thermal Model

The variables mentioned already are temperature and heat flow. In the compartments, the heat balance has to be calculated. The general form is:

$$\text{Storage} = \text{Inflow} - \text{Outflow} + \text{production} \qquad (4)$$

According to table 1, an 0-junction represents addition of flow variables according to half arrows; so, in an 0-junction of the thermal model, the heat balance is set up. The inflow has to come from outside (radiation), or from other compartments, and the outflow has to go to other compartments; so, by estimating the exchange of heat between the 0-junctions, one can build up a thermal model. This thermal model, which, in fact, is a set of differential equations, can then be solved. How the different terms of the heat balance are represented will now be shown.

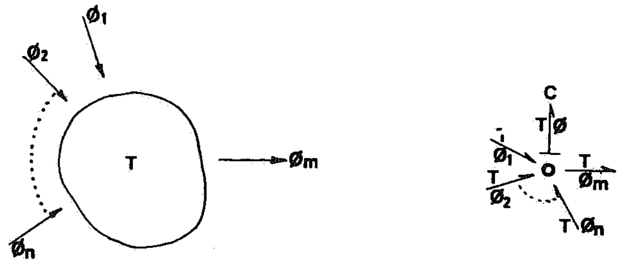

Fig. 4
Physical model (left) and bond graph (right) of heat capacity, with in- and outgoing flows.

In the bond graph of heat capacity (fig. 4), the 0-junction represents the heat balance, taking into account the direction of the half arrows:

$$\varnothing = \varnothing_1 + \varnothing_2 + \ldots \varnothing_n - \varnothing_m \qquad (5)$$

The bond graph also demonstrates that all heat flows are connected to the same temperature T. The C component (cf. table 1) represesents how much heat Q is stored:

$$Q(t) = Q(0) + \int_0^t \varnothing \, dt \qquad (6)$$

$$\text{or, also: } \frac{dQ}{dt} = \varnothing \qquad (7)$$

It also represents the specific relation between T and Q for the body under consideration. In the linear case:

$$T = \frac{1}{C} Q$$

with:

C : heat capacity $= \varrho \, C_p \, V$ (J/K)
ϱ : specific mass (kg/m^3)
C_p : specific heat at constant pressure (J/kg K)
V : volume (m^3) .

Finally, an important aspect for computation is whether the heat balance equation should be calculated by integration or by differentiation. This choice is also indicated in the bond graph, marking the bond graph to a computational scheme like a block diagram. The small stroke at the end of the bond to C is called the causal stroke. It indicates here that the effort variable (T) will be the result of the computation, the flow variable ($\varnothing$) being the cause. So, this placement of the causal stroke indicates that T is obtained by integration of $\varnothing$ (eq. 6). Placement at the C-end of the bond would indicate the computationally less attractive, but sometimes necessary, differentiation procedure by which $\varnothing$ is obtained from T.

Heat Transfer

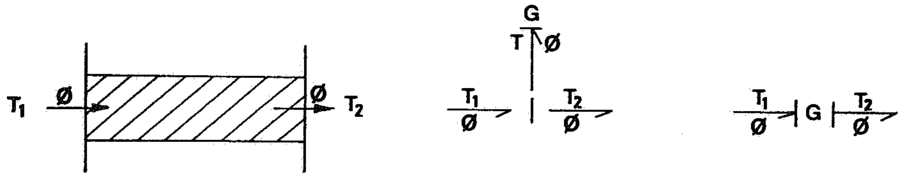

Fig. 5
Physical model and bond graph of heat transfer.

Heat transfer between two compartments with temperature T_1 and T_2 may be caused by conduction, convection, ventilation or radiation. When the temperature difference T_1-T_2 determines the heat flow, a 1-junction is used in the bond graph (fig. 5). According to table 1, all bonds have the same flow $\varnothing$; furthermore, $T = T_1 - T_2$ is obtained, respecting the directions of the half arrows. So, these arrows indicate the direction of the temperature drop. The G component expresses a linear or non-linear relationship between $\varnothing$ and T, depending on the heat transfer considered. The causal stroke now being placed at the G-end of the bond indicates that the flow variable ($\varnothing$) is the result of the computation, having the effort variable (T) as input.

It is easy now to represent the different forms of heat transfer :

Forced convection : $\varnothing = G.T$. G is a constant, equal to α A with α, partial heat transfer coefficient (W/m^2K), calculated with the variables wind velocity, air properties and geometrical factors from dimensionless relationships. In the model, forced convection exists between the outside air and the glass and between the inside air and the glass, the plants and the soil, when there is air movement in the house due to ventilation.

Free convection : $\varnothing = G.T$. Here, G is not a constant but a function of T, e.g., in the turbulent region along a vertical wall in air : $G = 1.4\ T^{0.33}.A$. In the greenhouse, free convection will occur along the heating system.

Conduction $\varnothing = G.T$. G is dependent on the thermal conductivity of the conducting materials: $G = \lambda\ A/L$, with λ = thermal conductivity (W/mK), L = distance between the centre of the two conducting compartments (m). λ can be either a constant, or be a function of different variables. In the model, conduction is considered in the soil with a constant λ.

Ventilation : the direction of the heat flow is given by the direction of the ventilation, so it does not depend on the temperature difference. This can be presented as an adapted G-component, but also by f-sources (cf. table 1). In the model, ventilation occurs with outside air and a ventilation air flux $\varnothing$ vent (m^3/s). In the air compartment, the inflowing heat is an independent heat source :

$$SF_{in} = \varnothing\ \text{vent}.\ \rho.C_p.T_{\text{outs air}} \qquad \text{(W)}$$

$\varnothing_{out}$ depends on the temp. of the air compartment itself and should be modeled by a G : $\varnothing_{out} = \varnothing_{vent}\ \rho C_p\ T_{air} = G\ T_{air}$

Radiation : The bond graph on the right in figure 4 shows a so-called two-port G. This form has to be used if the heat flow is not dependent on T_1-T_2. This is the case when heat is transfered by radiation, e.g., for black bodies :

$$\varnothing = \sigma A \; (T_1^4 - T_2^4), \text{ with } \sigma, \text{ constant of Stephan Boltzmann.}$$

In the greenhouse, heat is exchanged by thermal radiation between the opaque components (glass is opaque for thermal radiation). Corrections have to be made due to the emissivity of and the view factors between the compartments. In the literature (e.g. BUSINGER, 1963), it is reported that this thermal radiation is unimportant, because the temperature differences are small and other heat flows are much larger. So, in the model, the thermal radiation in the greenhouse is neglected.

On the other hand, radiation from outside (direct and diffuse shortwave and longwave) has to be incorporated in the model. These heat flows are input variables, which can be calculated from many other variables. In our case, they were calculated from the measurements of STANHILL *et al.* (1973). They were represented by time-dependent f-sources working on the glass, the plants and the upper soil layer.

On incorporating the above representations, a thermal bond graph for the simplified greenhouse model can be set up (fig. 6).

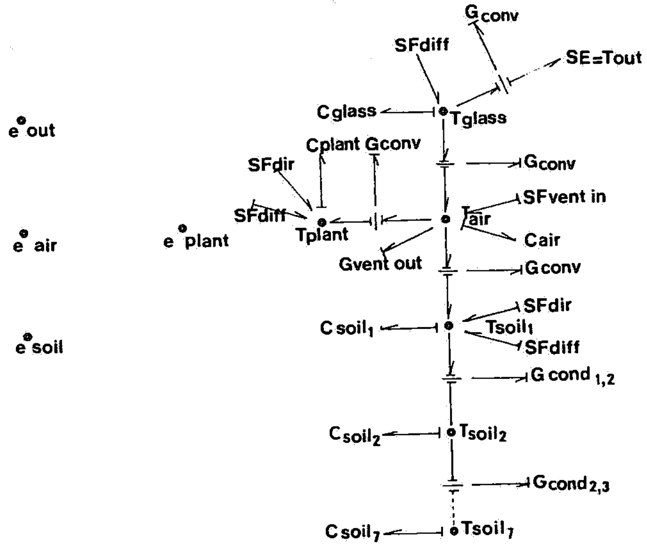

Fig. 6
Thermal bond graph of the simplified greenhouse model.

Variables and Components in the Water Vapour Model

The effort variable is the water vapour pressure e (N/m^2), while the flow variable is the water vapour mass flow f (kg/s). In figure 3, the compartmentation of the water vapour model is already given. As in the thermal model, one has again to represent the balances in the different compartments and the exchange of vapour between these compartments.

The balance here is also represented by the 0-junctions. Likewise, the terms are storage, in- and outflow by ventilation, convection, transpiration or evaporation and condensation.

Storage

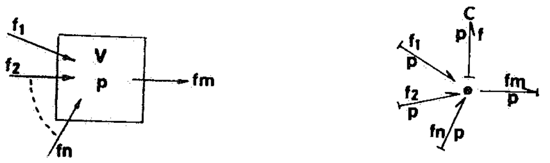

Fig. 7
Physical model (left) and bond graph (right) of vapour storage with in- and outgoing flows.

In figure 7, the vapour balance is stated by the 0-junction. The relation

$$p(t) = p(o) + \frac{1}{C} \int_{0}^{t} f \, dt$$

is represented by the C-component, where
$C = MV/RT$ (m.s^2)
with M = molar mass (kg/kmol) for water $M = 18$
V = volume of the compartment (m^3)
R = gas constant (= 8314 J/kmol K)
T = absolute temperature (K)

So, the water vapour capacity is temperature dependent.

Vapour Transfer

Vapour transfer by convection is represented in the same way as heat transfer, by a G-component. The value of G is

$$G = \frac{M.k.A}{RT} \quad (m.s)$$

with k = mass transfer coefficient (m/s).

Water Vapour Model (fig. 8)

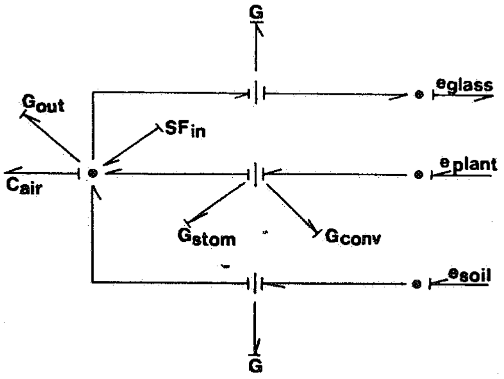

Fig. 8
Water vapour model.

In this sub-model, convective vapour transfer exists from soil to air and from leaf surface to air, or vice versa, corresponding to evaporation and condensation at the leaf or soil surface respectively. In the direction in which evaporation at the leaf surface takes place, the convective resistance from leaf to air is connected in series with the stomatal resistance. This resistance can be modelled as a function of many variables (e.g. PENNING DE VRIES, 1972). In our model, the measured data from STANHILL *et al.* (1973) were used to calculate the time-dependency of the stomatal resistance. Vapour transfer from air to the partial vapour pressure at the glass temperature can only take place in the direction air to glass, corresponding with condensation on the glass roof. As in the thermal model, vapour transfer by ventilation is represented by a flow source (S_f) for the inflow and a ventilation-dependent conductance (G) for the outflow :

$$S_f = \frac{M}{RT} \cdot \varnothing_{vent} \cdot e_{outside}$$

$$G = \frac{M}{RT} \cdot \varnothing_{vent}$$

Coupling Between Water Vapour and Temperature Model

At the surfaces where evaporation or condensation occurs, couplers or transducers (TD) are situated between the water vapour and the thermal model (fig. 9) :

$$\xleftarrow[f]{e} \mathrm{TD} \xleftarrow[\varnothing]{T}$$

Fig. 9
Water vapour - thermal coupling.

Like electrical transformers, they perform a transformation from the variable on one side to the corresponding variable on the other side. In this case, heat flow $\varnothing$ corresponds with vapour flow f :

$$f = \frac{\varnothing}{r} \text{ , r = heat of evaporation}$$

and temperature corresponds with saturated vapour pressure :

$$e = p(T) \text{ (vapour pressure table).}$$

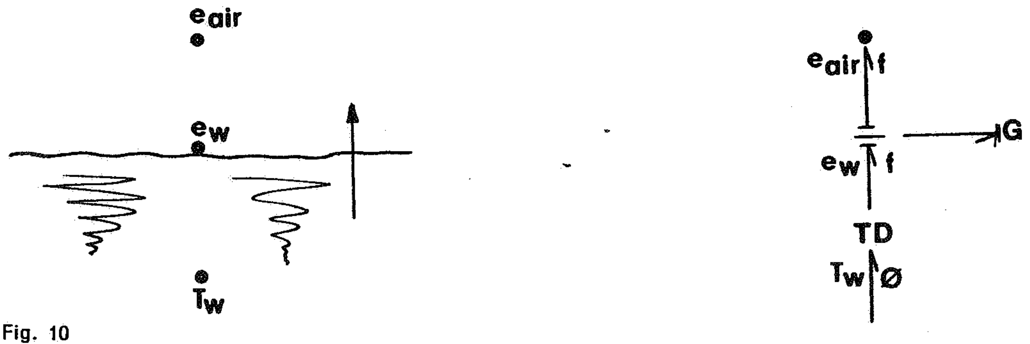

Fig. 10
Physical model (left) and bond graph (right) of exchange between water and air.

In figure 10, the above-defined transducer and a convective conductance G are used to represent the heat and vapour exchange at a free water surface.

If $e_w > e_{air}$, vapour flow f through conductance G, as well as heat flow $\varnothing$, are positive, so the heat content of the water is diminished by the evaporation heat flow $\varnothing$. If T_w is lower and $e_w < e_{air}$, f and $\varnothing$ reverse sign and condensation takes place. G is generally non-linear and dependent on the direction of f.

Combined bond graph (fig. 11)

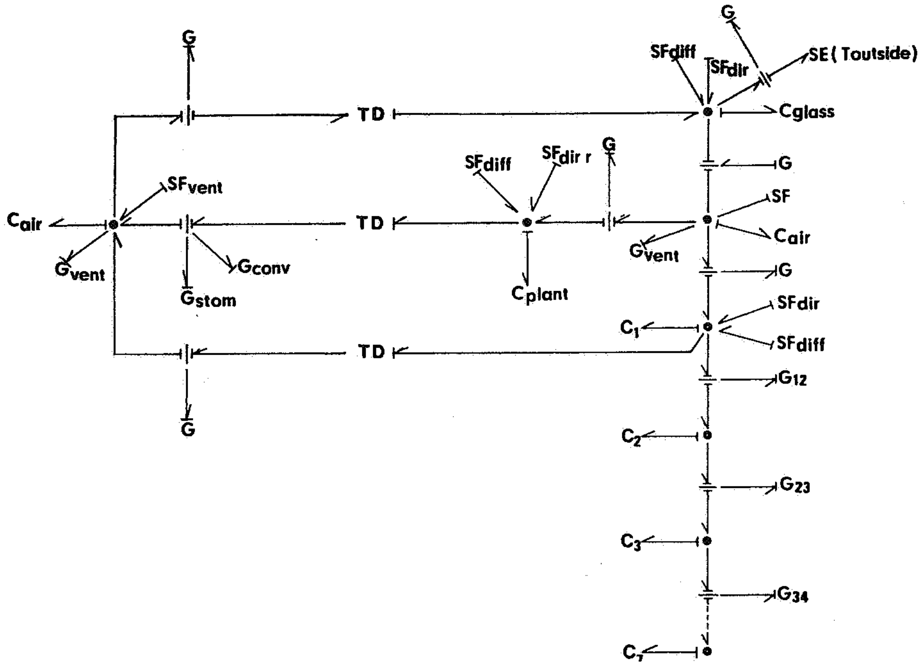

Fig. 11
Complete bond graph of the simplified greenhouse.

Simulation of the Model

The complete bond graph gives a clear insight into the structure of the model. Also, it represents the system equations in a well-ordered form. The solution of the system equations can be tackled in different ways. If it is preferred, a general simulation language like CSMP (IBM, 1966) can be used on a large computer.

The easiest way to solve a model written in bond graphs is to use a simulation language which accepts the bond graph components as input symbols. For linear systems, an elegant solution is the use of the ENPORT Program (ROSENBERG, 1974), which is suitable for large computers. It accepts the bond graph in its elementary form and supplies the user with the system response, the system matrix and its eigen values. On our department we use a minicomputer (PDP 11) with 16k-16bit memory, equipped with a display scope, XY plotter and some other in- and output facilities. The mini-computer has the advantage that the user has the possibility of direct conversation; a disadvantage is the relatively small memory. This disadvantage is decreased when a simulation language written in assembler language is used. For the PDP 11, such a simulation language is THT SIM (KRAAN, 1974, VAN DIXHOORN, 1977), used in our work.

As an illustration for this language, a simple soil model is given (fig. 12) as a physical model, bond graph, structure table and THT SIM table.

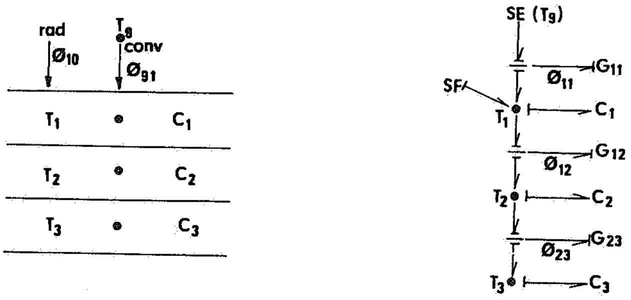

STRUCTURE TABLE

output		function		input
T9	=	SE		
∅11	=	G	,	T9-T1
T1	=	C	,	∅10+∅11—∅12
∅12	=	G	,	T1-T2
T2	=	C	,	∅12—∅13
∅23	=	G	,	T2-T3
T3	=	C	,	∅23

THT SIM INPUT TABLE

output		function		input
9	,	SE		
11	,	G	,	9,—1
1	,	C	,	10, 11,—13
12	,	G	,	1,—2
2	,	C	,	12,—13
23	,	G	,	2,—3
3	,	C	,	23

Fig. 12
Simple soil model and bond graph.

Setting up the bond graph with causal strokes will give no difficulties. In a simple procedure, explained in KARNOPP and ROSENBERG (1975) and VAN DIXHOORN (1977), computational difficulties such as dependent capacities or algebraic loops are found and remedied. In the example, no difficulties are encountered. Then, at the SE and C-components and their appropriate 0-junctions, the output variables T are named and numbered. The same is done with the SF and G components and their 1-junctions. Now, the structure table can be read from the bond graph, taking into account the half-arrows for the sign convention. Parameters like the numerical values of the C's and G's and the initial conditions of the effort variables at the 0-junctions must also be given. After specifying run data such as the time step, the desired output variable and its range on the display or plotter, the run command can be given and outputs as given in figure 13 result. Parameter or model structure changes can be typed in and will result immediately in different responses.

CSMP - SIMULATION

```
T 9 =
PHI 11 = G 11 * (T 9 - T 1)
T 1 = 1/C1 * INTGRL (0, PHI 10 + PHI 11 - PHI 12)
PHI 12 = G 12 * (T 1 - T 2)
etc.
```

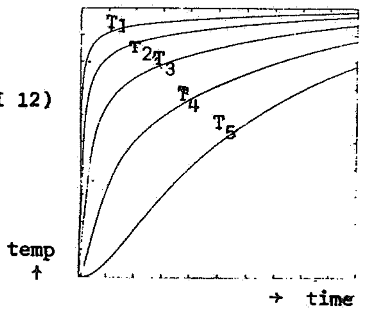

Fig. 13
Step response of soil model.

Result of the Simulation of the Simplified Greenhouse

The complete bond graph of figure 11 is programmed in THT SIM and simulated on the PDP 11. The time-dependent course of every interesting variable can be plotted. In figure 14, the temperatures during 24 h of the inside air, the plant, glass and upper soil compartments and the outside air are given. During the night, the plant

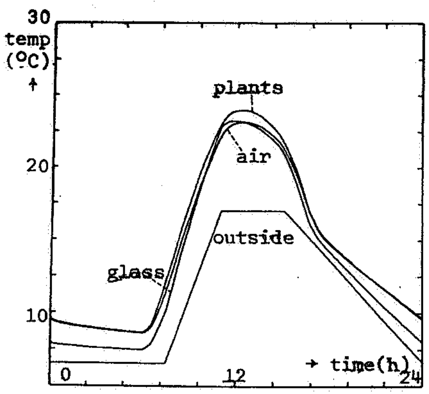

Fig. 14
Some temperatures in the unheated greenhouse.

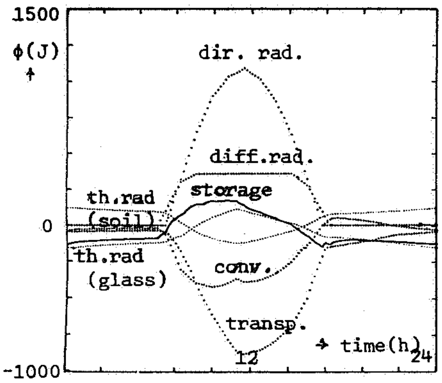

Fig. 15
Terms of the heat balance over the plant compartment (length 1 m).

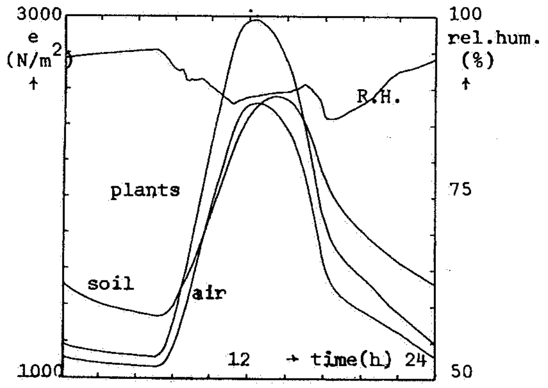

Fig. 16 Vapour pressures and relative humidity of air.

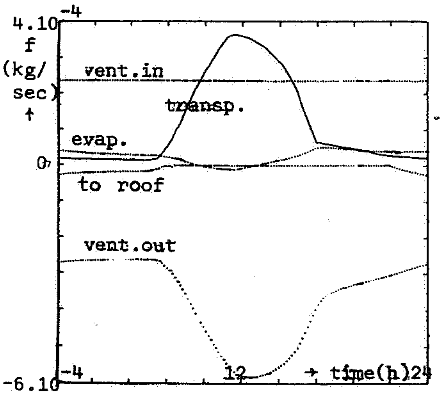

Fig. 17
Terms of water balance over air compartment (length 1 m).

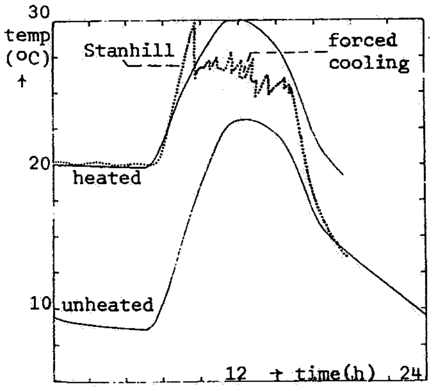

Fig. 18
Comparison of unheated, heated and Stanhill greenhouses.

and air temperature are almost the same ; by day, the plant temperature is higher than the air temperature. The adjustment of plant temperature is shown in figure 15, in which the terms of the heat balance over the plant compartment are given. By day, transpiration is the main negative term compensating the incoming radiation. At night, the thermal radiation from the soil and to the glass are the main heat fluxes, but they balance each other : the plant behaves as a radiation screen between soil and glass.

For plant transpiration, the driving force is the difference in vapour pressure between the plant and the air. In figure 16, vapour pressures over 24 h are given for the air, the plants, the upper soil and at the glass. The relative humidity (RH) of the air is also given. The air has a very high RH at night, due to the low temperature, and by day, due to the high transpiration and low ventilation grade. At night, the RH is controlled by condensation on the glass. As shown in figure 17 in which the terms of the vapour balance (except storage) over the air compartment are given, no condensation will occur on the plants.

In the same way, the response of a heated greenhouse can be given. The result for the temperatures is shown in figure 18. The air temperature measured by STANHILL *et al.* (1973) was higher during the day. The model reported here, however, cannot be accurate at the moment because several estimations were made of, e.g. transfer coefficients, and heat loss may therefore be too high. Compartmentation was also very rough, and more precise plant compartmentation will be especially important. Nevertheless, the method of simulation has proved to be suitable for modelling a greenhouse.

Bull. OEPP 9 (3) : 205-218 (1979)

RESUME

Utilisation du graphique « bond » et des mini-ordinateurs pour la régulation climatique des serres

par G.P.A. BOT et J.J. VAN DIXHOORN

Laboratory of Physics and Meteorology, Agricultural University,
Wageningen (Pays-Bas)

La présente étude concerne la mise au point d'une méthode pour l'établissement de modèles et de simulation permettant de régler les conditions climatiques en serre. Le graphique désigné par le terme de « bond » prend la forme d'un diagramme topologique, qui peut représenter tout type de réseau physique. Dans le cas considéré, le graphique « bond » sert de modèle aux flux de chaleur et de vapeur entre composants compartimentés en tenant compte du lien entre les flux de chaleur et de vapeur. La graphique « bond » se convertit facilement en un modèle d'équations différentielles qui peuvent, par exemple, être résolues par le système CSMP ; le graphique « bond » sert alors d'entrée directe à un programme interactif de simulation pour mini-ordinateur. Cette méthode a servi à l'établissement d'un modèle pour la serre expérimentale décrite par STANHILL *et al.* (1973).

REFERENCES

BUSINGER, J.A. (1963). *In* : W.R. VAN WIJK (ed.). Physics of Plant environment. N.H. Amsterdam : 277-318.

DIXHOORN, J.J. VAN (1977). Simulation of bond graphs on minicomputers. *J. Dyn. Syst. Meas. Control, Trans ASME, Series G* **99** : 9-14.

DIXHOORN, J.J. VAN & F.J. EVANS (1974). Physical Structure in Systems Theory. Acad. Press, London.

IBM (1966). IBM 1130 Continuous System Modelling Program, IBM Manuals, SH 20-0905 and H 20-0209.

KARNOPP, D.C. & R.C. ROSENBERG (1975). System Dynamics : A Unified Approach. Wiley, New York.

KRAAN, R.A. (1974). THT SIM : A conversational simulation program on a small digital computer. *Journal A* **15** : 186-190.

OSTER, G.F., A.S. PERELSON & A. KATCHALSKY (1973). Network Thermodynamics : dynamic modelling of biochemical systems. *Quarterly Rev. Biophysics* **6** : 1-134.

PENNING DE VRIES, G.W.T. (1972). A model for simulating transpiration of leaves with special attention to stomatal functioning. *J. appl. Ecol.* **9** : 55-77.

ROSENBERG, R.C. (1974). A Users Guide to Enport — 4. Wiley, New York.

STANHILL, G., M. FUCHS, J. BAKKER & S. MORESHET (1973). The radiation balance of a glasshouse rose crop. *Agric. Meteorol.* **11** : 385-404.

7.4. OUTLINE OF THE PRESENT MODEL

From the calculations with the first version of the model and comparison with climate measurements, it became very clear that detailed knowledge about various exchange processes was missing. Either literature data were not available or, on the other hand, it seems doubtful whether eventual literature data from isolated laboratory experiments could be applied without any adaptation. Evidently in the greenhouse environment reciprocal influence is to be expected. Therefore the emphasis was on the formulation and in-situ measurement of the various exchange processes in the greenhouse (chapter 3-6). Parallel to this research the present model was developed from the first version of the simulation model that was described in section 7.3.
With the present model we simulated the momentaneous greenhouse climate in an infinitely large multispan greenhouse, equipped with a thermal screen, as a function of the outside weather conditions, the control actions in the greenhouse and the physical properties of the various components of the greenhouse. The various exchange processes are formulated according to chapters 3-6, though the most recent results could not yet be incorporated completely. The compartmentation is according to section 7.2.
In figure 7.1 the corresponding 0-junctions are given for each component.
In additions to the low heating pipe system, also a high heating pipe system is represented. The number of pipes of the high system is small compared to that of the low system (mostly one high and four low pipes per span of a Venlo-greenhouse). The high pipes will only be used if the low system does not satisfy the energy demand of the greenhouse. So the high heating pipes do not create large vertical temperature gradients and thus do not interfere with the assumption of a homogeneous air temperature.

The energy and mass balance can be set up over each greenhouse component using bond-graph notation according to section 7.3. First the storage of energy and water vapour should be taken into account in each component. This is represented by a power bond to a C-symbol (figure 7.2).
From outside energy and vapour fluxes enter the various components. Shortwave radiation fluxes are absorbed by the roof cover, the thermal screen, the vegetation and the soil surface. These fluxes being system independent are represented as SF symbols (figure 7.2). The transmission of the cover for both direct and diffuse radiation has to be defined according to chapter 5 and from

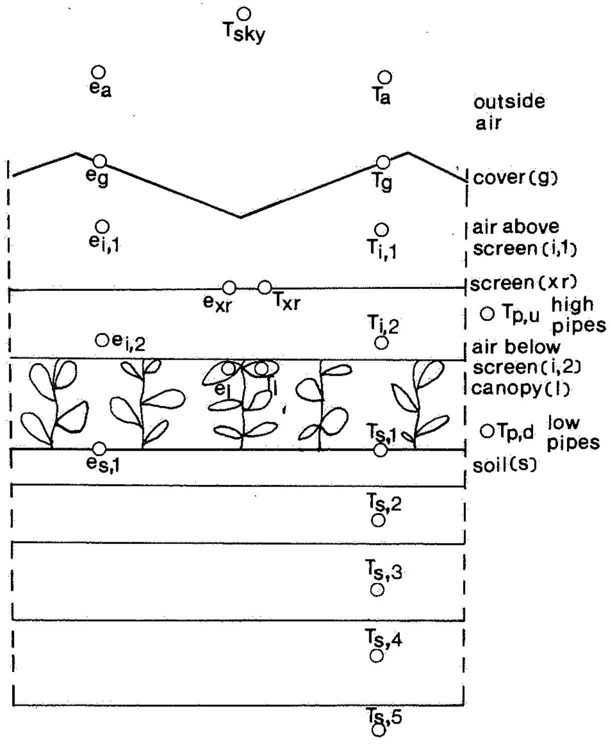
Tsky
ea
Ta
outside air
eg
Tg
cover(g)
ei,1
Ti,1
air above screen(i,1)
exr
Txr
screen(xr)
Ti,2
Tp,u
high pipes
ei,2
air below screen(i,2)
el
Tl
canopy(l)
Ts,1
Tp,d
low pipes
es,1
soil(s)
Ts,2
Ts,3
Ts,4
Ts,5

Fig. 7.1. Greenhouse compartmentation for the present model.

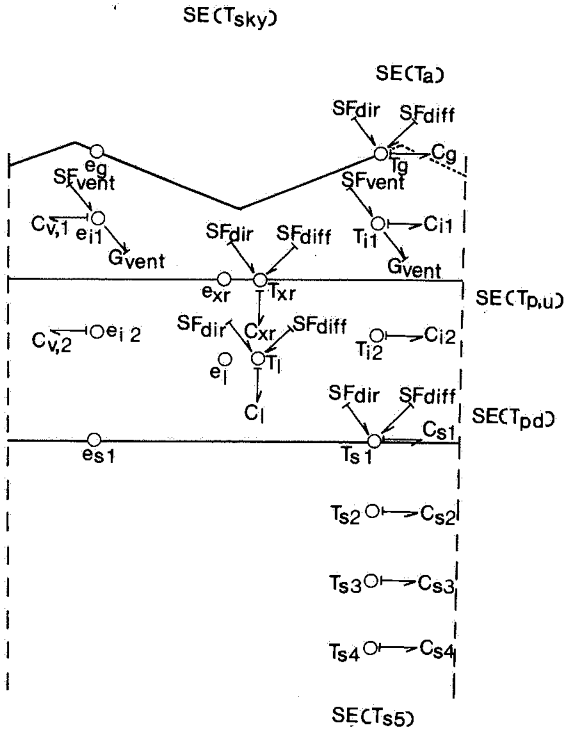
SE(Tsky)
SE(Ta)
SFdir
SFdiff
Cg
Tg
eg
SFvent
SFvent
Cv,1
ei1
Gvent
SFdir
SFdiff
Ti1
Ci1
Gvent
exr
Txr
SE(Tp,u)
SFdir
Cxr
SFdiff
Cv,2
ei 2
Ti2
Ci2
el
Tl
Cl
SFdir
SFdiff
SE(Tpd)
Cs1
es1
Ts1
Ts2
Cs2
Ts3
Cs3
Ts4
Cs4
SE(Ts5)

Fig. 7.2. Bond graph representation of direct and diffuse irradiation, ventilation, energy and vapour storage and the boundary conditions.

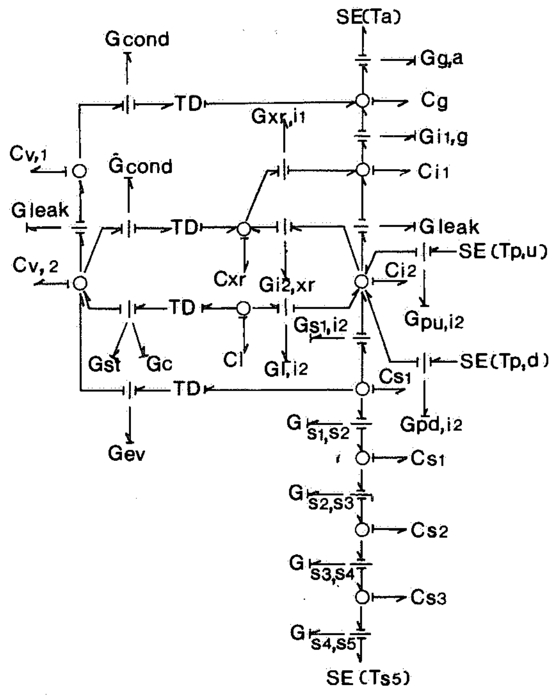
SE(Ta)
Gg,a
Gcond
TD
Cg
Gxr,i1
Gi1,g
Cv,1
Ĝcond
Ci1
Gleak
TD
Gleak
SE(Tp,u)
Cv,2
Cxr
Gi2,xr
Ci2
TD
Gs1,i2
Gpu,i2
Gst
Gc
Cl
Gl,i2
SE(Tp,d)
TD
Cs1
G s1,s2
Gpd,i2
Gev
Cs1
G s2,s3
Cs2
G s3,s4
Cs3
G s4,s5
SE(Ts5)

Fig. 7.3. Bond graph representation of the exchange of heat and water vapour between the various components.

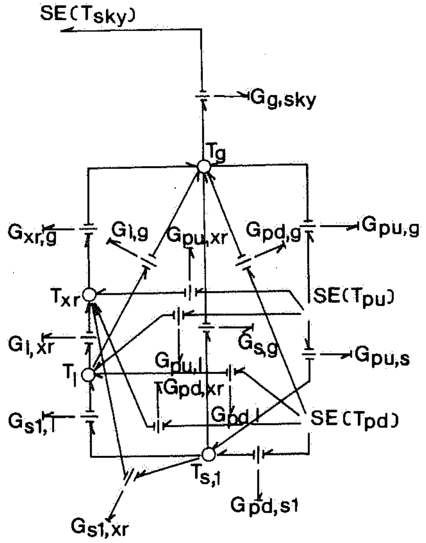
SE(Tsky)
Gg,sky
Tg
Gxr,g
Gl,g
Gpu,xr
Gpd,g
Gpu,g
Txr
SE(Tpu)
Gl,xr
Gs,g
Gpu,s
Tl
Gpu,l
Gpd,xr
Gs1,l
Gpd,l
SE(Tpd)
Ts,1
Gpd,s1
Gs1,xr

Fig. 7.4. Bond graph representation of the exchange of thermal radiation between the opaque components of the greenhouse.

this transmission and the canopy characteristics the distribution of the shortwave radiation over the various components is determined.

Other fluxes defined by outside conditions, and therefore also represented by SF-symbols, are the influx of energy and water vapour due to ventilation (figure 7.2). These fluxes enter the air-compartment between roof and screen. The outflux due to ventilation depends on the temperature and vapour pressure in this compartment, so it is system dependent. These fluxes are represented by a power bond to a G-symbol (figure 7.2). The ventilation characteristic of the multispan greenhouse is dependent on the outside windspeed, the window aperture and the type of window as defined in chapter 3 and 4.

Between the various greenhouse components, energy and water-vapour is exchanged due to convection and conduction. This is represented by bonds to a G-symbol in figure 7.3.

The energy model determines the temperatures of the leaf, the screen, the glass cover and the soil surface. As a result the vapour fluxes from the leaves due to transpiration, that from the soil surface due to evaporation and that to the screen and glass cover due to condensation are part of the energy balance over these components. This coupling between the thermal and water vapour model is represented by a TD symbol in figure 7.3.

The following boundary conditions are system independent and are thus represented in figure 7.3 as SE symbols: the outside air temperature, the temperatures of the low and high heating pipes and the soil temperature at a depth of about 1 m.

The outside air vapour-pressure is incorporated in the SF-symbol for the vapour influx due to ventilation.

The two air compartments exchange energy and water vapour directly due to air leakage through the screen. This exchange too is represented by a bond to a G-symbol.

The various exchanges represented by the G-bonds have been dealt with in chapter 6, except for the exchange through the screen. This exchange is assumed to be dependent on the temperature difference between the two air compartments according to ventilation due to temperature differences (chapter 3).

The opaque greenhouse components exchange energy due to thermal radiation. In figure 7.4 this, too, is represented by G-bonds. The sky temperature is a boundary condition that is represented as a SE symbol. In the G's due to thermal radiation, the emission coefficient of the surfaces involved, the view factor from one surface to the other and the area of the first surface are incorporated. Again the structure of the canopy has its impact on the radiation via the view factors of the vegetation, of the low heating pipes and of the soil surface to the other components. So a proper determination of the transmissivity of the canopy during the growing season is important for both the distribution of the shortwave and longwave radiation.

In the above the complete structure of the greenhouse climate model has been given as a combination of the figures 7.1 to 7.4. The given structure is that of the climate model for a greenhouse with a closed thermal screen. If the screen is opened, the two air compartments are lumped to one greenhouse air compartment. In the recent version of the model, the bond graph is directly translated into a computer program using CSMP as programming language.
The simulation is executed on the DEC 10 Wageningen University computer. This computer is able to handle large datafiles for the input of the measured boundary conditions. Besides, data files of measured state variables (section 7.5) can be handled to compare simulated and measured climate quantities. Subroutines for parameter estimation can be coupled to the model to adapt modelparameters and so improve the agreement between calculated and measured climate quantities.

7.5. EXPERIMENTAL SET-UP

To compare the response of the simulation model with that of a real greenhouse, detailed measurements were performed of the greenhouse climate. The results of the first versions of the model without vegetation were compared with measurements of climate quantities in one of the compartments of the 24-compartment greenhouse complex of the Glasshouse Crops Research and Experimental Station at Naaldwijk. The ventilation experiments (chapters 3 and 4) were also carried out in this greenhouse complex. The output of the present version of the model is compared with measured data in a 8-span Venlo greenhouse with an area of 560 m^2, sited at the Institute of Agricultural Engineering (IMAG) at Wageningen. The experiments on the exchange processes (chapter 6) were carried out in this greenhouse. An outline of the most recent experimental set-up will be given below.
The 8-span test greenhouse (figure 7.5) is oriented east-west, the span-width is according to a Venlo greenhouse equal to 3.2 m, the gutters are at a height of 2.45 m and a thermal screen was installed at a height of 2.05 m. The roof

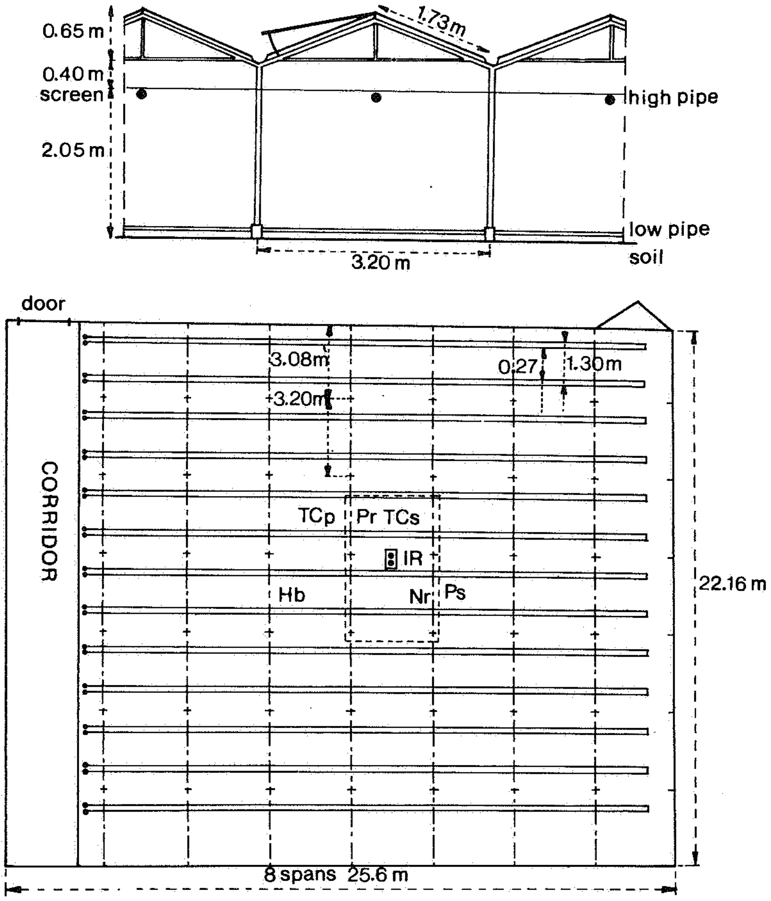
0.65 m
0.40 m
screen
2.05 m
1.73m
high pipe
low pipe
soil
3.20 m
door
CORRIDOR
3.08m
3.20m
0.27
1.30m
TCp
Pr TCs
IR
Hb
Nr
Ps
22.16 m
8 spans 25.6 m

Symbols	
▯	Lysimeter
Nr	Net-radiometers
Pr	Pyranometers
TCs	Thermocouples soil temperature
TCp	Thermocouples pipe temperature
Ps	Psychrometers
IR	IR thermometer
Hb	Hot-bulb anemometers

Fig. 7.5. Overview and dimensions of the test greenhouse, with the location of the climate sensors.

slope is 22^0. The greenhouse is equipped with ventilation windows only installed in the east side of the roof. The ventilation windows have a length of 1.73 m (ridge to gutter) and a width of 0.7 m (width of one glass pane) and they cover an area of 11.5% of the total roof area. Their maximum opening angle is 11^0. The heating system is a hot-water pipe system with 4 pipes at a height of 5 cm and 1 pipe at a height of 2 m, both per span-width. The low pipes are perpendicularly oriented to the ridge of the greenhouse while the high pipes are parallelly oriented to it. The gables of the greenhouse are insulated with air-bubble plastic and extra heating pipes along the gables compensate for the heat loss through the gables. The greenhouse air temperature was controlled by the Imag computer control system (Van Meurs, 1979).

The test period was in the winter and spring of 1982. The crop, tomatoes CV Marathon, was planted on 3 January 1982. It was grown on rockwool with drip irrigation. The soil of the greenhouse was completely covered with a white plastic sheet. In the centre of the greenhouse (figure 7.5) the sensitive lysimeter was located for the measurement of the transpiration of the crop (section 6.4).
The state variables were measured near to the lysimeter. These were the leaf temperature measured by means of an infra-red thermometer, the greenhouse air temperature and vapour pressure measured with dry and wet bulb thermometers (ventilated and radiation shielded), the temperature of the soil surface and the soil temperature at some depths (section 6.3), and the temperature of the thermal screen and the glass cover measured with very thin thermocouples glued against the glass and the screen material. The greenhouse air temperature and vapour pressure were measured at 4 locations: one above the screen, and three at even vertical distances below the screen. The surface temperatures of the low and high heating pipes were measured with thermocouples attached on the outside of the heating pipes. The outside air temperature and vapour pressure were measured with the type of dry and wet bulb thermometer as was used inside. Both shortwave and longwave radiation were measured using pyranometers and net-radiometers. Global radiation was measured outside the greenhouse and inside at various heights: just above the thermal screen, one just below the screen, one just above the canopy and one at ground level between the plants. Just above the canopy the reflected shortwave radiation too was measured. Unfortunately no distinction could be made between direct and diffuse radiation, because no equipment was available for a separate measurement. Therefore an estimation of the ratio of direct and diffuse radiation was made from the weather conditions (chapter 5). In addition to the shortwave radiation measurements, net radiation was measured, outside above the glass cover and inside at several positions: just above the screen, just above the canopy and at two lower positions: one just between the low heating pipes (without "seeing" these pipes) and one at the same height between the plants. Finally the net radiation was measured above a surface with a well defined temperature to calculate the sky temperature as a boundary condition (see section 5.3). Last of all we also measured the air movement inside, as well as outside the greenhouse. The outside wind speed is a parameter needed for the quantification of the ventilation exchange and of the heat transfer coefficient at the outside of the cover. It was measured together with the wind direction at a

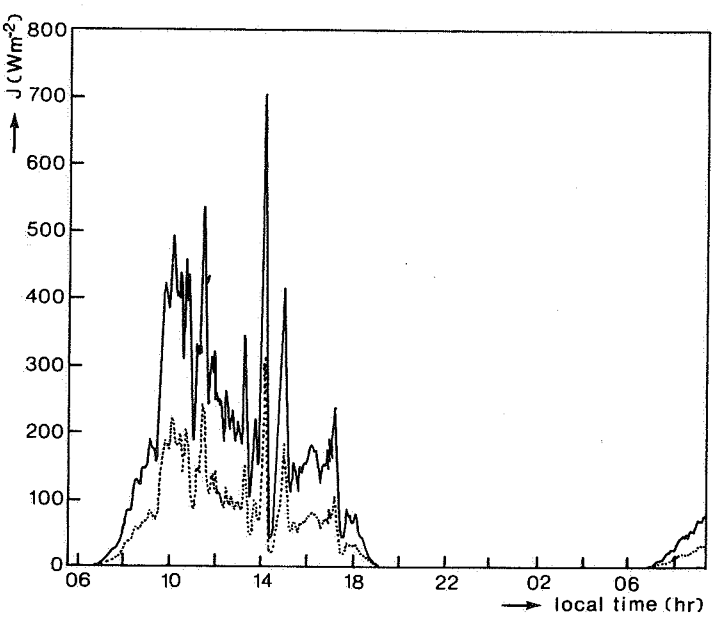

date: 1983, March 23 March 24

Fig. 7.6. Outside global irradiation (———) and by the canopy absorbed shortwave radiation (--------) during the test period in March.

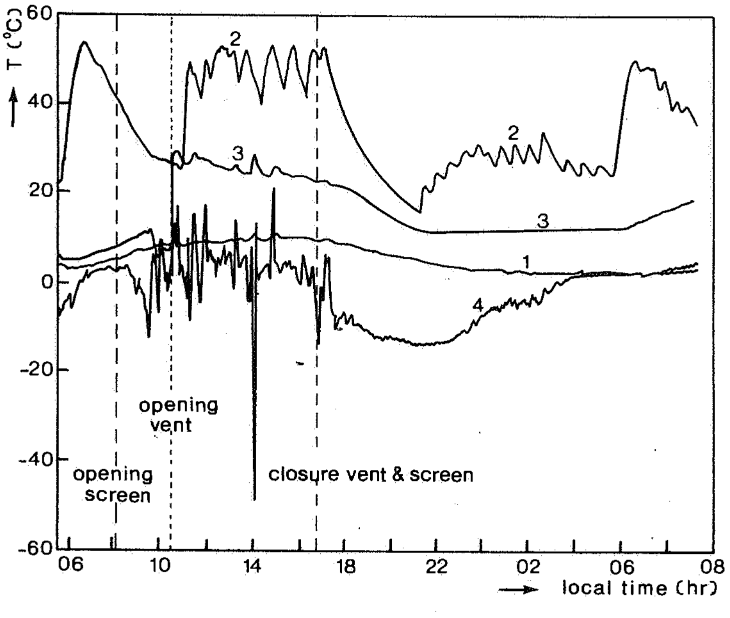

Fig. 7.7. The observed temperatures of the outside air (1), the high heating pipes (2), the low heating pipes (3) and the sky temperature (4). These data act in the simulation as boundary conditions.

height of about 3 m above ridge level. The inside air velocity was measured to check if this quantity is dependent on other climate quantities. It was measured with four hot-bulb anemometers at various locations in the greenhouse.
In total 53 sensors were placed to measure the above mentioned quantities. They were scanned by means of a computer controlled data-logging system during some measuring periods in the growing season. A scan interval of 3 min was chosen to obtain data with a short time interval and to conserve a manageable length of the data files. The data were stored on a TU58 magnetic cassette tape recorder. The tapes were copied on a hard disc of a PDP11-34 minicomputer and the files were rearranged. From the PDP11-34 the data files of the boundary conditions, some state variables, the transpiration, the outside wind speed and the window aperture, were transferred by telephone line to the DEC10 Wageningen University computer system for further processing.

7.6. SIMULATION AND EXPERIMENTAL RESULTS

Results of the measurements and of the simulation will be discussed in combination. As mentioned before not all physical processes have yet been incorporated according to the results of the chapters 3-6. The first as yet unadapted process is that of the convective heat transfer at the outside of the cover. In the simulation model this is assumed to be dependent on the outside wind velocity according to relation 6.1a with C_{fo},n,m equal to 0.036, 0.8 and 1/3 respectively. This results in a much stronger dependency of the outside heat transfer coefficient on the outside wind speed. The second point not yet incorporated is that of the separated consideration of the diffuse and direct radiation. The estimation afterwards of the ratio of the diffuse and direct radiation leads to great errors if there is a considerable amount of direct radiation. If the weather conditions point out that the diffuse radiation is predominant reliable results will be obtained. Therefore the results of a day with a high ratio of diffuse to direct radiation will be discussed, but with characteristic fluctuations of the global irradiation.
A daily course of the global irradiation that responds to this criterion is that of figure 7.6, measured on 23 March 1982. The weather was cloudy with a light cloud cover, so sharp fluctuations of the irradiation are observed with some pronounced peaks due to short periods of direct sunshine. On a cloudless day the maximum global irradiation on this date would be about 650 Wm^{-2}. From

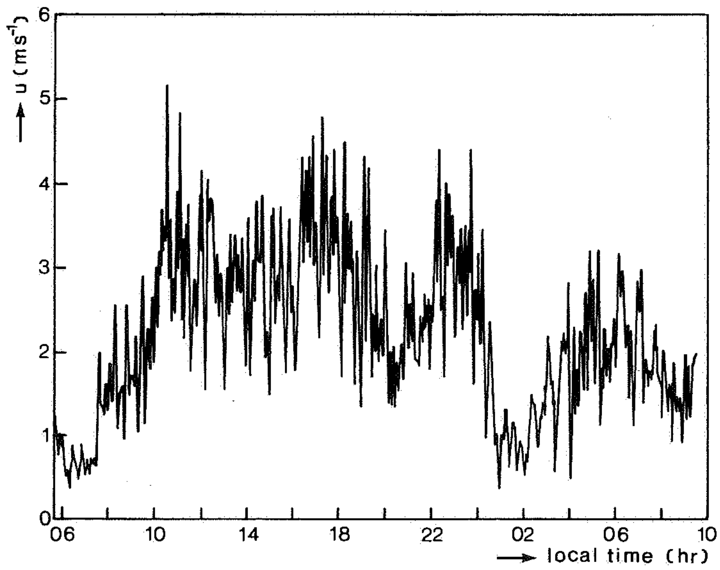

Fig. 7.8. The outside wind speed during the test period.

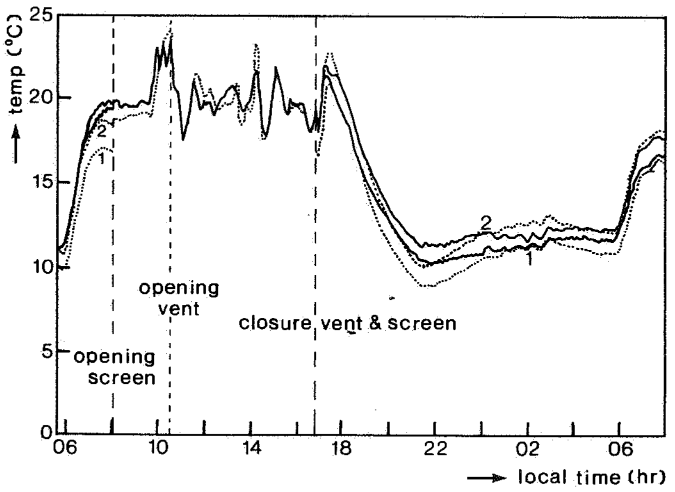

Fig. 7.9. Measured (———) and simulated (-------) temperatures of the air above (1) and below (2) the thermal screen. From 08.10 until 16.45 hr the screen is open, so in this period only one air compartment is considered.

the transmission of the cover and the characteristics of the canopy, the absorption of the canopy can now be calculated. This leads to the broken line in figure 7.6.

The boundary conditions , namely the temperatures of the high and low heating pipes, the temperature of the outside air and the sky temperature are given in figure 7.7. The temperature of the low heating pipes is strongly increased just before sunset to increase the greenhouse air temperature and hence the temperature of the vegetation before transpiration is actuated by the irradiation. By this procedure condensation on the vegetation and the fruits is prevented.

Just after 8.00 a.m. the screen is opened, and at about 10.30 a.m. the ventilation windows are opened under manual control. This would cause the air temperature in the greenhouse to become too low, so the temperature of the low heating pipes is increased. After the closing of the screen and the ventilation windows at about 5.00 p.m. the low heating pipes slowly cool down and their temperature is set on the night level. The next day this procedure is repeated exactly.

The measured temperature of the high heating pipes shows an erroneous shift of about -15°C, until 10.30 a.m. In this way the high heating pipes would withdraw energy from the greenhouse air during this period. In the simulation this actually occurs.

The outside air temperature shows a smooth daily course with an average temperature of about 5°C and an amplitude of 5°C. The variation in the sky temperature is much more important. By day it increases to about 5°C and during the night it drops to about -15°C at 9.30 p.m. In the evening the sky was clear,later on it became hazy and in the early morning at about 4.0 a.m. even mist occurred. The sky temperature then almost equals the outside air temperature. The variations at day are caused by the effect of shortwave radiation on the measurement of the sky temperature so it would be bettter to filter these variations in order to get rid of the erroneous fluctuations.

The vapour pressure of the outside air is not shown separately, it is very low especially compared to that of the greenhouse air.

The outside wind speed, as system parameter is shown in figure 7.8.

With the above boundary conditions and a soil temperature at about 1 m of 15°C simulation of the greenhouse climate was performed.

The simulated and measured air temperatures are shown in figure 7.9. If the

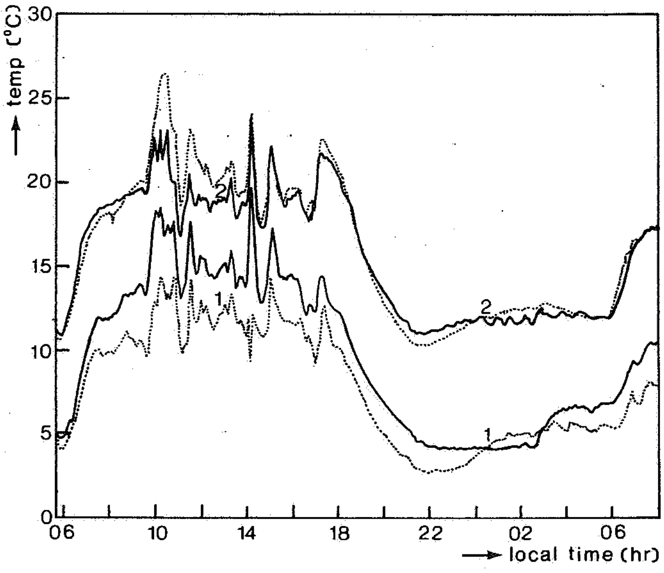

Fig. 7.10. Measured (———) and simulated (-------) temperature of the roof cover (1) and the leaves (2).

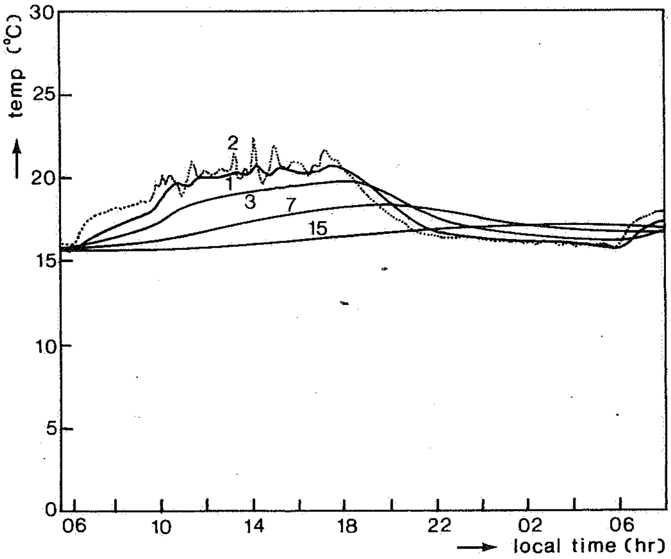

Fig. 7.11. Measured temperature at the soil surface (-----) and the simulated temperatures (———) at a depth of 1, 3, 7 and 15 cm.

screen is closed two air temperatures are obtained (both measured and simulated) and if it is open we get only one air temperature. The air temperature below the screen was measured at three equidistant heights. Very small differences were observed between these temperatures. This supports the assumption of a perfectly homogeneous air temperature. In general the agreement between the measured and simulated air temperatures is reasonable. Before the opening of the screen on 23 March the simulated temperatures are too low, that of the air below the screen about 1.5^{0}C and that of the air above the screen about 2.5^{0}C. This might originate from the erroneous temperature of the high heating pipes, but another cause may be that the outside heat transfer coefficient is too high. After the screen has been opened by day the agreement between the measured and simulated air temperature is good, especially when the ventilation windows are open.This confirms the proper incorporation of the natural ventilation mechanism. After closure of the screen and the ventilation windows the simulated air temperatur again decreases to a lower value than the measured ones. Later on the simulated temperatures recover and the agreement with the measured temperatures becomes reasonable.

The effect of the heat transfer coefficient at the outside on the simulated air temperatures can be demonstrated with the record of the measured and simulated roof cover temperature (figure 7.10). The simulated roof temperature is steadily too low. The development of the difference between the measured and simulated glass temperature can be compared to the behaviour of the outside wind speed (figure 7.3). The too strong dependency of the outside heat transfer coefficient on the wind speed can be recognized; the difference in measured and simulated glass temperature is proportional to the outside wind speed. At day the effect of a too low glass temperature on the inside air temperature is decreased by the ventilation.

The simulated and measured leaf temperatures are also presented in figure 7.10. The agreement is reasonable, the same effects as discussed in the glass-temperature and the air temperature can be recognized. The temperatures of the air, the glass and the leaves are in close correlation. The response to the irradiation is found during the day that to the temperature of the low heating pipes is demonstrable in the early morning and during the night.

A much smoother response is shown by the temperatures of the soil surface and the deeper soil layers. In figure 7.11 the measured temperature of the white plastic sheet at the soil surface and the simulated temperatures at a depth of 1, 3, 7 and 15 cm are represented. At 1 cm the fast fluctuations of the mea-

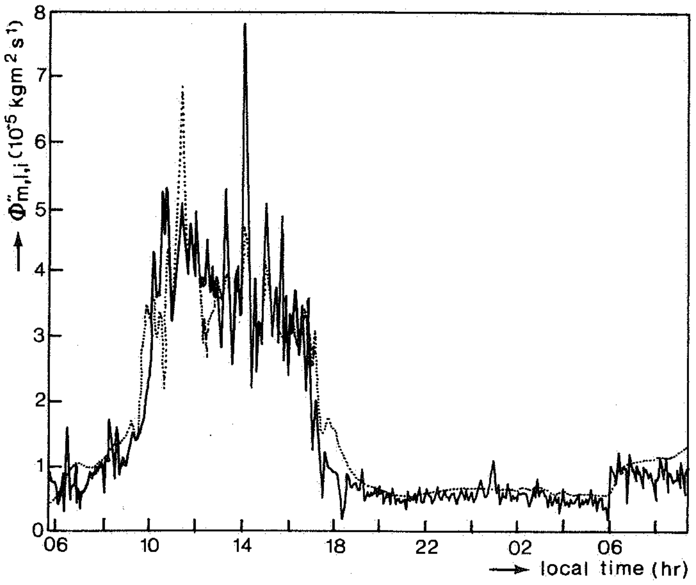

Fig. 7.12. Measured (———) and simulated (-------) transpiration.

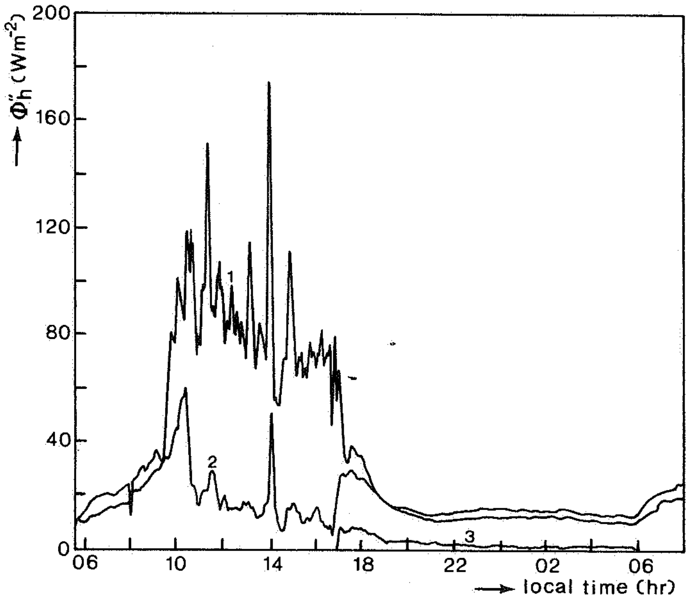

Fig. 7.13. Simulated energy flux densities (per unit ground area) due to transpiration (1), condensation on the glass (2) and condensation on the screen (3).

sured surface temperature are damped out, the absolute level of the temperature is reproduced in a proper way. By day the soil surface temperature has about the same value as the air temperature, at night the former is about 5^{o}C higher.

Besides the simulated and measured state variables, all simulated and measured energy and vapour fluxes can be represented. Only some of those which are characteristic of the greenhouse climate will be reproduced.
First of all the measured and simulated transpiration will be shown (figure 7.12). Again the agreement between simulation and measurement is reasonable, during the day as well as during the night. At day the transpiration correlates with the irradiation, the peaks in both quantities correspond very well. In the early morning the slight increase of the transpiration is caused by the sudden increase of the temperature of the low heating pipes. In general the simulated transpiration is slightly higher than the measured one.
The effect of the transpiration equals the absorption of latent heat due to the evaporation. This latent heat flux (figure 7.13) represents one of the terms in the energy balance over the canopy. In figure 7.13 the energy fluxes to the glass and to the screen due to condensation are represented as well. At night the transpiration is almost balanced by the condensation on the glass. Only a small portion of the transpiration condenses on the screen or is transported to outside by leakage ventilation. At day most of the transpiration is transported to outside due to the ventilation through the open windows, but still a considerable flux is condensing on the glass.
With the energy flux due to transpiration (figure 7.13) and that due to absorbed shortwave radiation (figure 7.6) two of the main terms in the energy balance over the canopy are given. The shortwave radiation is only a driving force for the transpiration by day, at night the longwave radiation from the heating pipes and from the soil surface are needed to supply the necessary energy. In figure 7.14 these radiant energy fluxes are represented. The contribution of the upper pipes can almost be ignored, the jump during the morning is caused by the erroneous measured temperature. By day the contribution of the soil surface is partly negative and partly positive; it fluctuates due to the fluctuations in the leaf temperature (figure 7.10). During the morning the simulated leaf temperature was too high, so the negative radiant flux will be overestimated in this period. The contribution of the low heating pipes by day is considerable due to the high pipe temperature by day (figure 7.7). Due

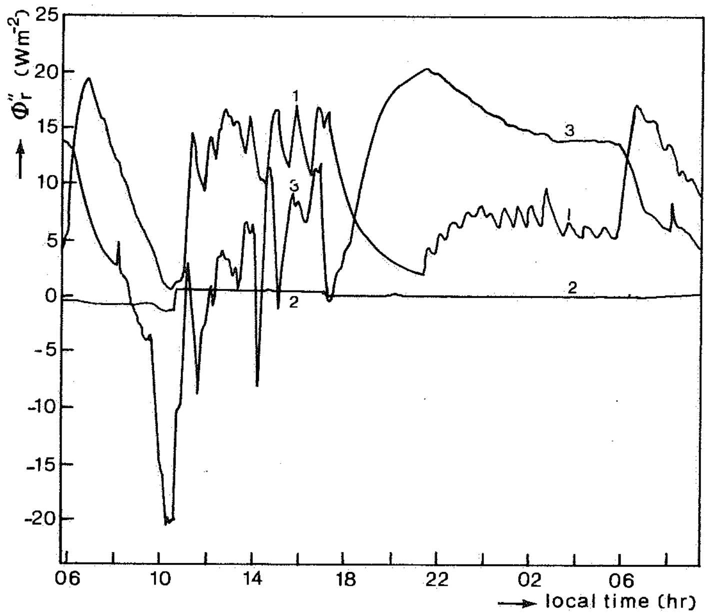

Fig. 7.14. Simulated radiant energy flux densities (per unit ground area) to the canopy from the low heating pipes (1), the high heating pipes (2) and the soil surface (3).

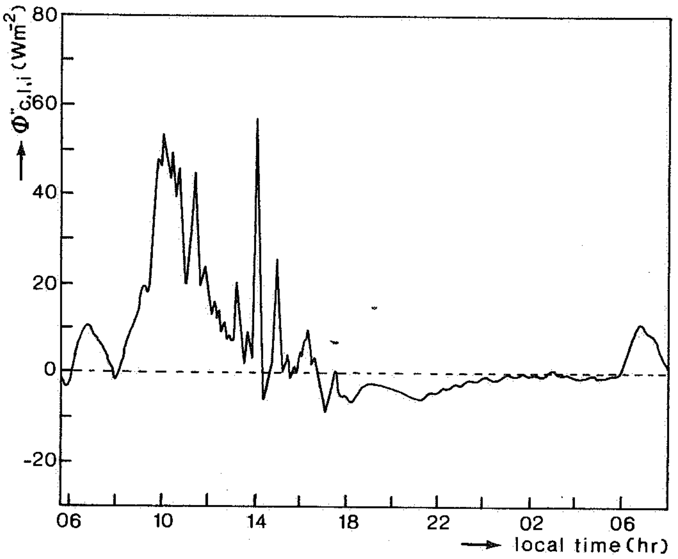

Fig. 7.15. Simulated energy flux density (per unit ground area) of sensible heat from the leaves to the greenhouse air.

to this high heating pipe temperature the radiant flux to the soil will be considerable too. This energy is stored in the soil by day and realeased at night which is marked by the high radiant flux from the soil to the vegetation at night. The contribution by the soil to the energy balance of the vegetation is even higher than that by the low heating pipes. This phenomenon is caused in this particular testing period by the effect of opening the windows by day under manual control. As a result of this action the heating pipes were activated to prevent a too low air temperature. In wintertime it will be normal for this day-night shift to appear because then the heating pipes will be continuously activated.

The remaining radiant heat fluxes from the vegetation are that to the thermal screen and to the glass cover. If the screen is closed almost immediately water condenses on the screen (figure 7.13). So, though the screen itself is partly transparent as regards thermal radiation, the transparency is greatly reduced due to the water film. So the thermal radiation exchange with the glass cover is shielded off during the period in which condensation on the screen exists. During the day the radiant energy exchange with the roof cover was observed to be about 15 Wm^{-2}, during the night the radiant flux to the screen was observed to be about 5 Wm^{-2}. So these two radiant fluxes are only small compared to that from the soil or the low heating pipes or compared to the absorbed shortwave radiation during the day.

Besides the net radiation and the energy flux due to transpiration convective heat is transferred from the leaves to the greenhouse air. This sensible heat is represented in figure 7.15. During the day the leaf temperature is higher than that of the greenhouse air, hence the convective heat transfer is positive. At night the leaf temperature is lower than the greenhouse temperature, but the difference is very small so a small amount of sensible heat is transferred to the leaves. The amount of energy exchanged during the morning is overestimated because the simulated leaf temperature was too high in this period (figure 7.10). In the afternoon the agreement between measured and simulated leaf temperature was good. Consequently the exchange of sensible heat in this latter period is more representative for the exchange during the day than that in the morning. This means that the convective energy exchange is only a minor term in the energy balance of the vegetation compared to the transpiration and the net radiation. So the net radiation to the canopy and the energy due to transpiration are almost balanced. This is in full accordance with the situation in the open air for a well-watered crop (e.g. Slatyer, 1967).

7.7. COMMENTARY ON THE SIMULATION RESULT AND PROCEDURE

The analysis of the energy balance over the vegetation demonstrates that detailed information can be gathered on the greenhouse climate. If the measured and simulated state and flow variables agree, then the information can be considered to be reliable.

In the present model detailed knowledge of the physical processes leads to reliable simulations. Because, as mentioned before some of the processes were not correctly incorporated, the occurring errors were reduced by the use of a parameter estimation technique. With this technique (Birta, 1977) the results of the calculations are compared to the measured ones for some quantities to a maximum of eight. The agreement between the various simulated and measured quantities is optimized by adaptation of some of the exchange coefficients, also to a maximum of eight. We only adapted four coefficients at a time because of the possibility of a physical interpretation of the results. The parameter estimation technique will lead to reliable results if the unadapted coefficients are beyond all doubt. If there is an error in one of these "fixed" coefficients, the parameter estimation will result in a compensation via the estimated coefficients. We optimized the air exchange through the screen, the heat transfer coefficient between the greenhouse air and the glass, the heat transfer coefficient between the heating pipes to the greenhouse air and the heat transfer coefficient between the soil surface and the air. Unfortunately the heat transfer coefficient from the glass cover to the outside air was considered to be correct at that time. As mentioned earlier this coefficient turned out to be dependent on the outside wind speed too strongly. In the parameter estimation this was compensated for by an unjustified adaptation of the heat transfer coefficients between the heating pipes and the air and between the greenhouse air and the glass cover. As a result of this the effective surface area for convective transfer from the heating pipes was increased and that of the glass cover was decreased. Thus the best fit was obtained as an average over the test period, so that the differences between measured and simulated temperatures correlate with the wind velocity. This result is comprehensible if we look after it in the light of the foregoing considerations. With the adaptation of the heat transfer coefficient at the outside to the correct relation with outside wind speed (section 6.1) the other mentioned coefficients too would be adapted to their correct value. Since the calculations are extremely time consuming we refrained from repea-

ting the complete procedure. The more so because other elements of the model also want improvement. Actually the results of the present calculation are sufficient to make clear our point and to illustrate how the simulation results can be improved.
Due to the increased convective exchange with the heating pipes the energy consumption is slightly overestimated in the present simulation. A reliable measurement of the heat consumption was impossible during the test period concerned. If carried out, it would be a powerful extra check in the results of the simulation model. Even with a correct implementation of the main exchange coefficients parameter estimation will be a useful technique to tune the simulation model to the measured greenhouse climate. To be really reliable, however, the results of this tuning have to be supported by a physical interpretation.
For a proper reproduction of the dynamic behaviour of the greenhouse climate quantities, the heat capacity of the various components should be introduced in a correct way. These heat capacities were calculated from the specific heat and the mass of the component concerned. For the air compartments another procedure was required, for, as it turned out, the heat capacity calculated in this way was too small to reproduce the dynamical behaviour of the greenhouse air temperature. A close consideration of the greenhouse air compartment proved that a considerable amount of energy was stored in constructive parts which were located in the air compartments. These parts have a large outside surface area (T, U, H profiles) so have a very small time constant. The heat capacity of these constructive elements can therefore be considered to be added to that of the air. With this increase of the heat capacity of the air the right short-terms dynamical response was obtained.

A physical model is only really reliable if it also reproduces the desired system behaviour in another course of the boundary conditions at another range. Though we do not consider the model to be fully developed at this moment, simulations were carried out with other measured data files as boundary conditions. The results were almost comparable to those of the test day discussed before. If the amount of direct radiation during the day was relatively high, then the differences between measured and simulated results were larger. The simulated and measured air temperature during a 48 hour period at the end of May is shown as an example (figure 7.16). We will briefly describe the outside weather instead of reproducing all recorded weather conditions. At 28 May

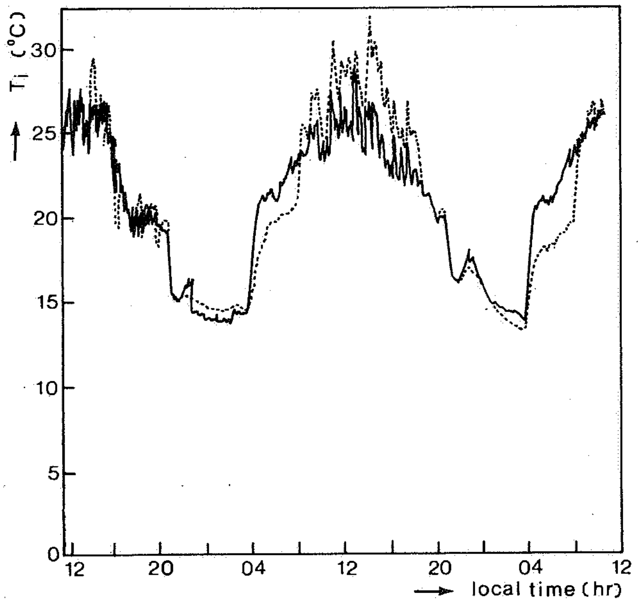

date: May 28 May 29 May 30

Fig. 7.6. Measured (———) and simulated (------) air temperatures during the test period at the end of May (screen open during the whole test period).

the weather was cloudy with most of the radiation being diffuse. The outside wind velocity at day was about 3 ms^{-1}, in the evening it decreased and at about 9 p.m. it was less then 0.5 ms^{-1}. At 29 May the weather was clear with most of the radiation being direct. The wind velocity increased during the day to about 15 ms^{-1}, during the night the increase continued to about 2 ms^{-1}. The outside air temperature varied between 3°C at night to 17°C at day during the measuring period. In the first night the sky temperature was about 4°C lower than the outside air temperature, in the second night about 12.5°C. In the early mornings of May 29 and 30 the sky temperature was observed as being about 60°C too low due to a measuring error. The ventilation windows were controlled by the automatic control system that opened them at varying apertures during the day and closed them at night. The low heating pipes were only activated by the control system just before sunrise.

During the day and night at 28 May the agreement between measurement and simulation was fair (figure 7.16). The temperature during the night was simulated at a slightly higher value then the measured one. In the early morning of May 29 the simulated temperature is lower than the measured one due to the error just mentioned. By day the simulated temperature is higher than the measured one due to the inproper incorporation of the direct radiation into the model. During the second night the agreement is fair again and in the early morning of May 30 the erroneous measured sky temperature once more depresses the simulated air temperature.

The difference between the measured and simulated air temperature show the same correlation to the outside wind speed as during the test day discussed before. During the first night of May 28-29 at very low wind speed the simulated temperature is higher, during the second night with increasing wind velocity, the difference between simulated and measured temperatures also increases. The same phenomenon was apparent in the records of the glass- and leaf temperatures. The transpiration during this period showed the same difference as that during the first test period; the simulated transpiration was about 15% too high.

The comparison of simulation and measurements during other periods gave the same results as discussed before. Improvement, then, can be expected with proper incorporation of the distinction between direct and diffuse irradiation and with the correct heat transfer coefficient on the outside of the cover. Moreover the measurement of the sky temperature has to be improved to prevent erroneous effects of the shortwave radiation.

7.8. APPLICABILITY OF THE MODEL

Though the results presented cannot yet be considered definite, they nevertheless characterize the type of model in such a way that possible applications can be outlined already.

In the introduction it was stated (chapter 1) that the need for more quantitative knowledge follows from the system approach and that it underlays the search for energy saving strategies. Therefore we will expose the possible model applications to these starting points:

In the system approach three levels were distinguished (chapter 1).

On the first level, that of momentaneous growth, the desired values of the controllable climate quantities have to be realized. On this level simple black box models can represent the relation between these quantities and the outside weather in a reliable way as indicated by Udink ten Cate (1983). In this way it is only the relation between a limited amount of quantities that

can be represented.
On the second level, that of short term crop growth and development, the growth conditions, or, a large number of climate quantities have to be taken into account. Both the relation between the momentaneous outside weather and the environmental conditions in the greenhouse and the impact of these conditions on the short term plant growth and development have to be known to accomplish a proper control on this level. The first relation is stated by the present model; recent plantphysiological research is aimed at the second relation (Challa and Schaapendonk, 1983). A combination will be possible if the present model is extended with a description of the distribution of the shortwave radiation in the canopy. Recent research is also focussed on this item (Nederhoff, 1983).
What was also introduced on the second level of the system description was the "speaking plant" approach, recently critically reconsidered by Udink ten Cate (1983). To employ plant measurements in a control system, both a model is needed of the plant behaviour in which the relation of the measured quantities to short term plant growth and development is defined and a model of the relation between the controllable climate quantities and the growth and crop conditions (e.g. irradiation, leaf temperature, water status). The present model defines the second relation and can easily be extended with a description of the plant water status. Hashimoto et al. (1981) reported on this kind of control. Hopmans (1981) suggests the incorporation of measurements on the water status of the crop in a control system.
An important item on the second level is the prevention of extreme greenhouse climate conditions. In general, these conditions are triggered by sharp changes of the outside weather. With the present model we can simulate what kind of weather conditions trigger extreme situations and how various control actions influence the prevention of these situations.
On the third level, that of long term crop growth and development, possible applications are hard to indicate because of the lack of relevant physiological and horticultural knowledge for this specific purpose. In on-line optimization schames (Seginer, 1980, Challa et al., 1980) the energy demand, hence the energy balance of the greenhouse, should be dealt with. It depends on the specific application whether a very simple balance or a more complex one must be dealt with.

In energy saving strategies, a physical model like the present one is able to simulate the effect of various measures on the greenhouse climate, hence on the growth conditions, and on the energy saving. The various physical properties of the greenhouse components (e.g. emission coefficients, leakage through the screen) can be varied very easily and adaptations to incorporate other types of equipment (e.g. insulating covers, heat recovery, low temperature heating) are easily accomplished. This can be a powerful tool in the preparation of full scale experiments in real greenhouses which in general are very expensive.

8. Final discussion, conclusions and suggestions

In this concluding chapter we offer a condensed review of the work reported under the present thesis. Apart from discussing our results and conclusions, we will also formulate some suggestions for continued research.
The greenhouse climate results from a combination of physical processes. This leads to the consideration of the separate processes and thereupon to their integration into a dynamic physical model. In this way the interrelation between the various greenhouse climate quantities and the energy and water vapour fluxes could be established, together with the dependency of these quantities on the outside weather conditions, the physical properties of the greenhouse construction, the physical interaction with the vegetation and the way ventilation and heating is performed. On the physical processes involved a few literature data were available, but they do not refer to observations on a greenhouse or a greenhouse environment. When actually applied to a greenhouse these data prove to be unrealistic. Moreover, for some processes adequate data were not available at all.
Therefore in this thesis the emphasis was on the quantitative description of the major physical processes with special reference to greenhouse conditions and on in situ measurements for the validation of these processes.
As a result the main characteristics of the greenhouse climate processes were established, theoretically as well as experimentally. Because of the approach of the greenhouse climate as a combination of physical processes and their separate in situ establishment the applicable knowledge about the greenhouse climate has considerably been improved. This approach may also serve as a starting-point in a survey of knowledge which is still missing so that this thesis may serve as a blueprint for future greenhouse climate research.
The various physical processes are discussed separately below.

The air exchange or ventilation through the cover of a multispan greenhouse proved to be linearly dependent on the outside wind speed. For lee-side ventilation it was exponentially dependent on the ventilation window aperture. For windward-side ventilation the dependency had to be separated into two regions of the window aperture as discussed later on. The wind direction proved to be a parameter of minor importance; a unique dependency could not be established.

The linear dependency on the outside wind speed confirmed the assumption of a linear relationship between the amplitude of the outside pressure fluctuations, as the driving force for the ventilation, and the volumetric mean kinetic energy of the outside wind. The combination of the results of the ventilation measurements in a full scale Veno-greenhouse, equipped with ventilation windows of a specific length-width ratio with those of flow resistance measurements in small scale models lead to the prediction of ventilation through windows of other length-width ratios. Application of this predicted ventilation in the simulation model indicated that the ventilation was accurately represented. However more experimental evidence is needed. *Suggestion one* is therefore to check this predicted ventilation in situ by full scale ventilation measurements.

The full scale ventilation measurements were performed in relatively small greenhouse compartments. If measurements are performed in large greenhouse compartments with one or more as side walls compartment walls, static pressure differences can be expected between the window openings in opposite side walls. By measurements of the fluctuations of the temperature and air velocity in the ventilation window openings we have made clear the fluctuative nature of the ventilation. The superposition of a static pressure difference over the window openings resulted in the addition of a continuous ventilation flux to the effective flux due to fluctuations. This added continuous flux is to be expected dependent on the wind direction. *Suggestion two* is to perform ventilation measurements in large greenhouse compartments to investigate what correction should be made on the ventilation when the side wall effects are taken into account.

The ratio of windward-side and lee-side ventilation was determined from the similarity of the sensible heat fluxes calculated from the tracer gas experiments with those obtained from the fluctuation measurements. This ratio was constant up to a window opening angle equal to the roof slope and increased at larger opening angles. *Suggestion three* is to perform full scale ventilation measurements for windward-side ventilation and also to investigate the combination of windward-side and lee-side ventilation. Though these kinds of ventilation are not relevant in winter, they will be during spring, summer and autumn, when high irradiation causes a high greenhouse air temperature and a high carbondioxide consumption. Under these conditions ventilation is necessary to keep the greenhouse air temperature sufficiently low and to minimize carbondioxide depression.

The temperature difference between the greenhouse air and the outside air will only have a sensible impact on the ventilation at low outside wind speed values. The height of the greenhouse itself does not have any effect on this ventilation effectuated by temperature differences. If only ventilation openings in the roof are involved, the height in these openings does affect the ventilation. If openings in the side walls are involved as well the vertical distance between the roof openings and the side wall openings has to be taken into account. The sealing of the side walls drastically reduces the ventilation due to temperature effects. *Suggestion four* is to set up experiments aimed at full-scale measurements of the type of ventilation for both ventilation through roof openings and a combination of roof and side wall openings.

The transmissivity for direct shortwave radiation could be calculated with the course of the solar position, the optical laws for reflection and transmission of a single transparent sheet and the geometry of the greenhouse. Though the light was assumed to be non-polarized, the calculations were set up in such a way, that, if necessary, polarization can easily be taken into account. Especially with respect to diffuse radiation this may be of importance. The combination of the transmission for direct and diffuse light yields the regions in the greenhouse with both direct and diffuse light (sunlit regions) and those with diffuse light only (shaded regions). This picture has to be corrected for the scattering of direct light on glass panes (e.g. due to the condensed water at the inside, imperfections in the glass, dust particles on the surface of the glass) and for the reflection on the constructive parts. This correction will slightly decrease the contribution of the direct light and will increase that of diffuse light. Due to the occurrence of sun lit and shaded regions in the greenhouse it is very hard to perform momentaneous measurements of the transmission for direct light. *Suggestion five* is to employ the effective transmission (ratio of the daily total irradiation inside and outside the greenhouse) as a check on the transmission model and to measure the diffuse and direct irradiation both inside and outside to establish the correction on the direct and diffuse transmission due to scattering. *Suggestion six* is to combine the computation of the transmission with a model of the penetration of direct and diffuse light into a vegetation. This allows a more proper calculation of the photosynthesis in the greenhouse which is the starting point for a short term plant growth model.
The loss of light through the roof cover is a limiting factor for greenhouse

crop growth. In the Netherlands glass is the most common greenhouse covering material; other materials have proved not to be suitable for application on a large scale in this country. Technically methods are known (e.g. coatings) to improve the optical properties of the glass so that light transmission is increased. In this way the transmissivity of a glasshouse can be improved or insulating glass panes can be constructed with a high light transmission. *Suggestion seven* is to investigate methods for the improvement of the optical properties of the glass for the economical application in glasshouse industry.

The convective heat transfer at the outside of the cover could be measured in a reliable way. Up to a wind speed of about 3-4 ms^{-1} the heat transfer happened to be in the transition region between free and forced convection. The saw tooth shape of the roof greatly affects the heat transfer in the forced convection regime and the flow field above the roof. *Suggestion eight* is to investigate the effect of the roof slope, the span width and the ridge shape on the heat transfer in the forced convection regime.

The convective heat transfer at the inside of the cover could not be measured accurately. However, the measurements on the outside at low wind speed provide evidence that this exchange is due to free convection and it stands to reason that the results equal those on the inside. The outside heat transfer at low wind speed is found to be nearly equal to that reported in the literature for free convection from inclined surfaces. Therefore the expectation is that the heat transfer coefficient at the inside slightly decreases with increasing roof slope and that it is not affected by the length of the glass pane i.e. by the span width. *Suggestion nine* is to repeat the measurements on the convective heat transfer on the inside in a greenhouse where no condensation appears on the inside of the cover, on the outside at higher outside wind speeds.

The convective heat transfer from the heating pipes showed a dependency on the temperature difference between pipe surface and greenhouse air that is not equal to what could be expected from literature data on free convection in the considered range of the Grashof number. This was understandable from the correlation between the pipe temperature and the cover temperature which causes an additional driving force besides the one calculated from the pipe temperature. The heat transfer is expected to be affected by the position of the heating pipes, the arrangement of the pipes and the structure of the vegetation. *Suggestion ten* is to investigate those dependencies in order to find

an optimum for the lay out of the heating system.
The transpiration could be measured on a short time base (one minute scale). The establishment of the boundary layer conductivity and stomatal conductivity resulted in a boundary layer conductivity which agreed with that found in literature for similar conditions and in a linear dependency of the stomatal conductivity on the irradiation. The night value of the stomatal conductivity (irradiation zero) was found to be higher than that found in literature data for transpiration in the open. The implementation of the linear dependency on the irradiation in the simulation model already gave satisfactory results. However the measurements gave some evidence of a "midday depression". *Suggestion eleven* is to investigate for a well watered crop, the dependency of the stomatal conductivity on other parameters besides shortwave irradiation in order to extend the applicability of the crop transpiration model.
The various convective exchange processes inside the greenhouse interact via the air circulation. Besides the above mentioned processes the exchange with the soil surface also plays a role in this respect. This system of convective exchanges and air circulation in principle can be schematized and tackled by numerical calculation methods. *Suggestion twelve* is to investigate the interrelation between the surface temperatures and the air circulation in the greenhouse in this way as a support for research on the inside exchange processes.

The implementation of the physical processes into a dynamic physical model resulted in a realistic simulation of the various climate quantities. This was achieved by a combination of the validation with in situ measurements of the major physical processes and on line parameter estimation for the adaptation of the minor processes. The differences between the simulated and measured climate quantities resulted from an improper implementation of the convective heat exchange the outside of the cover and the inaccurate determination of the direct and diffuse components of the shortwave radiation.
Suggestion thirteen is to update the simulation model with the most recent results of the research on the physical processes. The differences do not indicate a different dynamic behaviour for low and high frequencies as is the case for simple black box models of the greenhouse climate (Udink ten Cate, 1983). The detailed information gathered with the physical model presented in this thesis facilitates the evaluation of adaptations of the greenhouse construction and equipment e.g. in energy saving strategies and, therefore, the

preparation of full scale greenhouse climate experiments. *Suggestion fourteen* is to apply simulation models on a larger scale in greenhouse climate research.

Summary

In this thesis greenhouse climate has been studied as the set of environmental conditions in a greenhouse in so far as they affect crop growth and development. In chapter 2 this set has been defined in terms of temperatures and vapour pressures. Moreover we have indicated which physical processes co-operate in the greenhouse. So the dependency of the greenhouse climate on the outside weather, the physical properties of the greenhouse construction and the way ventilation and heating is performed has been described in causal relations. This description can be employed in short term as well as in long term crop growth models and it can be a powerful tool in the search for energy saving strategies. As the physical processes are at the basis of this approach, in this thesis the emphasis has been laid on a proper description of the major processes and their validation by in situ measurements.

In chapter 3 natural ventilation through window openings is considered. The airflow due to wind effects through the roof openings of a large multispan greenhouse is assumed to be driven by fluctuating pressure differences over the individual openings. Static pressure differences between the openings are not expected because of the corresponding flow conditions near each span. The driving force due to wind effects together with the flow resistance of the opening determines the ventilation flux through the window opening. Parameters in this relation are the area of the opening without window, a function $G(\xi)$ (being a function of the opening angle ξ) and the outside wind speed. In the function $G(\xi)$ (called the window function) various window parameters are combined with a pressure fluctuation coefficient. From full scale ventilation experiments with a tracer gastechnique, the window function was determined for lee-side ventilation. Only one type of ventilation window was investigated experimentally under full-scale conditions. In small scale greenhouse models the window parameters of various types of ventilation windows were measured. The pressure fluctuation coefficient was calculated from the window parameters and the window function of the experimental full-scale greenhouse. This coefficient was combined with the measured window parameters of other types of ventilation windows in order to predict the window function of these windows. So we could also calculate the ventilation due to wind effects through these windows of other types.

Also in chapter 3 the ventilation due to temperature effects has been investigated. In this case the driving force is derived from the density difference over the window opening. Introduction of the resistance to flow resulted in relations for the ventilation flux due to temperature effects. These relations were derived for flow through openings at the same height and for openings with some vertical distance. Theoretically ventilation due to temperature effects has been presumed to be important at low wind speeds only. From the experiments some support was obtained for this presumption. It was also theoretically argued that the sealing of ventilation openings in the side walls substantially reduces the ventilation due to temperature effects.

The fluctuative nature of the ventilation due to wind effects has been discussed in chapter 4. This fluctuative nature was concluded from the measured fluctuations of the air velocity and the air temperature in the opening. The frequency distribution of the fluctuations proved to be dependent on the window aperture; the window opening acts as a tuneable high pass filter. The measurements resulted in the calculation of the effective flux due to the fluctuating flow (represented by the RMS of the local air velocity) that may be compared with the results obtained by the tracer gas experiments. For lee-side ventilation the agreement between these fluxes is reasonable. So we concluded that the RMS at windward-side ventilation indicates the ventilation flux for this type of ventilation. The superposition of a static pressure difference over the window openings may give rise to an increase of the lee-side ventilation. For windward-side ventilation hardly any effect of this superposition was observed.

The interaction of a multispan greenhouse cover with shortwave direct and diffuse radiation has been described in chapter 5. For direct shortwave radiation this interaction is calculated from the solar position, the optical laws for reflection and transmission, the detailed dimensions of the roof construction and the orientation of the greenhouse. The calculations were made for non-polarized light; polarization can be taken into account, however, without much difficulty. Special attention was paid to the contribution of reflected direct light and to coinciding shadows of the constructive roof parts. Calculated transmissions are presented for various data from both a north-south and an east-west oriented multispan Venlo greenhouse at 52^{0} north latitude.

Because diffuse shortwave radiation is composed of radiation from the hemisphere, the calculation procedure for direct radiation was applied to calculate the interaction with the radiation from any defined direction of the hemisphere. Integration over the hemisphere then yields the interaction with the diffuse radiation. The effect of the intensity distribution for various types of diffuse radiation is investigated in this way. The experimentally measured transmissivity for diffuse radiation indicates that the calculations are accurate.

At the end of chapter 5 the interaction with the longwave sky radiation has been discussed. Since the momentaneous interaction had to be determined, no empirical formula for the time average sky temperature or the time average sky radiation could be applied. Therefore the momentaneous sky temperature was determined by means of measurements of the net radiation above a surface with a well-defined temperature.

The major convective exchange processes affecting greenhouse climate are treated in chapter 6.
An experimental set-up is described to measure the convective heat transfer on the inside and the outside of the cover directly in situ. Special attention was given to minimizing the effect of the radiant exchange. Due to condensation to the inside of the cover the convective exchange at this side could not be determined accurately. On the outside reliable measurements were obtained. The measured heat transfer coefficient is lower than we expected from literature data on forced convection over a flat plate. This defect can easily be understood if we remind ourselves that the roof is saw-tooth shaped, which gives rise to secondary flows. The heat transfer between the saw tooth roof surface and the outside air is in the transition region between free and forced conevection up to a wind speed of about 3-4 ms^{-1}. The measurements at the highest wind speeds occurring during our experiments (i.e. up to 4 ms^{-1}) actually indicate pure forced convection. The measurements at low wind speeds provided some evidence of pure free convective exchange at the outside. The exchange phenomena on the inside are expected to be similar to these latter results.
From local wind speed measurements above the greenhouse, isotachen pictures were constructed for some combinations of the wind speed and the wind direction, These pictures show some characteristic flow phenomena, especially the

appearance of a large eddy in the roof dale. It is precisely this secondary flow phenomenon which is responsible for the reduction of the outside heat transfer coefficient mentioned earlier.

The convective heat transfer from the heating pipes is experimentally determined in the greenhouse from cool-down curves of the pipes. Corrections were made for the radiative heat losses to the environment. The heat transfer was found to be due to free convection. The dependency of the Nusselt number on the Grashof number, however, is different from that found in literature on free convection from a horizontal cylinder. This is explained from the different experimental conditions.

The transpiration was measured on a short time scale, using a sensitive weighing lysimeter. We determined the total conductivity for water transport from the vegetation to the air from the steady state transpiration during the night and the vapour pressure difference between the leaves and the air. From the response of the leaf temperature during periods with intermittent irradiation from infra red lamps, we determined the combined conductivity for transport of sensible and latent heat from the leaves to the air. The heat transfer coefficient was calculated from this combined conductivity and the conductivity for water transport. This coefficient agrees with that from the literature under the same conditions. The calculated stomatal conductivity is much higher than what was reported in the literature for transpiration in the open. By day the total conductivity for water transport from the vegetation to the air was found to be approximately in proportion with the irradiation. Some evidence was found for a "midday depression" of the conductivity.

In chapter 7 the major physical processes have been combined into a physical model to simulate the momentaneous greenhouse climate as a function of the outside weather, the physical properties of the greenhouse construction and materials and the way heating and ventilation is performed. A thermal screen has been incorporated in the model. Parameter estimation techniques have been used to validate the minor physical processes. Bond graph notation is applied to obtain a transparent scheme.
In the model the temperatures of the greenhouse cover, the thermal screen, the greenhouse air above and below the thermal screen, the vegetation and several horizontal soil layers have been assumed to be homogeneous. The same

assumption was made for the vapour pressure of the greenhouse air compartments. The vapour pressures on the soil surface, inside the leaves, on the thermal screen and on the inside of the cover equal the local saturated vapour pressures. They were calculated from the respective temperatures.
For a greenhouse with low heating pipes and a vegetation with an open structure, the vertical gradients are small, so in that case the model assumptions are valid.
The agreement between the measured and simulated state variables is reasonable. Differences are due to the improper incorporation of the outside heat transfer coefficient and to the fact that the contribution of the direct and the diffuse radiation to the global radiation had to be estimated after the event. This reasonable agreement has been demonstrated for two different test periods.

A final discussion and suggestions for aims of future research have been presented in chapter 8.

Samenvatting

In dit proefschrift is het kasklimaat beschouwd als het systeem van omgevingsfactoren in de kas die de groei en ontwikkeling van een gewas beinvloeden. In hoofdstuk 2 wordt beschreven hoe dit in termen van temperaturen en dampspanningen kan worden uitgedrukt. Bovendien is aangegeven welke fysische processen in de kas samenhangend optreden. Op deze manier wordt het oorzakelijk verband beschreven tussen het kasklimaat en het buitenweer, de fysische eigenschappen van de kas en de manier waarop de kas wordt verwarmd en geventileerd. Deze beschrijving kan worden gebruikt in korte en lange termijn gewasgroeimodellen en het kan een krachtig hulpmiddel zijn bij het onderzoek naar methoden voor energiebesparing.

Omdat de fysische processen het uitgangspunt vormen van deze benadering wordt in dit proefschrift de nadruk gelegd op een zo goed mogelijke beschrijving van de belangrijkste processen en op de validatie hiervan met behulp van in situ metingen.

In hoofdstuk 3 wordt natuurlijke ventilatie door raamopeningen onder de loep genomen. Er is aangenomen dat de luchtuitwisseling ten gevolge van windeffecten door de openingen in het dak van een groot warenhuis worden veroorzaakt door fluctuaties in het drukverschil over de afzonderlijke openingen. Deze fluctuaties zijn weer het gevolg van lokale windsnelheidsfluctuaties. Statische drukverschillen tussen deze openingen worden niet verwacht omdat het stromingsveld rondom iedere kap identiek is.

Het ventilatiedebiet wordt bepaald door bovengenoemde oorzaak en de stromingsweerstand van de opening. Hieruit is afgeleid dat dit debiet afhangt van het oppervlak van de ventilatieramen, een raamfunctie $G(\xi)$ (die een functie is van de openingshoek ξ) en van de windsnelheid. In de raamfunctie $G(\xi)$ zijn verschillende parameters van de ventilatieopening (raamparameters) en een drukfluctuatiecoëfficiënt gecombineerd. De raamfunctie is experimenteel bepaald met behulp van een tracer gas in een kas van ware grootte voor één type ventilatieraam bij lijzijde luchting. De raamparameters van verschillende raamtypen werden bepaald met behulp van metingen in schaalmodellen van een kas. Door van het type ventilatieraam uit de ware grootte ventilatie-experimenten de raamfunctie en de raamparameters te combineren is de druk fluctuatiecoëfficiënt uitgerekend. Deze is gecombineerd met de raamparameters van andere typen ventilatieramen zodat hiervoor de raamfunctie kon worden voorspeld. Zodoende kan het ventilatiedebiet ten gevolge van windeffecten ook voor deze andere raamtypen worden berekend.

In hoofdstuk 3 is ook de ventilatie ten gevolge van temperatuureffecten onderzocht. Hierbij wordt het drukverschil over de ventilatieopeningen veroorzaakt door de dichtheidsverschillen aan beide zijden van de opening. Het invoeren van de stromingsweerstand leverde relaties op voor het ventilatiedebiet ten gevolge van temperatuureffecten. Deze relaties werden afgeleid voor zowel de uitwisseling door verschillende openingen op dezelfde hoogte alsmede voor die door openingen met een verticale afstand. Uit deze theoretische beschouwing bleek dat de ventilatie ten gevolge van temperatuureffecten alleen bij lage windsnelheden van belang is. Uit de ventilatieproeven kon hiervoor enige ondersteuning worden afgeleid. Ook bleek uit de theoretische beschouwing dat door het afsluiten van ventilatieopeningen in de zijwanden de ventilatie ten gevolge van temperatuureffecten relatief zeer sterk wordt gereduceerd.

In hoofdstuk 4 wordt het fluctuerende karakter van de ventilatie besproken. Dit karakter werd bevestigd door metingen van de fluctuaties van de luchtsnelheid en de luchttemperatuur in de raamopening. De frequentieverdeling van de fluctuaties bleek af te hangen van de stand van het ventilatieraam; de raamopening gedraagt zich als een afstembaar hoogdoorlaatfilter.
Uit de fluctuatiemetingen kon de effectieve flux ten gevolge van de fluctuerende luchtstroom (gerepresenteerd door de RMS van de lokale luchtsnelheid) worden berekend en deze kon worden vergeleken met de resultaten van de tracer gasexperimenten. Deze was redelijk voor de experimenteel bepaalde lijzijdeluchting. Daaruit trokken we de conclusie dat uit de RMS voor windzijdeluchting het ventilatiedebiet voor deze wijze van ventileren wordt aangegeven.
De superpositie van een statisch drukverschil over de raamopeningen kan een toename van het ventilatiedebiet bij lijzijde-luchting veroorzaken. In het geval van windzijde-luchting werd van zo'n superpositie nauwelijks enig effect geconstateerd.

De wisselwerking tussen het dek van een warenhuis met directe en diffuse kortgolvige straling wordt in hoofdstuk 5 beschreven. In het geval van directe straling kan deze wisselwerking worden berekend uit de stand van de zon,

de optische wetten voor reflectie en transmissie, de gedetailleerde afmetingen van de dakconstructie en de ligging van de kas. De berekeningen werden uitgevoerd voor ongepolarizeerd licht: met polarizatie kan echter zonder veel moeilijkheden rekening worden gehouden. Veel aandacht werd besteed aan de bijdrage van gereflecteerd direct licht en aan het samenvallen van de schaduwen van de constructieve elementen. Voor verschillende data werden transmissies uitgerekend voor zowel een noord-zuid als een oost-west georiënteerd Venlo warenhuis gelegen op 52^o noorderbreedte.
Omdat diffuse straling is samengesteld uit straling afkomstig van de halve hemelbol, is de rekenprocedure voor de transmissie van directe straling toegepast om de wisselwerking te berekenen met straling vanuit iedere richting van de hemelkoepel. Uit de integratie over de hemelkoepel wordt de interactie van diffuse straling met het kasdek verkregen. De invloed van de intensiteitsverdeling over de hemelkoepel voor verschillende typen diffuse straling is op deze manier onderzocht. De experimenteel gemeten doorlatendheid voor diffuse straling geeft aan dat de berekeningen nauwkeurig zijn.
Op het eind van hoofdstuk 5 wordt de wisselwerking met de langgolvige hemelstraling besproken. Omdat in ons geval de wisselwerking op ieder moment moet worden bepaald kunnen geen empirische formules voor de in de tijd gemiddelde hemeltemperatuur of hemelstraling worden toegepast. Daarom werd de momentane hemeltemperatuur bepaald uit metingen van de netto straling boven een oppervlak met een goed gedefinieerde temperatuur.

In hoofdstuk 6 worden de belangrijkste convectieve overdrachtsprocessen besproken.
De convectieve warmteoverdracht aan de binnen- en buitenkant van het kasdek is direct in situ gemeten. In de meetopstelling hiervoor is veel aandacht geschonken aan het zo klein mogelijk maken van de invloed van warmteoverdracht door straling. Omdat aan de binnenkant van het kasdek condensatie optrad aan het meetpaneel kon de convectieve overdracht aan deze zijde niet nauwkeurig worden bepaald. Aan de buitenkant werden wel betrouwbare meetresultaten verkregen. De gemeten warmteoverdrachtscoëfficiënt is lager dan we verwachtten op grond van literatuurgegevens over gedwongen convectie aan vlakke platen. Dat dit verschil optreedt kan gemakkelijk worden ingezien door te bedenken dat het kasdek een zaagtandvorm heeft waardoor secundaire stromingspatronen optreden. Tot een windsnelheid van ongeveer 3-4 ms^{-1} bevindt het warmteoverdrachtsmechanisme zich in het overgangsgebied tussen vrije en gedwongen con-

vectie. De metingen die verricht werden bij de hoogste gedurende het experiment optredende windsnelheid (4 ms^{-1}) wijzen op overdracht door gedwongen convectie. Bij lage windsnelheden wijzen de metingen op vrije convectieoverdracht. Verondersteld wordt dat de vrije convectieoverdracht aan de binnenzijde van het kasdek analoog is aan die aan de buitenkant.
Uit metingen van de lokale windsnelheid op verschillende plaatsen boven de kas werden verdelingen van de lijnen van gelijke windsnelheid bepaald voor een aantal combinaties van de windrichting en windsnelheid op referentiehoogte. Hieruit bleek dat er karakteristieke stromingsverschijnselen optreden waarbij vooral sprake is van een grote wervel boven de goot, tussen de nokken. Juist door deze secundaire stroming wordt de eerder vermelde vermindering van de warmteoverdrachtscoëfficiënt aan de buitenkant veroorzaakt.

De convectieve warmteoverdracht van de verwarmingsbuizen naar de kaslucht is experimenteel in de kas bepaald uit afkoelcurves van deze buizen. Hierbij werd gecorrigeerd voor het warmteverlies door straling naar de omgeving. Er werd geconstateerd dat de overdracht wordt bepaald door vrije convectie. De bepaalde relatie tussen het Nusselt getal en het Grashof getal was echter verschillend van die uit de literatuur over vrije convectie aan horizontale cylinders. Dit werd verklaard uit de verschillen in experimentele omstandigheden in de kas en het laboratorium.

De gewasverdamping is gemeten op basis van gewichtsmetingen met zeer korte tussenpozen. Hierbij is gebruik gemaakt van een zeer gevoelige wegende lysimeter. Uit de constante nachtverdamping en het dampspanningsverschil tussen de bladeren en de kaslucht is de totale stofoverdrachtscoëfficiënt voor verdamping van het gewas bepaald. De gecombineerde warmteoverdrachtscoëfficiënt voor latente en voelbare warmte is bepaald uit de responsie van de bladtemperatuur op een stapvormig aan het blad toegevoerde warmtestroom met behulp van "infrarood lampen". De warmteoverdrachtscoëfficiënt voor voelbare warmte van het gewas naar de kaslucht werd vervolgens berekend uit de gecombineerde warmteoverdrachtscoëfficiënt en de totale stofoverdrachtscoëfficiënt. Deze bleek goed overeen te komen met waarden die in de literatuur voor dezelfde omstandigheden worden vermeld. De berekende stomatale geleiding is veel hoger dan wat in de literatuur voor verdamping in het vrije veld wordt vermeld. Voor het gedrag overdag kon de totale stofoverdrachtscoëfficiënt voor verdamping van het gewas bij benadering recht evenredig met de irradiantie worden gesteld. Er werd enige aanwijzing gevonden dat er hiernaast een effect optrad waardoor deze coëfficiënt midden op de dag wat afnam.

In hoofdstuk 7 zijn de voornaamste fysische processen gecombineerd tot een fysisch model om het kasklimaat van moment tot moment te kunnen simuleren als functie van het buitenweer, de fysische eigenschappen van de kas en de manier waarop de kas wordt verwarmd en geventileerd. In het model is de werking van een energiescherm opgenomen. Parameterschatting is toegepast om de minder belangrijke fysische processen te valideren. Om het model in een overzichtelijk schema te kunnen weergeven zijn bond grafen gebruikt.
De temperaturen van het kasdek, het energiescherm, de kaslucht boven en onder het energiescherm, het gewas en enkele horizontale bodemlagen worden in het model homogeen verondersteld. Hetzelfde geldt voor de dampspanningen van de kasluchtcompartimenten. De dampspanningen aan het bodemoppervlak, het energiescherm, de binnenkant van het kasdek en in de bladeren zijn gelijk gesteld aan de verzadigingsdampspanning ter plaatse. Zodoende worden deze berekend uit de betrokken temperatuur. Voor een kas met lage, vlak bij de grond gelegen verwarmingsbuizen en een gewas met een open structuur zijn de verticale gradiënten klein en zijn de modelaannamen geldig.
De overeenstemming tussen de gemeten en de gesimuleerde toestandsvariabelen is redelijk. Verschillen zijn te wijten aan het gebruik van een verkeerde overdrachtscoëfficiënt aan de buitenkant van het kasdek en aan het feit dat de bijdrage van de directe en diffuse straling aan de globale straling achteraf moest worden geschat. De redelijke overeenstemming is voor enkele verschillende perioden aangetoond.

In hoofdstuk 8 wordt een slotbeschouwing gegeven en worden suggesties gedaan voor toekomstig onderzoek.

References

Abeels, P.F.J., 1981, Natuurlijke verluchting in stallen in de plaats van mechanische ventilatie |in Dutch| . Agricontact 114, IIIa: 1-8.

Ahmadi, G. and Glockner, P.G., 1982, Dynamic simulation of the performance of an inflatable greenhouse in the southern part of Alberta, I: Analysis and average winter conditions. Agr. Meteorol. 27: 155-180.

Ahmadi, G., Kessey, K.O. and Glockner, P.G., 1982, Dynamic simulation of the performance of an inflatable greenhouse in the southern part of Alberta, II: Comparisons with experimental data. Agr. Meteorol. 27: 181-190.

Ångstrom, A., 1915, A study of the radiation of the atmosphere. Smitsonion misc. coll. 65 (3): 159 p.

Bailey, B.J., 1978, Heat conservation in glasshouses with aluminised thermal screens. Acta Hort. 76: 175-278.

Baily, B.J., 1981, The evaluation of thermal screens in glasshouses in commercial nurseries. Acta Hort. 115: 663-670.

Baseaux, P., Deltour, J. and Nisen, A., 1973, Effect of diffusion properties of greenhouse covers on light balance in the greenhouse. Agr. Meteorol. 11: 357-372.

Behboudian, M.H., 1977, Water relations of cucumber, tomato and sweet pepper. Meded. Landb. Hogesch. Wageningen 77 (6): 1-85.

Bird, R.B., Stewart, W.E. and Lightfoot, E.N., 1960, Transport phenomena. J. Wiley & Sons, N.Y., 780 p.

Birta, L.G., 1977, A parameter optimization module for CSSL-based simulation software. Simulation (April): 113-121.

Bokhorst, D., Drenth, A. and Holsteijn, G.P.A., 1972, Lichtafhankelijke klimaatregeling voor kassen |in Dutch| . ITT publ. 74, Imag, Wageningen, 80 p.

Bot, G.P.A., Dixhoorn, J.J. van and Udink ten Cate, A.J., 1977, Dynamic Modelling of greenhouse climate and the application to greenhouse climate control. Proc. 1977 ICHMT seminar on "Heat Transfer in Buildings". Hemisphere N.Y.

Bot, G.P.A., Dixhoorn, J.J. van and Udink ten Cate, A.J., 1978, Beheersing van de teelt in kassen met behulp van de computer |in Dutch|. Bedrijfsontwikkeling 9 (10): 729-731.

Bot, G.P.A. and Dixhoorn, J.J. van, 1978, Dynamic modelling of greenhouse climate using a minicomputer. Acta Hort. 76: 113-120.

Bot, G.P.A., 1981, Heating load of a glasshouse from the physical point of view. Acta Hort. 115: 335-340.

Bovy, A.J. and Woelk, G., 1971, Untersuchungen zur freien Konvektion an ebenen Wänden |in German|. Wärme und Stoffübertragung 4: 105-112.

Bowman, G.E., 1970, The transmission of diffuse light by a sloping roof. J. Agric. Engng. Res. 15 (2): 100-105.

Bowman, G.E., and Weaving, G.S., 1970, A light-modulated greenhouse control system. J. Agric. Engng. Res. 15 (3): 255-264.

Braak, N.J. van de, 1980, Thermal problem solving by handcalculations, an application of network theory. Acta Hort. 115: 365-375.

Brandsma, C., 1977, Luchtstromingspatronen in en rond gebouwen |in Dutch|. Landbouwmechanisatie 28 (4): 407-410.

Brown, W.G. and Solvason, K.R., 1962, Natural convection through rectangular openings in partitions -1- Vertical partitions. Int. J. Heat and Mass Transfer 5: 859-868.

Breuer, J.J.G. 1976, 1983, Rekenmodel energiebehoefte in kassen deel 1 en 2. |in Dutch| (1st and 2nd ed.) Imag publ. 49. Imag, Wageningen 72 + 152 p.

Brunt, D., 1932, Notes on radiation in the atmosphere. Quart J. Roy. Meteorol. Soc. 58: 389-418.

Buckius, R.O. and King, R., 1978, Diffuse solar radiation on a horizontal surface in a clear sky. Solar Energy 21: 503-509.

Cannon, J.H., Krantz, W.B., Kreith, F. and Naot, D., 1979. A study of transpiration from porous flat plates simulating plant leaves. Int. J. Heat and Mass Transfer 22: 469-483.

Challa, H., 1976, An analysis of the diurnal course of growth, carbondioxide exchange and carbohydrate reserve content of cucumber. Agric. Res. Report 861. Pudoc, Wageningen 88 p.

Challa, H., Bakker, J.C., Bot, G.P.A., Udink ten Cate, A.J., and Vooren J. van de, 1980, Economical optimization of energy consumption in an early cucumber crop. Acta Hort. 118: 191-199.

Challa, H. and Schaapendonk, A.H.C.M., 1983, Dynamic optimalization of CO_2 enrichment in relation to climate control in greenhouses. In Enoch, H., Z and Kimball, B.A. (eds), Carbondioxide enrichment of greenhouse crops. CRC Boca Raton, U.S.A. (in press).

Chamberlain, J.E., Chantry, G.W., Findlay, F.O., Gebbic, H.A., Gibbs, J.E. Stone, N.W.B., and Wright, A.J., 1966. The spectral transmission of infra-red wavelengths of Michelson interferometers with dielectric film beam dividers. Infrared Physics 6: 195-203.

Chandrasekhar, S., 1960, Radiative transfer. Dover, 393 p.

Chen, T.S., Sparrow, E.M. and Mucoglu, A., 1977. Mixed convection in boundary layer flow on a horizontal plate. ASME J. Heat Transfer 99: 66-71.

Chiapale, J.P., Kittas, C. and Villêle, O. de, 1981, Estimation regionale des besoins de chauffage des serres. Acta Hort. 115: 493-502.

Chiapale, J.P., Van Bavel, C.H.M. and Sadler, E.J., 1982, Comparison of calculated and measured performance of a fluid-roof and a standard greenhouse. Report of Station de Bioclimatologie, INRA, Montfavet, France and The Texas Agric. Exp. Station, Texas A & M University, College Station, Texas, U.S.A., 36 p.

Churchill, S.W. and Chu, H.H.S., 1975, Correlating equations for laminar and turbulent free convection from a horizontal cylinder. Int. J. Heat and Mass Transfer 18: 1019-1053.

Cockroft, J.P. and Robertson, P., 1976, Ventilation of an enclosure through a single opening. Building and Environment 11: 29-35.

Corson, D.R., and Lorraine, P., 1962, Introduction to electromagnetic Fields and Waves, Ch. 11: 361-372. C.W. Freeman and Cy. San Francisco, 552 p.

Coulson, K.L., 1975, Solar and Terrestrial Radiation. Ac. Press, N.Y., 322 p.

Critten, D.L., 1983, A computer model to calculate the daylight integral and transmissivity of a greenhouse. J. Agric. Engng Res. 28: 61-76.

Damagnez, J., Van Bavel, C.H.M., Sadler, E.J. and Chouanière, M.P., 1980, Simulation of the effect of storage characteristics upon the dynamic response of a fluid-roof solar greenhouse. Acta Hort. 106: 27-38.

Dave, J.V., 1979, Isotropic distribution approximation in solar energy estimations. Solar Energy 22: 15-19.

Deltour, J., and Nisen, A., 1970, Les verres diffusants en couverture des serres |in French|. Bull. Rech. Agron. Gembloux NSV, 1: 232-255.

Dick, J.B., 1950, The fundamentals of natural ventilation of houses. J. Inst. Heat Vent. Engrs. 18: 123-134.

Dybwad, J.R., Hellickson, M.A., Johnson, C.E. and Moe, D.L., 1974, Ridge vent effects on model building ventilation characteristics. Trans ASAE 17: 366-370.

Edgan, R.K. and Hellickson, M.A., 1978, Ridge vent and wind direction effects on ventilation characteristics of a model open-front livestock building. Trans ASAE. 21: 146-152.

Edwards, R.I., 1963, Transmission of solar radiation by glasshouses. Expl. Hort. 9: 1-8.

Edwards, R.I. and Lake, J.V., 1964, Transmission of solar radiation in a large-span east-west glasshouse. J. Agric. Engng. Res. 9 (3): 245-249.

Edwards, R.I. and Lake, J.V., 1965, Transmission of solar radiation in a large-span east-west glasshouse II. J. Agric. Engng. Res. 10: 125-131.

Elsner, B. von, 1982, Das Kleinklima und der Wärmeverbrauch von geschlossenen Gwächshäusern |in German|. I.T.G. Heft 12, Universität Hannover, Germany. 197 p.

Fand, R.M. and Keswani, K.K., 1973, Combined natural and forced convection heat transfer from horizontal cylinders to water. Int. J. Heat and Mass Transfer. 16: 1175-1191.

Fand, R.M. and Bruckner, J., 1983, A correlation for heat and mass transfer by natural convection from horizontal cylinders that accounts for viscous dissipation. Int. J. Heat and Mass transfer 26: 709-726.

Farouk, B. and Güçeri, S.I., 1983, Natural convection from horizontal cylinders in interacting flow fields. Int. J. Heat and Mass Transfer 26: 231-243.

Freriks, J.H., 1981, Nieuwe staltypen voor mestvarkens: stallen met natuurlijke ventilatie zonder verwarming |in Dutch|. Boerderij/Varkenshouderij 66 (14): 9VA-10VA.

Froehlich, D.P., Hellickson, M.A. and Young, H.G., 1975, Ridge vent effects on model ventilation characteristics. Trans ASAE 18: 690-693.

Froehlich, D.P., Allbright, L.D., Scott, N.R. and Chandra, P., 1979, Steady periodic analysis of glasshouse thermal environment. Trans ASAE 22: 387-399.

Gaastra., 1959, Photosynthesis of crop plants as influenced by light, carbon dioxide, temperature and stomatal diffusion resistance. Meded. Landb. Hogesch. , Wageningen. 59 (13): 1-68.

Garzoli, K.V. and Blackwell, J., 1973, The response of a glasshouse to high solar radiation and ambient temperature. J. Agric. Engng. Res. 18: 205-216.

Garzoli, K.V. and Blackwell, J., 1981, An analysis of the nocturnal heat loss from a single skin plastic greenhouse. J. Agric. Engng. Res. 26 (39): 204-214.

Georgii, H.W., 1954, Untersuchungen über den Luftaustausch zwischen Wohnräumen und Aussenluft |in German|. Arch. Met. Geoph. Biokl . B 5 (2): 191-214.

Germing, G.H., 1978, Energy and protected cultivation in The Netherlands. Acta Hort. 87: 363-369.

Gids, W.F. de, 1978, Calculation method for the natural ventilation of Buildings. Verwarming en Ventilatie 1978 (7): 551-559.

Goldberg B. and Klein, W.H., 1980, A model to determine the spectral quality of daylight on a horizontal surface at any location. Solar Energy 24: 351-357.

Goudriaan, J., 1977, Crop meteorology: A simulation study. Simulation Monographs, Pudoc, Wageningen. 249 p.

Graaf, R. de, 1978, Onderzoek naar de waterhuishouding in het bijzonder het waterverbruik bij een teelt van stooktomaten in 1977 |in Dutch|. Report 36-1978, Glasshouse Crops Research and Experiment Station, Naaldwijk, The Netherlands.

Graaf, R. de and Ende, J. van de, 1981, Transpiration and evapotranspiration of the glasshouse crops. Acta Hort. 119: 147-158.

Gudehus, H. Chr., 1977, Determination of air exchange figures with regard to closed greenhouses. Acta Hort. 76: 301-304.

Gulik, D. van, 1910, Iets over het gebruik van glas in broeikassen |in Dutch| Meded. v. RHLTB 1910 (III): 108-118.

Hand, D.W., Slack, G. and Machin, D.R., 1970, Evaporation rates of capillary-watered tomatoes in an east-west house. J. Hort. Sci. 45: 3-14.

Haneghem, I.A., 1981, Een niet-stationaire naaldmethode (warmtegeleiding, warmtecapaciteit, contactweerstand) |in Dutch|. Ph. D. thesis Agr. University, Wageningen. 187 p.

Harnettt, R.F., 1974, The advantages of east-west multispans. The Grower 13, July: 64-66.

Harnett, R.F., 1975, Study of glasshouse type and orientation. Acta Hort. 46: 209:215.

Hashimoto, Y., Morimoto, T., Funada, S. and Sugi, J., 1981, Optimal control of greenhouse climate by the identification of water deficit and photosynthesis in short term plantgrowth. In proc. 8th Ifac World Congress, Kyoto, Japan XV: 5-10.

Hatfield, J.L., Giorgis, R.B. and Flocchini, R.G., 1981, A simple solar radiation model for computing direct spectral fluxes. Solar Energy 27: 323-329.

Hey, G. and Schaapendonk, A.H.C.M., 1983, CO_2 depletion in greenhouses. Acta Hort. 148: 8 p. (in press).

Heyna, B.J., 1975, Delta X - a new control system. Acta Hort. 46: 13-19.

Heyna, B.J. and Holsteijn, G.P.A., 1981, Buisligging en energiebesparing |in Dutch|. Tuinderij 21 (3): 18-21.

Hieber, C.A., 1973, Mixed convection above a heated horizontal surface. Int. J. Heat and Mass Transfer 16: 769-785.

Hitchin E.R. and Wilson, C.B., 1967, A review of experimental techniques for the investigation of natural ventilation in buildings. Building Science 2: 59-82.

Holmes, R.M., Gill, G.C. and Carson, H.W., 1964, A propellor type vertical anemometer, J. Appl. Meteorol. 3: 802-804.

Hopmans, P.A.M., 1981, In situ plant water relations monitoring for greenhouse climate control with computers. Acta Hort. 119: 137-145.

Hull, J.N., 1954, Spectral distribution of radication from sun and sky. Trans. Illum. Engn. Soc. 19 (1): 21.

Idso, S.B. and Jackson, R.D., 1969, Thermal radiation from the atmosphere. J. Geoph. Res. 74: 5397-5403.

Idso, S.B., 1971, Transformation of a net radiometer into a hemispherical radiometer. Agr. Meteorol. 9: 109-121.

Idso, S.B., 1974, On the use of equations to estimate atmospheric thermal radiation. Arch. Met. Geoph. Biokl. B 22: 287-299.

Iqbal, M. and Stoffers, J.A., 1975, Natural convection heat transfer in covered plant canopies. Agr. Meteorol. 15: 97-111.

Iqbal, M. and Khatry, A.K., 1977, Wind induced heat transfer coefficients from glasshouses. Trans. ASAE 20: 157-160.

Iqbal, M., 1980, Prediction of hourly diffuse solar radiation from measured hourly global radiation on a horizontal surface. Solar Energy 24: 491-503.

Jefimenko, O.O., 1966, Electricity and Magnetism. Ch. 8: 233-258. Appleton-Century-Crofts. N.Y. 591 p.

Jodlbauer, K., 1933, Das Temperatur und Geschwindigkeitsfeld um ein geheitztes Rohr by freier Konvektion. Forsch. Geb. Ingenieurw. 4: 157-172.

Kanemasu, E.T. and Tanner, C.B., 1969a, b, Stomatal diffusion resistance of

snap beans.
I Influence of leaf water potential. Plant Physiol. 44: 1547-1552.
II Effect of light.Plant Physiol. 44: 1542-1546.

Kasten, F. and Cseplak, G., 1980, Solar and terrestrial radiation dependent on the amount and type of cloudiness. Solar Energy 24: 177-189.

Kieboom, A.M.G. van de and Stoffers, J.A., 1982, Radiation properties of greenhouse roof covering materials and greenhouses. Imag report (March 1982). 24 p.

Kieboom, A.M.G. van de, 1983, Note on the transmission of a Venlo greenhouse. Personal communication.

Kimball, B.A., 1973, Simulation of the energy balance of a greenhouse. Agr. Meteorol. 11: 243-260.

Kindelan, M., 1980, Dynamic modelling of greenhouse environment. Trans ASAE 23 (5): 1232-1234.

King, W.J., 1932, The basic laws and data of heat transmission III: Free convection. Mech. Engng. 54: 347-353.

Kingham, H.G. and Smith, C.V., 1971, Calculated light transmission: the effect of orientation of single glasshouses. Expl. Hort. 22: 1-8.

Kirsten, W., 1973, Die natürliche Einstrahlung in Gewächshäuser in Abhängigkeit von deren Form und Aufstellungsrichtung sowie der Beschaffenheit des Hüllstoffes |in German|. Ph. D. thesis. Technische Universität, Hannover, 89 p.

Kondratyev, K, Ya, 1969, Radiation in the atmosphere. Int. Geoph. Ser. 12. Ac. Press, N.Y. 912 p.

Kondratyev, K. Ya, 1972, Radiation processes in the atmosphere. WMO rep. no. 309. WMO, Geneva. 214 p.

Koppe, R. and Stoffers, J.A., 1967, Berekening van de temperatuurfluctuaties in kassen bij wisselende uitstraling en van luchtvochtigheidsfluctuaties bij wisselende waterdamptoevoer |in Dutch|. In: Kassen en Kasklimaat. ITT publ. 13, Imag, Wageningen: 81-94.

Kozai, T. and Kimura, M., 1977, Direct solar light transmission into multispan greenhouses. Agr. Meteorol. 18: 339-349.

Kozai, T. and Sase, S., 1978, A simulation of natural ventilation for a multi-span greenhouse. Acta Hort. 87: 39-49.

Kozai, T., Goudriaan, J. and Kimura, M., 1978, Light Transmission and photosynthesis in greenhouses. Simulation Monographs, Pudoc, Wageningen. 99 p.

Kozai, T., Sase, S. and Nara, M., 1980, A modelling approach to greenhouse ventilation control. Acta Hort. 106: 125-136.

Kreith, F., 1976, Principles of Heat Transfer, 3rd ed. Intext Press Inc. N.Y. 656 p.

Kuiper, P.J.G., 1961, The effects of environmental factors on the transpiration of leaves with special reference to stomatal response. Meded. Landb. Hogesch. Wageningen. 61 (7): 1-49.

Lake, J.V., Postletwaite, J.D., Slack, G. and Edwards, R.I., 1965, Seasonal variations in the transpiration of glasshouse plants. Agr. Meteorl. 3: 187-196.

Lawrence, W.J.C., 1963, Science and the Glasshouse, 3rd ed. Oliver & Boyd, London, 139 p.

Lemeur, R. and Blad, B.L., 1974, A critical review of light models for estimating the shortwave radiation regime of plant canopies. Agr. Meteorol. 14: 255-286.

Liu, B.Y.H. and Jordan, R.C., 1960, The interrelation and characteristic distribution of direct, diffuse and total solar radiation. Solar Energy 4 (3): 1-19.

Los, G.J., 1964, The intensity and distribution of light in greenhouses. Proc. of the XVIth (1962) Int. Hort. Congress 16 (4): 211-219.

Maher, M.J. and O'Flaherty, T., 1973, An analysis of greenhouse climate. J. Agric. Engng. Res. 18: 197-203.

Manbeck, H.B. and Aldrich, R.A., 1967, Analytical determination of direct visible solar energy transmitted by rigid plastic greenhouses. Trans. ASAE 10: 564-567, 572.

McAdams, W.H., 1954, Heat Transmission, 3rd. ed. McGraw-Hill, N.Y. 532 p.

McKenzie, G.S., 1812, On the form which the glass of a forcing house ought to have. Trans.Hort.Soc. London 2: 171-177.

Meijer, J., Bot, G.P.A., Stanghellini, C. and Udink ten Cate, A.J., 1983, Development and application of a high precision weighing lysimeter. Submitted to J. Agric. Engng. Res.

Meurs, W.T.M. van, 1979, The climate control system at the Imag, Wageningen. Acta Hort. 106: 77-83.

Meyer, J., 1977, Reducing energy consumption of greenhouses by the choice of the heating system. In: Technical and physical aspects of energy saving in greenhouses. Commission of the European Comm. Eur. 5679e: 90-93.

Moon, P. and Spencer, D.E., 1942, Illumination from a non-uniform sky.

Trans. Illum. Eng. Soc. 37: 707-726.

Monteith, J.L., 1973, 1980. Principles of environmental Physics. Edw. Arnold. 241 p.

Monteith, J.L. (ed.), 1975, Vegetation and the Atmosphere I, II. Ac. Press London. 278, 439 p.

Morgan, V.T., 1975, The overall convective heat transfer from smooth circular cylinders. In: Advances in Heat Transfer 11. Ac. Press, N.Y.: 199-264.

Morris, C.W. and Lawrence, J.H., 1971, The anisotropy of clear sky diffuse solar radiation. Trans ASHRAE 77 (2): 136-142.

Morris, L.G. and Neale, F.E., 1954, The infra-red carbondioxide gasanalyzer and its use in glasshouse research. NIAE rep. Wrestpark, Silsoe, England.

Morris, L.G., Neale, F.E. and Postletwaite, J.D., 1957. The transpiration of glasshouse crops and its relationship to the incoming solar radiation. J. Agric. Engng. Res. 2: 111-122.

Morrison, J.E. and Barfield, B.J., 1981, Transpiring artificial leaves. Agr. Meteorol. 24: 227-236.

Muyzenberg, E.W.B. van den, 1943, Overzicht van de historische ontwikkeling van de kassenbouw- en de kasverwarming |in Dutch|. ITT meded. 1. Imag Wageningen: 505-515.

Muyzenberg, E.W.B. van den, 1948, Het licht in de kas |in Dutch|. Meded. Dir.Tuinb. 11: 514-521.

Nederhoff, E.M., 1983, Light interception of a cucumber crop at different stages of growth. Acta Hort. 148: 9 p. (in press).

Nederhoff, E.M., Vooren, J. van de and Udink ten Cate, A.J., 1983, Method to determine ventilation in greenhouses. Acta Hort. 148: 6 p. (in press).

Nisen, A., 1962, Calcul de l'éclairement naturel des constructions horticoles |in French|. Proc. of the XVIth (1962) Int. Hort. Congress 16 (4): 383-389.

O'Flaherty, T. and Maher, M.J., 1978, Evaluation of double-clad polythene greenhouses for energy saving in early tomato production. Acta Hort. 76: 335-339.

Okada, M. and Takakura, T., 1973, Guide and data for greenhouse air conditioning. 3: Heat loss due to air infiltration of heated greenhouses. J. Agric. Meteorol. (Tokyo) 28 (4): 223-230.

Okada, M. and Hayashim, 1978, Reducing heat consumption by curtain insulating systems. Acta Hort. 87: 103-110.

Okada, M., 1980, The heating load of greenhouses. I Convective heat transfer coefficients at the inside cover surface of a greenhouse as influenced by heating pipe positions. J. Agric. Meteorol. (Tokyo) 35 (4): 235-242.

Parkhurst, D.F., Duncan, P.R., Gates, D.M. and Kreith, F., 1968, Windtunnel modelling of convection of heat between air and broad leaves of plants. Agr. Meteorol. 5: 33-47.

Penning de Vries, F.W.T., 1972, A model for simulating transpiration of leaves with special attention to stomatal functioning. J. Appl. Ecol. 9: 57-77.

Pera, L. and Gebhart, B., 1973a, Natural convection boundary layer flow over horizontal and slightly inclined surfaces. Int. J. Heat and Mass Transfer 16: 1131-1146.

Pera, L. and Gebhart, B., 1973b, On the stability of natural convection boundary layer flow over horizontal and slightly inclined surfaces. Int. J. Heat and Mass Transfer 16: 1147-1163.

Pettenkofer, M. von, 1858, Über den Luftwechsel in Wohngebäuden |in German|. Cotta, München.

Pokrowski, G.J., 1929, Über die Helligkeitsverteilung am Himmel |in German|. Phys. Zeitschr. 30: 697-300.

Raithy, G.D. and Hollands, K.G.T., 1975, A general method of obtaining approximate solutions to laminar and turbulent free convection problems. In: Advances in Heat Transfer 11: 265-315. Ac. Press N.Y.

Raithby, G.D. and Hollands, K.G.T., 1976, Laminar and turbulent free convection from elliptic cylinders with a vertical plate and a horizontal cylinder as special cases. ASME J.Heat Transfer 98: 72-80.

Ramachandran, N., Armaly, B.F. and Chen, T.S., 1983, Mixed convection over a horizontal plate. ASME J.Heat Transfer 105: 420-423.

Raschke, K., 1975, Stomatal action. Ann. Rev. Plant Physiol. 26: 309-340.

Renard, W. and Stein, J., 1960, Der Einfluss des Windes auf die Gewächshauslüftung |in German|. Gartenbauwissenschaft 25:

Robinson, N., 1966, Solar Radiation. Elsevier, Amsterdam, 347 p.

Rose, C.W., 1966, Agricultural Physics, Pergamon Press. 226 p.

Rosenberg, N.J., 1974, Microclimate, the biological environment. Wiley & Sons. 315 p.

Ross, H.D. and Grimsrud, D.T., 1978. Air infiltration in buildings: literature survey and proposed research agenda. Nat. Techn. Inf. Service. U.S. Dept. of Commerce LBL-7822.

Rothwell, J.B. and Jones, D.A.G., 1961, The water requirement of tomatoes in relation to solar radiation. Expl. Hort. 5: 25:30.

Ruth, D.W. and Chant, R.E., 1976, The relationship of diffuse radiation to total radiation in Canada. Solar Energy 18 (2): 153-154.

Sase, S., Kozai, T., Nara, M. and Negishi, H., 1980, Ventilation of glasshouses I. Windtunnel measurements of pressure and discharge coefficients for a single-span greenhouse |in Japanese|. J. Agric. Meteorol. (Tokyo) 36 (1): 3-12.

Schaapendonk, A.H.C.M. and Gaastra, P., 1983a, Fysiological aspects of optimal CO_2 control in protected cultivation. Acta Hort. 148: 11 p. (in press).

Schaapendonk, A.H.C.M. and Gaastra, P., 1983b, Simulation study on CO_2 concentration in protected cultivation. Submitted to Scientia Horticulture.

Schenk, J., Altmann, R. and Wit, J.P.A. de, 1976, Interaction between heat and mass transfer in simultaneous natural convection about an isothermal vertical flat plate. Appl. Sci. Res. 32: 599-606.

Schockert, K. and Zabeltitz, Chr. von, 1978, Measurements of climate and heat consumption under double glass. Acta Hort. 76: 317-320.

Schockert, K. and Zabeltitz, Chr. von, 1980, Energy consumption in greenhouses. Acta Hort. 106: 21-26.

Sebesta, S. and Reiersen, D., 1981, A comparison of single glass and double acrilyc sheating with respect to heat loss and effects on plant environment. Acta Hort. 115: 409-416.

Seemann, J., 1952, Stralungsverhältnisse in Gewächshäusern |in German|. Archiv für Met. Geoph. Biokl. B 2: 193-206.

Seemann, J., 1974, Climate under Glass, WMO rep. no. 373. WMO, Geneva. 40 p.

Seginer, I. and Levav, N., 1971, Models as tools in greenhouse climate design. Publ. no. 115, Technion, Haifa, Israël: 80 p.

Seginer, I., 1980, Optimizing greenhouse operation for best aerial experiment. Acta Hort. 106: 169-178.

Selçuk, M.K., 1971, Analysis, design and performance evaluation of controlled environment greenhouses. Trans ASHRAE 8: 21-72.

Shaw, B.H., 1971, Heat and mass transfer by natural convection and combined natural convection and forced air flow through large rectangular openings in a vertical partition. Inst. Mech. Engrs Proc. of 1971 Conf. C117/71: 31-39.

Shaw, W.N., 1907, Air currents and the law of ventilation. C.U.P.

Slatyer, R.O., 1965, Plant-Water Relationships. Ac. Press, N.Y. 366 p.

Slavik, B., 1974, Methods of studying Plant-Water Relations. Ecological Studies 9. Springer, Berlin: 449 p.

Slob, W.H., 1982, Climatological values of solar irradiation on the horizontal and several inclined surfaces at De Bilt. Scient. Rep. W.R. 82-7. KNMI, De Bilt, The Netherlands. 19 p.

Smith, C.V. and Kingham, H.G., 1970, A contribution to glasshouse design. Agr. Meteorol. 8: 447-468.

Smith, M.R. and Hazen, T.E., 1968, Similitude study of inlet configuaration. Trans ASAE 11: 218-225.

Soribe, F.J. and Curry, R.B., 1973, Simulation of lettuce growth in an air supported plastic greenhouse. J. Agric. Engng. Res. 18: 133-140.

Sparrow, E.M., 1973, Radiant interchange between surfaces separated by non-absorbing and nonemitting media. In: Rohsenov, W.M. and Hartnett J.P. (eds), Handbook of Heat Transfer. Mc Graw-Hill: 15,1-15,28.

Stamnes, K. and Swanson, R.A., 1981, A new look at the ordinate method for radiative transfer calculation in anisotropically scattering atmospheres. J. Atmos. Sci. 38: 387-399, 2696-2706.

Stanghellini, C., 1981a, Estimation of energy requirement for evapotranspiration in greenhouses. Acta Hort. 115: 693-700.

Stanghellini, C., 1981b, Evapotranspiration and energyconsumption in greenhouses. Acta Hort. 119: 273-280.

Stanhill, G., 1966, Diffuse sky and cloud radiation in Israël. Solar Energy 10 (2): 96-101.

Stigter, C.J., Leaf diffusion resistance to water vapour and its direct measurement. I. Introduction and review concerning relevant factors and methods. Mededed. Landb. Hogesch. Wageningen 72 (3): 1-47.

Stoffers, J.A., 1967, Lichtdoorlatendheid van met vlakke materialen bedekte warenhuizen |in Dutch|. ITT publ. 14. Imag, Wageningen. 35 p.

Stoffers, J.A., 1971 Lichtdurchlässigkeit von Gewächshäusern in Blockbauweise |in German|. ITT publ. 39. Imag, Wageningen. 29 p.

Stoffers, J.A., 1975, Radiation absorbtion of canopy rows. Acta Hort. 46: 91-95.

Stoffers, J.A., 1977, Heat transfer measurements in screened greenhouses. In: Technical and physical aspects of energy saving in greenhouses. Commission of the European Comm. Eur. 5679e: 35-37.

Strijbosch, Th. and Vooren, J. van de, 1975. Developments in climate control. Acta Hort. 46: 21-22.

Swinbank, W.C., 1963, Long-wave radiation from clear skies. Quart. J. Roy Meteorol. Soc. 89: 339-348.

Takakura, T., 1967, Predicting air temperatures in the glasshouse I. J. Meteorol. Soc. Japan ser. II, 45 (1): 40-52.

Takakura, T., 1968, Predicting air temperatures in the glasshouse II. J. Meteorol. Soc. Japan ser. II, 46 (1): 36-44.

Takakura, T., Jordan, K.A. and Boyd, L.L., 1971, Dynamic simulation of plant growth and environment in the greenhouse. Trans ASAE 14: 964-971.

Takakura, T., Kozai, T., Tachibana, K. and Jordan, K.A., 1974, Direct digital control of plant growth. I. Design and operation of the system. Trans ASAE 17 (6): 1150-1154.

Tantau, H.J., 1978, The influence of single and double shelters on the climate and heat consumption of greenhouses. Acta Hort. 87: 119-123.

Taylor, A.H. and Kerr, G.P., 1941, The distribution of energy in the visible spectrum of daylight. J. Opt. Soc. Am. 31: 3.

Udink ten Cate, A.J., Bot, G.P.A. and Dixhoorn, J. van, 1978, Computer control of greenhouse climates. Acta Hort. 87: 265-272.

Udink ten Cate, A.J., 1983, Modelling and (adaptive) control of greenhouse climates. Ph. D. thesis. Agr. University, Wageningen. 159 p.

Van Bavel, C.H.M., Damagnez, J. and Sadler, E.J., 1981, The fluid roof solar greenhouse: energy budget analysis by simulation. Agr. Meteorol. 23: 61:76.

Vogel, S., 1970, Convective cooling at low air speeds and the shapes of broad leaves. J. exp. Bot. 21: 91-101.

Vooren, J. van de, 1975, A computer for crop research and climate control in glasshouses. Acta Hort. 51: 169-174.

Vooren, J. van de and Koppe, R., 1975, The climate glasshouse at Naaldwijk. Neth. J. Agric. Sci. 23: 238-247.

Vooren, J. van de, 1979, Data analysis. Acta Hort. 106: 39-42.

Vorst. P.G.T. and Postel, J.H.G., 1972, Bepaling bladoppervlak van tomatenplanten |in Dutch|. Intern rep. 46. Imag, Wageningen. 15 p.

Walker, J.N., 1965, Predicting temperatures in ventilated greenhouses. Trans ASAE 8 (3): 445-448.

Wang, X.A., 1982, An experimental study of mixed forced and free convection heat transfer from a horizontal flat plate to air. ASME J.Heat Transfer 104: 139-144.

Warren, P.R., 1977, Ventilation through openings in one wall only. Proc. 1977 ICHMT seminar on "Heat Transfer in Buildings". Hemisphere N.Y.

Wartena, L., Palland, C.L. and Vossen, G.H.L., 1973, Checking of some formulae for the calculation of long-wave radiation from clear skies. Arch. Met. Geoph. Biokl. B 21: 335-348.

Weel, P.A., 1981, Arbeidsbesparing door laaggelegenbuisverwarming |in Dutch|. Vakblad voor de Bloemisterij 39: 36-39.

Weerdhof, A.M. van de, 1982, Vergelijking tussen natuurlijke en mechanische ventilatie in slachtkuikenstellen. 2. |in Dutch|. Pluimveehouderij 12 (3): 14-15.

Whittle, R.M. and Lawrence, W.J.C., 1959, The climatology of glasshouses. I. Natural illumination. J. Agric. Engng. Res. 4: 326-340.

Whittle, R.M. and Lawrence, W.J.C., 1960, The climatology of glasshouses. II. Ventilation. J. Agric. Engng. Res. 5: 36-41.

Wijk, W.R. van (ed), 1963, Physics of Plant Environment. North Holland, Amsterdam.

Winspear, K.W., 1977a, Vertical temperature gradients in heated greenhouses. In: Technical and physical aspects of energy saving in greenhouses. Commission Eur. Comm. 5679e: 95-102.

Winspear, K.W., 1977b, Vertical temperature gradients and greenhouse energy economy. Acta Hort. 76: 97-103.

Wit, C.T. de, 1965, Photosynthesis of leaf canopies. Agric. Res. Rep. 663. Pudoc Wageningen. 57 p.

Youssef, W.W., Tarasuk, J.D. and McKeen, W.J., 1982, Freen convection heat transfer from upward facing isothermal horizontal surfaces. ASME J. Heat Transfer 104: 493-500.

Zabeltitz, Chr., von, 1978, Gewächshäuser, Planung und Bau |in German|. Eugen Ulmer, Stuttgart. 267 p.

Curriculum vitae

Gerardus Petrus Adrianus Bot werd geboren op 28 december 1944 te Grootebroek. Na het behalen van het HBSb diploma in 1963 aan het St. Werenfridus Lyceum te Hoorn werd de militaire dienstplicht vervuld.
In 1965 werd met de studie aan de Technische Hogeschool Delft begonnen aan de afdeling Technische Natuurkunde. Het kandidaatsexamen werd afgelegd in april 1971 en in april 1972 werd het diploma van natuurkundig ingenieur behaald. Hierbij werd tevens de onderwijsbevoegdheid in de Natuurkunde verkregen. Het kandidaats- en afstudeeronderzoek werden verricht in de groep Warmtetransport (prof. ir. C.J. Hoogendoorn) aan respectievelijk stromingsverschijnselen in gespiraliseerde buizen en warmteoverdracht in een horizontale hoek. Het laatstgenoemde onderzoek werd verricht in een aanstelling als student-onderzoeker bij de Technische Physische Dienst TNO-TH.
Per 1 juni 1972 volgde aanstelling als wetenschappelijk medewerker aan de Landbouwhogeschool Wageningen bij de vakgroep Natuur- & Weerkunde, belast met onderwijs en onderzoek in het taakgebied van de sectie Technische Natuurkunde.. De onderwijstaak omvat vooral het geven van onderwijs aan studenten in de kandidaats- en doctoraalfase. Daarnaast wordt als docent meegewerkt aan de 2 jarige MSc. opleiding "Bodem en Water" voor studenten uit ontwikkelingslanden.
In het onderzoek wordt gewerkt aan onderwerpen op het gebied van het binnenklimaat en de energietechniek. Het zwaarste accent lag hierbij op kasklimatologisch onderzoek.

Greenhouse climate: from physical processes to a dynamic model

G.P.A.Bot

Errata:

page	line ↓	line ↑	reads as:	should read:
11		8	$T_{g,1}$	$T_{g,i}$
12	1		e_1	e_l
13		8	...distint..	.. distinct..
18	15		..(fig.3.2.,..	.. (fig. 3.2.)..
19		9	.. sin (1+...	.. sin ζ (1+..
21		17	.. abject..	.. object ..
22	11		.. $\tilde{u}^2$	.. $\bar{u}^2$
29	5		$-\frac{mB}{H}[\ldots(H-R)]^{5/2}$	$-m\, \frac{S}{H}[\ldots(H-R)^{5/2}]$
29		2	with B =....	with S =....
31	1		..(figure 36)..	..(figure 3.6)..
33		13	..$K_u(\Psi)$	..$K_f(\zeta)$
33		11	..= $3 \frac{u}{\ldots}$	$= 3 \frac{\bar{u}}{\ldots}$
36		10	..τ (= $/\phi_v$)..	..τ (= V/ϕ_v)..
39	1		..+ 0.7 exp (- H_o/L_o)/..	..+ 0.70 exp (-(H_o/L_o)/..
39		11	..without F_o..	..without window F_o..
41	6		(relations 3.6.a and b)..	(relations 3.6.a, b and c)..
49	6		..4.8 10^{-5} Ag	..4.8 $10^{-5} A_g$
49	16		..from figure 3.17..	..from figure 3.19..
50	fig.3.21 vertical axis:		K_f (ζ)	K_f (ζ). 10^2
51		12	3.40 and 3.42..	3.40 and 3.41...
51		10	..relation (3.3.8.a).	..relation (3.38.a).
52	5		..- 0.28 exp(-ζ/35)}	..- 0.28 exp(-ζ/3.5)}
54		1	..is found.	..are found.
55		6	.. (3.52	.. (3.52)
56		2	Fig.24..	Fig.3.24..
57	4		..more than 400%..	..more than 300%..
57	6		.., high greenhouse. D is..	.., high greenhouse D is..
58		7	..and, rolled	..and rolled
59,61			H_z	Hz
63		7	..will be between..	..will be inbetween..

72	12		..occured..	..occurred..
75	8		..(figure 4.10b),..	..(figure 4.10 a),..
77		7	..(section 3.2.2).	..(section 5.2.2).
79	6		fects the..	fect the..
81	9		C =..	c =..
83	2		..flass..	..glass..
84	5		..arbit..	..orbit..
84	9		..number of the..	..number in the..
84		8	..co-ordination	..co-ordinate
85	12		..the q axis	..the q-axis..
86	4		..the wo glasspanes	..the two glasspanes
89		8	..number of pans..	..number of panes..
91	9		..(section 5.20.1a)..	..(section 5.2.1.a)..
99	2		d_2 = EFsin/(FED)	d_2 = EFsin(/FED)
105		2	..in figure 5.7,..	..in figure 5.18,..
105		1	..in figure 5.16.	..in figure 5.17.
107		5	34, 65°	34.65°
112	9		..hours are given..	..hours is given..
116		9	..the the required..	.. to the required..
116		5	..combinations..	..combination..
117		2	..relation 5.49..	..relation 5.59..
121	4		..Kondretyev..	..Kondratyev..
125	11,12		..W_m^{-2}..	..Wm^{-2}..
126	4		..geen given..	..been given..
128	5		τ	σ
136	17		C_{gr} (relation 6.1b)..	C_{fo} (relation 6.1.a)..
142	20		..The extended literature..	..The extensive literature..
144		6	..large differences.	..large variations.
152	7		.., 40 sm)..	.., 40 cm)..
153		1	larger	layer
155		8	..are not so large..	..are not that large..
157	13		..(section 6.12)..	..(section 6.1.2)..
158	3		..the greenhous..	..the greenhouse..
163	10		..(4.2 $10^3 JKg^{-1}$..	..(4.2 $10^3 Jkg^{-1}$..
165	horizontal axis of figures:		$J(Wm^{-2})$	$I(Wm^{-2})$

168		8	varous	various
183	fig. 12	(tables)	$\phi 13$	$\phi 23$
183	fig. 12	(tables)	12, -13	12, -23
183	fig. 12	(tables)(to add)		ϕ_{10} = SF
183	fig. 12	(tables)(to add)		10, SF
183	fig. 12	(tables)	10, 11, -13	10, 11, -12
187		16	In additions..	In addition..
197	7		sunset..	sunrise..
199		15	(figure 7.3)..	(figure 7.8)..
199		6-5	day that to the..is demonstrable..	day, the response to the.. is demonstrated..
206	5		15 ms^{-1}	1.5 ms^{-1}
206	1		Fig. 7.6	Fig. 7.16
206		2	then	than
208		5	..schames..	..schemes..
211	15		..as side walls..	..side walls as..
213		11	..cover on the..	..cover and on the..
214		9	..exchange the..	..exchange at the..
			Schaapendonk	Schapendonk
			Stephan-Boltzmann	Stefan-Boltzmann

226 to add:

Acock, B., Charles.Edwards, D.A. and Sawyer, S., 1979, Growth response of a chrysantemum crop to the environment. III, effects of radiation and temperature on dry matter partitioning and photosynthesis. Ann. of Bot. 44: 289-300.

227 to add:

Businger, J.A., 1963, The glasshouse (greenhouse) climate. In: Wijk, W.R. van (ed): Physics of plant environment. North Holland, Amsterdam.